

ANAYLSIS OF THE STRUCTURAL AND KINETIC PROPERTIES OF HUMAN SULT2A1
INDUCED BY THE BINDING OF 3'-PHOSPHOADENOSINE-5'-PHOSPHOSULFATE

by

IAN THOMAS COOK

STEPHEN BARNES, COMMITTEE CHAIR
CHARLES N. FALANY, MENTOR
MARY-ANN BJORNSTI
PETER PREVELIGE, JR.
YUHUA SONG

A DISSERTATION

Submitted to the graduate faculty of The University of Alabama at Birmingham,
in partial fulfillment of the requirements for the degree of
Doctor of Philosophy

BIRMINGHAM, ALABAMA

2011

ANAYLSIS OF THE STRUCTURAL AND KINETIC PROPERTIES OF SULT2A1
INDUCED BY THE BINDING OF 3'-PHOSPHOADENOSINE-5'-
PHOSPHOSULFATE (PAPS)

IAN COOK

PHARMACOLOGY AND TOXICOLOGY

ABSTRACT

Sulfation is an important Phase II drug metabolism reaction catalyzed by the cytosolic sulfotransferases (SULTs). SULT2A1 is a major SULT in liver and adrenal cortex that has been reported to sulfate a wide variety of substrates including bile acids, steroids, and drugs. The crystal structures of SULT2A1 suggest that PAPS binding causes a structural change. This study examines the kinetic changes in SULT2A1 caused by PAPS binding using computer modeling, enzyme kinetics, binding studies, and mammalian cells expressing SULT2A1. The data presented clearly demonstrate that the binding of PAPS changes the affinity of some substrates to SULT2A1 resulting in different apparent reaction mechanisms. With small substrates, such as dehydroepiandrosterone (DHEA), the binding of PAPS causes only a small change in substrate affinity to SULT2A1. For these substrates, either PAPS or acceptor may bind first resulting in a random Bi Bi reaction mechanism. With larger substrates, the binding of PAPS generated a conformational change in SULT2A1 that blocked the substrate from binding in a catalytic orientation. In these reactions, the substrate must bind before PAPS resulting in an ordered reaction mechanism. All human SULTs have been identified as homodimers. In SULT2A1, the addition of an amino-terminal maltose binding protein (MBP) tag disrupted dimerization. The MBP-SULT2A1 monomer was kinetically active and showed similar affinities for DHEA and PAPS as the SULT2A1 homodimer.

However, the MBP-SULT2A1 monomer did not show substrate inhibition. Analysis of MBP-SULT2A1 and dimeric SULT2A1 demonstrated that substrate inhibition of DHEA was caused by the binding of DHEA at an inhibitory allosteric site. The inhibitory binding site was blocked or disrupted when PAPS bound to the homodimer. The molecular rearrangements observed in SULT2A1 upon PAPS binding were hypothesized to occur in other SULT isoforms. Modeling and enzyme kinetics demonstrated that similar as well as different structural changes occur in SULT1A1. These changes had a significant effect on the binding and kinetic properties of SULT1A1. The study presents novel insights into SULT2A1 and SULT1A1 structural, kinetic, and binding properties, and provides valuable insights for improving the *in silico* predictions of the *in vivo* sulfation of therapeutic drugs.

Key words: Sulfotransferase, Phase II drug metabolism, docking, 3'-phosphoadenosine-5'-phosphosulfate, dehydroepiandrosterone, enzyme kinetics

DEDICATION

To my wife, Andrea Lundgren-Cook and two children, Christopher and Rachael
with all my love.

ACKNOWLEDGMENTS

I would like to thank my advisor, Dr. Charles N. Falany, for his patience and support, especially during the writing. I would also like to thank Josie Falany for taking the time to teach me the techniques that were critical for my work. A special thanks to Dr. Emily Salmen, my “lab sister” who spent a great deal of time with me in the laboratory.

I also wish to extend a thank you to Dr. Steven Barnes for guiding my early research and directing me to Dr. Falany’s laboratory. I thank Dr. Yuhua Song for teaching me the computational chemistry that proved critical to my dissertation. I also thank Dr. Tom Leyh of Albert Einstein College of Medicine for his helpful comments along the way and for accepting me to work in his laboratory as a post-doc. Finally, I wish to thank my wife, Andrea Lundgren-Cook for following me from Idaho to Alabama and her understanding of the demands of science and being a graduate student.

TABLE OF CONTENTS

| | Page |
|--|------|
| ABSTRACT..... | ii |
| DEDICATION..... | iv |
| ACKNOWLEDGMENTS..... | v |
| LIST OF TABLES..... | x |
| LIST OF FIGURES..... | xi |
| LIST OF ABBREVIATIONS..... | xv |
| INTRODUCTION..... | 1 |
| I. Drug Metabolism..... | 1 |
| A. Phase II Drug Metabolism..... | 4 |
| II. Sulfation..... | 5 |
| III. SULT Isoforms..... | 10 |
| IV. Hydroxysteroid Sulfotransferase (SULT2) Family..... | 17 |
| V. SULT2A1..... | 19 |
| A. Adrenal Production and Secretion of DHEA-Sulfate..... | 20 |
| B. SULT2A1 Drug and Oxysterol Metabolism..... | 24 |
| VI. General SULT Structure..... | 25 |
| A. SULT2A1 Crystal Structure..... | 30 |
| VII. Rational and Objective..... | 34 |
| A. Aim 1..... | 34 |
| B. Aim 2..... | 34 |
| C. Aim 3..... | 37 |
| METHODS..... | 38 |
| I. The Structural Rearrangements Associated with PAPS Binding in the SULT2A1 Subunit..... | 38 |
| A. Materials..... | 39 |
| B. DHEA Sulfation Activity Assay..... | 39 |

| | |
|---|----|
| C. SULT2A1 Purification | 39 |
| D. Sulfation of 24(S)-OH-Chol..... | 43 |
| E. Molecular Docking of Ligands to the SULT2A1 Active Site..... | 50 |
| F. Determination of DHEA Sulfation Kinetic Constants..... | 52 |
| G. DHEA Pre-Steady State Kinetics..... | 52 |
| H. Determination of RAL Sulfation Kinetic Constants | 53 |
| I. RAL Pre-Steady State Kinetics | 53 |
| J. Determination of the Affinity Constants for SULT2A1 Binding by Changes in Intrinsic Fluorescence | 54 |
| K. Stoichiometric Determination of Binding for Substrate to SULT2A1 Using the Change in Intrinsic Fluorescence | 56 |
| L. Pharmacophore Analysis of SULT2A1 | 56 |
| M. Pre-Steady State Kinetics of Pharmacophore Results..... | 57 |
| N. Computational Modeling of G234L/G233L SULT2A1 Mutant..... | 57 |
| O. Generation and Characterization of L233G/L234 SULT2A1 Mutant | 58 |
| P. Characterization of V260E, Q247A, and Q155A SULT2A1 Mutants..... | 60 |
| II. The Subunit Interactions of the SULT2A1 Homodimer Associated with PAPS Binding..... | 60 |
| A. Materials..... | 60 |
| B. SULT2A1 Dynamic Modeling of with GROMACS..... | 61 |
| C. Size Exclusion Chromatography of WT SULT2A1 and MBP-SULT2A1 | 62 |
| D. DHEA Sulfation Activity of MBP-SULT2A1 and SULT2A1..... | 63 |
| E. PAPS Concentration Curve of SULT2A1 and MBP-SULT2A1 at 2 μ M and 20 μ M DHEA..... | 64 |
| F. Pre-Steady State Sulfation of RAL by MBP-SULT2A1 | 64 |
| G. Docking of a Second DHEA Molecule to the Open SULT2A1 Model | 64 |
| H. Cos-7 Transfection with SULT2A1 and MBP-SULT2A1 | 65 |
| I. Transfected Cos-7 DHEA Sulfation Assay | 66 |
| III. The Structural Rearrangements of SULT1A1 and SULT1E1 Associated with PAPS Binding | 67 |
| A. Materials..... | 67 |
| B. Homology Modeling of SULT1A1 and SULT1E1..... | 67 |
| C. Docking Studies with SULT1A1 and SULT1E1 | 67 |
| D. SULT1A1 and SULT1E1 Generation and Purification | 68 |
| E. Steady State Kinetics of E2 with SULT1A1 | 69 |
| F. Sulfation of FUL by SULT1A1 and SULT1E1..... | 69 |
| G. Determination of K _d for E2 and FUL Binding to SULT1A1 and SULT1E1 Using Intrinsic Fluorescence | 70 |

| | |
|--|-----|
| RESULTS | 70 |
| I. The Structural Rearrangements Associated with PAPS Binding in the SULT2A1 Subunit | 70 |
| A. Sulfation of 24(S)-Chol by SULT2A1 | 89 |
| B. Docking of DHEA and RAL to the Open and Closed Models of SULT2A1 | 94 |
| C. DHEA and RAL Sulfation by SULT2A1 | 92 |
| D. Kd and Stoichiometry Determination of PAPS, PAPS, DHEA, and RAL Binding to SULT2A1 | 100 |
| E. Pharmacophore Screening of Potential Substrates | 111 |
| F. Docking of Emodin, Digitoxin, and 3-CTP to SULT2A1 | 117 |
| G. Sulfation of Emodin, Digitoxin, and 3-CTP by SULT2A1 | 120 |
| H. APS Binding to SULT2A1 | 125 |
| I. Mutation of the Substrate Active Site to Reduce the Structural Rearrangements of SULT2A1 by PAPS Binding | 125 |
| J) Specific Aim 1 Conclusions | 133 |
| II. The Subunit Interactions of the SULT2A1 Homodimer Associated with PAPS Binding | 136 |
| A. MBP-SULT2A1: Monomerization and Sulfation Activity | 136 |
| B. DHEA Stoichiometry in Substrate Inhibition | 145 |
| C. MBP-SULT2A1 Sulfation of RAL | 147 |
| D. Dynamic Modeling of SULT2A1 | 153 |
| E. Homodimer Mutations of SULT2A1 | 155 |
| F. Cos-7 Cell DHEA Sulfation | 159 |
| G. Specific Aim 2 Conclusions | 165 |
| III. The Structural Rearrangements of SULT1A1 and SULT1E1 Associated with PAPS Binding | 165 |
| A. Homology Modeling of SULT1A1 and SULT1E1 to the Open SULT2A1 Model | 166 |
| B. Molecular Docking to SULT1A1 and SULT1E1 | 171 |
| C. FUL Sulfation by SULT1A1 and SULT1E1 | 177 |
| D. SULT1A1 Sulfation of E2 | 183 |
| E. Specific Aim 3 Conclusions | 189 |
| DISCUSSION | 193 |
| I. The Structural Rearrangements Associated with PAPS Binding in the SULT2A1 Subunit | 196 |
| A. 24(S)-OH-Chol Sulfation | 196 |
| B. Structural Rearrangement of SULT2A1 by PAPS Binding | 199 |
| C. Pharmacophore Modeling of SULT2A1 Substrates | 201 |
| D. SULT2A1 Reaction Mechanism | 202 |
| II. The Subunit Interactions of the SULT2A1 Homodimer Associated PAPS Binding | 204 |

| | |
|--|-----|
| A. MBP-SULT2A1 Structural and Kinetic Properties | 206 |
| B. Mechanism of Substrate Inhibition in SULT2A1 | 208 |
| C. PAPS Concentration, Reaction Mechanism, and Substrate Inhibition <i>in vivo</i> | 210 |
| III. The Structural Rearrangements of SULT1A1 and SULT1E1 with Associated with PAPS Binding | 211 |
| A. SULT1A1 Structure and Kinetics | 212 |
| B. SULT1E1 Structure and Kinetics..... | 213 |
| C. SULT1A1 and SULT1E1 Activity and PAPS Dependent Substrate Specificity | 214 |
| IV. Conclusions..... | 215 |
| V. Importance of <i>In Vivo</i> PAPS Concentration and SULT Substrate Specificity | 219 |
| VI. Comparison of <i>In Vivo</i> UGT and SULT Activity..... | 222 |
| VII. Active Site Plasticity in Phase I and Phase II Drug Metabolizing Enzymes..... | 224 |
| VIII. Future Directions..... | 228 |
| BIBLIOGRAPHY..... | 232 |

LIST OF TABLES

| <i>Table</i> | <i>Page</i> |
|--|-------------|
| 1 Kinetic constants for 24(S)-OH-Chol sulfation by SULT2A1 | 81 |
| 2 Kis for PAP and E2-S product inhibition of E2 Sulfation by SULT1A1 | 189 |

LIST OF FIGURES

| <i>Figure</i> | <i>Page</i> |
|--|-------------|
| 1 Chemical structure of PAPS and the sulfation reaction..... | 6 |
| 2 PAPS synthesis reaction schematic | 8 |
| 3 Chemical structures of DHEA, raloxifene (RAL), and 24(S)-OH-Chol | 21 |
| 4 Pathway for biosynthesis of androgenic/estrogenic steroid hormones..... | 23 |
| 5 Sequence alignment of three major SULTs involved in drug and hormone metabolism..... | 26 |
| 6 DHEA concentration dependent sulfation activity by SULT2A1 | 28 |
| 7 The dynamics of loop 3 in SULT2A1 crystal structures | 32 |
| 8 Proposed mechanism for the shift of loop 3 in SULT2A1 | 33 |
| 9 Hypothesized dimerization of SULT2A1 at the KTVE domain..... | 35 |
| 10 Restriction maps of the vectors pMAL-4c and pcDNA 3.1 (-)..... | 42 |
| 11 Sulfation of 24(S)-OH-Chol by SULT2A1 and SULT2B1b | 73 |
| 12 LC/MS/MS of 24(S)-OH-Chol sulfates | 74 |
| 13 Mass fragmentation of 24(S)-Chol-24-sulfate | 76 |
| 14 Sulfation of 24(S)-OH-Chol by SULT2A1..... | 77 |
| 15 Sulfation of 24(S)-OH-Chol monosulfates | 79 |
| 16 Sulfation pathway of 24(S)-OH-Chol by SULT2A1 | 82 |
| 17 Modeling of 24(S)-OH-Chol in SULT2A1..... | 84 |

| | | |
|----|--|-----|
| 18 | Molecular modeling of 24(S)-Chol-24-sulfate to SULT2A1 with PAPS..... | 86 |
| 19 | Docking of 24(S)-Chol-24-sulfate to the open model of SULT2A1 | 88 |
| 20 | Molecular docking of DHEA to the open and closed models of SULT2A1 | 90 |
| 21 | Molecular docking of RAL to the open and closed models of SULT2A1 | 92 |
| 22 | Double reciprocal plots for DHEA and RAL sulfation by SULT2A1..... | 95 |
| 23 | Pre-steady state kinetics of DHEA and RAL sulfation by SULT2A1..... | 98 |
| 24 | SULT2A1 concentration dependent pre-steady state kinetics | 101 |
| 25 | Kd determination for the co-substrate PAPS and inactive cofactor PAP by intrinsic fluorescence titration..... | 103 |
| 26 | Stoichiometric determination of PAPS and PAP binding to SULT2A1 by intrinsic fluorescence titration..... | 105 |
| 27 | Kd determination of DHEA binding to SULT2A1 by intrinsic fluorescence | 107 |
| 28 | Stoichiometric determination of DHEA binding to SULT2A1 by intrinsic fluorescence | 109 |
| 29 | Kd determination for RAL binding to SULT2A1 using intrinsic fluorescence | 112 |
| 30 | Stoichiometric determination of RAL binding to SULT2A1 by intrinsic fluorescence. | 114 |
| 31 | Chemical structure of the commercially available predicted substrates of SULT2A1 based on pharmacophore analysis of SULT2A1 active sites..... | 116 |
| 32 | Docking of emodin to SUTL2A1 | 118 |
| 33 | Docking of digitoxin to SULT2A1 | 119 |
| 34 | Docking of 3-CTP to SULT2A1 | 121 |
| 35 | Sulfation of predicted substrates of SULT2A1 | 122 |
| 36 | Pre-steady state kinetics of SULT2A1 sulfation of emodin, digitoxin, and 3-CTP | 123 |

| | | |
|----|--|-----|
| 37 | Binding of APS to SULT2A1 using intrinsic fluorescence | 126 |
| 38 | Docking of RAL to the closed structure of the L233G/L234G SULT2A1 mutant | 128 |
| 39 | DHEA sulfation by L233G/L234G SULT2A1 | 129 |
| 40 | Kd determination of PAPS and PAP binding to L233G/L234G SULT2A1 using intrinsic fluorescence..... | 130 |
| 41 | Pre-steady state kinetics of RAL sulfation with the L233G/L234G SULT2A1 mutant..... | 132 |
| 42 | Kd determination of RAL binding to L233G/L234G SULT2A1 using intrinsic fluorescence | 134 |
| 43 | Size exclusion chromatography of SULT2A1 and MBPSULT2A1 | 138 |
| 44 | DHEA sulfation by SULT2A1 and MBP-SULT2A1 and the loss of substrate inhibition for the monomer isoform | 140 |
| 45 | Kd determination of PAPS and DHEA binding to MBP-SULT2A1 using intrinsic fluorescence. | 141 |
| 46 | Stoichiometry of binding of PAPS and DHEA to MBP-SULT2A1 | 143 |
| 47 | Docking of a second DHEA molecule to the open active site of the SULT2A1 | 146 |
| 48 | Double reciprocal plot of SULT2A1 activity at 2 μ M and 20 μ M DHEA with increasing PAPS | 148 |
| 49 | Double reciprocal plot of MBP-SULT2A1 activity at 2 μ M and 20 μ M DHEA with increasing PAPS | 150 |
| 50 | Pre-steady state kinetics for MBP-SULT2A1 with RAL | 152 |
| 51 | Dynamic modeling of the monomer and homodimer of SULT2A1 | 154 |
| 52 | Monomerization of SULT2A1 by the V260E mutation in the KTVE dimerization domain | 156 |
| 53 | DHEA sulfation with increasing concentration of DHEA and PAPS concentration curves with V260E SULT2A1 | 157 |

| | | |
|----|---|-----|
| 54 | DHEA sulfation of Q155A and Q243A SULT2A1 mutants | 160 |
| 55 | SDS-PAGE and Immunoblot analysis of Cos-7 stably transfected cells..... | 161 |
| 56 | Generation of sulfated DHEA by SUTL2A1 or MBP-SULT2A1 stably transfected Cos-7 cells | 163 |
| 57 | Homology modeling of SULT1A1 to the open SULT2A1 template..... | 167 |
| 58 | Homology modeling of SULT1E1 to the open SULT2A1 template | 169 |
| 59 | Docking of FUL to the open and closed models of SULT1A1 | 172 |
| 60 | Docking of E2 to the open and closed models of SULT1A1 | 174 |
| 61 | Docking of E2 to the open and closed models of SULT1E1..... | 175 |
| 62 | Docking of FUL to the open and closed models of SULT1E1..... | 176 |
| 63 | FUL sulfation by SULT1A1 | 178 |
| 64 | Kd determination of FUL binding to SULT1A1 using intrinsic fluorescence. | 180 |
| 65 | SULT1E1 sulfation of FUL | 181 |
| 66 | Kd determination of FUL binding to SULT1E1 using intrinsic fluorescence..... | 184 |
| 67 | Pre-steady state kinetics of SULT1A1 or SULT1E1 for FUL sulfation..... | 185 |
| 68 | SULT1A1 double reciprocal plot for E2 sulfation | 187 |
| 69 | Product inhibition of E2 sulfation with PAP and E2-S in SULT1A1..... | 188 |
| 70 | Determination of E2 and PAPS binding to SULT1A1 using intrinsic fluorescence | 190 |

LIST OF ABBRIVIATIONS

| | |
|---------------|---|
| 24(S)-OH-Chol | 24(S)-hydroxycholesterol |
| 3-CTP | 3-(3-chlorophenyl)-1-(2-thienyl)-1-propanol |
| aa | amino acid |
| ADP | adenosine diphosphate, |
| APS | adenosine-5'-phosphsulfate |
| ATP | adenosine triphosphate |
| BFE | binding free energy |
| cDNA | complementary DNA |
| CYP | cytochrome P450 monooxygenase |
| DEAE | diethylaminoethyl |
| DHEA | dehydroepiandrosterone |
| DHEAS | dehydroepiandrosterone sulfate |
| DMEM | Dulbecco's Modified Eagle Medium |
| DNA | deoxyribonucleic acid |
| DTT | dithiothreitol |
| E1 | estrone |
| E2 | 17 β -estradiol |
| E2-S | 17 β -estradiol-3-sulfate |
| EE2 | 17 α -ethinylestradiol |

| | |
|-------|--|
| ER | Endoplasmic Reticulum |
| FBS | fetal bovine serum |
| FUL | fulvestrant |
| ITPG | isopropyl β -D-1-thiogalactopyranoside |
| KTVE | KXXXTVXXE, dimerization motif |
| LC/MS | liquid chromatography mass spectrometry |
| LB | Luria broth |
| LXR | liver-X-receptor |
| MBP | maltose binding protein |
| MOE | Molecular Operating Environment |
| mRNA | messenger RNA |
| MWCO | molecular weight cut off |
| PAP | 3'5'-diphosphoadenosine |
| PAPS | 3'-phosphoadenosine-5'-phosphosulfate |
| PAPSS | PAPS synthetase |
| PAPST | PAPS transporter |
| PCR | polymerase chain reaction |
| PNP | para-nitrophenol |
| PNPS | PNP-sulfate |
| RAL | raloxifene |
| RMSD | root mean squared distance |
| RMSF | root mean squared fluctuations |
| RNA | ribonucleic acid |

| | |
|-------|--------------------------------------|
| RT | room temperature |
| rT3 | reverse triiodothyronine |
| SEM | standard error of the mean |
| SNP | single nucleotide polymorphism |
| STS | steroid sulfatase C |
| SULT | sulfotransferase |
| T2 | 3,3'-diiodothyronine |
| T3 | triiodothyronine |
| T4 | thyroxine |
| TLC | thin layer chromatography |
| UDPGA | uridine 5'-diphospho-glucuronic acid |
| UGT | UDP-glucuronosyltransferases |
| WT | wild type |

INTRODUCTION

I. DRUG METABOLISM

Drug metabolism is the chemical modifications of xenobiotic and endogenous compounds by the body and represents an important field of research in Pharmacology. In addition to absorption, distribution, and excretion, drug metabolism can greatly affect the biological activity of drugs, xenobiotics, and endogenous compounds. The body is exposed to a wide variety of toxic environmental compounds and must also regulate the concentration of many potentially toxic endogenous compounds. In most drug and xenobiotic metabolism, the primary mechanism of detoxification is by conversion of the typically lipophilic xenobiotics to water soluble forms that enhances excretion. The metabolism of endogenous or xenobiotic compounds can improve excretion, change the biological activity, activate a pro-drug to an active drug form, or activate a xenobiotic to generate a toxic metabolite (Parkinson 1996).

An important aspect of drug metabolism research is the study of drug-drug interactions. Many drug-drug interactions involve drug metabolism enzymes. The administration of a drug may cause the induction or inhibition of a drug metabolizing enzyme that may dramatically alter the pharmacokinetic and pharmacodynamic properties of a second drug. A classic example of a drug-drug interaction through a drug metabolism enzyme is the interaction of the anticoagulant warfarin and the bactericidal antibiotic rifampicin (Niemi, Backman et al. 2003). Warfarin is metabolized in part by CYP2C9, and

CYP2C9 has been reported to be strongly induced by rifampicin (Niemi, Backman et al. 2003). For a patient prescribed both drugs, the induction of CYP2C9 by rifampicin will significantly increase the metabolism of warfarin. The higher CYP2C9 activity increases the clearance of warfarin. The increased clearance will lower the plasma concentration of warfarin, potentially to a level insufficient for successful treatment and result in a failure of warfarin therapy.

Drug metabolism is divided into three phases: Phase I oxidation/reduction reaction, Phase II drug conjugation reaction, and Phase III drug transport (Parkinson 1996). In general, Phase I is the first step in drug metabolism. Phase I enzymes catalyze an oxidation/reduction reaction that can generate a hydroxyl, amino, or a carboxylic acid group and prepares a compound for Phase II metabolism. Phase II metabolism involves the addition of a charged group to the compound that substantially increases the charge of the compound, biologically inactivates a compound, and greatly enhances the excretion. Phase III metabolism is the active transport of xenobiotics and endogenous compounds across the cell membrane (Boylard and Chasseaud 1969). While the three phases of drug metabolism generally proceed in order from Phase I to Phase II and then Phase III, many drugs can undergo Phase II metabolism directly without Phase I metabolism. Other compounds can be excreted by Phase III transporters immediately after Phase I metabolism. Some compounds have been reported to be transported by Phase III without the involvement of Phase I or Phase II activity. Phase II metabolism can precede Phase I metabolism, but this is highly unusual (Parkinson 1996).

Phase I drug metabolism is catalyzed predominately by the cytochrome P450 monooxygenase enzyme family (CYP). Other Phase I drug metabolism enzymes include

the carboxyl-esterases, epoxide hydrolases, and the flavin-containing monooxygenases. The CYPs comprise the largest family in Phase I drug metabolism and most studied drug metabolism family, with 67,054 publications (March 2011) in the last 15 years. All CYPs are membrane bound enzymes, located in the endoplasmic reticulum (ER) and mitochondria (Smith 1994). The membrane dependency of the CYPs has made study difficult because of the use of detergents to solubilize the enzymes *in vitro* and the difficulty in forming crystal structures of the membrane domains. There are over 50 known CYPs in humans (Smith 1994). The CYPs also have a high number of single nucleotide polymorphisms (SNP) that contribute to interpatient variability. SNPs are changes in the nucleotide sequence that of a gene. A SNP can result in a change in the amino acid (aa) sequence of a protein that alters activity or expression. Patients with different CYP SNPs may have very different levels of activity for the same drug. Several of the CYPs have also been reported to be highly inducible by a variety of different drugs and xenobiotics (Smith 1994; Parkinson 1996; Niemi, Backman et al. 2003).

Three important CYPs for drug metabolism are CYP3A4, CYP2C9, and CYP2D6. CYP3A4 is the highest expressed CYP in the liver and has the largest substrate range of the CYPs (Hashimoto, Toide et al. 1993; Ekroos and Sjögren 2006). Approximately 50% of all known drugs have been identified to be potential *in vivo* substrates for CYP3A4 (Smith 1994; Ekroos and Sjögren 2006). The wide diversity of CYP3A4 substrates is a result of the large plastic active site of CYP3A4. CYP2C9 is important in the metabolism of many common drugs. Like CYP3A4, CYP2C9 is also highly expressed in the liver (Niemi, Backman et al. 2003); (Smith 1994). A variety of SNPs in CYP2C9 have been identified that have a significant change in expression and activity.

In addition to SNPs, patients with more than 2 copies of CYP2C9 have been identified, and the increase in copies of CYP2C9 has been reported to increase CYP2C9 activity (Parkinson 1996). The result of these findings is that CYP2C9 activity can vary by a 1000 fold between individuals. Differences in CYP2C9 activity have a large impact on a patient's response to drugs that are CYP2C9 substrates such as warfarin (Smith 1994; Niemi, Backman et al. 2003). Like CYP2C9 and CYP3A4, CYP2D6 is also expressed in the liver. CYP2D6 has a wide number of SNPs, and most CYP2D6 SNPs result in a diminished or loss of activity, although CYP2D6*2 can result in an increase in activity (Smith 1994; Yu, Idle et al. 2004). Differences in CYP2D6 activity can change a patient's response to CYP2D6 substrates such as opioids, like codeine and oxycodone.

A) Phase II Drug Metabolism

Phase II metabolism enzymes catalyze the conjugation of a charged molecule to the acceptor substrate. The reactions catalyzed by Phase II enzymes include glucuronidation, sulfation, acetylation, methylation, glutathione conjugation, and amino acid conjugation. Generally, Phase II reactions generate a biologically inactive compound with increased solubility compared to the unconjugated compound. While most Phase II reactions biologically inactivate a compound, there are exceptions where a conjugated metabolite is biologically active. One example is the activation of the pro-drug minoxidil to the active drug, minoxidil sulfate (Meisheri, Cipkus et al. 1988). The increased solubility of most metabolized compounds greatly enhances the body's ability to excrete the compound causing the product to be eliminated very quickly (Parkinson 1996). The excep-

tions to this pattern are usually caused by the metabolite binding to serum proteins or active retention in the urinary tract (Parker 1999).

The UDP-glucuronosyltransferases (UGT) comprise a major Phase II drug metabolism family. The glucuronidation reaction consists of the transfer of the glucuronosyl group from uridine 5'-diphospho-glucuronic acid (UDPGA) to substrate molecules that contain oxygen, nitrogen, sulfur, or carboxyl functional groups. The UGT are responsible for about 1/3 of Phase II drug metabolism, quantitatively the most important of the Phase II enzymes in human liver (Liston, Markowitz et al. 2001). While most UGTs have a high K_{cat} , the UGT tend to have a lower affinity for substrates compared to the cytosolic sulfotransferase (SULTs). The UGTs have been localized to the luminal side of the ER (Liston, Markowitz et al. 2001). Like the CYPs, the UGTs are a membrane dependent enzymes. The membrane dependence of the UGTs requires the use of detergents to solubilize UGTs for *in vitro* experiments and is a major obstacle in crystallization. A UGT of clinical significance is UGT1A1, which is important in bilirubin metabolism. Several mutations in UGT1A1 have been shown to result in severe jaundice (Mackenzie, Miners et al. 2000). Expression of the UGT1A1 is deficient in neonates, resulting in neonatal jaundice 60% of newborns, however in the overwhelming majority cases of neonatal jaundice; the jaundice clears within a few days as expression of UGT1A1 increases shortly after birth (Maisels and McDonagh 2008).

II. SULFATION

The work presented in this dissertation will focus on the human cytosolic sulfotransferase (SULT) family that transfers a sulfonate group from PAPS to an acceptor

molecule to generate a sulfonated product. The term sulfation is inaccurate because the reaction is actually a sulfonation. In the 19th century, when sulfated phenol was found in the urine of patients treated with phenol, the activity was called sulfation and the term sulfation has been used ever since (Baumann 1876). There are two superfamilies of SULTs, the Golgi SULTs and cytosolic SULTs, named for their cellular localizations. The SULTs catalyze the transfer of the sulfonate group from the universal donor, 3'-phosphoadenosine-5'-phosphosulfate (PAPS) to a hydroxyl on an acceptor substrate. The reaction generates a sulfated product and the inactive co-factor, 3',5'-diphosphoadenosine (PAP) (Fig 1). While the typical site of conjugation is a hydroxyl group, in some cases a sulfamate can be formed with a N-containing compounds (Parkinson 1996). The sulfamate formation by the SULTs has been reported to be an important part in the toxicity of several N-containing xenobiotics in rats and other animal models (Glatt 1997; Glatt 2000; Arlt, Glatt et al. 2002; Arlt, Glatt et al. 2003).

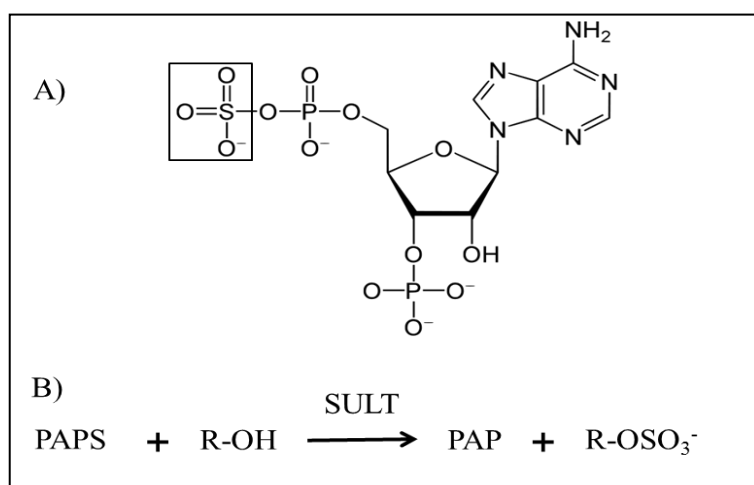


Figure 1. Chemical structure of PAPS and the sulfation reaction. A) The structure of the universal sulfate donor, PAPS with the sulfonate group highlighted. B) The SULTs catalyze the transfer of the sulfonate group from PAPS to an acceptor molecule to form PAP and a sulfate ester.

The synthesis of PAPS was first observed in 1953 by Demeio et al. (Demeio, Wizerkaniuk et al. 1953). Demeio et al. described an intermediate product from ATP, Mg^{+2} , and inorganic sulfate with rat liver homogenates that mediated the sulfation of phenol. Subsequently, Robbins and Lipmann in 1958 identified the intermediate as PAPS (Robbins and Lipmann 1957). PAPS is generated by the PAPS synthetase complex in a two-step reaction that utilizes ATP and inorganic sulfate (Fig 2) (Robbins and Lipmann 1958). The first step is the formation of adenosine-5'-phosphosulfate (APS) from ATP and inorganic sulfate by ATP-sulfurylase activity (Robbins and Lipmann 1958). The equilibrium for the reaction of ATP and inorganic sulfate to form APS is thermodynamically unfavorable. The second reaction is the formation of PAPS from APS and ATP by APS-kinase. The APS-kinase reaction is thermodynamically favorable and the energy from the APS-kinase reaction improves the ATP-sulfurylase thermodynamics. The ATP-sulfurylase and APS-kinase activities are tightly coupled *in vivo* (Robbins and Lipmann 1958). In prokaryotes, the reactions are performed by two separate enzymes (Robbins and Lipmann 1958; Robbins and Lipmann 1958). However, in eukaryotes, both reactions are catalyzed by a single peptide called PAPS synthetase (PAPSS) (Faiyaz ul Haque, King et al. 1998; Kurima, Warman et al. 1998; Franzon, Gibson et al. 1999). In humans, there are two isoforms of PAPSS, PAPSS-1 and PAPSS-2 located on chromosome 4 and 10, respectively (Faiyaz ul Haque, King et al. 1998; Franzon, Gibson et al. 1999). PAPSS-1 is ubiquitously expressed and is the predominant isoform in the brain. Initial investigations of PAPSS were based upon the hypothesis that PAPS synthesis occurred in the cytosol; however, PAPSS-1 has been shown to be localized to the nucleus (Besset, Vincourt et al. 2000). PAPSS-2 is localized to the nucleus as

well when co-expressed with PAPSS-1 (Besset, Vincourt et al. 2000). PAPSS-2 shows lower levels of expression than PAPSS-1 in most tissues, but is the major PAPSS isoform in mouse liver (Alnouti and Klaassen 2006) and human liver (Xu, Wood et al. 2001). Additionally, PAPSS-2 is reported to have an approximately six-fold higher catalytic efficiency than PAPSS-1 (Xu, Wood et al. 2001). Preliminary attempts to knockdown PAPSS expression in cells by Drs. Runge-Morris and Kocarek have shown that *in vivo*, down-regulation of one isoform is compensated by up-regulation of the other isoform (Runge-Morris and Kocarek 2011). Because PAPSS activity is dependent on the availability of inorganic sulfate, PAPSS activity is expected to be low in environments where inorganic sulfate is low, such as where glutathione activity is high (Klaassen and Boles 1997). PAPS levels may also be low due to genetic variants, particularly in PAPSS-2 (Venkatachalam 2003).

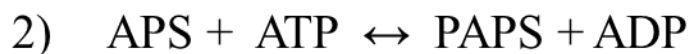
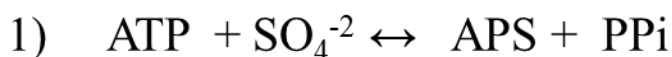


Figure 2. PAPS synthesis reaction schematic. PAPS synthesis is a two-step reaction mechanism catalyzed by PAPSS. 1) The first step is the conversion of ATP and inorganic sulfate to APS by ATP sulfurylase activity. 2) The second step is the conversion of APS to PAPS by APS kinase activity, utilizing one molecule of ATP.

In addition to PAPS synthesis, transport of PAPS in the cell plays a major role in the availability of PAPS. With a significant proportion of PAPS production in the nucleus and the necessity for PAPS transport to the Golgi for glycoaminoglycon SULF activity-

ty, the cell must transport PAPS from the site of synthesis to the SULTs in the cytosol and Golgi. Currently there are two identified PAPS transporters (PAPST) called PAPST-1 and PAPST-2 (Mandon, Milla et al. 1994; Kamiyama, Suda et al. 2003). The PAPST-1 gene is located on chromosome 6 and is highly expressed in placenta and pancreas with lower expression in the colon and heart (Mandon, Milla et al. 1994). PAPST-2 is also on chromosome 6 and is the dominant PAPST in the colon (Kamiyama, Ichimiya et al. 2011). Both PAPST isoforms transport PAPS from the cytosol into the Golgi and are critical for Golgi SULT activity (Bhattacharya, Townley et al. 2009). No transporter has yet been identified for transporting PAPS out of the nucleus and into the cytosol of the cell, though PAPS may be transported by a variety of nucleotide transporters.

There are two SULT families, the Golgi SULTs and the cytosolic SULTs. The Golgi SULTs are responsible for sulfation of glycol proteins, glycoaminoglycans, and glycopeptides that are required for cell function and destined for extracellular transport (Shworak, Liu et al. 1997; Grunwell and Bertozzi 2002). The Golgi SULT proteins are membrane bound, and localization to the luminal side of the Golgi limits their exposure to xenobiotics and thus their utility in drug metabolism. Sulfation by the Golgi SULTs is critical for several cell functions including cell-cell adhesion (Bistrup, Bhakta et al. 1999; Tangemann, Bistrup et al. 1999), cell proliferation (Rapraeger 1995), cell differentiation (Fan, Uchimura et al. 1999; Cornelison, Filla et al. 2001; Rapraeger 2001), blood clotting (Michnick, Pittman et al. 1994; Barbucci, Lamponi et al. 1998; Anderson, Fredenburgh et al. 2001), and chemokine activation (Selvan, Ihrcke et al. 1996; Lipscombe, Nakhoul et al. 1998). However the data presented in this dissertation will focus on the cytosolic SULTs.

III. SULT ISOFORMS

Cytosolic SULTs are responsible for the conjugation of drugs, xenobiotics and endogenous small compounds such as steroid hormones and monoamine neurotransmitters (Falany 1997). The sulfate acceptors have been reported to include phenolic hydroxyls (Anderson, Weinshilboum et al. 1981; Tseng and Liu 1981; Falany and Falany 1996), secondary alcohols (Barnes, Waldrop et al. 1986; Okuda, Hiratsuka et al. 1986; Falany, Vazquez et al. 1989; Aksoy, Otterness et al. 1993) and aromatic hydroxyamides (Wu and Straub 1976; Sekura, Duffel et al. 1981). Early classification of the SULTs used substrate specificity to classify individual isoforms, but as new SULTs with overlapping substrate specificities were identified this nomenclature became cumbersome. As the sequences of new SULT isoforms were determined, a new nomenclature was adopted (Blanchard, Freimuth et al. 2004). The current accepted nomenclature is based on the sequence identity of the SULT isoforms. The human cytosolic SULTs are divided into 4 families based on sequence similarity. SULTs that share greater than 45% identity are grouped as a family, and SULTs with at least 60% are grouped in the same sub-family. If the cDNA of two SULTs are 97% identical, then they are classified as two isoforms of a single SULT. The SULT1 family is the largest family and the most important for drug metabolism (Blanchard, Freimuth et al. 2004).

The first member of the SULT1A subfamily is SULT1A1 and was the first SULT identified, originally named thermostable phenol-sulfotransferase, P-PST (Wu and Straub 1976; Rein, Glover et al. 1982; Heroux and Roth 1988; Heroux, Falany et al. 1989). Expression of SULT1A1 has been reported in a variety of tissues including the intestine,

platelets, kidney, brain, prostate, skin, lungs, and liver (Whittemore, Pearce et al. 1986; Heroux, Falany et al. 1989; Nowell and Falany 2006). SULT1A1 is the highest expressed SULT in the liver (Whittemore, Pearce et al. 1986; Falany 1997; Alnouti and Klaassen 2006; Alnouti, Petrick et al. 2006) and has a large range of substrates including β -naphthol (Frame, Ozawa et al. 2000), para-nitrophenol (PNP) (Wu and Straub 1976), 17 β -estradiol (E2) (Gamage, Tsvetanov et al. 2005), resveratrol (Murias, Miksits et al. 2008), and acetaminophen (Reiter and Weinshilboum 1982).

The pharmacogenetics of SULT1A1 has been the most studied of the SULTs, with several identified allelic variants (Raftogianis, Wood et al. 1999) and reported changes in the gene copy number (Hebbring, Adjei et al. 2007). The SULT1A1 gene is located on chromosome 16 with the other SULT1A genes (Glatt, Boeing et al. 2001). The major SNP for SULT1A1 is SULT1A1*2, a R213H mutation with a 31% allelic frequency (Raftogianis, Wood et al. 1997). Mutational studies have reported that SULT1A1 is capable of activating many dietary compounds to electrophilic mutagens (Coughtrie, Gilissen et al. 1999; Glatt, Boeing et al. 2001; Arlt, Glatt et al. 2003). Some studies also found significant reduction in formation of some, but not all, toxic metabolites with the SULT1A1*2 allele (Arlt, Glatt et al. 2002). Another major SULT1A1 SNP is SULT1A1*3, a M233V mutation, with an allelic frequency of 11% in African Americans. SULT1A1*3 is almost always found linked to the SULT1A1*2 mutation and has been reported to reduce SULT1A1 activity (Nagar, Walther et al. 2006). In addition to the SULT1A1 allelic variants, SULT1A1 also can have different copy numbers between patients. The copy number of the SULT1A1 gene has been reported as high 5 copies in a single patient, with 63% of African Americans having 3 copies (Hebbring, Adjei et al.

2007). An increase in SULT1A1 copy number has been shown to increase SULT1A1 expression and activity, though the increase is not additive (Hebbring, Adjei et al. 2007).

The first SULT1A1 crystal structure was made in 2003 by Gamage et al. with bound PNP and PAP (1LS6) (Gamage, Duggleby et al. 2003). In the crystal structure, two PNP molecules were observed in the active site. SULT1A1 has been crystallized with PAP alone (1Z28) (Lu, Li et al. 2010) and with E2 and PAP (2DO6) (Gamage, Tsvetanov et al. 2005). The core of the crystal structure is conserved across all three structures with less than a 1.0 Å root mean squared distance (RMSD); however, the region of loop 1 (K85-P90) shows a significant amount of variation, up to 5 Å between the different crystal structures. Loop 1 forms the lip of the substrate binding domain and is apparently able to greatly influence the affinity of substrates. What regulates the orientation and the role in SULT1A1 catalysis for the loop region is still unclear (Allali-Hassani, Pan et al. 2007).

The second member of the SULT1A family is SULT1A2 and is closely related to SULT1A1. SULT1A2 has a similar range of substrates as SULT1A1 but with different affinities for phenolic compounds. The SULT1A2 gene is located next to SULT1A1 on chromosome 16 and shares a 96% sequence identity with SULT1A1 (Raftogianis, Wood et al. 1999). RNA expression of SULT1A2 has been identified in the kidney and gastrointestinal (GI) tract (Nowell, Green et al. 2005) and protein expression has been detected in some but not all human livers (Meinl, Pabel et al. 2006). SULT1A2 protein expression in the liver, when it is detected, is significantly less than SULT1A1 expression and SULT1A2 protein expression has not been detected in any other tissues (Meinl, Pabel et al. 2006).

The third member of the SULT1A family is SULT1A3, an isoform unique to humans and potentially other primates (Falany 1997; Weinshilboum, Otterness et al. 1997). The SULT1A3 gene is located on chromosome 16 about 150 kb from SULT1A1 and SULT1A2 (Dajani, Sharp et al. 1999) and has a sequence identity of 93% with SULT1A1. Compared to SULT1A1, SULT1A3 has a relatively low affinity for PNP, but a high affinity for catecholamines such as dopamine and epinephrine (Whittemore, Pearce et al. 1985; Heroux and Roth 1988; Weinshilboum, Otterness et al. 1997). SULT1A3 protein has been reported in all tissues expressing SULT1A1, but with different levels of protein expression between the isoforms (Whittemore, Pearce et al. 1985; Weinshilboum and Otterness 1994). No SNPs have been reported in the coding sequence of SULT1A3.

Mutational analysis of SULT1A1 and SULT1A3 have identified residue 146 as being critical to the substrate specificity of the two SULTs. The E146 in SULT1A3 is in the acceptor binding site of SULT1A3, and mutation to an alanine caused the active site to become more hydrophobic. This results in a change in substrate specificity from dopamine to more hydrophobic compounds like PNP. When the A146 of SULT1A1 was mutated to a glutamic acid, the A146E SULT1A1 mutant substrate specificity was similar to SULT1A3 (Dajani, Hood et al. 1998). The A146E SULT1A1 mutant had a more hydrophilic active site that preferentially bound compounds like dopamine over PNP. Another SULT1A member has been discovered recently, SULT1A4, and is located on chromosome 16. SULT1A4 has a 99% identity with SULT1A3 and appears to be the result of a recent gene duplication event (Hildebrandt, Salavaggione et al. 2004).

SULT1B1, the second SULT1 subfamily, was first isolated and characterized in rats in 1995 (Yamazoe, Nagata et al. 1994). In 1998, the human SULT1B1 gene was cloned by Wang et al. (Wang, Falany et al. 1998). The SULT1B1 gene is located on chromosome 4 (Wang, Falany et al. 1998). SULT1B1 protein has been reported in the colon, small intestine, and the liver (Wang, Falany et al. 1998). Substrates of SULT1B1 include the thyroid hormones: 3,3'-diiodothyronine (T2), triiodothyronine (T3), reverse triiodothyronine (rT3), and thyroxine (T4). Physiologically, the sulfation of thyroid hormones greatly enhances the irreversible deiodination reaction, making the sulfation of thyroid hormones an important inactivating pathway (Visser 1994). SULT1B1 sulfation activity was highest with T2, and was 2-fold lower for the active thyroid hormone T3 and 40-fold lower for the inactive prohormone T4 (Wang, Falany et al. 1998).

The SULT1C family is the third sub-family of the phenol SULTs. Like most other SULTs, the initial characterization was performed in rats (Gong, Ozawa et al. 1991). Early work with SULT1C1 in rats showed that expression was sex-related (Her, Kaur et al. 1997). However, the human homologue did not show any gender differences in expression. In addition to SULT1C1, humans have three other SULT1C family members, SULT1C2, SULT1C3, and SULT1C4. All SULT1C isoforms are located on chromosome 2 (Her, Kaur et al. 1997; Sakakibara, Yanagisawa et al. 1998). The SULT1C subfamily can all sulfate PNP and N-OH-2-acetylaminofluorene, while SULT1C2 has also been reported to sulfate estrone, bisphenol A, and diethylstilbestrol. SULT1C1 expression has been identified in the stomach, kidney, and thyroid in adults and the fetal liver and kidney (Her, Kaur et al. 1997). SULT1C2 expression has been reported in the fetal heart and adult kidney, ovary, and spinal cord (Sakakibara, Yanagisawa et al. 1998). A

genome search by Freimuth et al. revealed two more SULT1C members in humans, SULT1C3 and SULT1C4 (Freimuth, Wiepert et al. 2004). Expressed SULT1C3 has been reported to have no or very little activity for normal SULT1C substrates like PNP and α -naphthol but has been shown to sulfate large substrates like 1-hydroxymethylpyrene and 1'-hydroxysafrole (Meinl, Donath et al. 2008). SULT1C4 has been reported to sulfate catecholestrogens and methoxyestrogens (Hui, Yasuda et al. 2008). SULT1C3 and SULT1C4 have not been well characterized.

The fourth SULT1 subfamily is SULT1D. The SULT1D family was first reported in canines and has also been isolated from rodents (Tsoi, Falany et al. 2001; Teramoto, Sakakibara et al. 2008). In humans, the SULT1D1 homologue is a pseudogene located on chromosome 6. The human SULT1D1 gene contains an in frame stop codon, resulting in a premature truncation and a non-functional transcript (Meinl and Glatt 2001; Tsoi, Falany et al. 2001).

SULT1E1 is the only member of the fifth SULT1 subfamily, and is located on chromosome 4 close to the SULT1B1 gene (Aksoy, Wood et al. 1994; Falany, Krasnykh et al. 1995; Her, Szumlanski et al. 1996; Falany 1997; Zhang, Varlamova et al. 1998). Also called estrogen sulfotransferase (EST), SULT1E1 is unique among SULTs for its high affinity for estrogens. SULT1E1 is important in the metabolism of endogenous estrogens like E2 and estrone (E1) and some but not all exogenous estrogens such as 17 α -ethynyl estradiol (EE2). While most SULTs have K_m s in the low μ M range, SULT1E1 has a K_m for some (E1, E2, EE2) but not all estrogens (estriol) in the low nM range (4-10 nM). In humans, SULT1E1 has been identified in the liver, endometrium, jejunum, and mammary epithelial cells (Falany 1997). SULT1E1 expression has been found to be reg-

ulated in the endometrium by the menstrual cycle and pregnancy, with increased expression correlated with the increase of estrogen levels (Falany, Krasnykh et al. 1995). In addition to estrogens, SULT1E1 has also been shown to sulfate DHEA, pregnenolone and 1-naphthol; however these substrates generally have K_m s in the low μM range typical of phenolic substrates. SULT1E1 also shows potent substrate inhibition with E2. The K_m for estradiol is reported at 4 nM, with maximum activity observed at 20 nM; however, due to substrate inhibition the activity is only 20% of the maximum at 100 nM (Falany, Krasnykh et al. 1995).

SULT4A1 and SULT6A1 are the only members of their respective families. Little is known about these two families in humans or any other species. SULT4A1 is highly expressed in the brain, and the gene is located on chromosome 22. The region on chromosome 22 where SULT4A1 is located has a reported association with schizophrenia (Condra, Neiberger et al. 2007). SULT4A1 is highly conserved with an 89% identical amino acid sequence from humans to zebra fish (Condra, Neiberger et al. 2007). No sulfation activity for SULT4A1 has been reported. Recent SULT4A1 crystal structure shows that the active site is very small compared to all other SULTs, and it is not clear whether PAPS can even bind to SULT4A1. In addition, the active site is surrounded by a large hydrophobic surface, which suggests that the SULT4A1 active site may have a binding partner that is critical for activity. However, this hypothesis remains unproven (Allali-Hassani, Pan et al. 2007). Similar to SULT4A1, SULT6A1 also has no known substrate. SULT6A1 expression has been reported in the testis in humans (Freimuth, Wiepert et al. 2004). In chickens, SULT6A1 has also been isolated and the chicken SULT6A1 has a 56% identical amino acid sequence with humans. Expressed chicken

SULT6A1 showed sulfation activity with E2, but no activity has been reported with human SULT6A1 (Wilson, Reyns et al. 2004).

IV. HYDROXYSTERIOD SULFOTRANSFERASE (SULT2) FAMILY

The SULT2 family catalyzes the sulfation of primary and secondary aliphatic hydroxyl groups, with a preference for secondary hydroxyls. Substrates of the SULT2 family include bile acids, DHEA, oxysterols, and pregnenolone (Aksoy, Otterness et al. 1993; Wood, Her et al. 1996; Her, Wood et al. 1998). While the SULT2 family has a significant role in drug metabolism, the SULT2 family also has an important role in steroid and bile acid sulfation. In humans, there are two SULT2 genes with three proteins named SULT2A1, SULT2B1a, and SULT2B1b. Both SULT2 genes are located on chromosome 19 and separated by 500 kb (Otterness and Weinshilboum 1994; Her, Wood et al. 1998).

Sulfation of bile acids is a significant pathway of bile acid metabolism in rats but is a secondary pathway in humans and mice (Takahashi, Tanida et al. 1990). In humans, bile acid sulfation is important in the detoxification of bile acids during cholestasis (De Witt and Lack 1980). Cholesterol is converted to cholic and chenodeoxycholic acids by the liver and is conjugated to glycine or taurine before excreted from the liver. Gut bacteria can convert primary bile acids to the secondary bile acids deoxycholic and lithocholic acid (Hoffman 1988). During cholestasis, the accumulation of the bile acids can result in severe liver toxicity especially by lipophilic secondary bile acids. Sulfation of the bile acids inhibits the re-absorption of the bile acids preventing the accumulation of toxic bile acids levels in the enterohepatic circulation (De Witt and Lack 1980).

Although detoxification is an important function of steroid metabolism, it is not the sole function of steroid metabolism. Sulfated steroids can serve as a mechanism of transportation in the plasma and a reservoir for rapid activation of the prohormone in the peripheral tissues. Sulfated steroids cannot bind to their respective receptors, at least in peripheral tissues and are able to circulate in the blood stream at much higher concentration than the unsulfated steroid. The sulfated steroids can bind to proteins such as albumin, and as well as be readily reabsorbed by the kidney back into the blood, which results in a long half-life in the serum. The active hormones can be regenerated in the peripheral tissues by sulfatase activity (Pion, Conrad et al. 1966; Parker 1999).

The SULT2B1 gene is located on chromosome 19 and was cloned in 1998 by Her et al (Her, Wood et al. 1998) and encodes two proteins, SULT2B1a and SULT2B1b. The proteins are generated by alternative exon splicing of the SULT2B1 gene that result in different transcription start sites. SULT2B1a shares a 94% identical aa sequence with SULT2B1b, the only difference between SULT2B1a and SULT2B1b is in the amino terminal peptide due to the unique start sites for the proteins. The mRNA of SULT2B1a has been identified in placenta, prostate, skin, colon, kidney, and ovary (Meloche and Falany 2001; Falany, He et al. 2006). Despite the presence of mRNA in a wide range of tissues, no SULT2B1a protein has been identified in any tissue. SULT2B1b protein expression has been reported in a wide range of tissues including the brain, skin, prostate, uterus, placenta, and lung (Meloche and Falany 2001; Falany, He et al. 2006). The substrate specificity of SULT2B1b is much narrower than that of other SULTs, sulfating cholesterol, oxysterols, DHEA, and pregnenolone (Meloche and Falany 2001). Structurally, SULT2B1b differs from the classic SULT structure because of the presence of the

aa extensions at the amino and carboxyl terminals. The aa extensions have no homology to any other SULTs (Lee, Fuda et al. 2003). The role of the amino terminal extension is not known; however, the carboxyl terminal extension has been shown to be important in nuclear localization of SULT2B1b, in some tissues (He and Falany 2006). SULT2B1b is the only SULT to demonstrate nuclear localization (Falany, He et al. 2006). Phosphorylation of S348 in the carboxyl terminal extension has been shown to be important for nuclear localization of SULT2B1b, and recent unpublished results show that this phosphorylation is important in the stability of the SULT2B1b. In addition to phosphorylation, expression of SULT2B1b with a 6 His tag at the amino terminal greatly enhances enzyme stability (Meloche and Falany 2001). While SULT2B1b has been crystallized, the unique amino and carboxy peptide extensions were not resolved in the crystal structures. The probable reason for why the aa extensions did not crystallize is that they are unstructured and highly flexible. The structural interactions and properties of the aa extensions of SULT2B1b remain unknown (Lee, Fuda et al. 2003).

V. SULT2A1

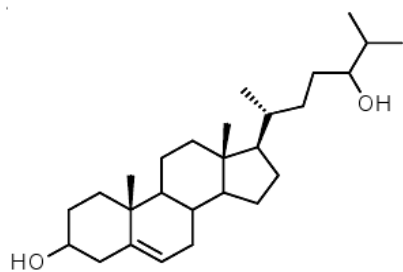
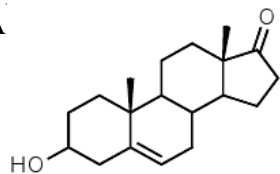
The focus of this dissertation is the first member of the SULT2 family to be identified, SULT2A1. SULT2A1 was first isolated from human liver in 1989 by Falany et al. (Falany, Vazquez et al. 1989). Expression of SULT2A1 has been identified in the liver (Falany 1991), adrenals (Comer, Falany et al. 1993; Falany 1997) stomach, and GI tract (Otterness and Weinshilboum 1994). The cDNA for SULT2A1 was cloned by Otterness et al. (Otterness, Wieben et al. 1992) in 1992 and the SULT2A1 gene was described in 1995 described by Otterness et al. (Otterness and Weinshilboum 1994). The SULT2A1

gene is comprised of 6 exons and is located on chromosome 19, 500 kb from the SULT2B1 gene. The cDNA is 855 nucleotides in length and the SULT2A1 protein is 285 aa long. An important physiological substrate for SULT2A1 is DHEA (Fig. 3), but SULT2A1 has also been reported to sulfate estrogens, hydroxysteroids, testosterone, and cholesterol (Aksoy, Otterness et al. 1993; Park, Lee et al. 1999). SULT2A1 can sulfate both alpha and beta hydroxyls and has been shown to sulfate some aliphatic hydroxyls (Falany 1997; Cook, Duniac-Dmuchowski et al. 2009). The maximum activity for SULT2A1 DHEA sulfation is observed at 3-4 μ M DHEA. At higher concentrations of DHEA, substrate inhibition decreases the total activity (Falany, Vazquez et al. 1989; Comer, Falany et al. 1993).

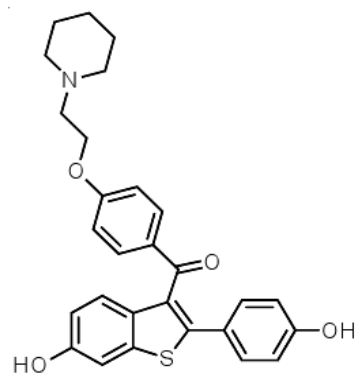
A) Adrenal Production and Secretion of DHEA-Sulfate

DHEA sulfation by SULT2A1 in the adrenals is an important physiological function for SULT2A1. The adrenal glands are a pair of endocrine organs adjacent to the kidneys that are divided into two regions, the medulla and the cortex. The medulla region is made of secretory cells and vesicles which are filled with epinephrine and norepinephrine. The release and regulation of these cells is by the sympathetic nervous system (Miller and Tyrrell 1995). The adrenal cortex is composed of three different regions. The zona glomerulosa is the outer layer and regulates the secretion of the mineralocorticoid, aldosterone that regulates blood pressure and volume. The next region is the zona fasciculata, which secretes glucocorticoids and is involved with regulating glucose metabolism. The last region is the zona reticularis; this is the region responsible for the secretion of androgens, the major one being DHEA-sulfate (DHEAS), and the region of

DHEA



24(S)-OH-Chol



Raloxifene

Figure 3. Chemical structures of DHEA, Raloxifene (RAL), and 24(S)-OH-Chol

SULT2A1 expression in the adrenal glands (Hadley 1992; Comer, Falany et al. 1993; Miller and Tyrrell 1995).

DHEAS is one of the major secretory products of the adrenal, with plasma concentrations reported to be in the low μM range in young adults (Elmlinger, Kühnel et al. 2002). DHEA is an important precursor for the synthesis of other androgens (Fig 4) and DHEAS acts as a reserve of androgens in the body that may be readily converted in the peripheral tissues to androgens and estrogens (Labrie 1991). The large reservoir of pro-hormone is the main source of estrogen in the peripheral tissue of post-menopausal women. In adult men, DHEAS is the circulating prohormone responsible for 30-50% of androgen synthesis (Labrie 1991).

The highest level of DHEAS secretion from the adrenal is just before birth. The fetal adrenal cortex of humans and higher primates is disproportionately enlarged and secretes 100-200 mg/day of DHEAS (Elmlinger, Kühnel et al. 2002). The fetal secretion of DHEAS is the major precursor for the formation of E2 and estriol in the placenta (Bocuzzi and Brignardello 1996). When the fetal adrenal cortex involutes after birth the levels of DHEAS secretion declines dramatically and remains low for the first several years of childhood. DHEAS secretion increases again during adrenarche, at the age of 5-6 years (Parker 1999). The secretion of DHEAS remains elevated till about 20 years of age, when a significant decline in DHEAS secretion occurs (Migeon, Keller et al. 1957; Labrie, Bélanger et al. 1998). In elderly individuals (over 65), the levels of DHEAS are only 10-20% of the levels during young adulthood (Labrie, Bélanger et al. 1998; Parker 1999). The cause for the age related change is reported to be a decrease in size ratio of

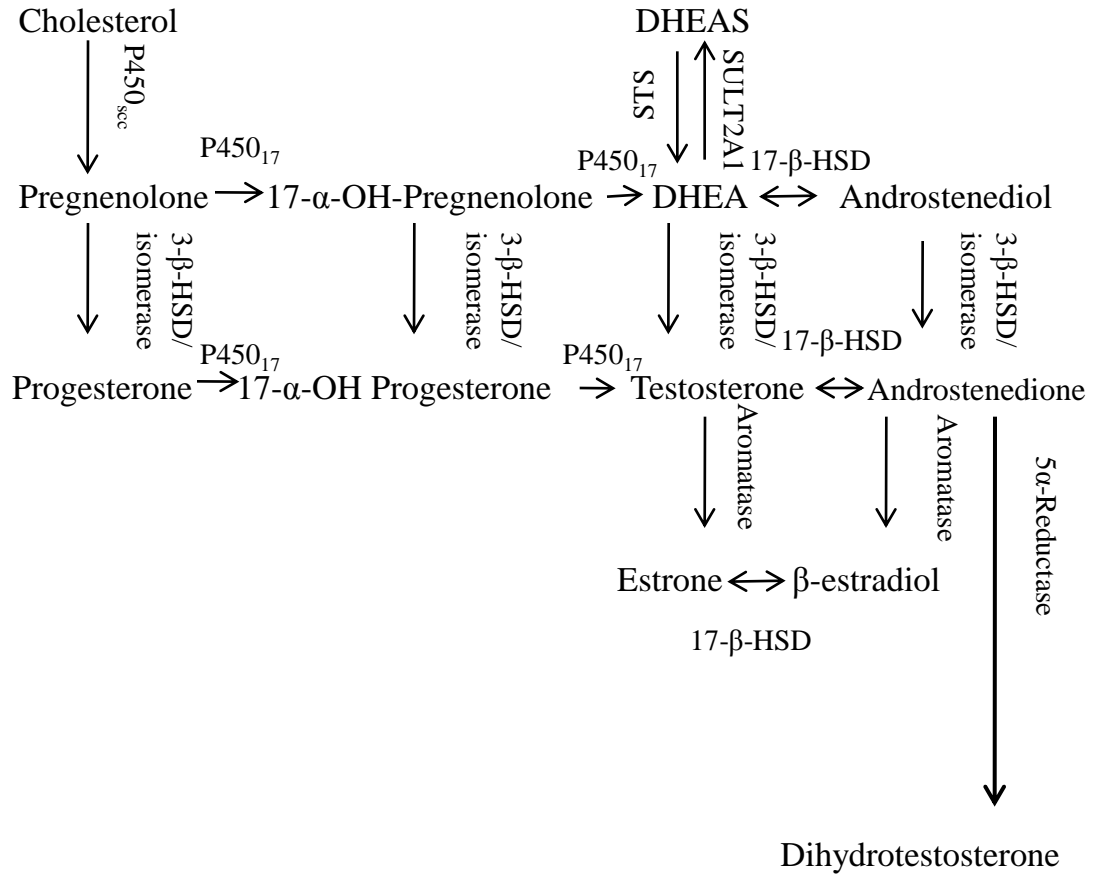


Figure 4. Pathway for biosynthesis of androgenic/estrogenic steroid hormones. DHEA is an important intermediate in the formation of androgenic and estrogenic hormones.

the zona reticularis relative to the other two regions of the adrenal cortex (Parker 1999). The effects of the age related decrease in DHEAS and DHEA production is not known.

B) SULT2A1 Drug and Oxysterol Metabolism

In addition to the DHEA, SULT2A1 is also a major drug metabolizing SULT with a high level of expression in the liver and is reported to sulfate a variety of xenobiotics and endogenous compounds (Meloche, Sharma et al. 2002; Falany, Pilloff et al. 2006; Ren, Li et al. 2007). One group of substrates for SULT2A1 is a class of cholesterol metabolites called oxysterols. The oxysterols are made by the hydroxylation of cholesterol by the CYPs and many oxysterols have been reported to be endogenous Liver-X-Receptor (LXR) activators (Lehmann, Kliewer et al. 1997). LXR is an important nuclear receptor that regulates cholesterol and lipid homeostasis (Peet, Turley et al. 1998). A major physiological oxysterol is 24(S)-hydroxycholesterol (24(S)-OH-Chol) (Fig 3) (Björkhem, Lütjohann et al. 1997). Synthesized in the brain by CYP46 (Vega and Weiner 2007), 24(S)-OH-Chol is involved in the regulation of the cholesterol levels in the brain (Björkhem, Lütjohann et al. 1997). The brain contains over 25% of total body cholesterol, and the level of cholesterol in the brain must be highly regulated to maintain healthy neural activity (Björkhem, Lütjohann et al. 1997; Björkhem and Meaney 2004). 24(S)-OH-Chol is also an endogenous LXR agonist (Peet, Turley et al. 1998). Sulfation of 24(S)-OH-Chol has been reported to be a major pathway of metabolism *in vivo* (Meng, Griffiths et al. 1997). In addition, the sulfation of 24(S)-OH-Chol has been shown to change 24(S)-OH-Chol from an LXR agonist to an LXR antagonist (Cook, Duniac-Dmuchowski et al. 2009).

SULT2A1 can also sulfate raloxifene (RAL), a selective estrogen receptor modulator (SERM) (Falany, Pilloff et al. 2006) (Fig 3). The clinical use of RAL is in the prevention of breast cancer in women at high risk, and the prevention of osteoporosis (Snyder, Sparano et al. 2000). RAL is sulfated by all of the major SULTs to some degree and can also be di-sulfated by SULT1E1. In SULT1E1, di-sulfate formation is preferred at low concentrations of RAL. The three most active SULTs *in vitro* for RAL sulfation are SULT1E1, SULT2A1 and SULT1A1 (Falany, Pilloff et al. 2006). Despite RAL sulfation observed *in vitro*, no RAL sulfates have been detected *in vivo* (Jeong, Liu et al. 2005).

VI. GENERAL SULT STRUCTRE

The SULTs show significant sequence and structural homology. Sequence alignment of the SULTs shows a highly conserved PAPS binding domain, active site histidine and KXXXTVXXXE (KTVE) dimerization domain (Fig 5) (Petrotchenko, Pedersen et al. 2001). Nearly all characterized SULTs have been reported to be homodimers (Allali-Hassani, Pan et al. 2007), with the one exception being mouse SULT1E1 which has been reported to be a monomer (Petrotchenko, Pedersen et al. 2001; Stjernschantz, Reinen et al. 2010). There has been a single report of a heterodimer formation in the SULTs, between SULT1A1 and SULT1A3 in an *in vitro* system by over expressing the two enzymes (Kiehlbauch, Lam et al. 1995). However, heterodimers have not been reported *in vivo* despite many years of isolating SULTs from tissues. The lack of heterodimers is inconsistent to the highly conserved dimerization domain proposed for

PAPS

```

2A1  1  MSDDLWFEGIAFPTMGFRSETLRKVRDEFVIRDEDVILTYPKSG 46
1E1  1  MNSELDY-YEKFEVHVGILMYKDFVKYWDNVEAFQARPDDLVIATYPKSG 49
1A1  1  MELIQDTSRPPLEYVKGVPLIKYFAEALGPLQSFQARPDDLLTYPKSG 50

2A1  47 TNWLAEILCLMHSGDAKWIQSVPIWERSPWVES-----EIGYTALSETE 91
1E1  50 TTWVSEIVYMIYKEGDVEKCKEDVIFNRIPFLECRKENLMNGVKQLDEMN 99
1A1  51 TTWVSQILDMIYQGGDLEKCHRAPIFMRVPFLEFKAPGIPSGMETLKDTP 100

Active Site

2A1  92 SPRLFKSHLPIQLFPKSFFSSKAKVIYLMRNPRDVLVSGYFFWKNMKFIK 141
1E1 100 SPRIVKTHLPPELLPASFWEKDCKIIYLCRNAKDVAVSFYYFFLMVAGHP 149
1A1 101 APRLLKTHLPLALLPQTLLDQKVVVYVARNAKDVAVSYHFYHMAKVHP 150

2A1 142 KPKSWEEYFEWFCQGTVLYGSWFDHIHGWMPMREEKNFLLLSYEELKQDT 191
1E1 150 NPGSFPEFVEKFMQGQVPYGSWYKHVKSWWEKGKSPRVLFLFYEDLKEDI 199
1A1 151 EPGTWDSFLEKFMVGEVSYGSWYQHVQEWWELSRTHPVLYLFYEDMKENP 200

Loop 3

2A1 192 GRTIEKICQFLGKTLEPEELNLILKNSSFQSMKENKMSNYSLLSVDYVVD 241
1E1 200 RKEVIKLIHFLERKPSEELVDRIIHHTSFQEMKNNPSTNYTTLPDEIMNQ 249
1A1 201 KREIQKILEFVGRSLPEETVDFMVQHTSFKEMKKNPMTNYTTVPQEFMDH 250

KTVE

2A1 242 KAQ-LLRKGVSGDWKNHFTVAQAEDFDKLFQEKMADLPRELFPWE 285
1E1 250 KLSPFMRKGITGDWKNHFTVALNEKFDKHYEQQMKESTLKFRTEI 294
1A1 251 SISPFMRKGMAGDWKTTFTVAQNERFDADYAEKMAGCSLSFRSEL 295

```

Figure 5. Sequence alignment of three major SULTs involved in drug and hormone metabolism. Sequence alignment of SULT2A1, SULT1A1 and SULT1E1 was generated using the McVector program. The residues of the PAPS binding domain (green), the active site histidine and lysine (pink), and KTVE dimerization domain (blue) are highlighted. Loop 3 of SULT2A1 is highlighted in red.

the SULT family (Petrotchenko, Pedersen et al. 2001), indicating some level of selection of dimerization that is not well understood.

The structural and kinetic importance of the SULT homodimer has not been well characterized. A recent publication by Sun and Leyh, indicates that the dimerization in SULT1E1 results in half-site reactivity, and dimerization enhances the internal equilibrium of the enzyme (Sun and Leyh 2010). Alternatively, the dimerization of the SULTs may be important for enzyme stability (Lu, Chiang et al. 2009). The lack of substrate inhibition in mouse SULT1E1 suggests that the dimerization of the enzyme may be important for substrate inhibition (Stjernschantz, Reinen et al. 2010). How dimerization of the SULTs influence structure and function is still unknown.

Substrate inhibition is a common characteristic of the SULTs and is the decrease in activity with increasing concentrations of substrate (Anderson, Weinshilboum et al. 1981; Falany, Vazquez et al. 1989; Zhang, Varlamova et al. 1998; Tyapochkin, Cook et al. 2009). Many SULTs show substrate inhibition for some, but not all of their substrates, and the level of substrate inhibition varies between substrates and SULTs. In the case of SULT2A1 and DHEA, maximum activity is at 3 μ M DHEA and then the activity comes down to 66% of the total activity at 20 μ M DHEA (Fig 6) (Falany, Vazquez et al. 1989). In addition to DHEA sulfation with SULT2A1, substrate inhibition is also observed with E2 and SULT1E1 (Zhang, Varlamova et al. 1998) as well as PNP and SULT1A1 (Anderson, Weinshilboum et al. 1981). The mechanism of substrate inhibition is not known. Theories for the mechanism of substrate inhibition include the formation of a dead end complex with the SULT*PAP complex (Sun and Leyh 2010), allosteric binding of the substrate to the enzyme at a second binding site (Zhang, Varlamova et al.

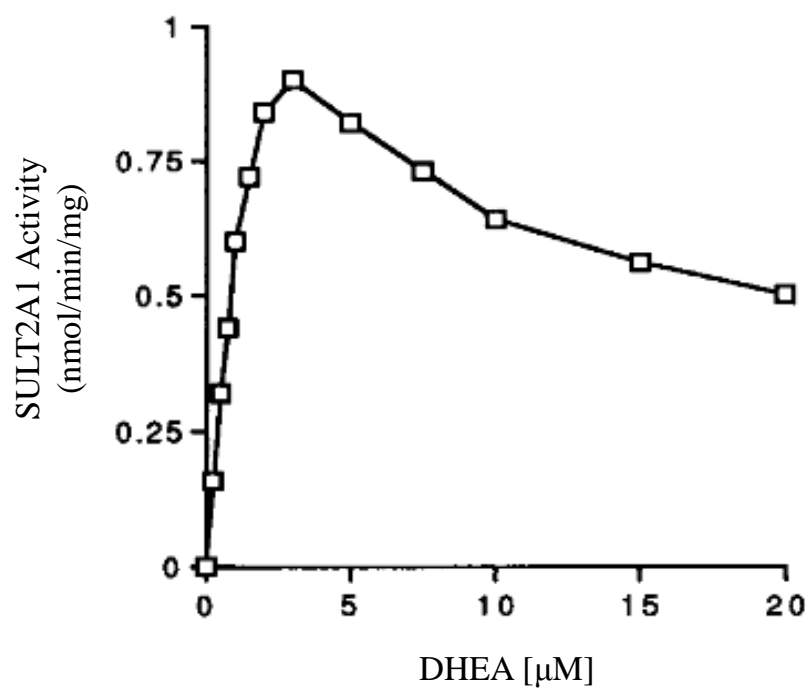


Figure 6. DHEA concentration dependent sulfation activity by SULT2A1. DHEA sulfation activity was assayed using SULT2A1 with [^3H]-DHEA in a chloroform extraction

1998), the binding of two substrates in the active site (Gamage, Duggleby et al. 2003), enzyme gating of the active site (Lu, Hsieh et al. 2008) and alternative binding orientations of the substrate (Rehse, Zhou et al. 2002; Lu, Hsieh et al. 2008). The dead end substrate complex formation is the most accepted theory and is supported by several studies showing substrates able to bind to the PAP*SULT complex using fluorescence and isotope exchange (Tyapochkin, Cook et al. 2009; Gulcan and Duffel 2011). Intrinsic fluorescence of SULT1E1 with E2 has indicated that two E2 molecules can bind to each subunit (Zhang, Varlamova et al. 1998) and crystallization of PNP in SULT1A1 resolved two PNP molecules in active site, supporting the multiple substrate binding or allosteric binding hypothesis (Gamage, Duggleby et al. 2003). Lin et al. have reported that two residues, Tyr240 and Met137 regulate gating of the active site, and the gating is a molecular mechanism for substrate inhibition (Lu, Hsieh et al. 2008). The SULT2A1 crystal structure (1J99) resolved two binding orientations of DHEA, with electron density indicating only a single molecule binding per monomer (Rehse, Zhou et al. 2002). The SULT2A1 crystal structure with bound DHEA suggests that substrate inhibition is caused by alternative binding angles of DHEA in the active site of SULT2A1.

The reaction mechanism for the SULTs has remained unclear despite several decades of research. An early study by Barnes et al. (Barnes, Waldrop et al. 1986) indicated that bile acid sulfation by SULT2A1 is an ordered reaction mechanism with the bile acid as the leading substrate in rhesus monkeys. However, Duffel et al. (Duffel and Jakoby 1981) and Zhang et al. (Zhang, Varlamova et al. 1998) have reported that the reaction mechanism is a random Bi-Bi reaction mechanism for human SULT1A1 sulfation of β -naphthol and human SULT1E1 sulfation of E2, respectively. Tyapochkin et al. have re-

ported that the reaction mechanism is an ordered reaction mechanism with PAPS binding first; however, this was based on the kinetics of the reverse reaction for human SULT1A1 (Tyapochkin, Cook et al. 2008; Tyapochkin, Cook et al. 2009). The different reaction mechanisms reported in the literature suggest that the reaction mechanism in the SULTs may be substrate dependent.

A) SULT2A1 Crystal Structure

There are currently 33 SULT crystal structures available in the Protein Data Bank. The first crystal structure reported was mouse SULT1E1 resolved with bound PAP and E2 (Kakuta, Pedersen et al. 1997). All of the SULTs show significant conservation in their basic structure with a central four stranded β -sheet surrounded by twelve α -helices and 2-3 loops that are usually disordered in the absence of bound PAP or substrate. The β -sheets, α -helices and loops are numbered from the N-terminal to the C-terminal, so that loop 1 is the first loop from the N-terminal. Despite the significant molecular evidence for a conserved SULT dimerization domain (Petrotchenko, Pedersen et al. 2001), only SULT1A1 and SULT1E1 have formed crystal dimers with the KTVE domain. Most SULTs form monomers in the crystal structures; however, several of the SULTs including human SULT1B1, SULT1C2, SULT4A1, and SULT2A1 have formed dimers using different interfaces other than the predicted KTVE dimerization domain. However, *in vitro* experiments using site directed mutagenesis and chemical cross linking have not identified any other region of dimerization. Allali-Hassani et al. recently published a review of all the SULT crystal structures that showed a significant difference between

SULT2A1 without PAP and SULT2A1 with PAP in the loop 3 region, but did not examine the kinetic implications of the observation (Allali-Hassani, Pan et al. 2007).

Several SULT2A1 crystal structures have become available in the last 10 years. The first SULT2A1 crystal structure was generated with bound PAP by Pedersen et al. (Pedersen, Petrotchenko et al. 2000). While the resolved crystal structure was a dimer, the interface was not at the KTVE site, but over the substrate binding site. Later monomer crystal structures of SULT2A1 were generated, with bound DHEA (Rehse, Zhou et al. 2002; Lu, Hsieh et al. 2008) and bound androsterone (Chang, Shi et al. 2004). The core of the crystal structures showed less than a 1.5 Å (RMSD) (Allali-Hassani, Pan et al. 2007). The exception was loop 3, which spans the region from aa 230 through 258 (Fig 7). In the structures without PAP, the region is often poorly defined and extends away from the core of the enzyme. When PAP binds, the crystal structure indicates that loop 3 was better resolved and moves closer to the core of the enzyme (Allali-Hassani, Pan et al. 2007). The structure with PAP was examined and a strong electrostatic interaction with the 3'phosphate and the R247 was observed (Fig 8) (Pedersen, Petrotchenko et al. 2000). As SULT2A1 is the only SULT to be crystallized without PAP(S) to a high resolution, data on the possible interactions of PAPS binding in other SULTs was not available. High resolution crystal structures with PAP(S) are available for all of the major SULTs, and all show an electrostatic interaction with the conserved Arg and the 3' phosphate of PAPS. (Allali-Hassani, Pan et al. 2007).

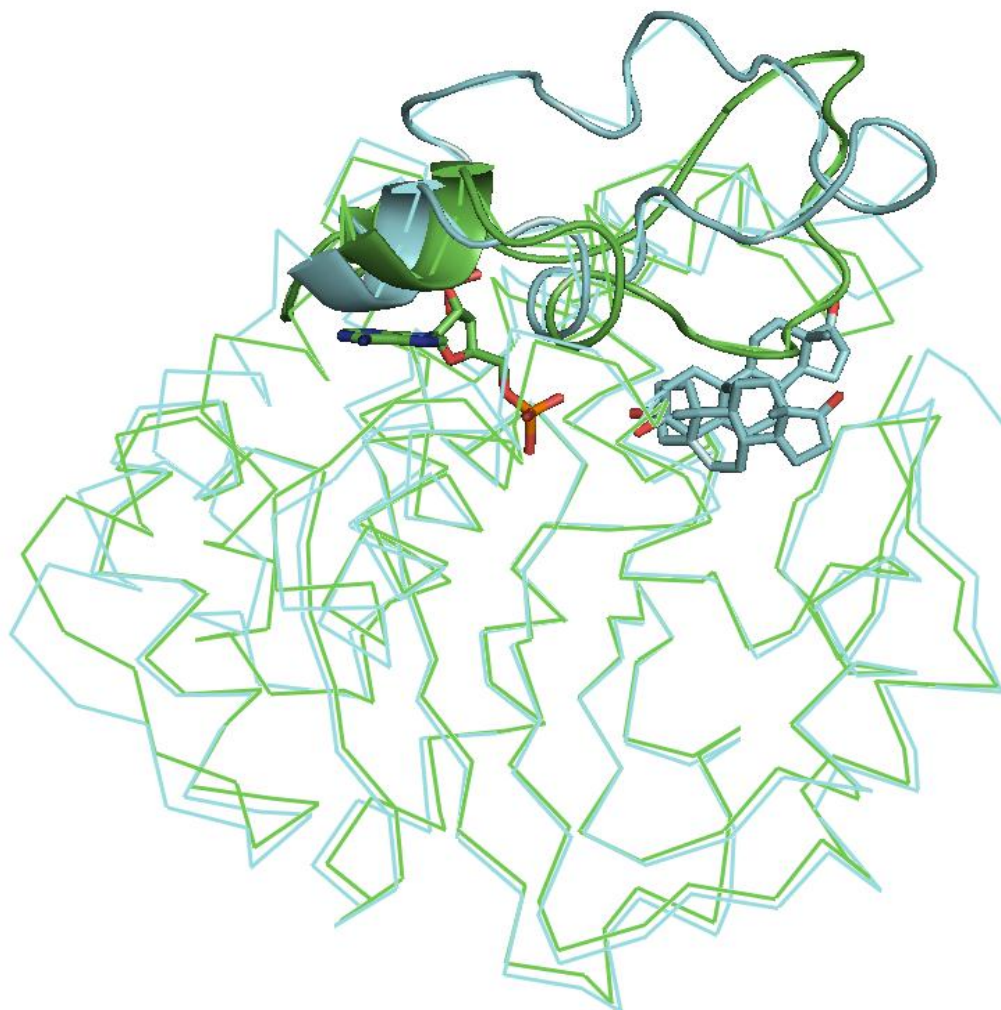


Figure 7. The dynamics of loop 3 in SULT2A1 crystal structures. The crystal structures of SULT2A1 were downloaded from the RCSB protein structure data bank. The backbone of each crystal structure is shown in ribbon format with the loop 3 region highlighted in cartoon. The SULT2A1 crystals structures were generated with bound PAP (1EFH) or DHEA (1J99). The 1EFH is shown green and 1J99 is shown in cyan.

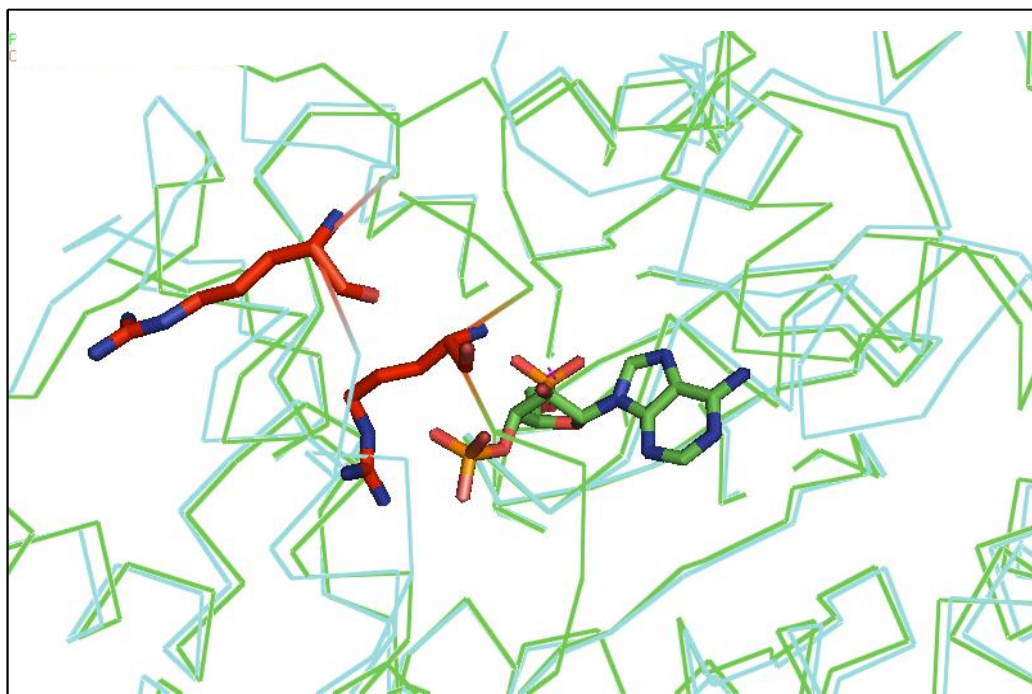


Figure 8. Proposed mechanism for the shift of loop 3 in SULT2A1. The crystal structures of SULT2A1 were made with bound PAP (1EFH-green) or DHEA (1J99-cyan). The backbone of SULT2A1 in each crystal structure is shown in ribbon. In stick is the PAP molecule in the 1EFH crystal structure. The R247 of SULT2A1 is highlighted in red.

VII. RATIONALE AND OBJECTIVE

The hydroxysteroid SULTs are an important family of the SULTs, and SULT2A1 is an important member for drug and xenobiotic metabolism and endogenous steroid metabolism. SULT2A1 is the primary enzyme involved in DHEA sulfation and along with SULT1A1, is an important isoform in the liver for drug metabolism. The crystal structures of SULT2A1 suggest that the binding of PAPS can alter the substrate specificity of the enzyme. While there were some preliminary data suggesting some change in the affinity of substrates with PAPS binding, there was no kinetic study to show how these structural changes impact sulfation. This thesis is focused on describing the structural rearrangement induced by PAPS and substrate binding and the impact on the kinetics.

A) Aim 1

The first aim of this study was to examine the structural interactions of PAPS binding to human SULT2A1 in the monomer subunit. Crystal structures present strong evidence that the binding of PAPS causes a significant structural rearrangement at the acceptor substrate binding site. The objective of this study was to demonstrate how the binding of PAPS changes the kinetics of SULT2A1. This was accomplished by examining the SULT2A1 substrates 24(S)-OH-Chol, DHEA, and RAL.

B) Aim 2

The second aim of this study was to examine the intermolecular interactions across the homodimer (Fig 9). While the KTVE domain is the highly conserved dimerization domain, evidence indicates that the dimerization domain may also be involved in

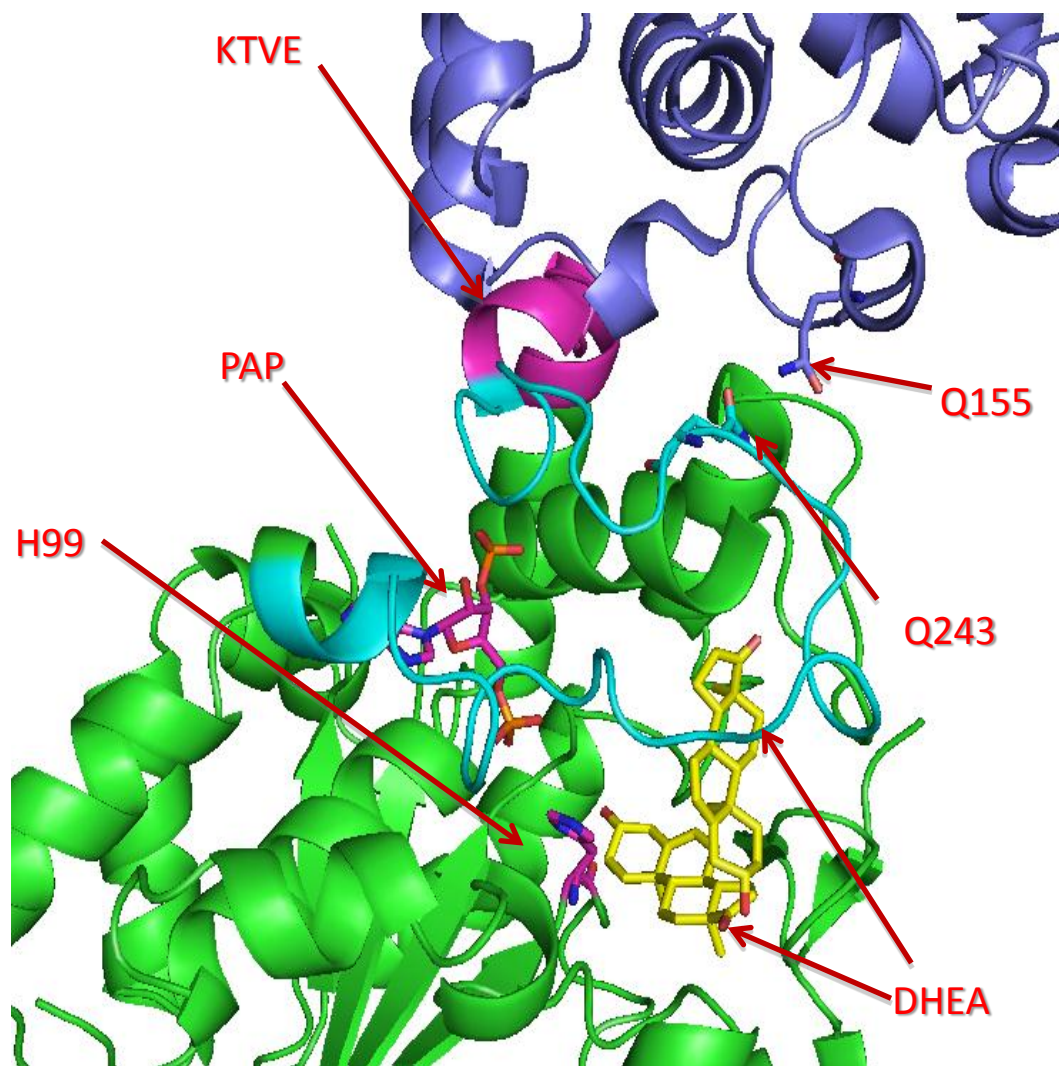


Figure 9. Hypothesized dimerization of SULT2A1 at the KTVE domain. The SULT2A1 homodimer was made by aligning the SULT2A1 subunits at the KTVE dimerization domain. The subunits were generated from the SULT2A1 crystal structure made with DHEA (1J99). The position and orientation of DHEA (yellow) and PAP (violet) are based on the crystal structures of SULT2A1. The lower subunit is green and the upper subunit is blue with the dimer interface in purple. In the lower subunit, loop 3 region is colored cyan and the active site H99 is highlighted in stick. The Q155 of the upper subunit and Q243 of the lower subunit are shown in stick and are close enough to form a hydrogen bond.

improving enzyme stability, substrate inhibition, and half-site reactivity. The objective of this aim was to identify the mechanism of this interaction and determine how dimerization regulates the kinetics of SULT2A1.

C) Aim 3

The final aim of this dissertation was to examine of the molecular rearrangements induced by PAPS in other members of the SULT family. In particular, this objective focused on SULT1A1 and SULT1E1 because of the unique features of these two SULTs. SULT1A1 is considered the most important SULT in drug metabolism due to the large range of substrates and high expression in the liver and peripheral tissues. SULT1E1 has a very high affinity for estrogens and 1000-fold lower affinity for other substrates. The reason for this large difference in affinity has not been determined. The objective of this study was to determine whether the molecular rearrangement induced by PAPS binding is a general characteristic of the SULT family.

METHODS

I. THE STRUCTURAL REARRANGEMENTS ASSOCIATED WITH PAPS BINDING IN THE SULT2A1 SUBUNIT

A) Materials

[1,2,6,7-³H]-DHEA (60 Ci/mmol), [1,2,6,7-³H] DHEAS (60.0 Ci/mmol), and [³⁵S]-PAPS (2.2 Ci/mmol) were purchased from Perkin Elmer (Waltham, MA). PAPS was purchased from Dr. Sanford Singer at the University of Dayton (Dayton, OH). DHEA, emodin, digitoxin, and RAL were purchased from Sigma Chemical (St Louis, MO). Silica gel thin-layer chromatography (TLC) plates (250 mm) were obtained from Whatman Inc. (Clifton, NJ). Con A-Sepharose and DEAE-Sepharose Cl-6B were from GE Healthcare (Pittsburgh, PA). The pMAL-c2 vector, amylose resin, and Factor Xa were purchased from New England Biolabs (Ipswich, MA). The 24(S)-OH-Chol was purchased from BioMol (Plymouth Meeting, PA). 3-CTP was purchased from Key Organics (Camelford, Cornwall, UK). QuikChange™ Site-Directed Mutagenesis Kit was purchased from Stratagene (La Jolla, California). Advantage Taq polymerase was purchased from BD Bioscience (Franklin Lakes, NJ). The Molecular Operating Environment (MOE) license was purchased from Chemical Computing Group (Montreal, Quebec, Canada). All other reagents are reagent grade and purchased from Fisher Scientific (Norcross, GA).

B) DHEA Sulfation Activity Assay

DHEA sulfation activity was assayed by a chloroform extraction method described previously (Falany, Vazquez et al. 1989; Comer, Falany et al. 1993; Cook, Leyh et al. 2010). Reactions were performed in 10 mM sodium phosphate (pH 7.4) and 5 mM MgCl₂. The concentration of DHEA was 3 μM and [³H]-DHEA was added for a specific activity of 200 dpm pmol⁻¹ in a volume of 87.5 μL. SULT2A1 was added to each reaction in a volume of 25 μL. Each reaction was initiated with the addition of 12.5 μL of PAPS for a concentration of 20 μM in a volume of 125 μL. Reactions were typically incubated for 5 min at 37°C, and stopped with the addition of 375 μL of stop buffer (50 mM Tris, pH 8.8) and 3 mL of chloroform, then mixed by vortexing. Reactions were centrifuged at 600 X g for 5 min to separate the phases. [³H]-DHEAS was measured in 200 μL of the aqueous phase by scintillation spectroscopy with a Beckman LS 6500 scintillation spectrometer.

C) SULT2A1 Purification

1. *Partial Purification of SULT2A1 following expression using SULT2A1-pKK233-2 Vector in E. coli*

SULT2A1 has been previously cloned into the pKK233-2 vector and transfected into *E. coli* DH5-α to generate SULT2A1-pKK expressing bacteria (Comer, Falany et al. 1993; Falany, Wheeler et al. 1994). A volume of 20 mL SULT2A1-pKK *E. coli* cells were grown in Luria broth (LB) with 100 μg mL⁻¹ of ampicillin for 12-16 h at 37°C. The 20 mL was added to 500 mL of LB with 100 μg mL⁻¹ of ampicillin. Cells were grown to an OD₆₀₀ of 0.4-0.6, then induced with a concentration 0.3 mM isopropyl β-D-

1-thiogalactopyranoside (IPTG) and incubated for 2 h. Cells were centrifuged at 2,800 X g for 15 min to pellet the cells. The supernatant fraction was discarded and cells were frozen at -80°C. After the cells were frozen, 65 mL of DEAE-sepharose Cl-6B resin (in 20% ethanol) was poured into a column for a final bed volume of 50 mL. The ethanol was removed and the column was equilibrated in DEAE column buffer. Cells were thawed on ice and re-suspended in 5 mL of DEAE column buffer (10 mM sodium phosphate, pH 7.4, 1 mM DTT, 10% glycerol, 5 mM EDTA) gram⁻¹ of wet cell weight. Lysozyme was added to a concentration of 1.0 µg mL⁻¹, and samples were incubated on ice for 30 min. The solution was then sonicated for 10 sec and then incubated for 10 sec on ice. The sonication was repeated 12 times. Lysis was monitored by release of protein detected using the BioRad protein detection assay. The lysate was then centrifuged for 1 h at 100,000 X g. The supernatant fraction (cytosol) was saved in a 50 mL conical tube. The cytosol was loaded onto the DEAE column at a flow rate of 1.0 ml min⁻¹, and the column was washed with 50 mL of DEAE buffer, followed by a similar wash with DEAE buffer containing 50 mM NaCl. SULT2A1 activity was eluted from the column using a gradient of 50 mM to 250 mM NaCl in DEAE column buffer and collected in 3 mL fractions. SULT2A1 was detected by DHEA sulfation activity, described in section I-B. The concentration of SULT2A1 was determined by immunoblot analysis with pure enzyme for standardization and purity of the SULT2A1 pool was determined by SDS-page electrophoresis with 10% polyacrylamide gel and staining with Coomassie brilliant blue.

2. Purification of SULT2A1 from SULT2A1-pMAL-c2 Vector in *E. coli*

SULT2A1 was cloned into the pMAL-c2 vector as described previously (Cook, Leyh et al. 2010). The SULT2A1 cDNA (Comer, Falany et al. 1993) was inserted into the pMAL-c2 vector (Fig 10) using the DNA restriction enzymes XmnI and HindIII (Falany 1997). The vector was transfected into Z-competent *E. coli* XL1-blue cells. Cytosol was generated as described in section I-C-1. A 15 mL amylose column was equilibrated in DEAE column buffer. The cytosol was loaded onto the amylose column at a flow rate of 0.5 mL min⁻¹ at 4°C. The column was washed with 45 mL DEAE column buffer. SULT2A1 activity was eluted with 30 mL of 10 mM maltose in DEAE buffer. Fractions were assayed for DHEA sulfation activity as described in section I-B. The activity and purity of the MBP-SULT2A1 by SULT2A1 activity and SDS-PAGE as described in section I-C-1.

To generate WT SULT2A1, 2.0 mg of the MBP-SULT2A1 was cleaved with 20 µg of Factor Xa for 12 hours at 4 °C. The cutting reaction was monitored by SDS-page electrophoresis with a 10% polyacrylamide gel and staining with Coomassie brilliant blue. After cutting, the reaction was loaded onto a DEAE column with a 2 mL bed volume, equilibrated in DEAE column buffer as described in the previous section. The column was washed with 2 mL of DEAE column buffer, and then washed with 2 mL of DEAE column buffer containing 50 mM NaCl. SULT2A1 activity was eluted from the column with a gradient from 50 mM to 250 mM NaCl in DEAE column buffer. DHEA sulfation activity was assayed for each fraction. The SULT2A1 prep was then passed through a 1 mL amylose column, to remove contaminating fusion protein and MBP. The purity and

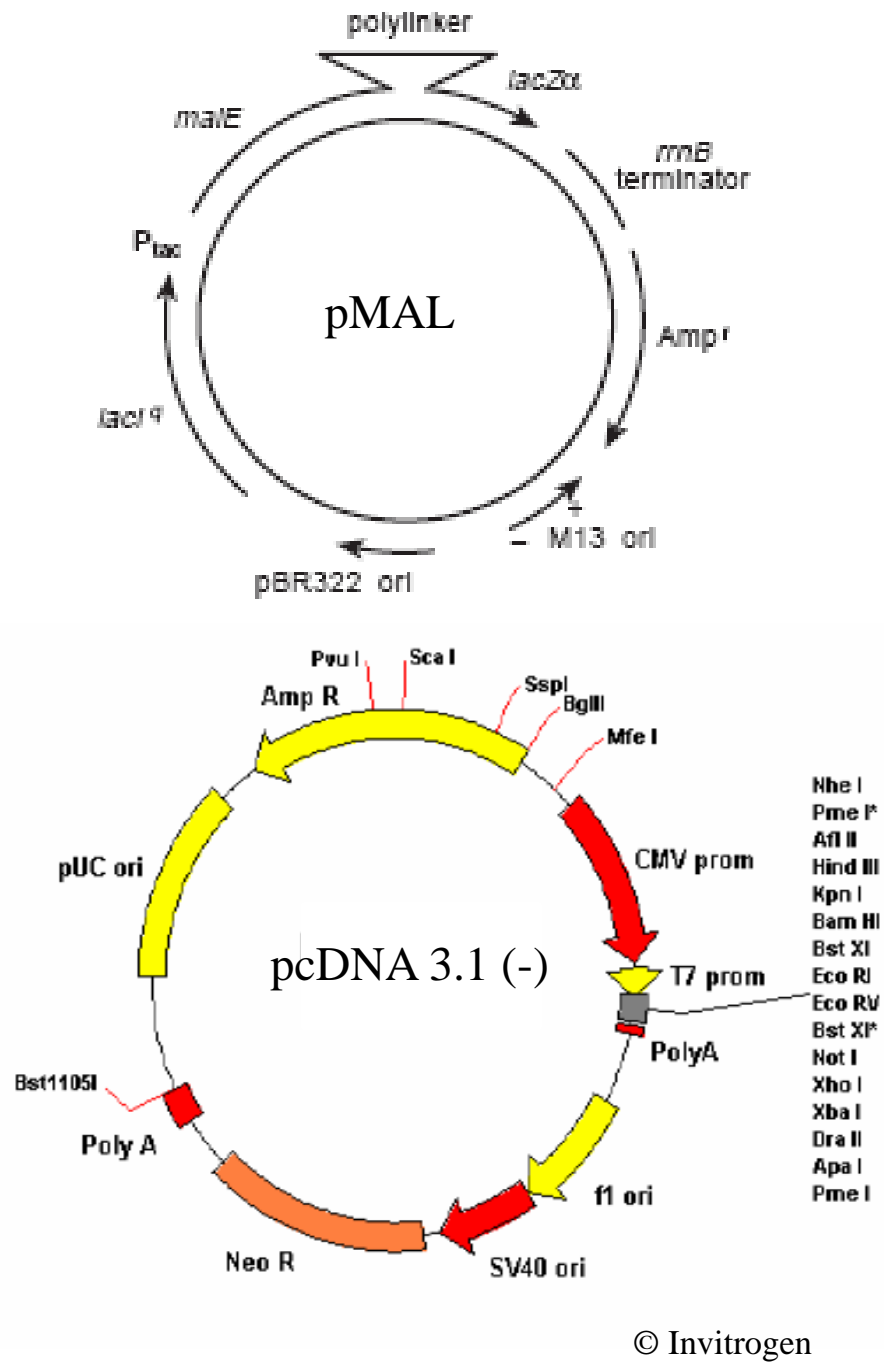


Figure 10. Restriction maps of the vectors pMAL-4c and pcDNA 3.1 (-).

activity of the pure SULT2A1 was evaluated by SDS-PAGE and DHEA sulfation activity as described in section I-C-1.

D) Sulfation of 24(S)-OH-Chol

1. *Sulfation of 24(S)-OH-Chol by SULT2A1*

24(S)-OH-Chol sulfation activity was measured using [³⁵S]-PAPS radiolabeled co-substrate and a TLC method described previously (Falany, Wheeler et al. 1994; Falany, Pilloff et al. 2006; Cook, Duniac-Dmuchowski et al. 2009; Cook, Leyh et al. 2010). For each reaction, the buffer was 50 mM Tris (pH 7.4) with 5 mM MgCl₂, 5 μL of SULT2A1 and 0.1 to 20 μM 24(S)-OH-Chol. The reaction was initiated with the addition of 10 μM [³⁵S]-PAPS (50 dpm pmol⁻¹) for a final volume of 100 μL. The reaction was stopped after 10 min with the addition of 100 μL of chloroform and mixed by vortexing. The reaction was then centrifuged for 5 min at 1000 X g and 40 μL of the aqueous phase was spotted onto to a TLC plate and dried. The sulfated products were separated using a solvent system containing 84 mL of methylene chloride, 16 mL of methanol, and 5 mL of ammonium hydroxide. The radioactive products were identified by exposure to autoradiograph film and the bands were scraped and quantified using scintillation spectroscopy.

2. *Kinetic Analysis of 24(S)-OH-Chol Sulfation by SULT2A1*

The product bands were identified using 24-48 h exposure to autoradiograph film. Following visualization of the bands, the products were physically scraped from the TLC plate with a razor into a vial; 4.5 mL of EcoLume biodegradable scintillation cocktail was

added to each vial and mixed well by vortexing. The [^{35}S]- SO_4 of each vial was quantified by scintillation spectroscopy and the level of sulfated product was calculated using the specific activity of [^{35}S]-PAPS. The activity was plotted vs. starting concentration of 24(S)-OH-Chol. The K_m and V_{max} for the formation of disulfate and monosulfate was calculated using the Enzyme Kinetics program.

3. *STS Hydrolysis of 24(S)-OH-Chol Sulfates*

a) *STS purification from human placenta*

Steroid sulfatase C (STS) was isolated from placenta using a modified method described in Hernandez-Guzman et al. (Hernandez-Guzman, Higashiyama et al. 2001). Term human placental tissue was obtained from the Tissue Procurement Service of the UAB Comprehensive Cancer Center. The placental tissue was homogenized in 67 mM phosphate buffer, pH 7.4 containing; 0.5 mM DTT and 0.24 M sucrose and stored at -80°C . For purification the homogenate was thawed on ice and diluted with 10 mM potassium phosphate, pH 7.4, 20% glycerol, 0.5 μM androstenedione and 0.1 mM EDTA, then centrifuged at 105,000 X g for 60 min. The pellet was then homogenized in the same buffer using a Dounce homogenizer. The buffer was adjusted to 0.3% Na cholate and 0.3% Emulgen 911, stirred at 4°C for 30 min, then centrifuged at 100,000 X g for 1 h. The supernatant fraction was diluted 2 fold with the same buffer then loaded onto a 60 mL DE-52 anion-exchange column equilibrated in the same buffer. The column was washed with buffer containing 0.15% Emulgen 911 then with 20 mM Tris-HCl, pH 7.4 containing 0.1% Triton X-100. STS activity was then eluted with 0.15 M NaCl in the same buffer in 3 ml fractions. Fractions containing STS activity were pooled and adjust-

ed to Con-A buffer containing 20 mM Tris-HCl pH 7.4, 0.1% Triton X-100, 5 mM CaCl₂, 5 mM MgCl₂, 5 mM MnCl₂ and 1 M NaCl. The pool was stirred for 30 min at 4°C then centrifuged at 100,000 X g for 30 min. A 5 ml Con-A Sepharose column was equilibrated in Con-A buffer. The supernatant fraction was loaded on to the Con-A column at 1.0 mL min⁻¹. The column was washed with 10 mL of Con-A buffer. STS activity was eluted with 10% α-mannopyranoside in Con-A buffer and fractions containing STS activity were pooled. The α-mannopyranoside was removed by repeated concentration and dilution using a Centricon 30,000 MWCO membrane.

STS activity was monitored over the purification process using the hydrolysis of [³H]-DHEAS to form [³H]-DHEA (Falany and Falany 2007). Reactions were prepared with 20 μM [³H]-DHEAS and 10 μL of the STS fraction in a reaction buffer of 50 mM Tris (pH 7.4) in 100 μL. After 10 min at 37 °C, the reaction was stopped with the addition of 400 μL of stop buffer (50 mM Tris, pH 8.8) and 500 μL of ethyl acetate. Reactions were centrifuged at 1200 X g. The formation of [³H]-DHEA was measured with 200 μL from the ethyl acetate phase and quantified using scintillation spectroscopy.

b) STS hydrolysis of 24(S)-OH-Chol-3-sulfate.

The sulfation of 24(S)-OH-Chol by SULT2A1 was re-evaluated using STS to remove the 3-sulfate from the 24(S)-OH-Chol sulfated products. The initial sulfation of 24(S)-OH-Chol by SULT2A1 was performed using the same method described in section I-D-1. After sulfation and chloroform extraction, 40 μL of the aqueous phase was transferred to a fresh 1.5 mL tube. The 3-sulfate was removed from the disulfate and 24(S)-OH-Chol-3-sulfate by adding the purified STS activity and incubated for 20 min at 37 °C.

The reaction was then spotted onto a TLC plate and dried. The TLC plate was resolved with the same solvent system used previously in section I-D-1. The bands were identified by exposure to autoradiograph film. The K_m and V_{max} values for the formation of 24(S)-Chol-24-sulfate were determined as described in section I-D-2.

4. *SULT2B1b* Sulfation of 24(S)-OH-Chol

a) *Purification of SULT2B1b.*

SULT2B1b was expressed in a *E. coli* XL1-Blue cells transfected with a *SULT2B1b*-pQE-31 vector transfected as described previously (Meloche and Falany 2001; He, Frost et al. 2005; Falany, He et al. 2006). The pQE-31 vector placed a 6 X His tag on the carboxyl terminal of *SULT2B1b*, generating 6-His-*SULT2B1b*. *E. coli* containing the *SULT2B1b* pQE-31 vector was cultured in 10 mL LB with $100 \mu\text{g mL}^{-1}$ ampicillin for 12-16 h at 37°C . The culture was added to 500 mL of LB with $100 \mu\text{g mL}^{-1}$ of ampicillin and incubated at 37°C to an OD_{600} of 0.4-0.6. Expression of 6-His-*SULT2B1b* was induced with 0.5 mM IPTG. The cells were incubated for 14 h at 37°C , then pelleted at $1200 \times g$ for 20 min and the pellet was frozen at -80°C . The thawed pellet was re-suspended in buffer containing 50 mM sodium phosphate (pH 7.8), 10% glycerol, and 1 mM β -mercaptoethanol (Ni-NTA affinity buffer). The solution was incubated for 30 min on ice with 0.5 mg mL^{-1} lysozyme. The cells were centrifuged at $1000 \times g$ for 15 min, and cytosol was generated as described in section I-C-1. A 5 mL Ni-NTA column was equilibrated in Ni-NTA buffer. The 6-His-*SULT2B1b* cytosol was loaded on the Ni-NTA affinity resin column at 0.5 mL min^{-1} and eluted with a gradient of imidazole from 50 to 250 mM in Ni-NTA buffer. Elution of 6-His-*SULT2B1b* was detected by

DHEA sulfation activity using the sulfation assay described in section I-B. Fractions containing 6-His-SULT2B1b were pooled and dialyzed 1:50 in storage buffer (10 mM sodium phosphate pH 7.4, 10% glycerol and 1 mM BME) for 4 h at 4°C. After 4 h, the buffer was replaced with fresh storage buffer and the 6-His-SULT2B1b was dialyzed 1:50 overnight at 4°C.

b) 24(S)-OH-Chol sulfation by SULT2B1b

24(S)-OH-Chol sulfation activity with 6-His-SULT2B1b was assayed using the TLC method described in section I-D-1. Each reaction was run for 20 min at 37°C, and the sulfated products were identified by 48 h exposure to autoradiograph film.

5. Liquid Chromatography Mass Spectrometry of 24(S)-OH-Chol Sulfates

To identify 24-OH-Chol and the sulfated reaction products, non-radioactive PAPS was used to sulfate 20 µM 24(S)-OH-Chol in a reaction using the method described in section I-D-1 and I-D-3-b. The formation of product in the reactions was quantified by TLC in comparison to control reactions with radiolabeled [³⁵S]-PAPS. The non-radiolabeled sulfated products were loaded onto a C-18 Sep-Pak cartridge, washed with water and eluted with 100% methanol. The methanol was evaporated under N₂ and the sulfated products were suspended in water.

Identification of the 24(S)-OH-Chol monosulfates and disulfate were carried out by HPLC-mass spectroscopy using a Sciex API-4000 triple quadrupole mass spectrometer with two Shimadzu micropumps and a Synergi Fusion (100 x 2 mm ID) analytical C-18 column with a C-18 guard column (Phenomenex). The mobile phases were: A, 10

mM ammonium acetate; and B, 100% acetonitrile/10 mM ammonium acetate. The gradient profile was 0 to 5 min, 100% A; 5 to 10 min, 20% A (linear); 10 to 15 min 20% A; and 15 to 20 min 100% A (step). Mass spectroscopy results were analyzed with the Analyst 1.4 software (Applied Biosystems, Foster City, CA). Identification of the 24(S)-OH-Chol-monosulfates and disulfate was carried out by tandem mass spectrometry (MS/MS) to generate the parent 24(S)-OH-Chol and sulfate ions. MS/MS analysis of the 24(S)-OH-Chol-monosulfates was attempted with increasing collision energies (30-120eV). Structure specific fragmentation other than the parent and sulfate ion was observed with only the 24(S)-Chol-24-sulfate and not with the 3-sulfate.

6. *Conversion of 24(S)-OH-Chol Monosulfates to Disulfate by SULT2A1*

a) Enzymatic synthesis of 24(S)-OH-Chol monosulfates.

To determine the K_m and V_{max} for the sulfation of the monosulfates, 24(S)-OH-Chol monosulfates were synthesized using SULT2A1 and SULT2B1b and separated by TLC. The 24(S)-OH-Chol-3-sulfate was synthesized using 6-His-SULT2B1b as described in section I-D-3-b in a volume of 1 mL. The reaction was incubated for 1 h at 37°C and spotted onto multiple lanes of a TLC plate (50 μ L each lane) and dried. The TLC plate was resolved with the solvent system described in section I-D-3-b. Bands were identified by 48 h exposure to autoradiograph film. The bands were scraped from the plate into a 1.5 mL tube. The 24(S)-OH-Chol-3-sulfate was eluted from the silica with 100% methanol and transferred to another 1.5 mL tube. The methanol was evaporated under N_2 and the 24(S)-OH-Chol-3-sulfate was re-suspended in 50 mM Tris (pH

7.4). The concentration of [^{35}S]-24(S)-OH-Chol-3-sulfate was determined by scintillation spectroscopy.

The synthesis of the 24(S)-Chol-24-sulfate was made by sulfation of 24(S)-OH-Chol with SULT2A1 followed by hydrolysis of the 24(S)-OH-Chol-3-sulfate and the 3-sulfate of the disulfate by STS (Cook, Duniac-Dmuchowski et al. 2009). 24(S)-OH-Chol sulfation was performed using the method described in section I-D-1, with 20 μM 24(S)-OH-Chol and 20 μM [^{35}S]-PAPS in a volume of 1 mL. The reaction was incubated for 1 h at 37°C and stopped by chloroform extraction. The aqueous phase was transferred to a fresh 1.5 mL tube. To remove the 24(S)-OH-Chol-3-sulfate, STS was added to the aqueous phase and incubated for 1 h at 37 °C. The sample was spotted onto a TLC plate with 50 μL per lane and the [^{35}S]-24(S)-sulfate-Chol was separated using the solvent system described in I-D-1. [^{35}S]-24(S)-sulfate-Chol was identified by 24 h exposure to autoradiograph film. The [^{35}S]-PAPS was scraped and collected in a 1.5 mL tube and eluted from the TLC silica with 100 % methanol. The methanol was evaporated under N_2 and the [^{35}S]-24(S)-Chol-24-sulfate was re-suspended in 50 mM Tris (pH 7.4). The concentration of [^{35}S]-24(S)-Chol-24-sulfate was determined by scintillation spectroscopy.

b) SULT2A1 sulfation of 24(S)-Chol-24-sulfate and 24(S)-OH-Chol-3-sulfate to 24(S)-Chol-24,3-disulfate.

The monosulfates sulfation by SULT2A1 was assayed using the radiolabeled [^{35}S]-24(S)-OH-Chol-3-sulfate or [^{35}S]-24(S)-sulfate-Chol synthesized as described in the previous section. Sulfation activity was assayed with a modified TLC method described in section I-D-1 with 10 μM PAPS. The concentration of [^{35}S]-24(S)-OH-Chol-3-sulfate

was 0.2 to 10 μM . The [^{35}S]-24(S)-Chol-24-sulfate concentration was 50-300 nM. Reactions were incubated for 10 min at 37°C and spotted onto a TLC lane and resolved with the solvent described in section I-D-1. The disulfate was identified by exposure to autoradiograph film and quantified by scintillation spectroscopy as described in section I-D-2.

E) Molecular Docking of Ligands to the SULT2A1 Active Site

Molecular docking of 24(S)-OH-Chol in the active site of SULT2A1 was performed using the Molecular Operating Environment (MOE). The SULT2A1 model was made from the SULT2A1 crystal structure generated with bound PAP (1EFH) (Pedersen, Petrotchenko et al. 2000). The water molecules in the crystal structure were deleted and the missing atoms of the crystal structure were added using MODELLER (Eswar, Webb et al. 2006). MODELLER threaded the SULT2A1 sequence onto the SULT2A1 crystal structure and the missing atoms added. A sulfate was added to the PAP molecule in the model using LigX (Labute 2005) to convert the PAP to PAPS. LigX constructs a three dimensional chemical structure in MOE. The entire system was then protonated with Proton 3D (Bower, Cohen et al. 1997) assuming a pH of 7.0. The system was energy minimized using the AMBER force field (Aehle, Sobek et al. 1993). The 24(S)-OH-Chol and the monosulfates were constructed with LigX. The ligands were then energy minimized using AMBER. The active site in the SULT2A1 model was defined by the resolution of DHEA in the SULT2A1 crystal structure generated with bound DHEA (1J99) (Rehse, Zhou et al. 2002). The 24(S)-OH-Chol was then docked into the active site using Alpha Triangle for an initial placement and FlexX for refinement using the scoring functions, London dG and Affinity. Alpha Triangle is a docking program that uses a simpli-

fied ligand in a random walk and is useful for generating initial placement (Wildman and Crippen 2002). FlexX is a Monte Carlo algorithm based program that was used to refine the orientation of the ligand searching the local space for the lowest energy (Wildman and Crippen 2003). The London dG scoring function favors hydrophobic interactions (Wildman and Crippen 2001), which increases the predicted binding of hydrophobic compounds to the active site of SULT2A1. The Affinity scoring function favors electrostatic interactions (Feher and Schmidt 2000), and underestimates the hydrophobic interactions of the SULT2A1 active site. The use of two scoring functions reduces the inherent biases of both functions. The top ten models of each docking were analyzed by cluster analysis using MOE for the major predicted orientations. An active orientation for a ligand was defined as a BFE of -6 kJ or less and a predicted hydrogen bond with the His99 defined as an angle for the hydroxyl relative H99 of 150° to 210° and a distance of 1.5 to 3.5 Å.

24(S)-Chol-24-sulfate could not bind to the SULT2A1 model with PAPS in an active orientation, therefore a new model of SULT2A1 was modeled using the SULT2A1 crystal structure with bound DHEA as the template (1J99) (Rehse, Zhou et al. 2002). A PAPS free model of SULT2A1 was made using the same method as described in the previous paragraph except no PAPS was included in the model. The docking of the 24(S)-Chol-24-sulfate was performed using the same method as described in the docking to the PAPS-bound SULT2A1 model. The PAPS bound model was referred to as the “closed model” and the PAPS free SULT2A1 was referred to as the “open model” for the rest of this dissertation.

DHEA and RAL were constructed with LigX and energy minimized as described previously. The docking of DHEA and RAL to the “open” and “closed” model of SULT2A1 was also performed using the same method described for 24(S)-OH-Chol docking. The top ten structures of each docking were examined by cluster analysis in MOE for active orientations.

F) Determination of DHEA Sulfation Kinetic Constants

The sulfation of DHEA was evaluated using the chloroform extraction assay described in section I-B. To determine the K_m and V_{max} values, the concentration of [3H]-DHEA in each reaction was 0.1, 0.5, 1, or 2 μM and 0.05, 0.1, 0.2, or 1 μM PAPS. The reactions were stopped after 5 min with stop buffer and chloroform extraction as described in section I-B. The Lineweaver-Burk plots of each PAPS concentration were made relative to the DHEA concentration. The K_m s and V_{max} values were calculated by the re-plot of the slopes and Y-intercepts vs PAPS concentration, as described for two substrate kinetics by Bell and Bell (Bell and Bell 1988).

G) DHEA Pre-Steady State Kinetics

Pre-steady state kinetics for DHEA sulfation was evaluated with a method similar to the chloroform extraction assay described in section I-B. [3H]-DHEA (3 μM) or PAPS (20 μM) was added to 10 pmol of SULT2A1 in the reaction buffer and equilibrated for 2 min at 37 °C. The reaction was initiated with the addition of [3H]-DHEA (3 μM) or PAPS (20 μM) for a volume of 1 mL. At each time point from 0-300 sec, 50 μL was sampled and added to 450 μL of stop buffer (50 mM Tris pH 8.8) and 3 mL of chloro-

form then mixed by vortexing. The formation of [^3H]-DHEAS was determined in the aqueous phase by scintillation spectroscopy.

H) Determination of RAL Sulfation Kinetic Constants

The sulfation of RAL by SULT2A1 was performed using [^{35}S]-PAPS and TLC separation similar to the method described in section I-D-1. Each reaction was performed with 10 mM sodium phosphate (pH 7.4), 5 mM MgCl_2 , SULT2A1, and 0.5, 1.0, 2.0 or 5.0 μM RAL. The reactions were initiated with the addition of 0.2, 0.5, 1.0, or 5 μM [^{35}S]-PAPS in a volume of 100 μL . After 10 min, the reactions were stopped with 100 μL of chloroform and mixed by vortex. The reactions were centrifuged at 1200 X g for 3 min and 45 μL of the aqueous phase was spotted on a TLC plate. The products were separated with a solvent solution of 85 mL of methylene chloride, 15 mL of methanol, and 5 mL of ammonium hydroxide. The sulfated RAL was identified by exposure to autoradiograph film and scraped. [^{35}S]-RAL-sulfate formation was quantified by scintillation spectroscopy. The K_m s for RAL and PAPS, as well as the V_{max} , were calculated based on the re-plots of the Lineweaver-Burk plots as described with DHEA kinetics in the section I-F (Bell and Bell 1988).

I) RAL Pre-Steady State Kinetics

RAL pre-steady state kinetics was examined using a modified protocol of the RAL sulfation with [^{35}S]-PAPS described in section I-H. In 1 mL of buffer, 10 pmol of SULT2A1 was incubated with a saturating concentration of either RAL (20 μM) or 10 μM [^{35}S]-PAPS. For the burst kinetics, the specific activity of the [^{35}S]-PAPS was 500

dpm pmol⁻¹. After 2 min at 37°C, the reactions were started with the addition of 20 μM RAL or 10 μM [³⁵S]-PAPS in a final volume of 1000 μL. At the each time point (0-300 sec), 50 uL was added to 100 μL of chloroform and mixed by vortex to stop the reaction. The samples were then centrifuged at 1200 X g for 5 min and 45 μL of the aqueous phase was spotted onto a TLC plate and resolved in the solvent system described in section I-H. Bands were identified by exposure to autoradiograph. RAL-sulfate was quantified by scintillation spectroscopy and the total amount of RAL-sulfate in the reaction was determined for each time point.

J) Determination of the Affinity Constants for SULT2A1 Binding by Changes in Intrinsic Fluorescence

Intrinsic fluorescence of an enzyme is a measurement of the local environment of the aromatic residues of a protein. When ligands bind to a protein, the local environment of the ligands can be blocked directly by the binding ligand or indirectly by the binding causing structural changes in the enzyme. The intrinsic fluorescence of 50 nM SULT2A1 in PBS was measured using an excitation of 275 nm and an emission of 340 nm with a Perkin-Elmer LS-5 Fluorescence Spectrophotometer using a previously described protocol (Zhang, Varlamova et al. 1998). A control cuvette with only PBS was used to zero the fluorescence spectrophotometer. The initial fluorescence of SULT2A1 was measured, and the value was defined as I_0 . At each titration step, 2 μL of 40 μM PAPS or PAP was added to the SULT2A1 and control samples and mixed by pipetting. The solution was then equilibrated for 2 min at room temperature (RT). During the equilibration, the spectrophotometer light shutter was closed to prevent bleaching of the enzyme. The in-

intrinsic fluorescence was then measured for each cuvette, and the blank cuvette was subtracted from the SULT2A1 cuvette. The net fluorescence was normalized to the starting fluorescence to generate the I/I_0 value. Each substrate was added until no change in intrinsic fluorescence was observed for 5 consecutive additions. PAPS and PAP K_d titrations were repeated at least 3 times. The K_d of PAP and PAPS to SULT2A1 was determined using a single binding site model described by Bell and Bell (Bell and Bell 1988). The single site binding equation is $Y=Y_{\max} * X / (K_d + X)$ where X is the ligand concentration, Y_{\max} is the maximum change in fluorescence in the titration, and Y is the change in fluorescence. This equation assumes a concentration of enzyme less than the K_d .

RAL and DHEA titrations were performed with the same method described in the previous paragraph, with one change. Because of the higher K_d of RAL and DHEA relative to PAP and PAPS, the concentration of SULT2A1 was increased to 100 nM to improve the signal to noise ratio. In addition to titration with free SULT2A1, DHEA and RAL were titrated to SULT2A1 with 10 μ M PAP to determine the change in affinity for substrate with the binding of sulfate donor. The K_d for RAL was determined using a single binding site fit as described for PAP and PAPS. The DHEA titration curve to SULT2A1 in the absence of PAP was not consistent with a single binding site, but did correlate with a two binding site model (Bell and Bell 1988). The two substrate binding model equation is $Y=Y_{\max 1} * X / (K_{d 1} + X) + Y_{\max 2} * X / (K_{d 2} + X)$. $K_{d 1}$ is the K_d for the high affinity site, and $Y_{\max 1}$ was the maximum change in fluorescence by the high affinity site. The $Y_{\max 1}$ was determined by the binding of DHEA to SULT2A1 with 10 μ M PAP. $K_{d 2}$ is the low affinity active site and $Y_{\max 2}$ is the change in fluorescence caused by the low affinity site. $Y_{\max 2}$ was determined by the equation $Y_{\text{total}} = Y_{\max 1} + Y_{\max 2}$. When

SULT2A1 was saturated with PAP, DHEA titration was consistent with a single binding site model.

K) Stoichiometric Determination of Binding for Substrate to SULT2A1 Using the Change in Intrinsic Fluorescence

The titration of PAPS, PAP, RAL, and DHEA for determining the stoichiometry of binding to SULT2A1 was performed as described in the K_d titrations described in section I-J. The only difference was that the SULT2A1 concentration was increased to 5 μ M. RAL and DHEA were titrated to SULT2A1 with a concentration of 0 and 10 μ M PAP. DHEA was also titrated to SULT2A1 in the presence of 2.5 μ M PAP.

L) Pharmacophore Analysis of SULT2A1

Pharmacophore simulation was performed using the internal MOE program, PhamQuarry (Kastenholz, Pastor et al. 2000) to identify novel substrates. For both the open and closed models, a PhamQuarry quarry was generated by replacing the atoms of the active site with a generalized scaffold that defined hydrophobic, charged, and pi-stacking regions. A second scaffold was added that defined the volume of the active site. A hydrogen bond at the H99 was designated as a required interaction. The pharmacophore quarry was screened to a chemical library of over 35,000 compounds and the hit level for PhamQuarry was set to a probability of 0.95. Hits were then submitted to the web site www.emolecules.com to identify commercial availability and research interest of the predicted hits. The compounds emodin, digitoxin, and 3-(3-chlorophenyl)-1-(2-thienyl)-1-propanol (3-CTP) were selected and docked to the active site of both the

closed and open models of SULT2A1 using the docking method described in section I-E.

M) Pre-Steady State Kinetics of Pharmacophore Results

The predicted substrates emodin, digitoxin, and 3-CTP were assayed for SULT2A1 sulfation activity using a [^{35}S]-PAPS and TLC method described in section I-H with 20 μM emodin, 3-CTP, or digitoxin. Reactions were run for 30 min at 37° C, and spotted onto a TLC lane. Sulfated products were separated with the solvent system described in section I-H. The sulfated products were identified after 24 h exposure to autoradiograph film.

The pre-steady state kinetics of emodin, digitoxin and 3-CTP were performed using a modified method with [^{35}S]-PAPS and TLC as described in section I-I. Reactions were performed with 1 pmol SULT2A1, 10 μM [^{35}S]-PAPS, and 20 μM emodin, 3-CTP, or digitoxin for 0-120 sec. The bands were identified by exposure to autoradiograph film. Product bands were scraped and quantified by scintillation spectroscopy. Each reaction was repeated twice.

N) Computational Modeling of G234L/G233L SULT2A1 Mutant

Computational modeling of SULT2A1 was performed to predict the change in SULT2A1 sulfation of RAL. The closed SULT2A1 model based on the co-crystal structure with PAP was modified using LigX to mutate the L233 and L234 to glycines. After the generation of the mutant, the loop 3 region was minimized with AMBER. RAL was docked to the active site using the same method as described in section I-E. The top ten

orientations were analyzed by cluster analysis and compared to the initial closed docking of RAL to wild type SULT2A1 (WT).

O) Generation and Characterization of L233G/L234G SULT2A1 Mutant

Docking of RAL to the L233G/L234G SULT2A1 construct predicted that RAL could bind to the open and closed conformation of the L233G/L234G SULT2A1. The L233G/L234G SULT2A1 mutant was generated using custom mutagenesis primers, QuikChange™ Site-Directed Mutagenesis Kit, and Advantage Taq Polymerase. The SULT2A1-pMAL-c2 plasmid was purified using the plasmid midi-prep protocol described by Sambrook and Russel (Sambrook and Russel 2001). SULT2A1-pMAL-c2 transfected cells were grown for 12-14 h at 37 °C in 10 mL of LB with 100 µg mL⁻¹ of ampicillin. The cells were pelleted at 2800 X g for 5 min and the supernatant fraction was discarded. The pellet was re-suspended in 200 µL of 50 mM glucose, 25 mM Tris (pH 8.0), 100 µg mL⁻¹ lysozyme, and 10 mM EDTA (solution I) and transferred to a 1.5 mL micro centrifuge tube. A solution of 0.2 N NaOH and 1% SDS (solution II) was added (400 µL) and mixed gently by inversion. A solution of 66.7% potassium acetate and 12.7% glacial acid (solution III) was chilled to 4 °C. After solution III was chilled, 400 µL was added to the lysate. After 3-5 min at 4 °C, the 1.5 mL micro centrifuge tube was centrifuged for 5 min at 1200 X g and 600 µL was transferred to a new tube. A 1:1 phenol and chloroform mixture was added (600 µL) and the solution was centrifuged again and the aqueous phase was transferred to a new tube. The DNA was precipitated with 600 µL of isopropanol and centrifuged at 1200 X g for 5 min and the supernatant fraction was discarded. The DNA was washed with 100% ethanol and then 70% ethanol and then

re-suspended in 100 μL water. The concentration of DNA was evaluated by DNA electrophoresis with a 1% agarose gel. Each PCR reaction was performed with the Advantage PCR buffer provided by BD Bioscience (40 nM Tricine-KOH pH 8.7, 15 mM KOAc, $\text{Mg}(\text{OAc})_2$, $3.75 \mu\text{g mL}^{-1}$, 0.005% Tween 20, and Nonident-P40 0.005%), 10 mM dNTPs, 10 μM forward primer, 10 μM reverse primer, 100 ng SULT2A1-pMAL-c2 and 1 μg of Advantage Taq polymerase. The PCR reaction was heated at 95°C for 2 min. PCR reactions were run with a melting step of 95°C for 30 sec, an annealing step of 50°C for 1 min, and an elongation step of 68°C for 8 min for each cycle. After 30 cycles, the PCR reaction was run for 8 min at 68°C then held till ready at 4°C . The PCR product was isolated from a 1 % agarose gel with the QIAquick Gel Extraction Kit. DH5- α *E. coli* bacteria was made competent with a Z-Competent™ *E. coli* Transformation Kit. The L233G/L234G SULT2A1-pMAL-c2 vector was mixed with the competent cells, 1 μg per 100 μL of competent cells. Cells were plated on LB and $100 \mu\text{g mL}^{-1}$ ampicillin agar and grown overnight at 37°C . Individual colonies were picked and grown in 5 mL of LB with ampicillin at 37°C overnight. Glycerol blots were made of the mutants and the L233G/L234G SULT2A1-pMAL-c2 plasmid was isolated as described previously. L233G/L234G pMAL-c2 vector was submitted to the UAB sequencing core for confirmation of the mutation. L233G/L234G SULT2A1 was expressed using the same protocol described for wild type (WT) SULT2A1 in section I-C-2.

After the L233G/L234G SULT2A1 was purified, the kinetic properties of the mutant enzyme were compared to the WT SULT2A1 using the same protocol described in sections I-B and I-F with a fixed PAPS concentration of 10 μM . The [^3H]-DHEA concentration was varied from 0.5 to 20 μM . The K_d for PAPS and PAP to the mutant

SULT2A1 was evaluated using intrinsic fluorescence titrations as described in section I-J. RAL pre steady state sulfation was also performed with the mutant using the same protocol described in section I-I.

P) Characterization of V260E, Q247A, and Q155A SULT2A1 Mutants

SULT2A1 mutants V260E, Q247A, and Q155A were generated using QuikChange™ Site-Directed Mutagenesis Kit with the same protocol as described in section I-O. Plasmids were sent to UAB sequencing core for confirmation of the mutation. Purification of the mutants was performed using the pMAL vector system with the methods described in section I-C-3. The Q155A, Q243A, and V260E mutants were loaded onto G-100 Sephadex resin for detection of dimer formation, using the same protocol as described for WT SULT2A1 in section II-C. DHEA sulfation activity of the mutants was performed using the same method as described in section I-B and I-G.

II. THE SUBUNIT INTERACTIONS OF THE SULT2A1 HOMODIMER ASSOCIATED WITH PAPS BINDING

A) Materials

The Sephadex G100 resin was purchased from Sigma-Aldrich (St. Louis, MO). The pcDNA 3.1 (-) vector was purchased from Invitrogen (Carlsbad, CA). GROMACS is a free program under a general public license (gpl) from the University of Uppsala (Stockholm, Sweden) and was computed on the UAB College of Engineering server. Cos-7 cells were obtained from the ATCC (Manassas, VA). DMEM media was pur-

chased from CellGro (Manassas, VA). DNA restriction enzymes were purchased from New England Bio Labs (Ipswich, MA).

B) SULT2A1 Dynamic Modeling of with GROMACS

GROMACS is a dynamic modeling program provided under a general public license (gpl) (Van Der Spoel, Lindahl et al. 2005). The SULT2A1 monomer model was based on the SULT2A1 co-crystal structure with DHEA (1J99) (Rehse, Zhou et al. 2002). The missing atoms were added using the homology modeling method in MOE described in section I-E. The pdb file was transferred using Secure Shell to the UAB College of Engineering server. In GROMACS, the complete SULT2A1 monomer was converted to a topology file using the `pdb2gmx` function. The topology file includes information on angles, dihedrals, positional restraints and partial charges in addition to the position and atom type in the pdb file. A box was constructed in GROMACS around SULT2A1 using the “newbox” function. The box was a cube of 143 Å sides and SULT2A1 occupied approximately 70% of the volume. The system was then solvated using a simple 3 point water model, TIP3P. NaCl was added to the box to simulate 150 mM NaCl, replacing water molecules in the solvent. The net charge of the molecule was calculated during the writing of the topology file to be -4, therefore it was necessary to add 4 additional Na⁺ to balance the total charge. The system was then minimized using the “mdrun” function in GROMACS with a `minimize.mdp` file, an energy file written for 0°K in GROMACS. The system was then warmed up in a series of `mdrun` simulations using “mdp” topology files for the temperatures of 50, 100, 150, 200, 250, and 300°K in GROMACS. The warming mdp files were provided by the Collage of Engineering. Each warming step

was performed with a 2 psec time step and simulated for 100 psec. The production simulation was performed using the AMBER energy field, with a time step of 2 psec and simulated a 5 nsec period of time using an all atomistic simulation with an explicit solvent. The root mean squared fluctuations (RMSF) of the backbone α -carbons were measured.

The SULT2A1 dimer was constructed using MOE. The SUTL2A1 open model was duplicated and the two subunits were aligned to the SULT1E1 crystal structure made with PAPS (Pedersen, Petrotchenko et al. 2002) (1HY3) with the KTVE interface. The SULT2A1 dimer was then simulated using the same method described for the monomer in GROMACS in the previous paragraph in a cube with sides of 252 Å.

C) Size Exclusion Chromatography of WT SULT2A1 and MBP-SULT2A1

MBP-SULT2A1 was purified using the SULT2A1-pMAL-c2 expression system as described in section I-C-2. After isolation of MBP-SUTL2A1 from the amylose column, the MBP-SULT2A1 protein was pooled, and the purity and activity were determined as described in section I-C-2. To make the column, 5 grams of Sephadex G100 resin was hydrated in 200 mL of column buffer (10 mM potassium phosphate pH 7.4, 10% glycerol). The slurry was heated and decanted 3 times to remove air bubbles and the resin was equilibrate in the buffer. The slurry was loaded into a 1.5 cm diameter column, with 10 mL of buffer injected from the bottom of the column to remove air bubbles. The slurry was allowed to settle by gravity, and the final volume was 45 mL. The column was equilibrated in column buffer, and standardized with colorimetric molecular weight standards from Bio Rad: blue dextran (2000 kDa) bovine albumin (66.7 kDa), equine fumarase (48.5 kDa), and human cytochrome C (12 kDa). The flow rate of the col-

umn was 0.75 mL h^{-1} and fractions were collected every 30 min. The standards were detected by their UV absorbance at 260 nm. The elution of the standards was plotted relative to the volume to generate a standard curve of their molecular weights.

After the column was standardized, it was washed with 3 column volumes of buffer. Then the column was loaded with 200 μg of SULT2A1 or MBP-SULT2A1 in 300 μL volume, with a flow rate of 0.75 mL h^{-1} . Fractions were collected every 30 min. The elution of SULT2A1 was monitored by UV absorbance at 260 nm and with DHEA sulfation activity.

D) DHEA Sulfation Activity of MBP-SULT2A1 and SULT2A1

MBP-SULT2A1 elution from the Sephadex G100 column indicated that unlike SULT2A1, MBP-SULT2A1 was a monomer. DHEA sulfation activity was examined for MBP-SULT2A1 and SULT2A1 using the protocol described in section I-B and I-F. A concentration curve of DHEA sulfation was set up with increasing concentrations from 0.1 to 20 μM [^3H]-DHEA in the standard reaction buffer and 20 μM PAPS. The reactions contained either MBP-SULT2A1 or SULT2A1. Each reaction was stopped after 5 min. The sulfated product was separated by chloroform extraction and quantified by scintillation spectroscopy as described in section I-B. The K_d of binding for substrates to MBP-SULT2A1 were examined by intrinsic fluorescence as described in section I-J.

E) PAPS Concentration Curve of SULT2A1 and MBP-SULT2A1 at 2 μ M and 20 μ M DHEA

MBP-SULT2A1 had no detected substrate inhibition, in contrast to SULT2A1. To determine the influence of PAPS concentration on substrate inhibition, a PAPS concentration curve from 0.05 to 20 μ M was performed. DHEA sulfation activity was assayed using the established protocol from section I-B, with a concentration of [3 H]-DHEA of 2 μ M or 20 μ M.

F) Pre-Steady State Sulfation of RAL by MBP-SULT2A1

Pre-steady state kinetics of RAL sulfation by MBP-SULT2A1 were examined using the method described in section I-I with the only change in the protocol being the use of 10 pmole of MBP-SULT2A1 instead of SULT2A1.

G) Docking of a Second DHEA Molecule to the Open SULT2A1 Model

Computational modeling was used to predict the binding of a second DHEA molecule to the active site of SULT2A1. The open SULT2A1 model was constructed using the method described in section I-E. The lowest energy DHEA docking structure was added to the active site and included in the docking simulation. A second DHEA molecule was made using the method described in section I-E. The second DHEA molecule was docked to the active site with the protocol described in section I-E with the only change being the inclusion of a DHEA molecule fixed at the catalytic site. The top ten structures were analyzed by cluster analysis in MOE.

H) Cos-7 Transfection with SULT2A1 and MBP-SULT2A1

SULT2A1 cDNA was isolated from human liver in 1992 (Comer and Falany 1992), and was inserted into pcDNA 3.1 (-) using the DNA restriction enzymes HindIII and XmnI (Comer, Falany et al. 1993). The MBP-SULT2A1 DNA was cut from the pMAL vector using HindIII and EcoRV and then ligated into the pcDNA 3.1(-) vector. The vector (10 µg) was mixed with 100 µL of Z-component DH5- α *E. coli* cells and plated onto LB agar plates with 100 µg mL⁻¹ of ampicillin. Colonies were picked and grown in 10 mL of LB with 100 µg mL⁻¹ for 16 h. Plasmid was isolated with using the plasmid midi-prep protocol described in section I-O. Insertion of the SULT2A1 or MBP-SULT2A1 sequence was confirmed with a 1% agarose DNA gel. The African Green monkey kidney Cos-7 cells were grown in DMEM media with 7.5% fetal bovine serum to 50-60% confluency on 60 mm polystyrene cell culture plates. The pcDNA 3.1 (-) vector with MBP-SULT2A1 or SULT2A1 was diluted into 500 µL of Opti-MEM media (100 ng µL⁻¹) and gently mixed. Lipofectamine (10 µL) was diluted in 500 µL of Opti-MEM and the diluted lipofectamine and vector were then mixed and incubated for 30 min at RT. The Cos-7 cells were washed twice with PBS and the lipofectamine-vector solution was added to the cells. After 12 h at 37°C, 1 mL of DMEM 7.5% FBS was added to the cells. After 24 h, the media was removed and replaced with fresh DMEM media with 7.5% FBS, and 48 h after transfection, the cells were washed with PBS and treated with 100 µL of trypsin and transferred to a 100 mm polystyrene tissue culture plate. The cells were then grown for 48 h with DMEM and 7.5% FBS. After 48 h, the media was changed to a selection media of DMEM and 7.5% FBS with 400 µg mL⁻¹ G418 sulfate. The cells were grown until colonies were large enough to be visibly identified by the naked eye. The

colonies were transferred to 12 well plates using cloning cylinders. The wax was autoclaved and applied to the bottom of the cloning cylinders to form a water tight seal. The cloning cylinder was then placed over the colony and 50 μ L of trypsin was added to the cloning cylinder. After 10 min at 37°C, the colony was transferred to 1.5 mL of DMEM media, 7.5% FBS and 200 μ g of G418 in a 12 well plate. A 10% polyacrylamide gel was loaded with 100 ng of the cell lysate, WT and MBP-SULT2A1 for SDS-page electrophoresis. The gel was transferred to nitrocellulose using a Trans-Blot® SD Semi-Dry Electrophoretic Transfer cell at 10 V for 30 min. After blocking for 1 h with 5% non-fat milk in TEA buffer, the nitrocellulose was probed using a polyclonal rabbit anti-human SUTL2A1 IgG at a dilution of 1:2000 for 1 h. The primary antibody was detected with goat anti-rabbit horseradish peroxidase IgG (Heroux, Falany et al. 1989; Falany, Wheeler et al. 1994; Falany 1997).

I) Transfected Cos-7 DHEA Sulfation Assay

The sulfation of DHEA was evaluated in intact Cos-7 cells transfected with SULT2A1 or MBP-SULT2A1 pcDNA 3.1 (-). Cells were grown in 24 well plates in DMEM media with 7.5% FBS to 80% confluency. The number of cells in each well was determined using two wells, each counted twice by hemocytometer. Each well was then washed twice with PBS and serum free media was added to each well containing 1, 2, 5, 7.5, 10, 12.5, 15, 17.5, or 20 μ M [3 H]-DHEA. After 30 min at 37 °C, 100 μ L of the media was removed and the concentration of [3 H]-DHEAS was determined by chloroform extraction scintillation counting.

III. THE STRUCTURAL REARRANGEMENTS OF SULT1A1 AND SULT1E1 ASSOCIATED WITH PAPS BINDING

A) Materials

[1,2,6,7-³H]-E2 (60 Ci/mmol) was purchased from Perkin Elmer (Waltham, MA). FUL was purchased from Sigma-Aldrich (St. Louis, MO).

B) Homology Modeling of SULT1A1 and SULT1E1

The sequences of SULT1A1 and SULT1E1 were aligned to the SULT2A1 open model, built using the method described in section I-E. The sequences of SULT1A1 and SULT1E1 were aligned to SULT2A1 using MODELER with a gap setting of 5 residues (Eswar, Webb et al. 2006). The backbone of SULT1A1 and SULT1E1 were threaded on the SULT2A1 open template and then the side chains were added to the structure. After the side chains were added, the protein was energy minimized with the AMBER energy field (Labute 2005). The predicted open models of SULT1A1 and SULT1E1 were then submitted to the NIH SAVES server (<http://nihserver.mbi.ucla.edu/SAVES/>) and analyzed by the programs PROCHECK (Laskowski, MacArthur et al. 2001), VERIFY (Eisenberg, Luthy et al. 1997), and ERRAT (Luthy, Bowie et al. 1992) which checks bond angles, atom distances, and dihedrals properties for disallowed structural characteristics in the model.

C) Docking Studies with SULT1A1 and SULT1E1

Docking was also performed with the SULT1A1 and SULT1E1 using the protocol described in section I-E. The closed structure with of SULT1A1 was based on the

SULT1A1 crystal structure with bound E2 and PAP (2D06) (Gamage, Tsvetanov et al. 2005). The SULT1E1 crystal structure with bound PAPS was used for the closed SULT1E1 model (1HY3) (Pedersen, Petrotchenko et al. 2002). The active site of SULT1E1 was defined using the location of 3,5,3',5'-tetrachloro-biphenyl-4,4'-diol in the SULT1E1 crystal structure with bound PAP and 3,5,3',5'-tetrachloro-biphenyl-4,4'-diol (1G3M) (Shevtsov, Petrotchenko et al. 2003). The open model used in docking for SULT1A1 and SULT1E1 was the homology model generated in section III-C. E2 and FUL were built using LigX and docked to SULT1A1 and SULT1E1.

D) SULT1A1 and SULT1E1 Generation and Purification

The sequences for SULT1A1 and SULT1E1 were ligated into the pMAL vector as described previously (Falany, Krasnykh et al. 1995). Pure SULT1A1 and SULT1E1 were generated using the method described in section I-C-2. SULT1A1 activity was detected using PNP sulfation with [³⁵S]-PAPS using a barium precipitation assay (Falany 1997). The assay was performed in a reaction buffer consisting of 10 mM sodium phosphate buffer (pH 7.4) and 5 mM MgCl₂. Each reaction contained 25 μL of SULT1A1 and was started with the addition of 10 μM [³⁵S]-PAPS in a volume of 125 μL. Reactions were incubated for 5 min at 37°C and were stopped with the addition of 50 μL of 0.1 M Ba(OH)₂, 0.1 M Ba(C₂H₃O₂)₂, and 0.1 M ZnSO₄. The reaction was centrifuged at 1000 X g for 5 min, and the supernatant fraction was transferred to a 1.5 mL tube. The precipitation was repeated and the formation of PNPS concentration was measured with 125 μL of the reaction by scintillation spectroscopy.

SULT1E1 activity was assayed using a [^3H]-E2 sulfation with the chloroform extraction assay. The assay was performed using a method similar to the chloroform extraction assay described in section I-B. Instead of 3 μM [^3H]-DHEA, the reaction mixture contained 20 nM [^3H]-E2 with a specific activity of 32 dpm fmol $^{-1}$ and 25 μL of the SULT1E1.

E) Steady State Kinetics of E2 with SULT1A1

E2 sulfation by SULT1A1 was measured using [^3H]-E2 and the chloroform extraction method described in section I-B and III-D. The V_{max} and K_{m} were determined as described previously in section I-F (Bell and Bell 1988). Sulfation of E2 by SULT1A1 was repeated, with PAP and E2-S product inhibitors to determine the reaction mechanism. The concentration of PAP was 0.5, 1, 2, or 5 μM and E2-S was 0.5, 1, 2, or 5 μM .

F) Sulfation of FUL by SULT1A1 and SULT1E1

FUL was measured using [^{35}S]-PAPS and TLC method described in section I-D-1 and I-H. Each reaction used either SULT1A1 or SULT1E1. The concentration of FUL was 1, 5, 10, or 20 μM with SULT1A1 or 0.5, 1, 2, or 5 μM for SULT1E1. The concentration of [^{35}S]-PAPS was 0.5, 1, 2, or 5 μM for SULT1A1 and SULT1E1. The reactions were run 10 min at 37°C. Pre-steady state kinetics of FUL were performed with time points of 10, 30, 60, and 120 sec as described in section I-I.

G) Determination of K_d for E2 and FUL Binding to SULT1A1 and SULT1E1 Using
Intrinsic Fluorescence

Intrinsic fluorescence of SULT1A1 was measured using an excitation of 280 nm and an emission of 345 nm in PBS buffer using the previously described protocol in section I-J. For SULT1E1, the excitation was 285 nm and 340 nm for emission.

RESULTS

I. THE STRUCTURAL REARRANGEMENTS ASSOCIATED WITH PAPS BINDING IN THE SULT2A1 SUBUNIT

We propose that the binding of PAPS to SULT2A1 significantly changes the structure of the acceptor binding site, resulting in a change in substrate selectivity?

The crystal structures of SULT2A1 suggest that the binding of PAPS to SULT2A1 can change the substrate specificity of SULT2A1. In this aim, the changes induced by PAPS binding in the structure and function of the SULT2A1 monomer were examined using *in silico* modeling, *in vitro* kinetics, and enzyme binding. The initial observation was with 24(S)-OH-Chol sulfation by SULT2A1, were inconsistencies between the predicted activity and the *in vitro* activity required a new model of SULT2A1. Changes in the structure of the SULT2A1 subunit were examined in detail through side by side comparison of RAL and DHEA binding and conjugation using a wide range of methods. Pharmacophore modeling was performed to determine if the structural and kinetic changes observed were a general pattern in SULT2A1 sulfation of substrates.

A) Sulfation of 24(S)-Chol by SULT2A1

1. Kinetic Analysis of SULT2A1 Sulfation of 24(S)-OH-Chol

24(S)-OH-Chol is an important oxysterol produced in the brain. Physiologically, 24(S)-OH-Chol is an endogenous LXR agonist and is important for cholesterol homeo-

stasis in the brain (Björkhem and Meaney 2004). Sulfation of 24(S)-OH-Chol was tested with all of the major human SULTs. The highest 24(S)-OH-Chol sulfation activity detected was with SULT2A1 and SULT2B1b. Some 24(S)-OH-Chol sulfation activity was also observed with SULT1E1; however the activity was twenty fold less than either SULT2A1 or SULT2B1b (Cook, Duniac-Dmuchowski et al. 2009). SULT2B1b formed only a single monosulfate of 24(S)-OH-Chol while SULT2A1 formed a disulfate (Cook, Duniac-Dmuchowski et al. 2009). After sulfation, reactions were treated with STS to hydrolyze the 3-sulfate to measure the concentration of 24(S)-Chol-24-sulfate. When the monosulfate generated by SULT2B1b was treated with STS, no 24(S)-Chol-24-sulfate was detected; however, when the 24(S)-OH-Chol sulfates generated by SULT2A1 were treated with STS, only one of the two sulfated hydroxyls was sensitive to STS hydrolysis (Fig. 11).

The 24(S)-OH-Chol sulfates were identified by the UAB mass spectrometry core facility. The monosulfates were detected in the negative ion mode as they eluted from the C-18 column by an ion of 481.0 Da and a sulfate ion of 96.9 Da. The disulfate was detected by an ion of 560.1 Da and a sulfate ion of 96.9 Da. The monosulfates generated by SULT2A1 eluted in two peaks; a large peak at 9.0 and a smaller peak at 8.3 min (Fig. 12A). The disulfate generated by SULT2A1 was detected at 7.3 min (Fig. 12B). After STS hydrolysis, no disulfate was detected and only one monosulfate detected, at 8.3 min peak (Fig. 12C). In contrast to SULT2A1, only one monosulfate was generated by SULT2B1b and it eluted from the column at 9.0 min. The monosulfate generated by SULT2B1b was completely hydrolyzed by STS (Fig. 12D). When further fragmentation of the monosulfates was performed, the STS insensitive monosulfate generated an addi-

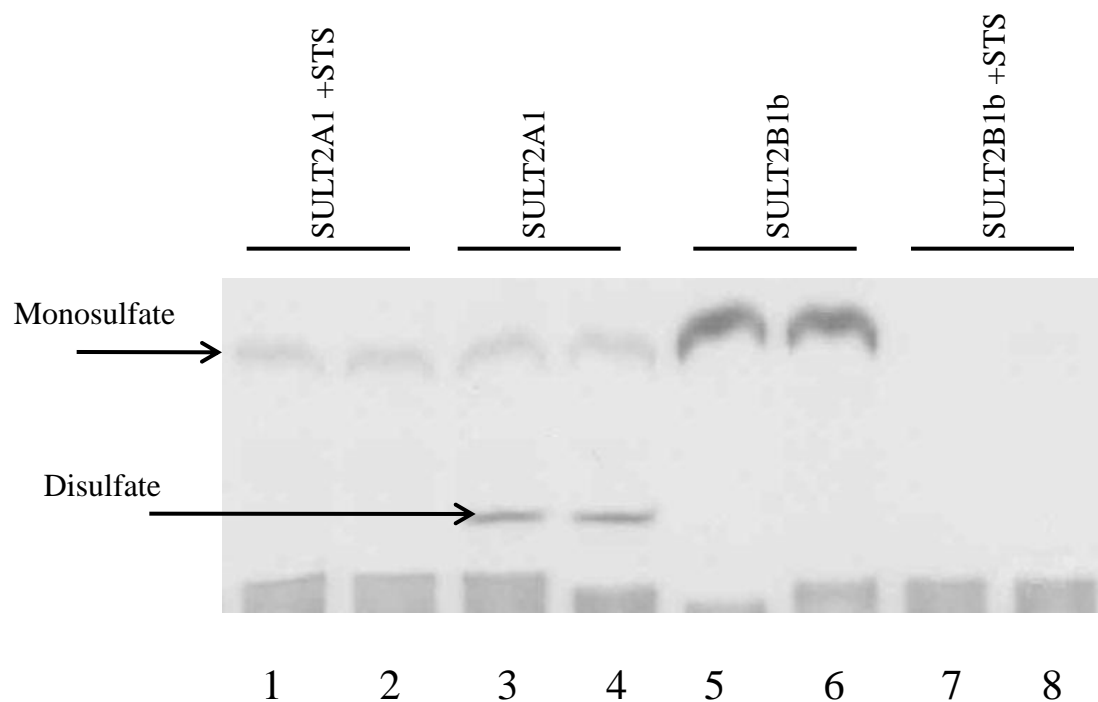


Figure 11. Sulfation of 24(S)-OH-Chol by SULT2A1 and SULT2B1b. Sulfation of 24(S)-OH-Chol by SULT2A1 (lanes 1-4) and SULT2B1b (lanes 5-8) is shown. The concentration of 24(S)-OH-Chol was 20 μ M and [35 S]-PAPS was 10 μ M. After sulfation, lanes 1, 2, 7 and 8 were treated with STS activity. The TLC plate was resolved as described in section I-D-1. Radiolabeled [35 S]-sulfate was detected after 24 h exposure to autoradiograph film.

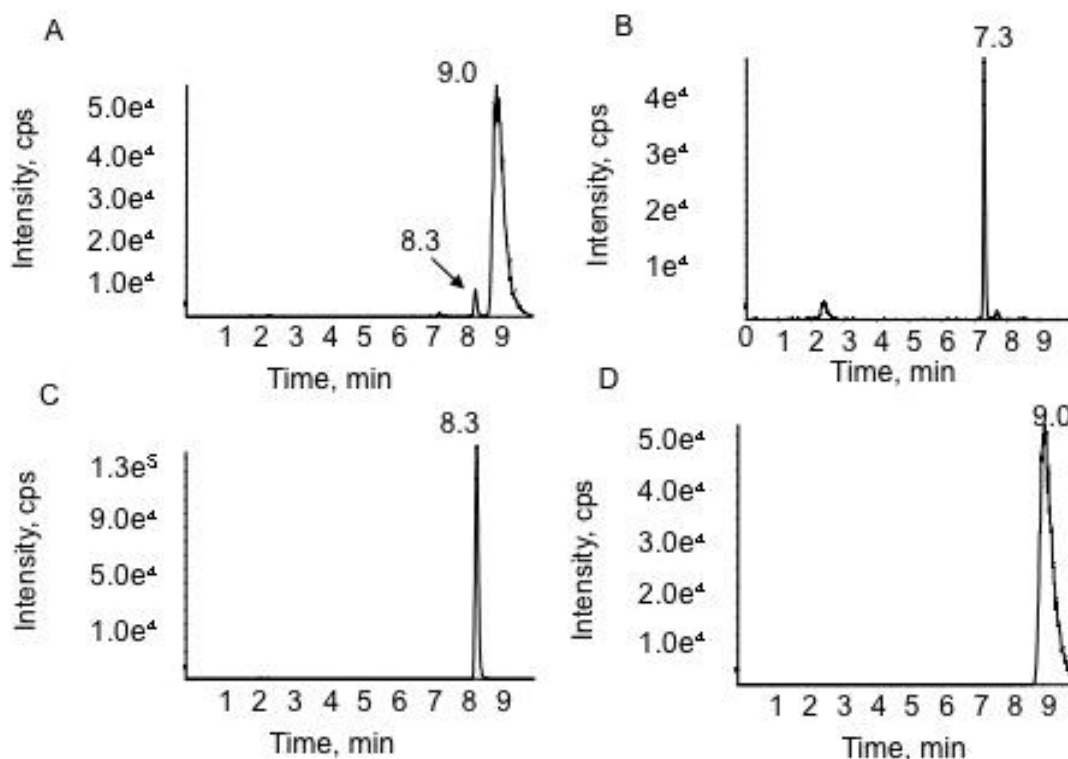


Figure 12. LC/MS/MS of 24(S)-OH-Chol sulfates. The 24(S)-OH-Chol sulfates were identified using LC/MS/MS in the negative ion mode. Monosulfates were detected by a parent ion mass of 481 Da and a sulfate ion of 97 Da. Disulfate was detected by a parent ion mass of 560 Da and a sulfate ion of 97 Da. Panel A) shows the elution of 24(S)-OH-Chol monosulfates generated by SULT2A1. Panel B) represents the elution of 24(S)-OH-Chol disulfate generated by SULT2A1. Panel C) shows the elution of 24(S)-OH-Chol monosulfate generated by STS treatment of the disulfate. Panel D) shows the elution of 24(S)-OH-Chol monosulfate generated by SULT2B1b.

tional fragment of 59.1 Da. The 59.1 Da mass is consistent with the predicted mass of the 3-OH group of 24(S)-Chol-24-sulfate, demonstrating that the STS insensitive monosulfate is the 24(S)-Chol-24-sulfate (Fig. 13). The 24(S)-OH-Chol-3-sulfate is therefore the STS sensitive monosulfate.

SULT2A1 sulfation of 24(S)-OH-Chol had an unusual characteristic with increasing concentrations of 24(S)-OH-Chol. At low concentrations of 24(S)-OH-Chol, disulfate formation was favored over monosulfate formation. As the concentration was increased, the production of disulfate reached a maximum rate at 10 μM and started to decline after 15 μM . Monosulfate was not detected below 0.2 μM and the monosulfate formation reached a maximum rate at 20 μM , with no decrease observed (Fig. 14A). The concentration of 24(S)-Chol-24-sulfate detected after treatment with STS was not statistically different from the level of disulfate. The result indicates that almost all of the monosulfate formed in the reaction was the 24(S)-OH-Chol-3-sulfate (Fig. 14B). To further investigate the mechanism for the formation of disulfate, the individual monosulfates were synthesized. SULT2A1 activity was assayed for each of the monosulfates (Fig. 15). The K_m for the formation of disulfate from 24(S)-OH-Chol-3-sulfate and 24(S)-Chol-24-sulfate was 8.0 and 0.1 μM , respectively. The K_m and V_{max} values for the reactions are shown in Table 1.

In summary, the sulfation of 24(S)-OH-Chol by SULT2A1 is a multi-step processes. The first step is the binding of 24(S)-OH-Chol to SULT2A1 followed by sulfation of either the 3-OH or 24-OH group at similar K_m s (Table 1). After sulfation, the monosulfates are released from SULT2A1. The release of the monosulfates is demonstrated by the fact that the formation of disulfate decreased at high concentrations of

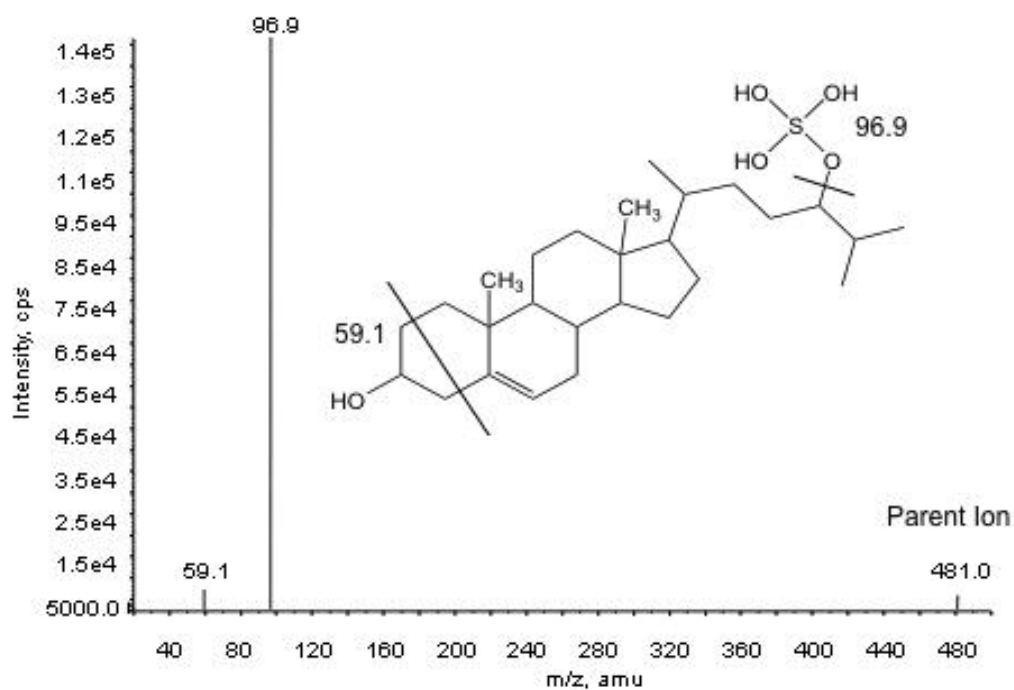


Figure 13. Mass fragmentation of 24(S)-Chol-24-sulfate. Fragmentation of the 24(S)-Chol-24-sulfate was identified by an initial parent ion of 481 Da, a sulfate ion of 97 Da, and the 3-OH ion of 59 Da. Fragmentation of the 24(S)-OH-Chol-3-sulfate resulted in detection of only the parent ion and sulfate ion.

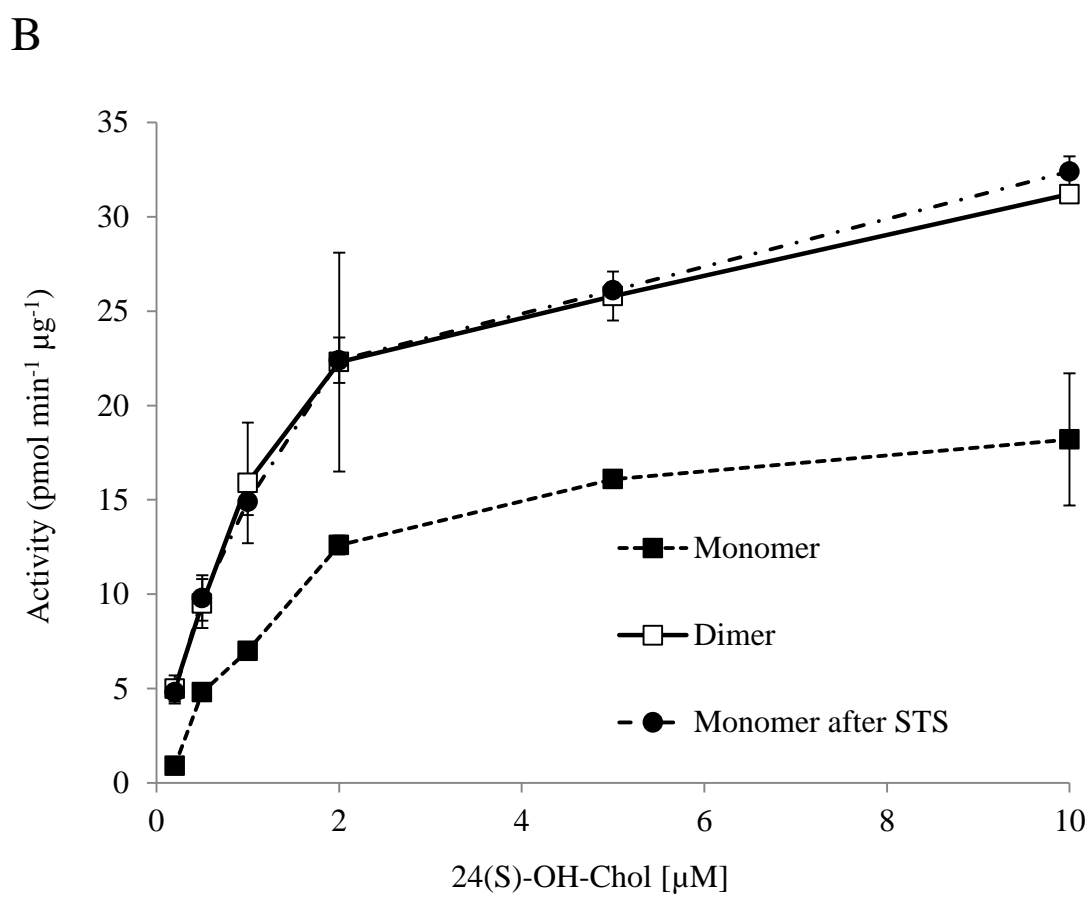
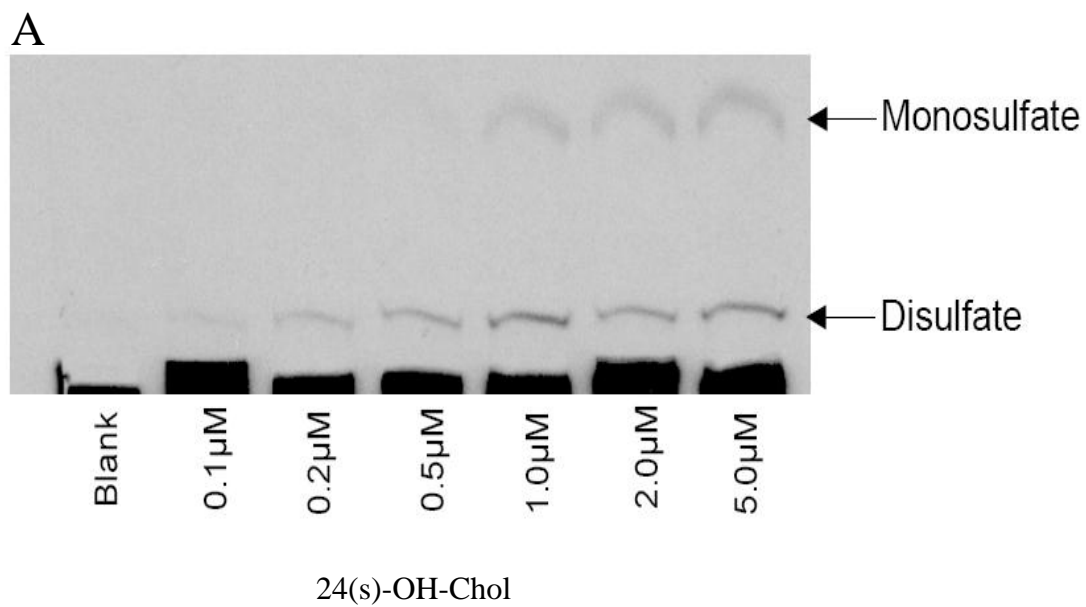


Figure 14. Sulfation of 24(S)-OH-Chol by SULT2A1. Increasing concentrations of 24(S)-OH-Chol was assayed with SULT2A1 and 10 μM [^{35}S]-PAPS. Each reaction was performed as described in section I-D-1. For STS treatment, the aqueous phase was treated with STS activity for 30 min at 37° C. Reactions were spotted onto a TLC plate and the sulfated products were resolved as described in the Methods. A) Radiolabeled [^{35}S]-sulfate was identified after 24 h exposure to autoradiograph film. The bands were then scraped and quantified by scintillation spectroscopy. B) Product formation was plotted vs. 24(S)-OH-Chol concentration: monosulfate (black squares), disulfate (white squares), and the residual monosulfate after STS (black circles). The approximate K_m and V_{max} were derived using non-linear regression analysis in the Enzyme Kinetics program and are presented in Table 1. Each concentration was evaluated 4 times and represented as the mean \pm SEM.

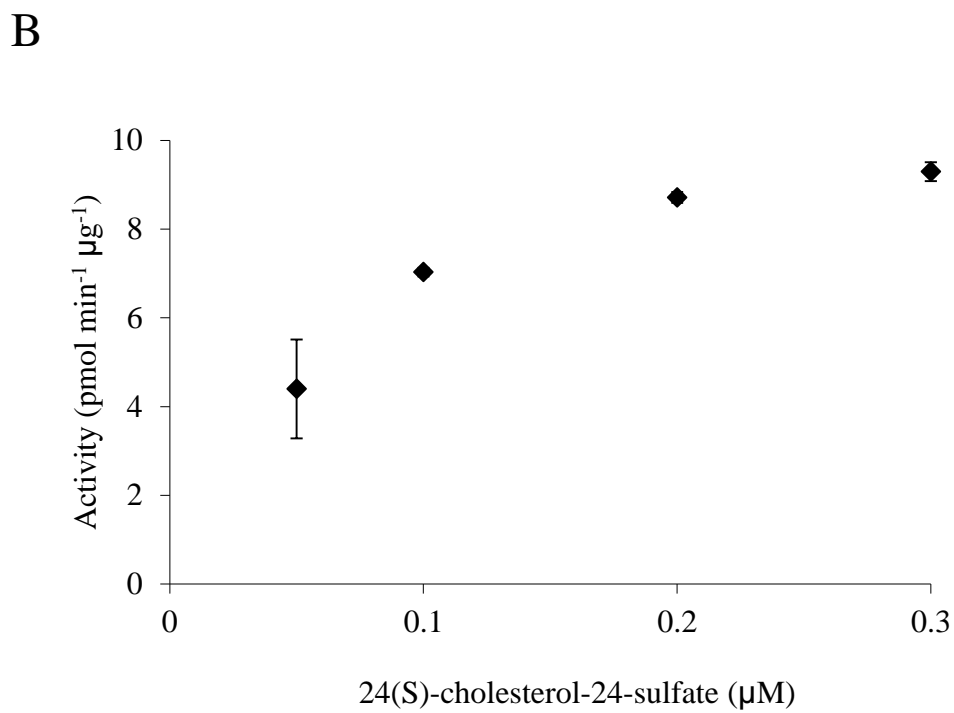
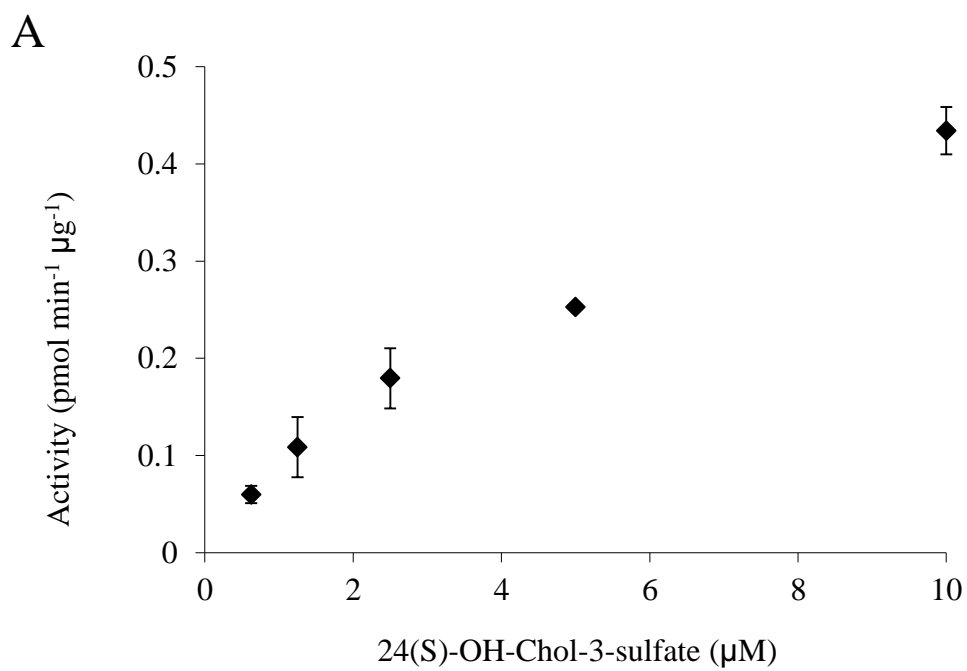


Figure 15. Sulfation of 24(S)-OH-Chol monosulfates. [³⁵S]-24(S)-OH-Chol-3-sulfate and [³⁵S]-24(S)-Chol-24-sulfate were generated as described in section I-D-6-a. The formation of disulfate with increasing concentrations of A) 24(S)-OH-Chol-3-sulfate and B) 24(S)-Chol-24-sulfate were assayed as described in section I-D-6-b. Each concentration was evaluated in triplicate and reported as the mean ± SEM. The Km and Vmax values were determined using non-linear regression analysis and are shown in Table 1.

24(S)-OH-Chol (greater than 20 μM). The 24(S)-Chol-24-sulfate then binds to SULT2A1 with a high affinity and is sulfated to form a disulfate (Table 1). The affinity for 24(S)-Chol-24-sulfate is greater than the affinity of 24(S)-OH-Chol for SULT2A1. Because of the poor affinity of 24(S)-OH-Chol-3-sulfate for SULT2A1 (Table 1), the 24(S)-OH-Chol-3-sulfate accumulates as the predominate monosulfate. The K_m (2.0 μM) for the formation of monosulfate with 24(S)-OH-Chol generated by SULT2A1 is approximately equal to the formation of 24(S)-OH-Chol-3-sulfate by SULT2A1. The formation of disulfate from 24(S)-Chol-24-sulfate had a K_m of 0.1 μM , indicating that the rate limiting step in the formation of disulfate is the sulfation of the 24-OH group. The K_m for the formation of disulfate from 24(S)-OH-Chol by SULT2A1 is therefore equal to the K_m for formation of 24(S)-Chol-24-sulfate by SULT2A1 (Fig. 16).

| Substrate | Product | K_m (μM) | V_{max} (nmol/min/mg) | V_{max}/K_m |
|------------|-------------|-------------------------|-----------------------------------|----------------------|
| 24(S)-OH | Monosulfate | 2.0 ± 0.4 | 19.6 ± 4.1 | 9.8 |
| 24(S)-OH | Disulfate | 1.5 ± 0.7 | NA | NA |
| 3-sulfate | Disulfate | 0.1 ± 0.06 | 9.2 ± 1.3 | 92 |
| 24-sulfate | Disulfate | 8.0 ± 2.1 | 0.9 ± 0.3 | 10 |

Table 1. Kinetic constants for 24(S)-OH-Chol sulfation by SULT2A1. The K_m and V_{max} were determined using the Enzyme Kinetics program. Each reaction was performed 4 times and presented with the mean \pm SEM.

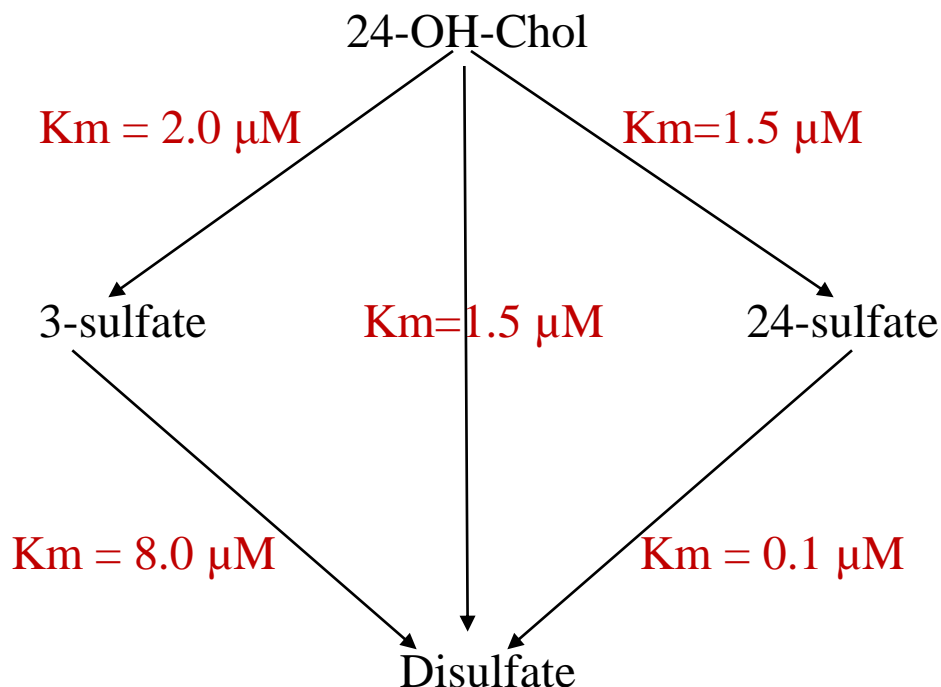


Figure 16. Sulfation pathway of 24(S)-OH-Chol by SULT2A1. The K_m s for the conversion of 24(S)-OH-Chol to disulfate by SULT2A1 are shown in the pathway schematic above. Sulfation of the 3-OH position causes an accumulation of 24(S)-OH-Chol-3-sulfate as the dominate monosulfate. This is because of the poor affinity of 24(S)-OH-Chol-3-sulfate to SULT2A1. The rate limiting step in the formation of disulfate is sulfation of the 24-OH position. The 24(S)-Chol-24-sulfate is rapidly converted to disulfate due to the high affinity of 24(S)-Chol-24-sulfate to SULT2A1. Because the 24(S)-Chol-24-sulfate is rapidly disulfated, very little 24(S)-Chol-24-sulfate accumulates. All the K_m and V_{max} values are shown in Table 1.

2. *Molecular Modeling of 24(S)-OH-Chol and Monosulfates to the SULT2A1 Active Site*

Docking of 24(S)-OH-Chol and the monosulfates to SULT2A1 was examined using MOE. The closed SULT2A1 model was made from the SULT2A1 crystal structure generated with bound PAP (1EFH). A sulfate was added to the 5'phosphate of PAP to convert the PAP to PAPS. The model was then protonated and energy minimized. 24(S)-OH-Chol was then docked to the model at the acceptor binding site. The top ten lowest energy orientations of 24(S)-OH-Chol were ranked based on the predicted binding free energy (BFE). The BFE represents a relative ranking of the predicted docking orientations. The orientations were then examined by cluster analysis to identify the major binding orientations of 24(S)-OH-Chol. The cluster analysis grouped the top ten orientations based on their positions and orientations relative to each other. For two orientations to be classified in the same group, the RMSD between the two orientations had to be less than 2.0 Å. The lowest energy binding was with the 24-OH group in position for sulfation with a BFE of -10.2 kJ (Fig. 17A). The lowest energy with the 3-OH group in position for sulfation had a BFE of -9.7 kJ (Fig. 17B). The 24(S)-OH-Chol-3-sulfate docking showed that in the lowest energy orientation, 24(S)-OH-Chol-3-sulfate docked with the 24-OH group in position for sulfation at a BFE of -8.7 kJ (Fig. 17C).

The docking of 24(S)-Chol-24-sulfate to SULT2A1 predicted that the monosulfate was not a substrate for SULT2A1. The lowest energy orientation showed the 24(S)-Chol-24-sulfate was on the surface of the active site with an electrostatic interaction between the 24-sulfate group of 24(S)-Chol-24-sulfate and the K138 of SULT2A1 with a predicted BFE of -13.2 kJ (Fig. 18). The interaction of the 24-sulfate with K138 was ob-

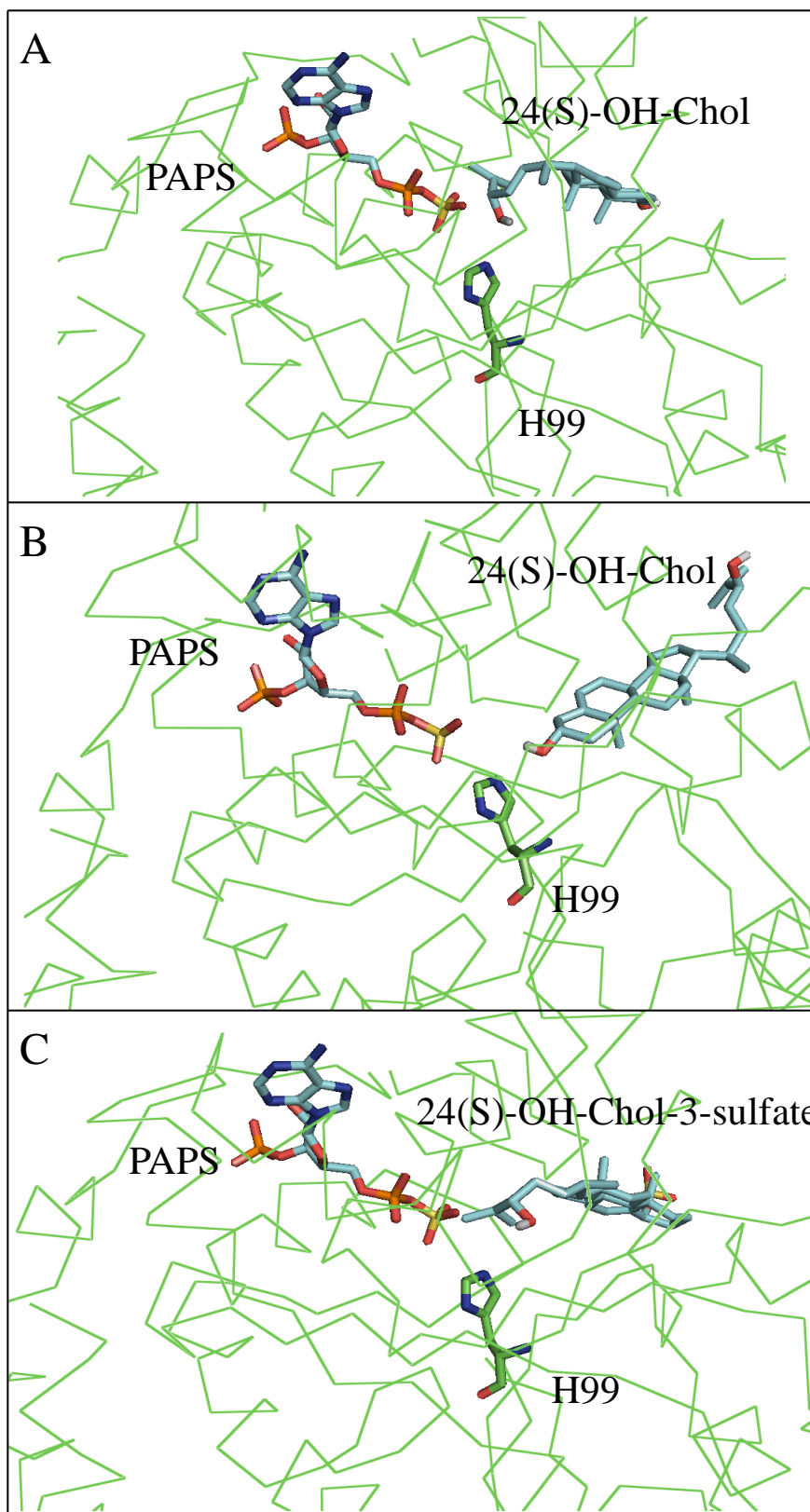


Figure 17. Modeling of 24(S)-OH-Chol in SULT2A1. 24(S)-OH-Chol and 24(S)-OH-Chol-3-sulfate were docked to a model of the SULT2A1, based on the SULT2A1 crystal structure generated with bound PAP (1EFH), as described in section I-E. A) The lowest energy structure of 24(S)-OH-Chol had a predicted BFE of -10.2 kJ and a hydrogen bond between the 24-OH position and the H99. B) Cluster analysis of the top 10 orientations for 24(S)-OH-Chol showed a second orientation for 24(S)-OH-Chol with a predicted BFE of -9.7 kJ and a hydrogen bond between the 3-OH position and the H99. C) The lowest energy structure for 24(S)-OH-Chol-3-sulfate monosulfate had a BFE of -8.7 kJ and a hydrogen bond with the H99. SULT2A1 is in green and the ligand and PAPS is in cyan, with the active site H99 and the ligands in stick format and SULT2A1 in ribbon format.

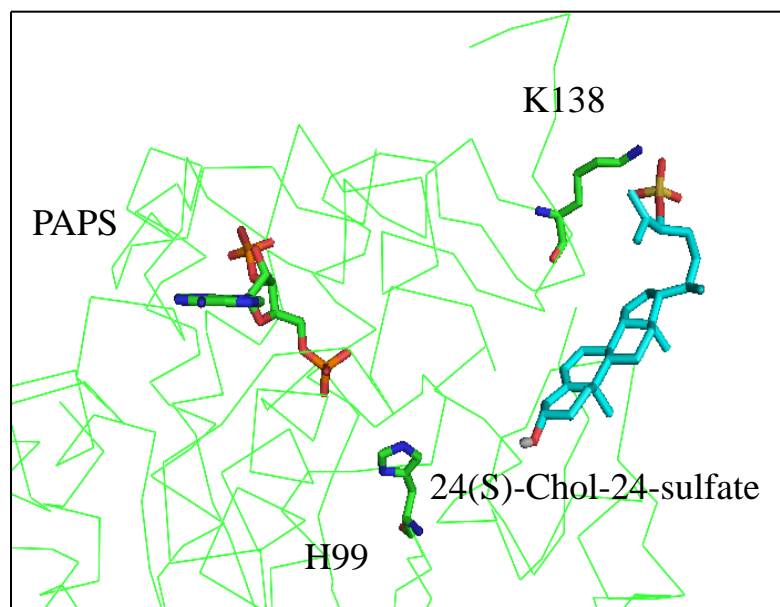


Figure 18. Molecular modeling of 24(S)-Chol-24-sulfate to SULT2A1 with PAPS. The 24(S)-Chol-24-sulfate was docked to SULT2A1 as described in section I-E. The lowest predicted BFE was -13.2 kJ. The docking showed no competent orientation for the formation of disulfate in the top ten lowest energy structures. 24(S)-Chol-24-sulfate and PAPS are in cyan and SULT2A1 is green. H99, K138, PAPS, and 24(S)-Chol-24-sulfate are shown in stick format with the SULT2A1 backbone in ribbon format.

served in nine of the top ten orientations, none of which were able to form a competent orientation for sulfation of the 3-OH group. The docking results are inconsistent with the kinetic data because the kinetic data demonstrated that the 24(S)-Chol-24-sulfate was a better substrate for SULT2A1 than 24(S)-OH-Chol or 24(S)-OH-Chol-3-sulfate and the docking predicted that 24(S)-Chol-24-sulfate was not a substrate.

Examination of the SULT2A1 crystal structures showed that the binding of PAPS caused a significant structural rearrangement in SULT2A1. The structural change in SULT2A1 was most significant in the region loop 3 (L224 to W259) and is likely caused by an electrostatic interaction between the 3'-phosphate of PAPS and R247 (Fig. 8). To model the structural rearrangement of the SULT2A1 active site by PAPS, an open model of SULT2A1 was made using the SULT2A1 crystal generated with bound DHEA (1J99). The 1J99 SULT2A1 crystal structure has the highest resolution of all the SULT2A1 structures without PAP. Compared to the 1EFH structure, loop 3 in 1J99 is extended into the solvent by 10 Å and the active site was more "open". When 24(S)-Chol-24-sulfate was docked to the open model of SULT2A1, the lowest energy orientation had an electrostatic interaction between the K138 and the 24-sulfate group of 24(S)-Chol-24-sulfate with a BFE of -13.8 kJ (Fig. 19), similar to the docking observed in the closed model. In contrast to the closed model, 24(S)-Chol-24-sulfate was in the active site of SULT2A1 with the 3-OH group 2.8 Å from the H99 in a catalytic orientation for sulfation. The BFE for 24(S)-Chol-24-sulfate was -13.8 kJ, significantly lower than the BFE for 24(S)-OH-Chol (-10.2 kJ) or 24(S)-OH-Chol-3-sulfate (-8.7 kJ). These results are consistent with the calculated K_m s for 24(S)-OH-Chol sulfation by SULT2A1 (Fig. 16).

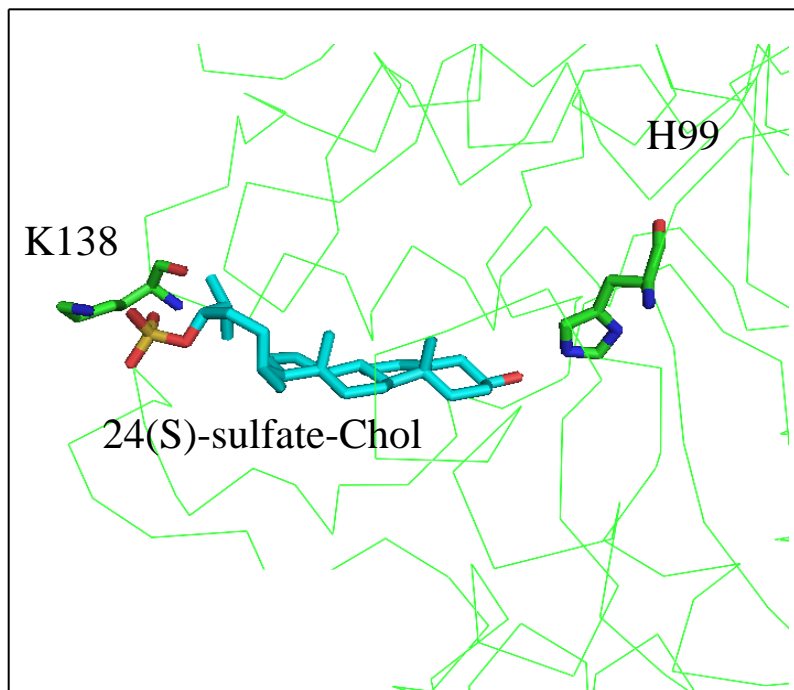


Figure 19. Docking of 24(S)-Chol-24-sulfate to the open model of SULT2A1. The SULT2A1 model was generated using the SULT2A1 crystal structure with bound DHEA (1J99) and the docking of 24(S)-Chol-sulfate to the model was performed as described in section I-E. The lowest energy predicted had a BFE of -13.8 kJ and a predicted hydrogen bond with the H99. The 24(S)-Chol-24-sulfate and PAPS are in cyan and SUTL2A1 is in green. The H99, K138, 24(S)-Chol-24-sulfate, and PAPS are in stick format and the SULT2A1 backbone is in ribbon format.

B) Docking of DHEA and RAL to the Open and Closed Models of SULT2A1

Kinetic and computational modeling of 24(S)-OH-Chol demonstrated that structural rearrangement of SULT2A1 upon the binding of PAPS has a significant influence on the activity of SULT2A1. To examine the change in activity caused by PAPS binding, the substrates DHEA and RAL were selected for docking, kinetic and binding analysis. Both compounds are reported substrates for SULT2A1 with similar K_m s, but have significant structural differences. DHEA is a small planar steroid while RAL is a much larger compound with a long side chain (Fig. 3). The docking of DHEA and RAL was evaluated with the closed model made with the SULT2A1 crystal structure generated with bound PAP (1EFH) and the open model made with the SULT2A1 crystal structure with bound DHEA (1J99).

Docking of DHEA to the open and closed models of SULT2A1 showed no preference for either model. In both models, the DHEA molecule formed a pi-stacking interaction with W76 that stabilized DHEA in an orientation that placed the 3-OH group in position to form a hydrogen bond with H99 that allowed sulfation. The predicted BFE of binding was -10.9 kJ for the open and -11.6 kJ for the closed model (Fig. 20). Based upon the docking models, SULT2A1 shows a random Bi Bi reaction mechanism during sulfation of DHEA.

In contrast to DHEA, RAL docking showed a significant change in the predicted affinity between the open and closed models. RAL was able to bind to the open model with a BFE of -11.1 kJ and a predicted hydrogen bond between H99 and the thiophenol OH group (Fig. 21A) and would be catalytically competent for sulfation. However, when RAL was docked to the closed SULT2A1 model, no catalytically competent orientation

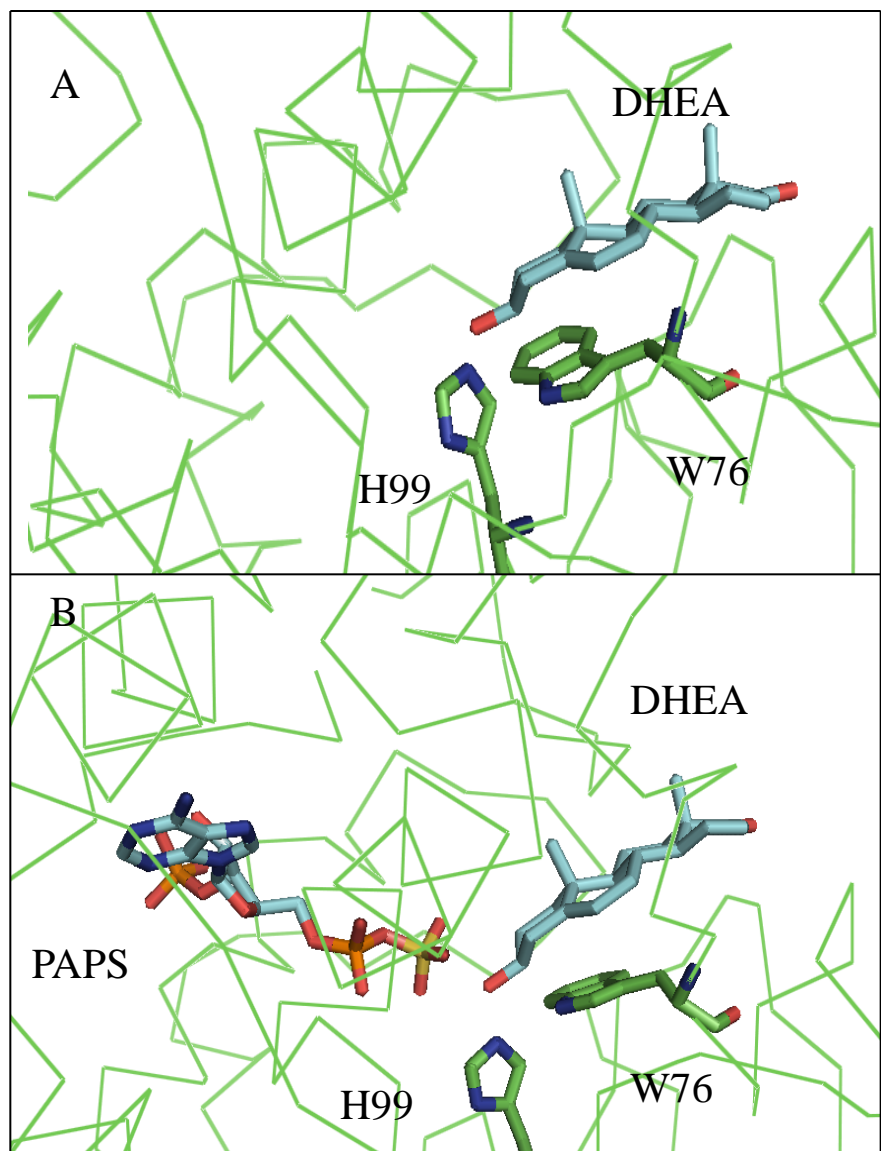


Figure 20. Molecular docking of DHEA to the open and closed models of SULT2A1. The docking of DHEA to the open and closed models of SULT2A1 was performed as described in section I-E. The open model is based on the SULT2A1 crystal structure with DHEA (1J99). The closed model is based on the SULT2A1 crystal structure with PAP (1EFH). A) The lowest predicted orientation for DHEA with the A) open model and B) closed model. The BFE was -10.9 kJ for the open model and -11.6 kJ for the closed model. In both models, a hydrogen bond was predicted between the H99 and 3-OH group. DHEA and PAPS are in cyan and SULT2A1 is in green. The H99, W76, DHEA and PAPS are in stick format with the SULT2A1 backbone in ribbon format.

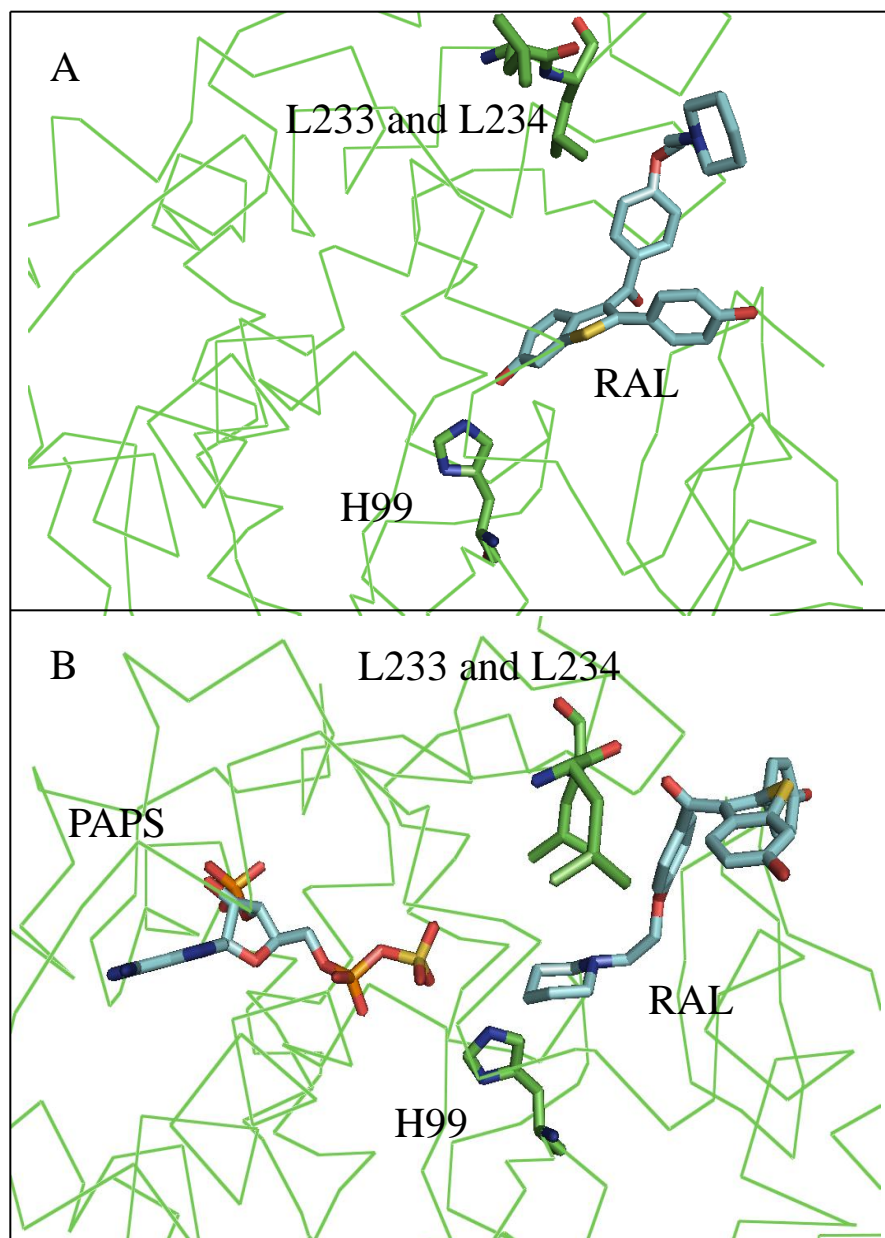


Figure 21. Molecular docking of RAL to the open and closed models of SULT2A1. RAL was constructed and docked to the open and closed models of SULT2A1 as described in section I-E. A) The lowest predicted orientation for RAL with the A) open model and B) closed model. In the open model, RAL had a BFE of -11.1 kJ and a hydrogen binding between the H99 and the OH group of the thiophenol ring. RAL had a BFE of -9.1 kJ in the closed model. No hydrogen bond was predicted in the closed docking. PAPS and RAL are cyan and SULT2A1 is green. The H99, L33, L234, RAL, and PAPS are in stick format and the backbone of SULT2A1 is in ribbon format.

was predicted in any of the top ten orientations. The most common orientation placed the core of the RAL structure on the surface with the side chain in the active site and a BFE of -9.1 kJ (Fig. 21B). RAL was blocked from the active site by L233 and L234 in loop 3 in the closed SULT2A1 model. In the open model loop 3 is extended into the solvent by 10 Å compared to the closed model and the residues L233 and L234 do not interfere with RAL binding. When PAPS binds, the loop 3 close on the active site and the leucines restricts access to the active site.

C) DHEA and RAL Sulfation by SULT2A1

1. *Steady-State Kinetics of DHEA and RAL Sulfation by SULT2A1*

DHEA sulfation by SULT2A1 was assayed using a chloroform extraction assay with [³H]-DHEA as described in the Methods. To accurately measure the K_m and V_{max} of the reaction, the DHEA sulfation activity was measured at different concentrations of DHEA and PAPS (Fig. 22A). Kinetic constants were determined using two substrate double reciprocal plots, and the K_m s were calculated to be 1.7 μM for DHEA and 0.2 μM for PAPS with a V_{max} of 17.8 $\text{nmol min}^{-1} \text{mg}^{-1}$. The double reciprocal plots of DHEA sulfation intercepted on the x-axis, indicating that binding of PAPS had no change on the affinity of DHEA and the same characteristic was observed for PAPS. These results are consistent with a random-order Bi Bi reaction mechanism as predicted by the modeling.

For RAL sulfation, a TLC method was utilized with radiolabeled [³⁵S]-PAPS as described in the Methods. Kinetic constants were determined using two substrate double reciprocal plots. The K_m s were 1.3 μM for RAL and 1.1 μM for PAPS, with a V_{max} of

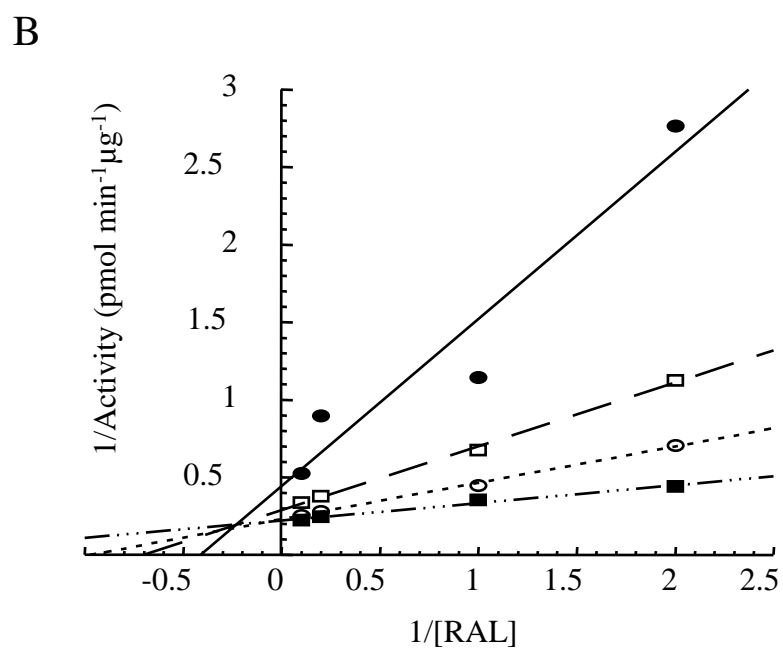
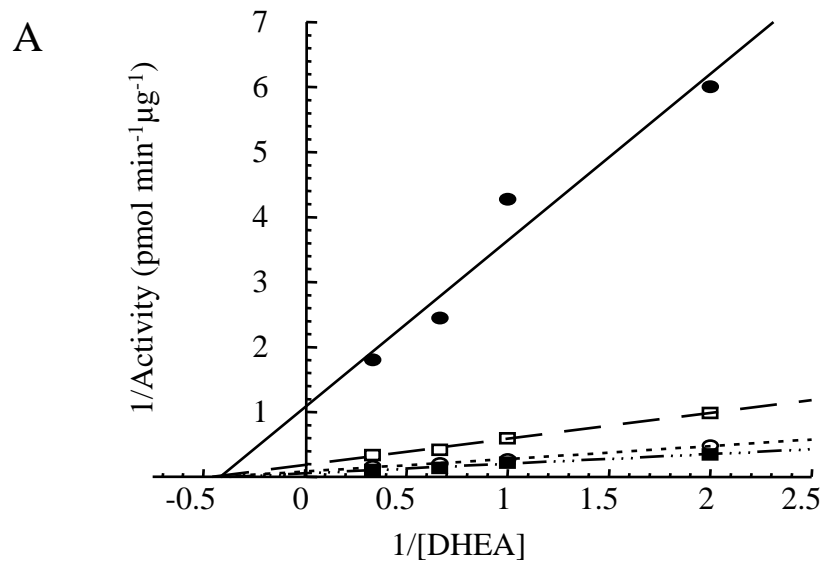


Figure 22. Double reciprocal plots for DHEA and RAL sulfation by SULT2A1. DHEA sulfation was examined with [³H]-DHEA and chloroform extraction assay as described in section I-F. RAL sulfation was examined with a TLC assay using [³⁵S]-PAPS as described in section I-H. Each concentration was assayed in duplicate. The kinetic constants were determined by the re-plots of the intercepts and slopes vs. the concentration of PAPS.

4.3 nmol min⁻¹ mg⁻¹ (Fig. 22B). A significant increase in the K_m for PAPS demonstrates that binding of RAL likely changes the affinity of the enzyme for PAPS. This suggests that the binding of RAL inhibits the closing of SULT2A1 when PAPS binds and inhibiting PAPS affinity for SULT2A1.

2. *Pre-Steady State Kinetics of DHEA and RAL by SULT2A1*

After the kinetic constants for the steady state sulfation of DHEA and RAL were determined, pre-steady state kinetics were examined to determine the order of binding in the sulfation reactions. The pre-steady state kinetics of DHEA showed a non-linear burst of DHEAS formation in the first 10 sec, followed by a linear increase with time for DHEA sulfation activity (Fig. 23A). The initial non-linear burst was 10 pmol of DHEAS, equal to the pmol of SULT2A1 active sites in the reaction. These results indicate that the burst is a single turnover of SULT2A1 and the linear increase was the steady state activity of SULT2A1. RAL pre-steady state activity was examined with the TLC method used to evaluate RAL steady state kinetics (Fig. 23B). When the reaction was initially saturated with RAL, there was an initial non-linear burst of RAL-sulfate formation, followed by a linear formation with time of RAL-sulfate. As observed for DHEA, the non-linear burst was 10 pmole of product; equal to the active sites of SULT2A1 in the reaction. These results indicate that the burst represents a single turnover and the linear curve is the steady state. In contrast to DHEA, when SULT2A1 was initially saturated with PAPS, no burst of activity observed when RAL was added. This demonstrates that RAL cannot bind to the active site when PAPS binds first. PAPS must dissociate from the enzyme in order for RAL to bind. These results show that SULT2A1

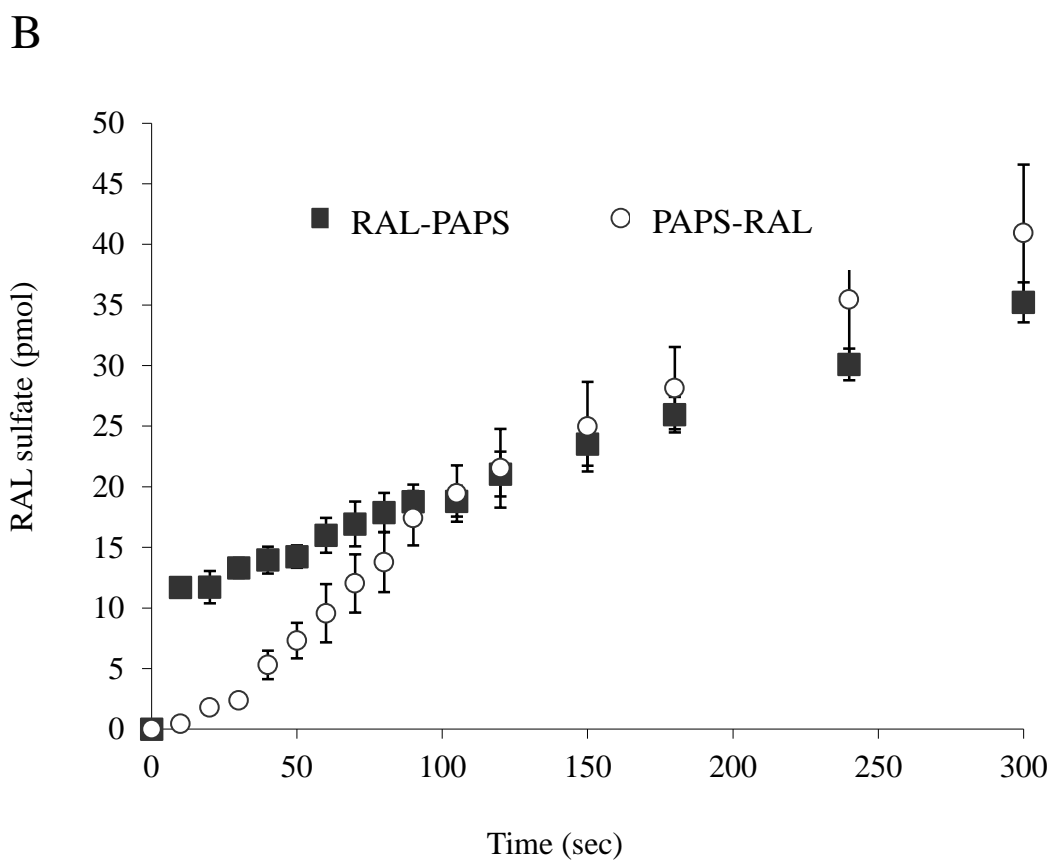
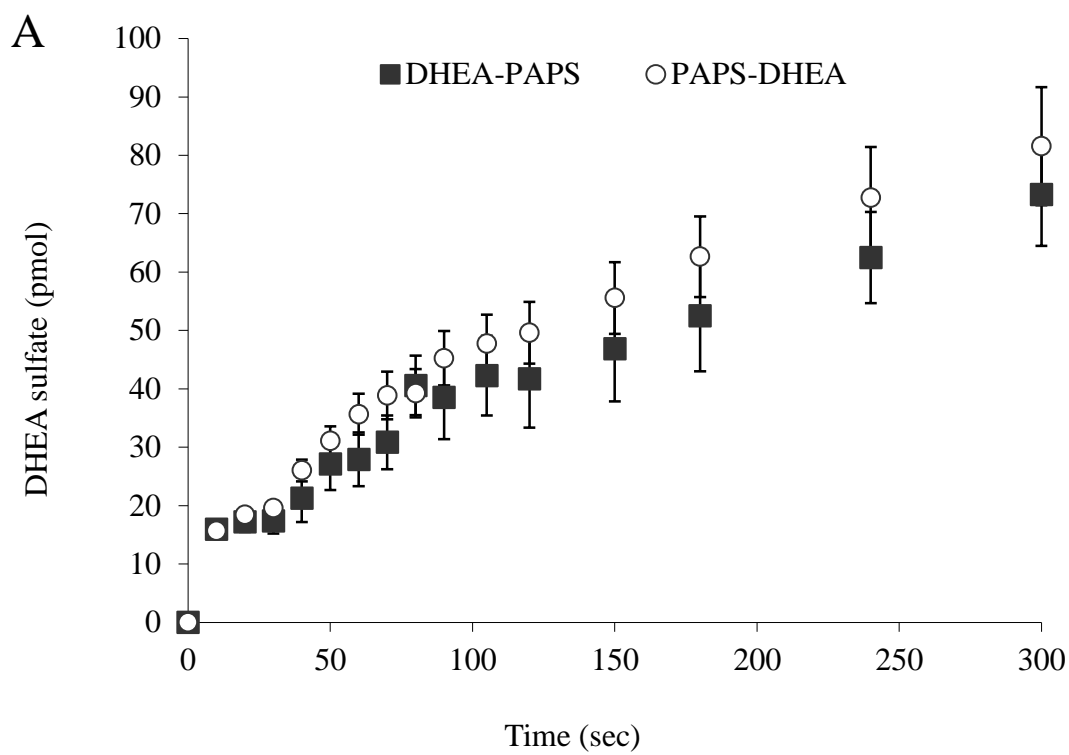


Figure 23. Pre-steady state kinetics of DHEA and RAL sulfation by SULT2A1. Pre-steady state kinetics were assayed with 10 pmol of SULT2A1. A) DHEA pre-steady state kinetics were performed using a chloroform extraction assay described in section I-G. B) RAL pre-steady state kinetics were performed using the TLC method described in section I-I. Each reaction was initiated with the addition of PAPS (white circles) or sulfate acceptor (black squares). Each reaction was evaluated in triplicate and presented as the mean \pm SEM.

sulfation of DHEA is a random ordered Bi Bi reaction mechanism while SULT2A1 sulfation of RAL is an ordered reaction mechanism with RAL as the leading substrate.

The RAL pre-steady state kinetics study was repeated, with different concentration of SULT2A1 to confirm that the initial burst was proportional to the number of SULT2A1 active sites. At all concentrations of SULT2A1, when SULT2A1 was saturated with RAL a burst of product was observed in the first 10 sec and amount of product formed in the burst was equal to the active sites of SULT2A1 in the reaction. These results confirm that the burst is a single turnover. At all concentrations when the reaction was saturated with PAPS first, RAL could not bind to the enzyme and no activity was observed until the PAPS dissociated from SULT2A1 and RAL bound to the active site (Fig. 24).

D) K_d and Stoichiometry Determination of PAPS, PAPS, DHEA, and RAL Binding to SULT2A1

The intrinsic fluorescence of SULT2A1 was used to measure the affinity and stoichiometry of binding for PAPS, PAP, DHEA, and RAL. The intrinsic fluorescence of a protein is dependent on the local environment of the aromatic residues. When ligands bind to an enzyme, the binding can bind directly to an aromatic residue or cause a structural change that changes the local environment of some of the aromatic residues. These interactions can change the intrinsic fluorescence of a protein and can be used to characterize binding of a ligand. By titrating a ligand to the protein, the K_d and stoichiometry of binding can be determined as described in the Methods. PAPS had a K_d of 180 nM and PAP had a K_d of 240 nM for binding SULT2A1 based on a single binding site model

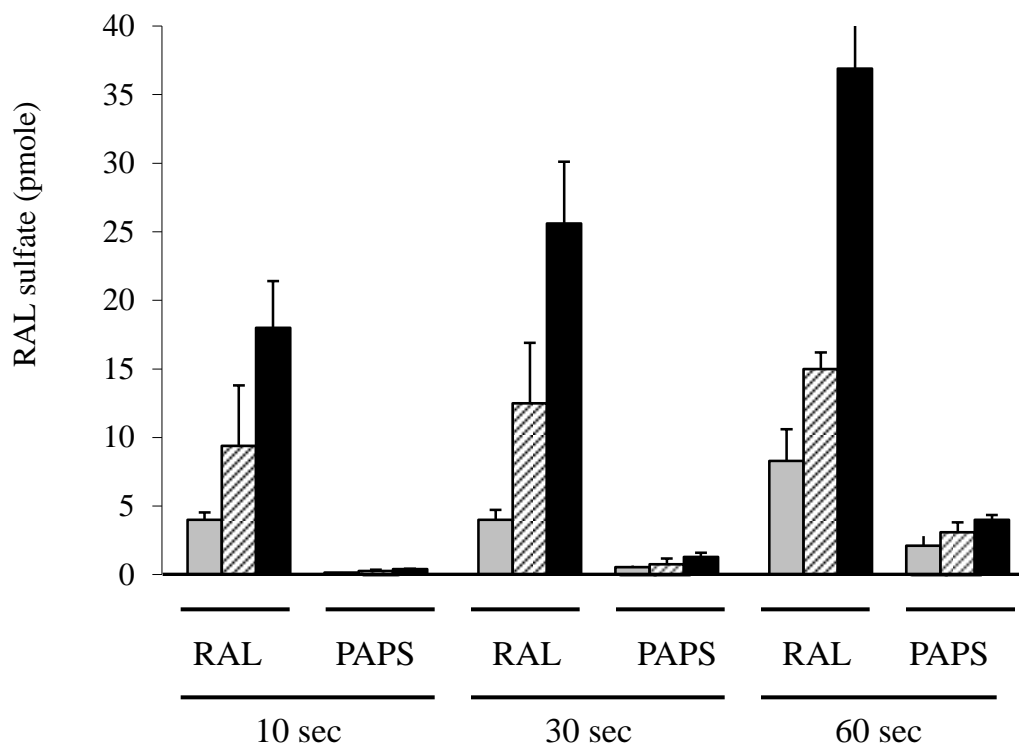


Figure 24. SULT2A1 concentration dependent pre-steady state kinetics. Reactions were evaluated using the methods described in section I-I. The reaction were performed in 300 μ L of buffer and sampled at 10, 30, and 60 sec. Each reaction contained 20 μ M RAL, 10 μ M PAPS, and 4 pmol (grey bars), 8 pmol (striped bars), or 16 pmol (black bars) of SULT2A1. Reactions were evaluated in triplicate and presented as the mean \pm SEM.

(Fig. 25). The affinity of PAPS was similar to the K_m for PAPS calculated in DHEA sulfation. To determine the ratio of binding, the concentration of SULT2A1 was increased to at least 5 times the K_d . At this concentration of SULT2A1, ~100% of the ligand will bind with each titration and the concentration of free ligand will be very small. When the concentration of ligand surpasses the concentration of binding sites, no additional ligand will bind to SULT2A1 and the intrinsic fluorescence will not change. The stoichiometry of binding was determined by the ratio of ligand to enzyme where no more change in fluorescence was observed with increasing PAPS or PAP indicating that the active sites were saturated. Both PAPS and PAP had a stoichiometry of 1:1 to SULT2A1 (Fig. 26).

In contrast to PAPS, the titration of DHEA to SULT2A1 indicated there was not a normal single binding site as was observed with PAPS and PAP. The intrinsic fluorescence titration data indicated that there are two binding sites for DHEA in SULT2A1. The calculated K_d was 240 nM for the high affinity site and 1400 nM for the low affinity site (Fig. 27). When a saturating concentration of PAP (10 μ M) was added to the solution, the titration curve of DHEA to SULT2A1 showed only a single binding site with a K_d of 240 nM. These results indicate that the binding of PAP, and by extension PAPS, results in the loss of the low affinity binding site but does not alter the high affinity binding site.

Titration of DHEA to a high concentration of SULT2A1 showed two molecules of DHEA bound to each subunit of SULT2A1 (Fig. 28A). The stoichiometric results support the two binding sites observed in the affinity titrations of DHEA. When a saturating concentration of PAP was added to the solution, the second binding site was lost and only a single DHEA molecule could bind to each subunit (Fig. 28C). To confirm the

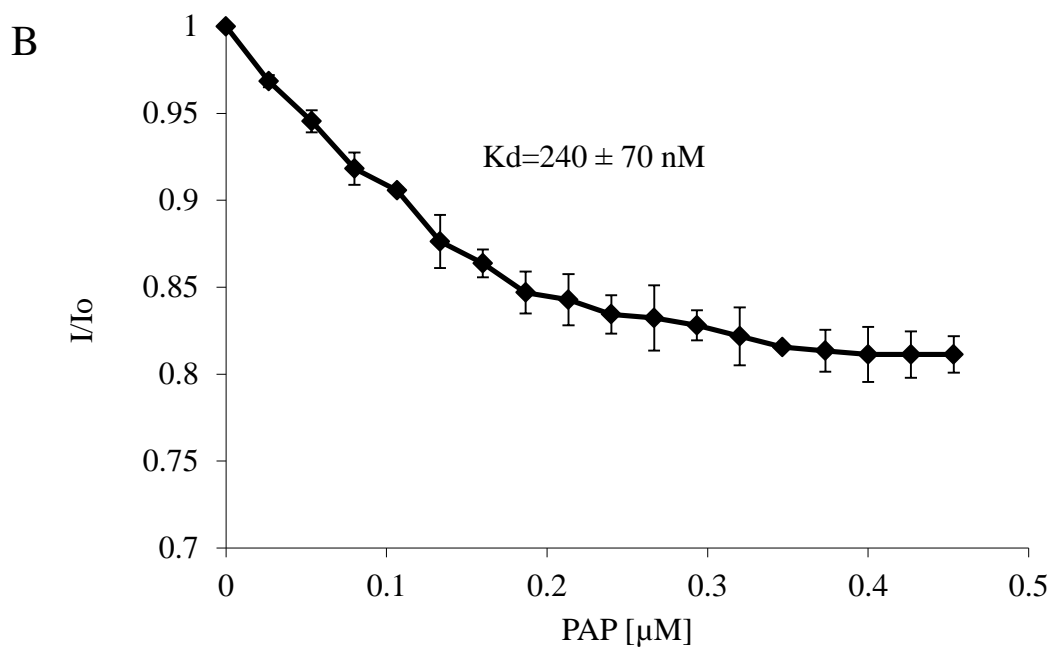
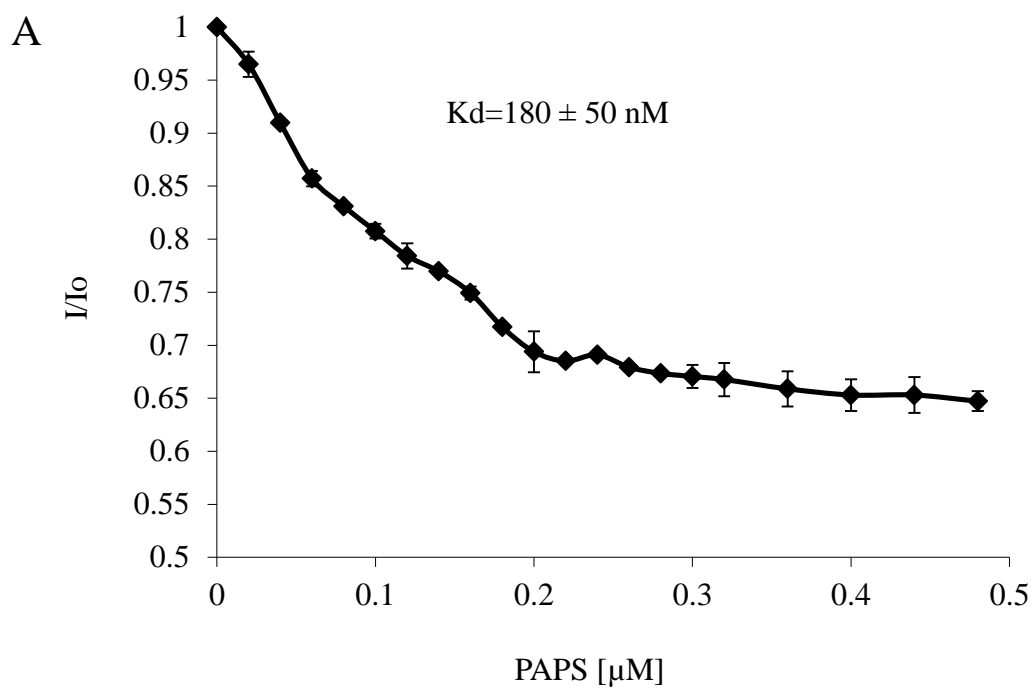


Figure 25. K_d determination for the co-substrate PAPS and inactive co-factor PAP by intrinsic fluorescence titration. PAPS and PAP were titrated to 50 nM SULT2A1 in PBS at RT as described in section I-J. The change in fluorescence was normalized to the initial fluorescence and plotted vs. the concentration of A) PAPS or B) PAP. The K_ds were determined in KaleidaGraph using non-linear analysis with a single binding site model. Each titration was evaluated in triplicate and presented as the mean \pm SEM

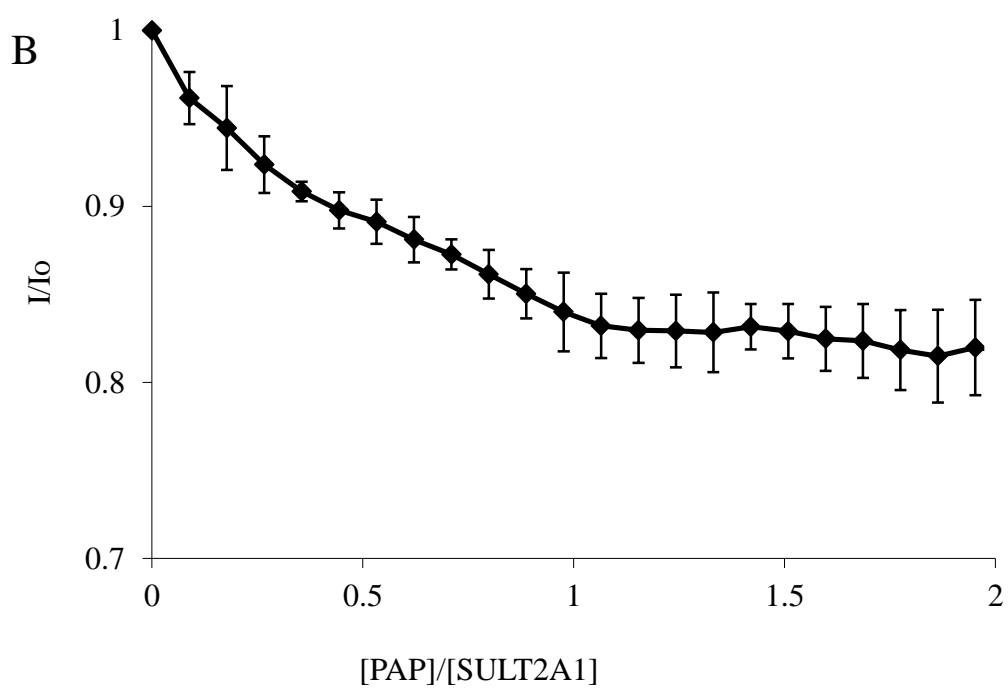
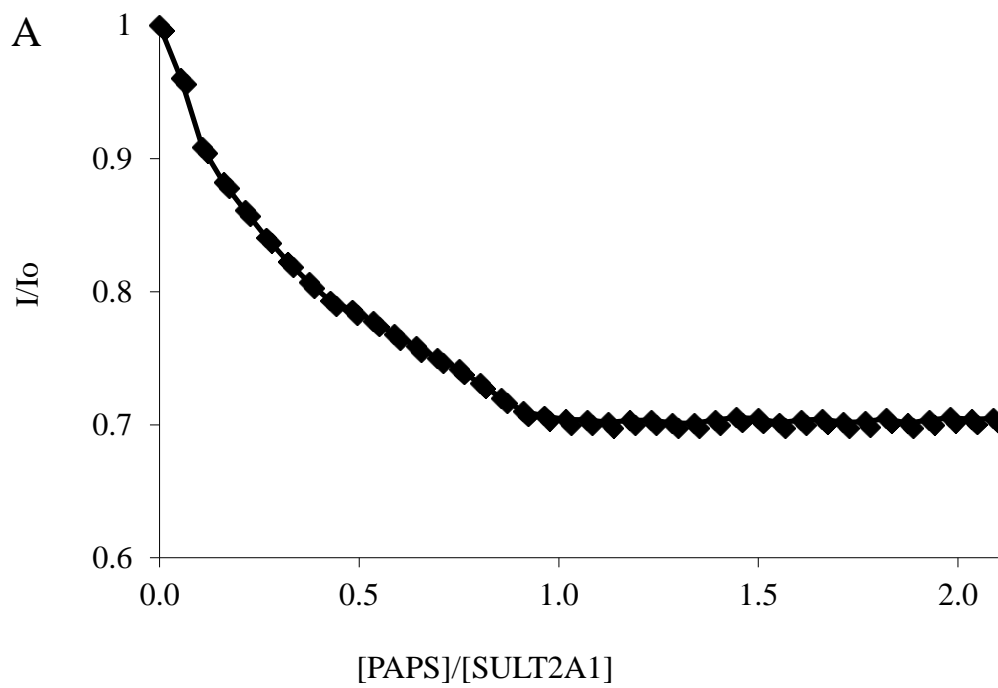


Figure 26. Stoichiometric determination of PAPS and PAP binding to SULT2A1 by intrinsic fluorescence titration. The binding stoichiometry of PAPS and PAP to SULT2A1 were determined using the change in intrinsic fluorescence with 5 μ M SULT2A1 at RT as described in the methods section I-K. The change in fluorescence was normalized to the initial fluorescence and plotted vs. the ratio of A) PAPS or B) PAP to SULT2A1. Each titration was evaluated at least five times and presented as the mean \pm SEM.

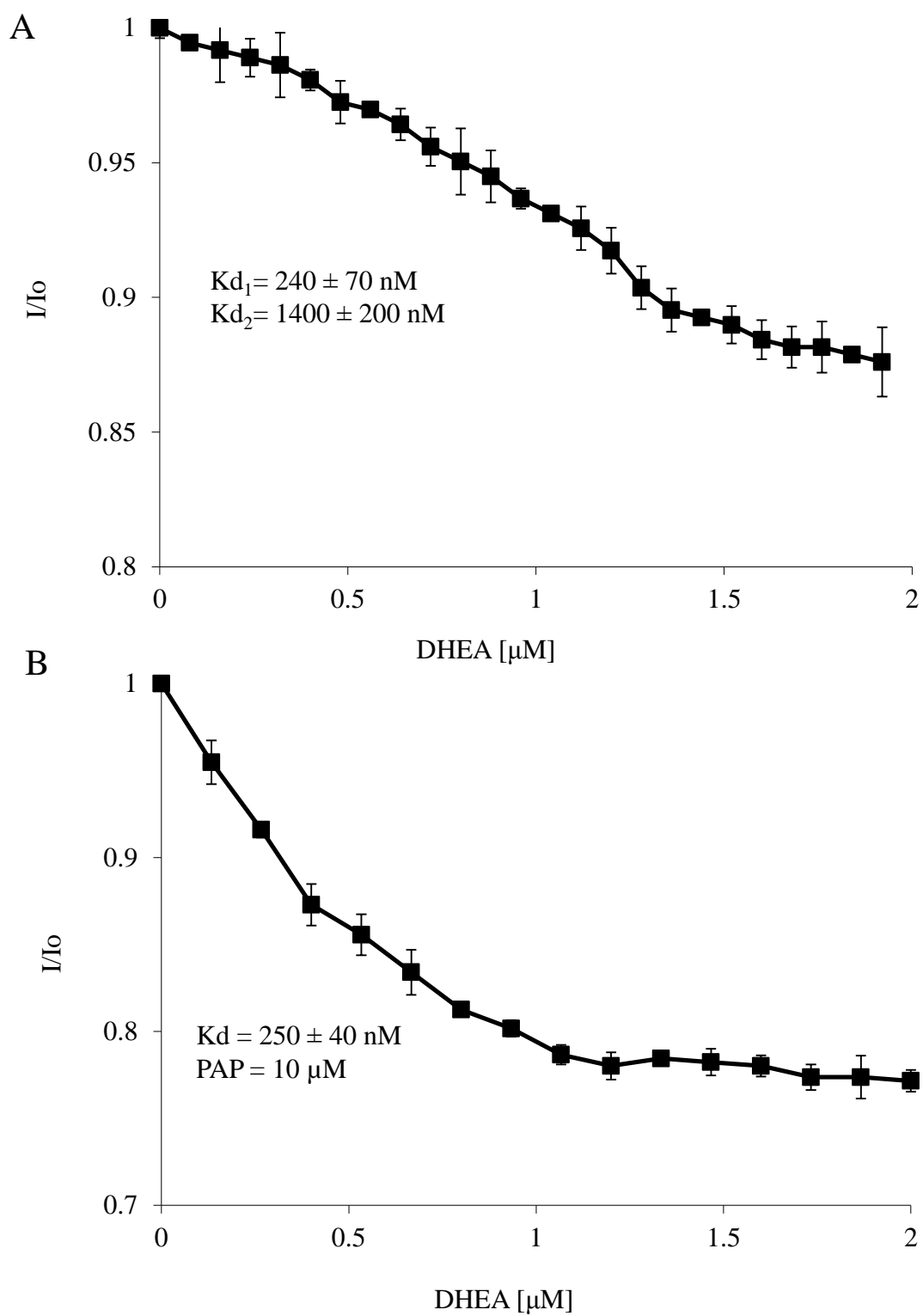


Figure 27. K_d determination of DHEA binding to SULT2A1 by intrinsic fluorescence. DHEA was titrated into a solution with 100 nM SULT2A1 in PBS. DHEA titration was performed A) without PAP and B) pre-incubated with 10 μ M PAP as described in the section I-J. The change in fluorescence was plotted vs. the concentration of DHEA. Each titration was evaluated in triplicate and presented as the mean \pm SEM. The K_ds were determined in KaleidaGraph using non-linear analysis with the two binding site and single binding site models.

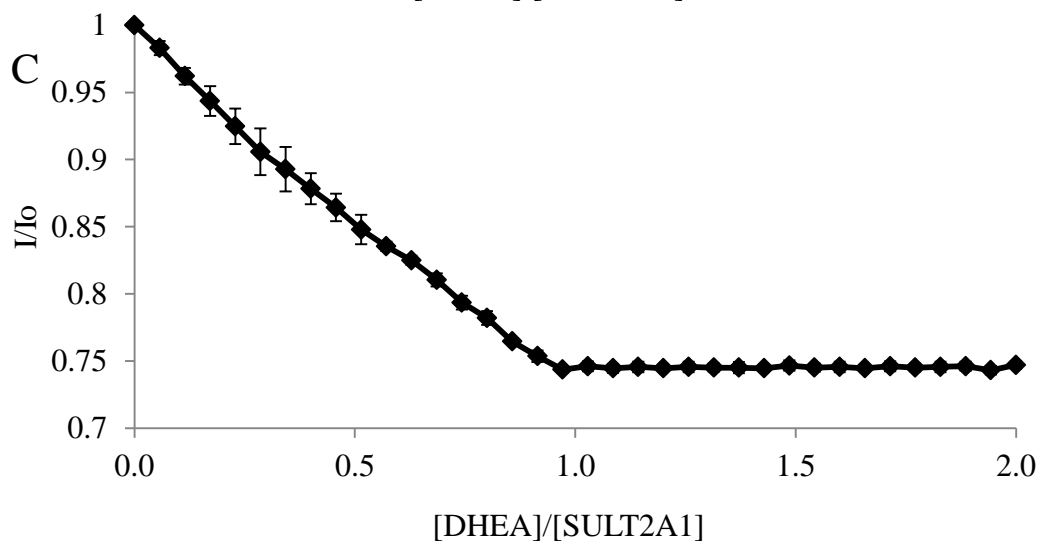
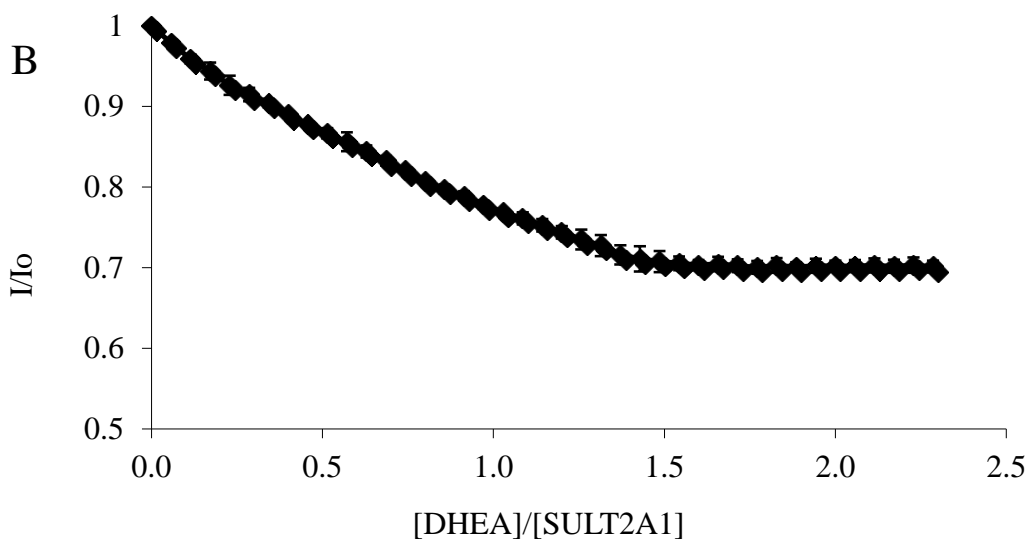
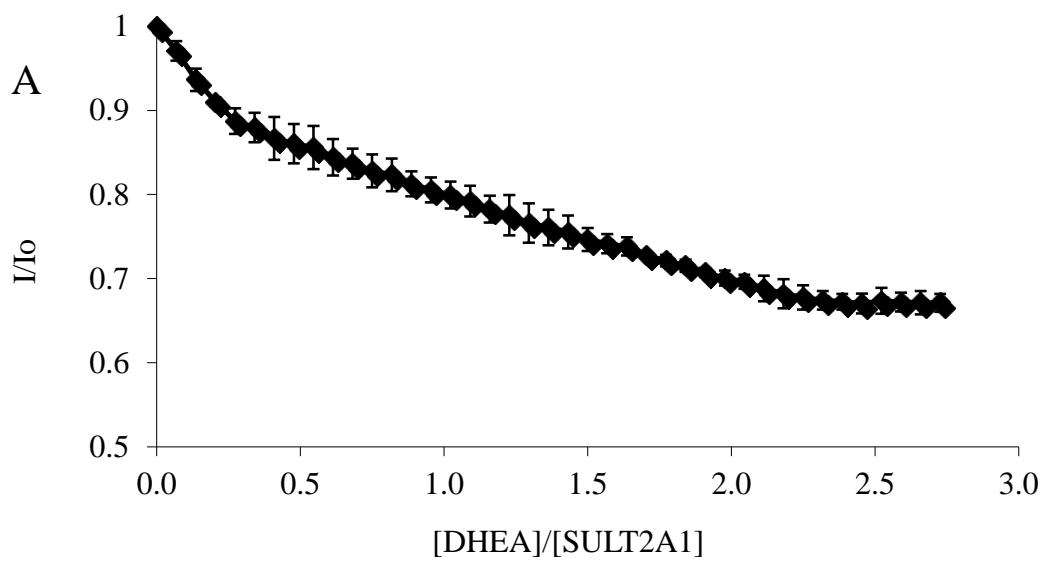


Figure 28. Stoichiometric determination of DHEA binding to SULT2A1 by intrinsic fluorescence. DHEA was titrated into 5 μM SULT2A1 in PBS. Titrations were performed with a stock solution of DHEA at 100 μM in a 50% ethanol solution as described in section I-K. DHEA stoichiometric titrations were pre-incubated A) without PAP, B) 2.5 μM PAP, or C) 10 μM PAP. Each titration was evaluated in triplicate and presented as the mean \pm SEM.

association of DHEA binding and the concentration of PAP, a 50% saturating concentration of PAP (2.5 μ M) was added to the SULT2A1 before titration of DHEA. This titration indicated that the binding of PAPS at half the active sites eliminated half the low affinity DHEA binding sites. To determine if the DHEA binding to the low affinity site was inversely proportional to the binding of PAPS to SULT2A1, DHEA was titrated to SUTL2A1 with a 50% saturating concentration of PAPS. The titration of DHEA to the 50% saturated SULT2A1 identified 1.5 molecules of DHEA bound to each subunit of SULT2A1 (Fig. 28B). These results support the conclusion that the low affinity DHEA binding site (1400 nM Kd) is available only in the absence of PAPS.

The titration of RAL to SULT2A1 was performed using the same buffers and concentrations as used in DHEA titrations. The Kd for RAL was 600 nM for binding in the absence of PAP, and was increased 10 fold to 6400 nM when PAP was added (Fig. 29). These results are consistent with the computational docking of RAL to the active site of SULT2A1. While RAL was able to bind to SULT2A1 even when PAP was present, the docking studies suggest that the orientation may be in a non-catalytic. To determine the stoichiometry of binding, RAL was titrated to 5 μ M SULT2A1. The ratio of binding for RAL to SULT2A1 was 1:1, regardless of the presence of PAP (Fig. 30).

E) Pharmacophore Screening of Potential Substrates

A pharmacophore model was constructed using the open and closed models of SULT2A1. Pharmacophore is similar to docking, except pharmacophore is optimized to model thousands of substrates in a day or less. To achieve the high-throughput in pharmacophore modeling, the enzyme is represented by a generalized model of the active site,

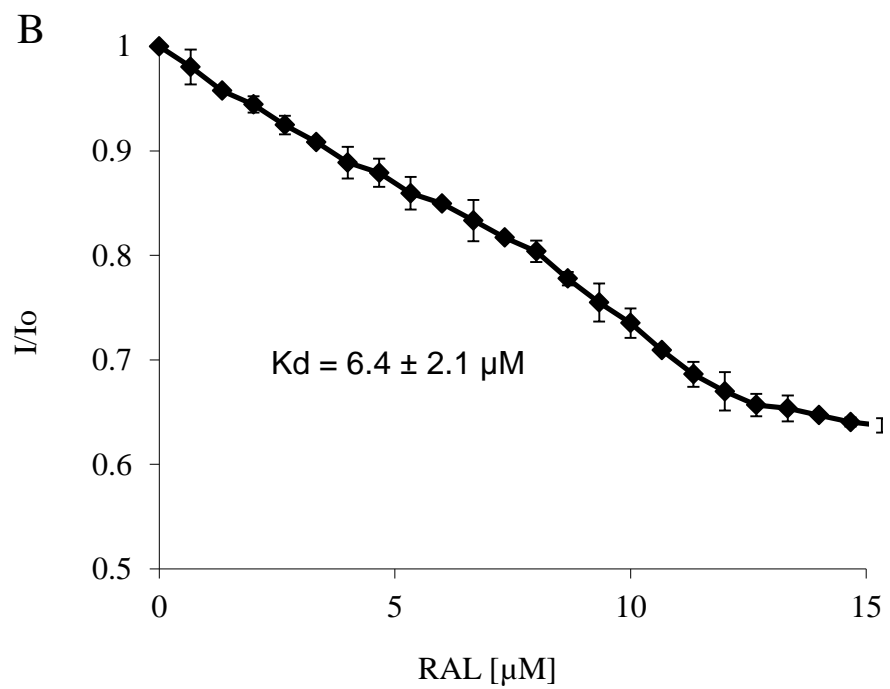
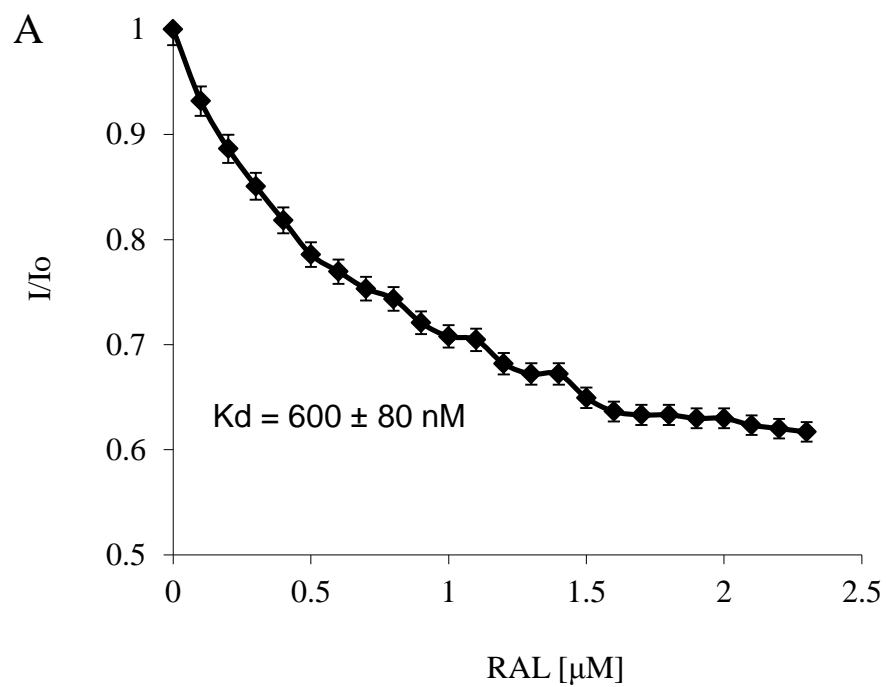


Figure 29. K_d determination for RAL binding to SULT2A1 using intrinsic fluorescence. RAL was titrated to 100 nM of SULT2A1 pre-incubated with A) no PAP or B) 10 μ M PAP as described in section I-J. The K_d for RAL binding to SULT2A1 was determined using non-linear regression analysis in KaleidaGraph. Each titration was evaluated in triplicate and presented as the mean \pm SEM.

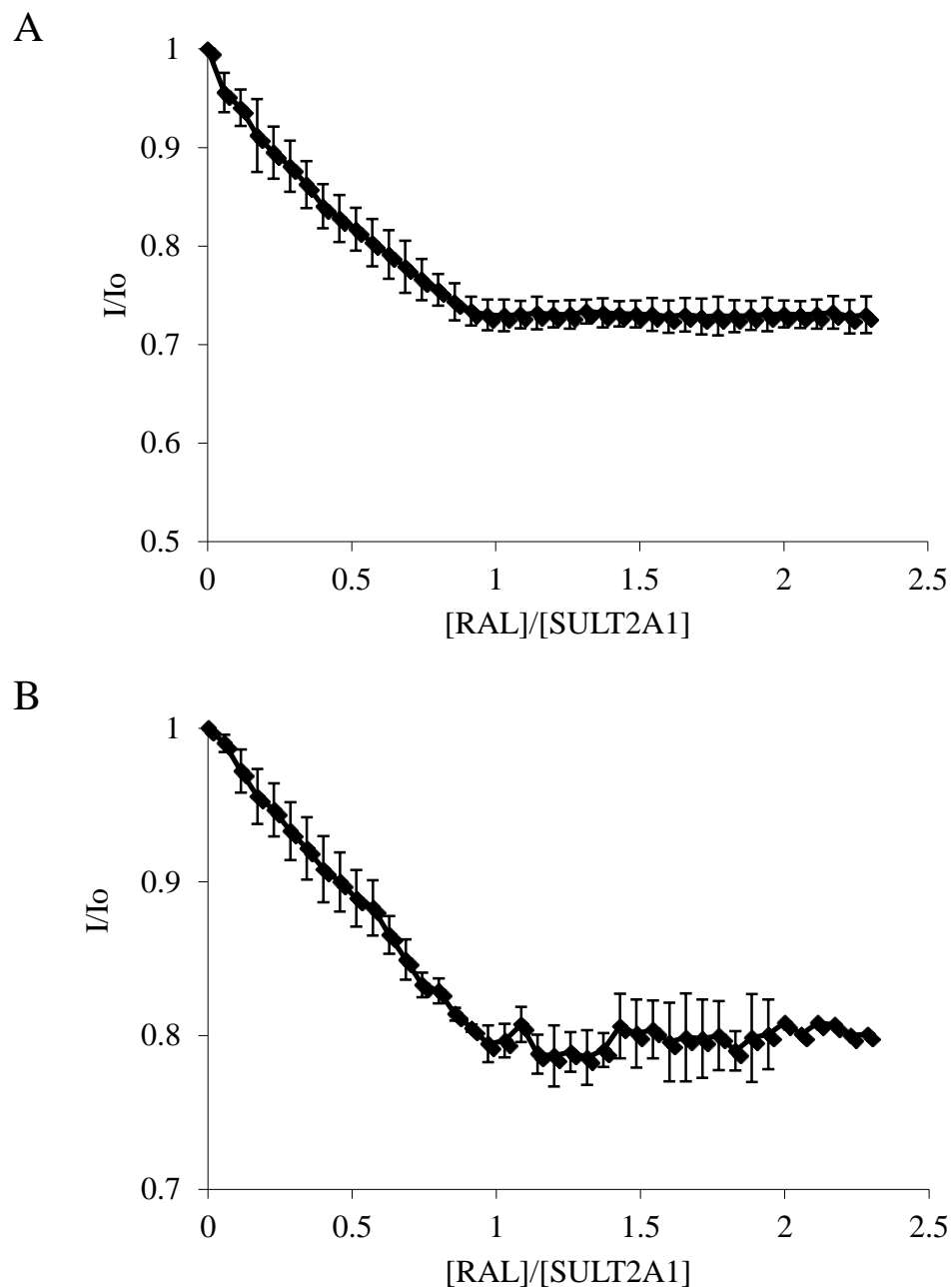
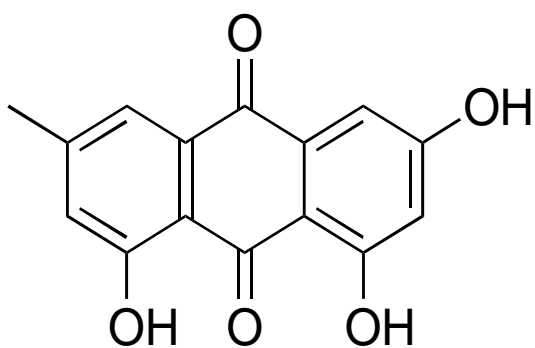
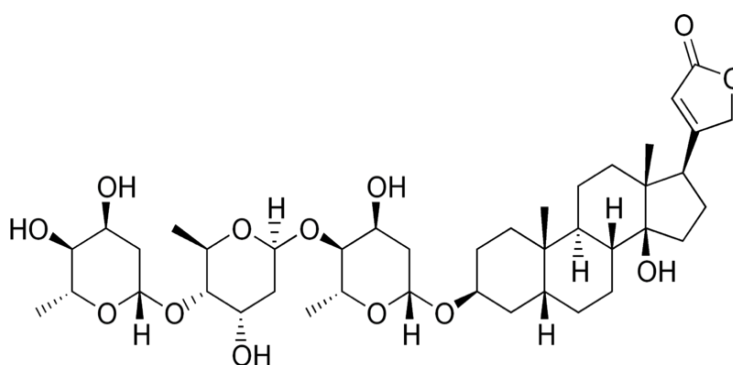


Figure 30. Stoichiometric determination of RAL binding to SULT2A1 by intrinsic fluorescence. RAL was titrated to 5 μ M SULT2A1 in PBS at RT as described in section I-K. Before each titration, SULT2A1 was pre-incubated with A) no PAP or B) 10 μ M PAP. Each titration was evaluated in triplicate and presented as the mean \pm SEM.

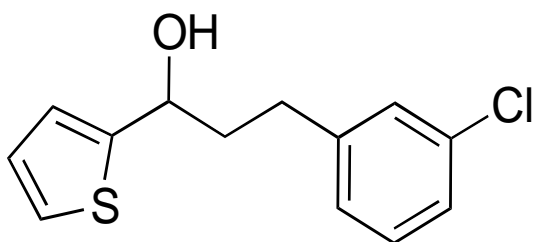
with charged and hydrophobic regions represented by a simple sphere instead of an explicit model of the residues that are used in docking. The pharmacophore models were screened with a library containing 35,000 compounds. The search criteria required a hydrogen bond with the active site H99, which is necessary for sulfation. Other interactions included in the model were the hydrophobic and charged residues of the active site. These interactions were included to improve the modeling, but were not mandatory for binding in the models. In addition to these interactions, the total volume of the active site was limited by a series of overlapping spheres, based on the SULT2A1 open and closed docking models. The screening of the 35,000 compounds to the open model resulted in 1250 compounds that were predicted to bind. When the same library was screened with the closed model, only 598 compounds were predicted to bind. With the exception of 2 compounds, all of the predicted closed model compounds were also in the open model results. The resulting compounds were screened on www.emolecules.com for commercial availability; three compounds were picked for further study to investigate the predictability of the pharmacophore modeling (Fig. 31). The first compound was emodin, a selective kinase inhibitor that has been studied as a dietary compound that may reduce Type 2 diabetes risk (Chao, Kuo et al. 2010). Emodin was predicted to be a substrate in both the open and closed models. The other two compounds were predicted to bind only in the open SULT2A1 conformation. The second compound of interest was digitoxin, a cardiac glycoside used instead of digoxin when poor renal clearance limits the use of digoxin (Belz, Breithaupt-Grögler et al. 2001). Digitoxin is eliminated by the liver and has been shown to be sulfated by SULT2A1 (Schmoltdt, Blömer et al. 1992), although little else about digitoxin sulfation by SULT2A1 has been reported. The third compound of



Emodin



Digitoxin



3-(3-chlorophenyl)-1-(2-thienyl)-1-propanol (3-CTP)

Figure 31. Chemical structure of the commercially available predicted substrates of SULT2A1 based on pharmacophore analysis of SULT2A1 active sites.

interest was 3-(3-chlorophenyl)-1-(2-thienyl)-1-propanol (3-CTP), that has been tested as an immunosuppressant (Scherer, Magness et al. 2007), although there is no FDA approval for clinical use.

F) Docking of Emodin, Digitoxin, and 3-CTP to SULT2A1

Each substrate was docked to the active site of SULT2A1 in both the open and closed models by the same methods used for docking DHEA and RAL. The docking of emodin to the open and closed active sites of SULT2A1 predicted a BFE of -10.9 kJ for the open model and -12.5 kJ for the closed model (Fig. 32). In both models, emodin was predicted to bind to SULT2A1 in a competent orientation for sulfation. The results predict that emodin sulfation by SULT2A1 will show a random-order Bi Bi reaction mechanism.

In the open model, digitoxin was able to bind in a competent orientation for sulfation with SULT2A1. The predicted BFE of docking was -12.7 kJ. When digitoxin was docked to the closed model, the digitoxin would not bind to the active site. The lowest energy structure in the closed model was on the surface of SULT2A1, with a predicted BFE of -4.5 kJ. No competent orientations for sulfation were observed in the top ten orientations of digitoxin with the closed model. The docking models predict that sulfation by digitoxin is an ordered reaction mechanism with digitoxin as the lead substrate (Fig. 33).

The third predicted substrate, 3-CTP, docked to the open model in a competent orientation for sulfation, but not in the closed model of SULT2A1. 3-CTP is a small compound; however the location of the OH group in the middle of the chain means that

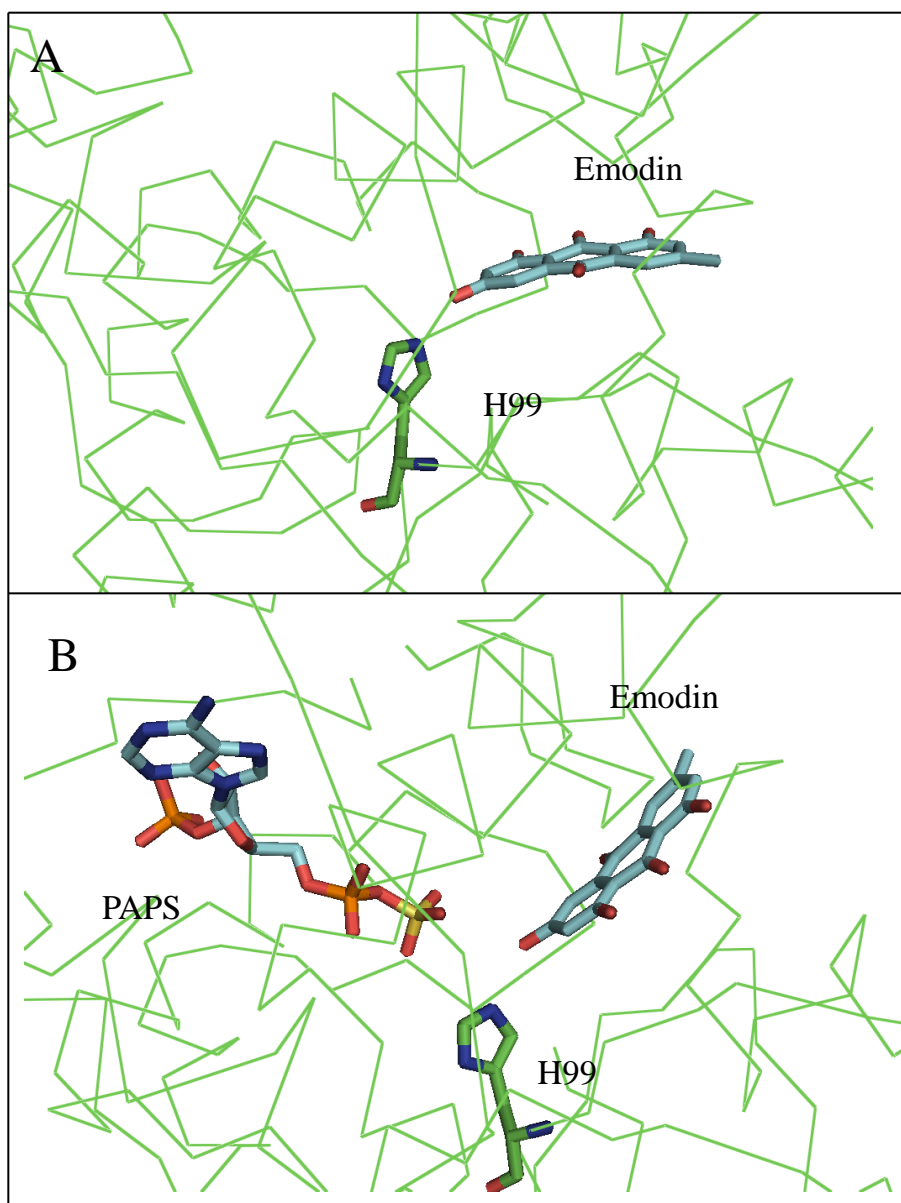


Figure 32. Docking of emodin to SULT2A1. Docking of emodin to the open and closed models of SULT2A1 was performed as described for DHEA docking in section I-E. A) Docking of emodin to the open model of SULT2A1 had a predicted BFE was -10.9 kJ. B) Docking of emodin to the closed model of SULT2A1 had a predicted BFE was -12.5 kJ. Both models predicted a hydrogen bond between H99 and emodin. The PAPS and emodin are shown in cyan and SULT2A1 is shown in green. H99, PAPS and emodin are represented in stick and the backbone of SULT2A1 is in ribbon.

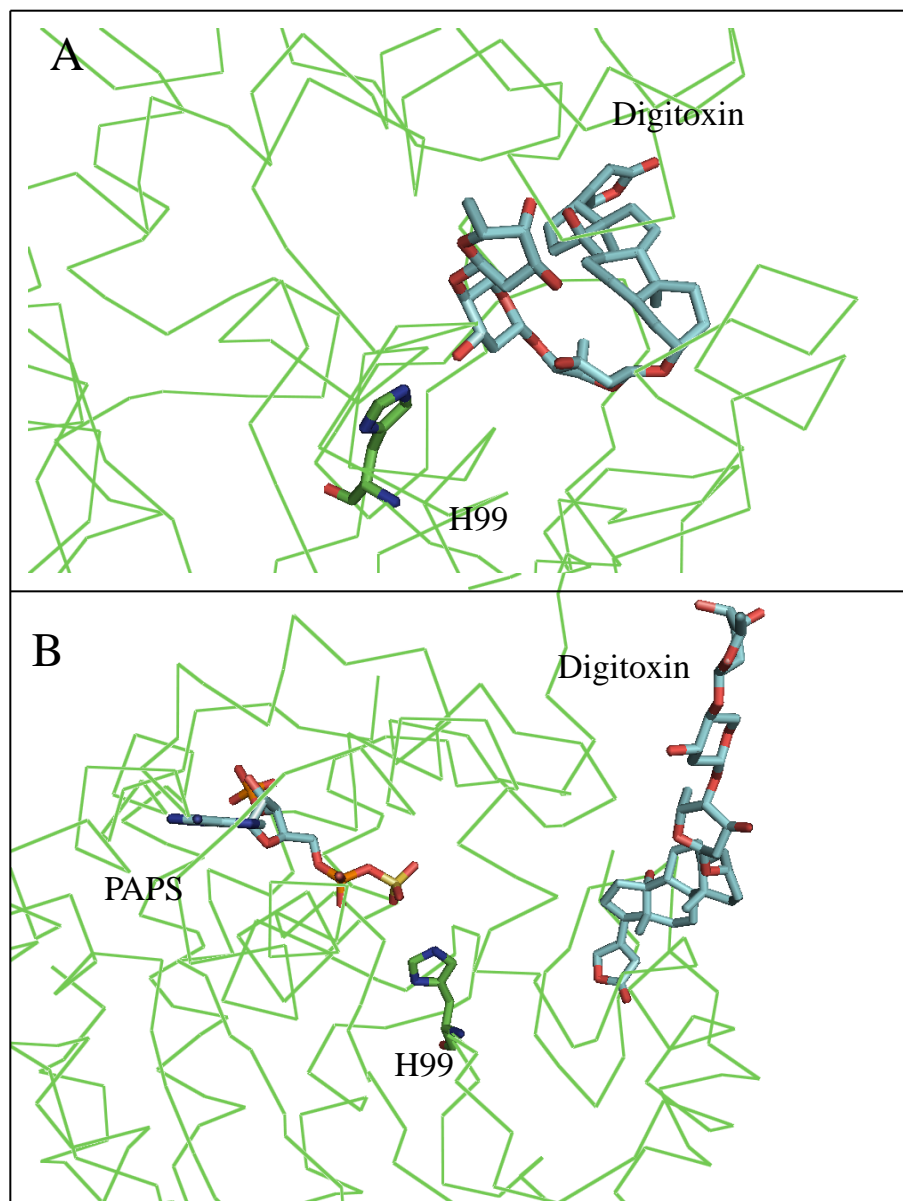


Figure 33. Docking of digitoxin to SULT2A1. Docking of digitoxin to the SULT2A1 models was performed as described in section I-E. A) The lowest energy orientation of digitoxin predicted in the open model. Digitoxin docked with a BFE of -12.7 kJ. A hydrogen bond was predicted between digitoxin and H99. B) The lowest energy orientation of digitoxin predicted in the closed model. The BFE was -4.5 kJ and no hydrogen bond predicted. Digitoxin and PAPS are in cyan and SULT2A1 is shown in green. H99, PAPS and digitoxin are shown in stick and the SULT2A1 backbone is shown in ribbon2

3-CTP must angle the OH group to the active site histidine in a non-planar orientation for sulfation (Fig 34). The angle of the OH group means that 3-CTP must occupy a large non-planar space more consistent with the large substrates, like digitoxin and RAL, than small substrates like DHEA or emodin. With the open model, 3-CTP bound in an orientation for sulfation with a BFE of -12.0 kJ. Due to the three dimensional space, 3-CTP could not bind to the closed model of SULT2A1 and was bound to the surface of the enzyme with a BFE of -11.5 kJ. Based on the modeling, 3-CTP will have an ordered reaction mechanism with 3-CTP as the lead substrate (Fig. 34).

G) Sulfation of Emodin, Digitoxin, and 3-CTP by SULT2A1

SULT2A1 activity for emodin, digitoxin, and 3-CTP were tested using the TLC assay described in the Methods. An initial assay was performed using 20 μM of each substrate and 10 μM [^{35}S]-PAPS with SULT2A1. Reactions were incubated at 37° C for 30 min and sulfated products were examined by the TLC method described for RAL sulfation. The results demonstrate that all of the substrates are sulfated by SULT2A1 (Fig. 35).

The pre-steady state kinetics were performed to determine the order of binding for emodin, digitoxin, and 3-CTP. All reactions were performed with of 1.0 pmol of SULT2A1, 10 μM PAPS and 20 μM emodin, digitoxin, or 3-CTP. The formation of product with time was monitored by TLC. Emodin had a burst of activity equal to the amount of SULT2A1 regardless of whether emodin or PAPS was bound first (Fig 36A). The burst was 1.0 pmol of product, indicating a single turnover. These results are consistent with a random ordered Bi Bi reaction mechanism for emodin sulfation by

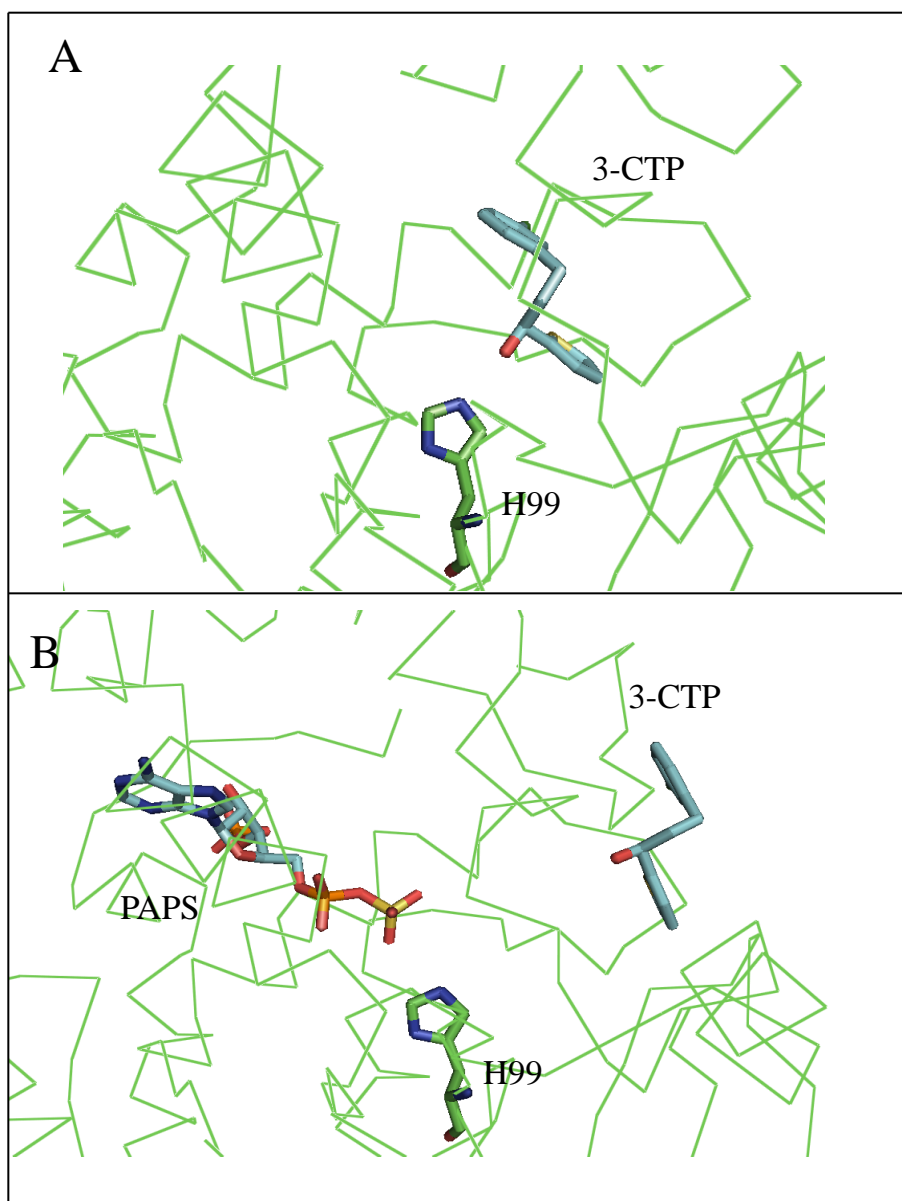


Figure 34. Docking of 3-CTP to SULT2A1. 3-CTP was docked to the open and closed models of SULT2A1 as described in section I-E. A) The lowest energy orientation of 3-CTP in the open model. 3-CTP docked with a predicted BFE of binding of -12.0 kJ. A hydrogen bond was predicted between the H99 and 3-CTP. B) The lowest energy orientation of 3-CTP docked in the closed model, with a BFE of -11.5 kJ. No hydrogen bond predicted in the docking. 3-CTP and PAPS are shown in cyan and SULT2A1 is in green. H99, PAPS and 3-CTP are shown in stick and the SULT2A1 backbone is in ribbon.

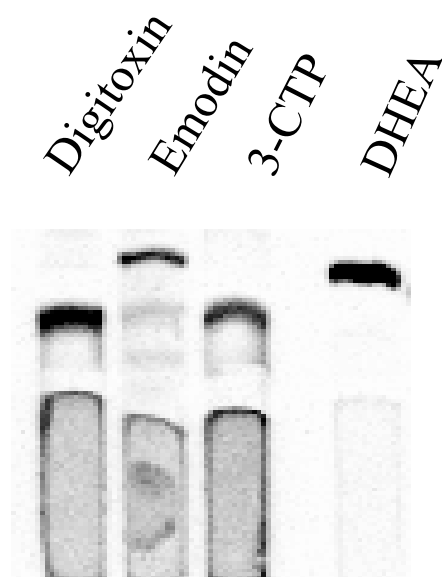


Figure 35. Sulfation of predicted substrates of SULT2A1. SULT2A1 was incubated with 20 μM of each predicted substrates and 10 μM of radiolabeled [^{35}S]-PAPS for 30 min at 37° C. DHEA sulfation was assayed as a positive control. Reactions were performed using the TLC method described in section I-H.

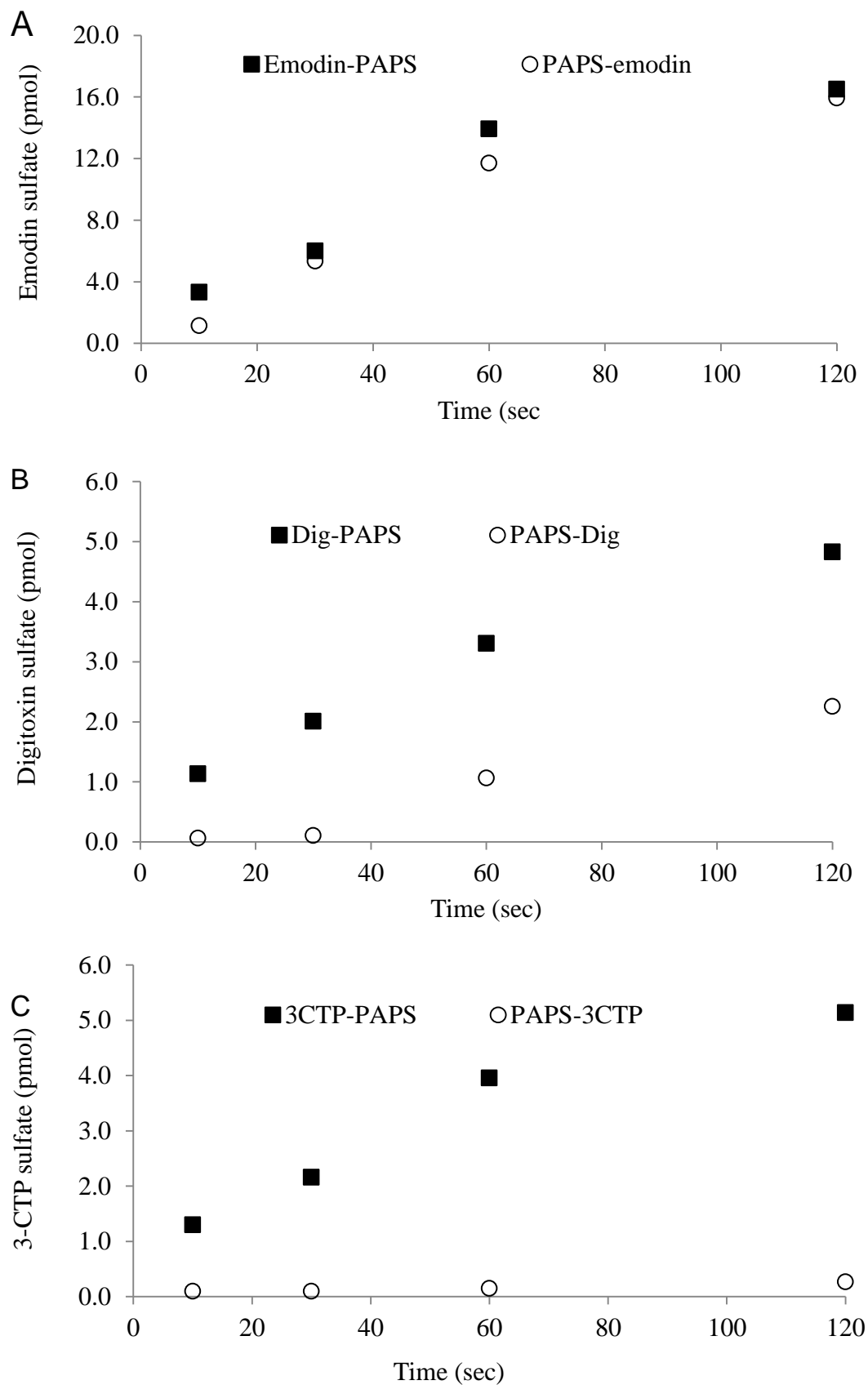


Figure 36. Pre-steady state kinetics of SULT2A1 sulfation of emodin, digitoxin, and 3-CTP. The pre-steady state kinetics were assayed using the TLC method described in I-M. Each reaction was performed with 1.0 pmol of SULT2A1, 10 μ M [35 S]-PAPS, and 20 μ M of acceptor substrate. The formation of sulfated product was plotted vs time for A) emodin, B) digitoxin, and C) 3-CTP. The reactions were started with the addition of sulfate acceptor (black squares) or PAPS (white circles). Each time point represents the average of duplicate reactions.

SULT2A1. In contrast to emodin, digitoxin and 3-CTP both showed an ordered reaction mechanism based on the pre-steady state kinetics. When digitoxin or 3-CTP was bound to SULT2A1, there was a single burst of sulfated product equal to 1 pmole, equal to the concentration of SULT2A1 active sites (Fig. 36 B and C). If SULT2A1 was saturated with PAPS first, the initial single turnover was not observed, indicating that PAPS had to leave the active site before the substrate could bind.

H) APS Binding to SULT2A1

Analysis of the crystal structures of SULT2A1 predicted that the mechanism of the structural rearrangement involved the attraction of the R247 to the 3'-phosphate of PAPS. The PAPS synthesis intermediate APS lacks the 3'-phosphate of PAPS and could provide a sulfate source without the structural rearrangement. However, when APS was titrated to SULT2A1, no evidence of binding was observed (Fig. 37). In addition, no SULT2A1 DHEA sulfation activity was observed with APS as the sulfate donor. A report on mutating the R247 to an alanine indicates that while the enzyme is active, the activity is very poor (Pedersen, Petrotchenko et al. 2000). The results indicate that the electrostatic interaction of the 3'-phosphate and the R247 is important for the activity of SULT2A1, though it is not critical.

I) Mutation of the Substrate Active Site to Reduce the Structural Rearrangements of SULT2A1 by PAPS Binding

In the docking of RAL to the SULT2A1 closed model, the L233 and L234 were shown to block RAL from the active site H99 (Fig. 21). Using MOE, the L233 and L234

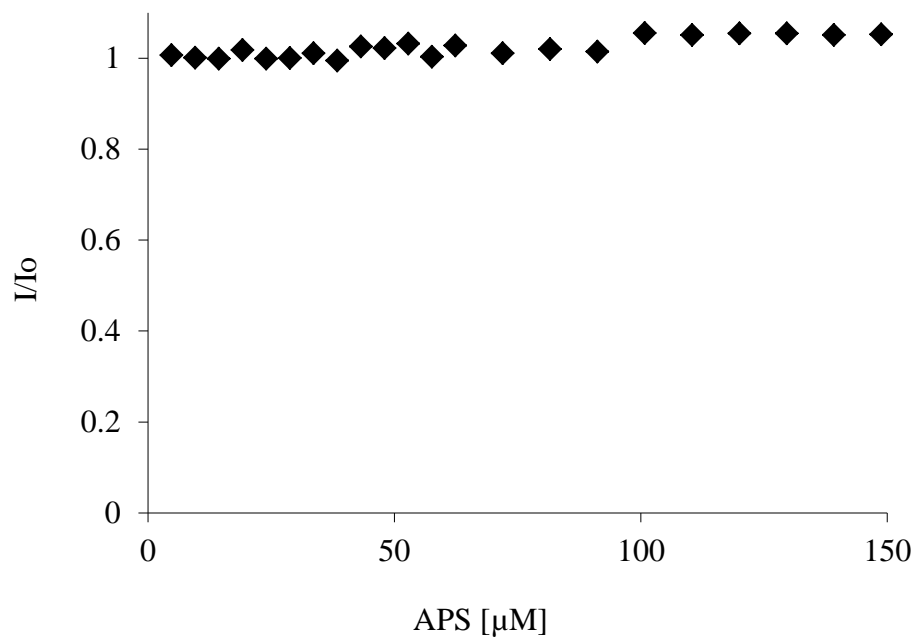


Figure 37. Binding of APS to SULT2A1 using intrinsic fluorescence. APS was titrated to 100 μM of SULT2A1 in PBS buffer as described in section I-J. Each titration was performed in duplicate and is presented as the average. No binding was observed.

were mutated to glycines *in silico*. The closed model was then energy minimized and checked on the NIH SAVES server for structural faults. RAL was docked to the mutant structure and the result was that RAL could bind to the closed mutant model in an orientation for sulfation with a predicted BFE of -12.2 kJ (Fig. 38). If the docking is accurate, then mutating L233 and L234 to glycine would make RAL sulfation by SULT2A1 a random order Bi Bi reaction mechanism.

The L233G/L234G SULT2A1 mutant was generated using the QuickChange II site-directed mutagenesis kit and the mutations were confirmed by sequence analysis. Basic kinetics of L233G/L234G SULT2A1 was examined to identify any change in activity. The change in activity with increasing DHEA concentrations was assayed using the chloroform extraction assay as described in methods. DHEA sulfation activity of the dileucine mutant was not significantly different from that of the WT enzyme (Fig. 39). The lack of any change with DHEA sulfation by SULT2A1 indicates that the mutation does not change the affinity of DHEA for SULT2A1. To ensure that the PAPS binding site had not been altered, the affinity of PAPS and PAP were examined using intrinsic fluorescence. No significant change was observed with the dileucine mutant for its affinity of PAPS or PAP (Fig. 40).

The pre-steady state kinetics for RAL sulfation by the mutant were studied using the same method and conditions as described for the WT enzyme, with 2 pmol of active sites. When L233G/L234G SULT2A1 was saturated with RAL or PAPS, a single turnover of RAL was observed followed by a linear with time formation of RAL-sulfate (Fig. 41). The absence of a lag indicates that the reaction mechanism for RAL sulfation with L233G/L234G SULT2A1 is a random order Bi Bi reaction mechanism.

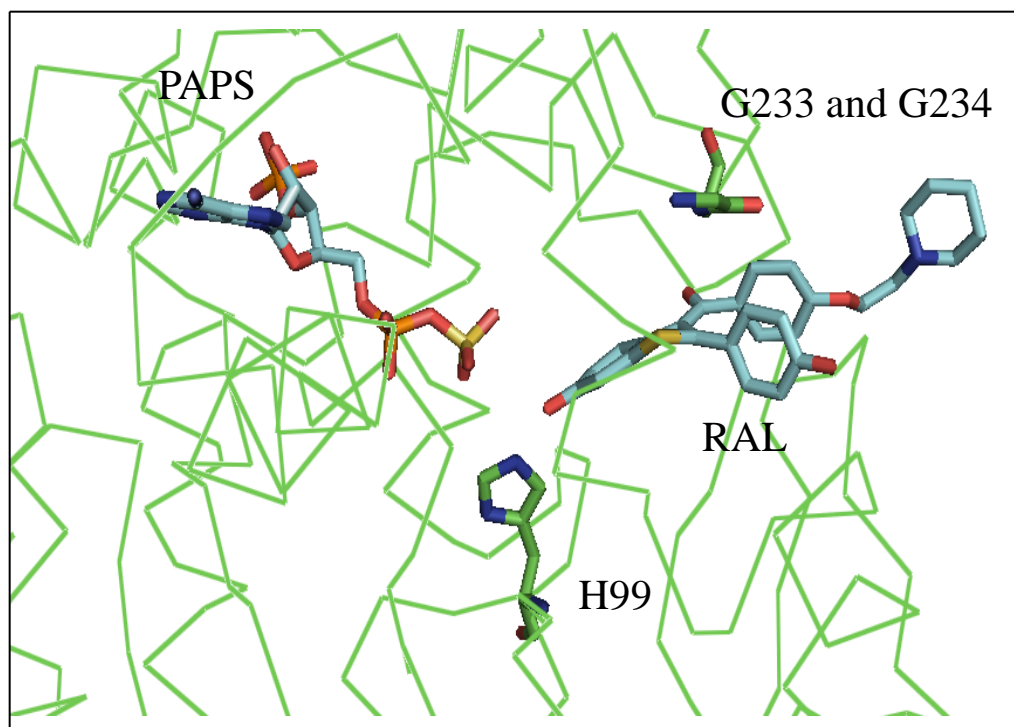


Figure 38. Docking of RAL to the closed structure of the L233G/L234G SULT2A1 mutant. The L233G/L234G mutant was made in *in silico* as described in section I-N. RAL was docked to the model using the protocol described in section I-E. RAL docked to the closed mutant model with a BFE of -12.2 kJ and a hydrogen bond predicted with the H99 and the thiophenol hydroxyl. PAPS and RAL are shown in cyan and SULT2A1 is shown in green. RAL, PAPS, H99, G233, and G234 are represented in stick and the SULT2A1 backbone is shown in ribbon

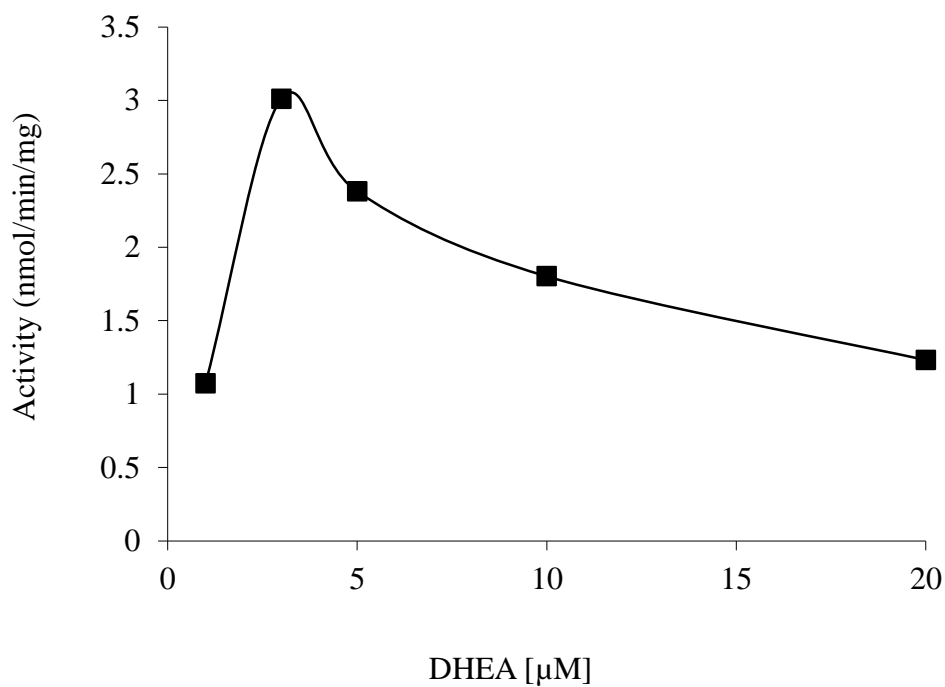


Figure 39. DHEA sulfation by L233G/L234G SULT2A1. DHEA sulfation activity of L233G/L234G SULT2A1 was measured using [^3H]-DHEA and the chloroform extraction assay described in section I-B. The concentrations of [^3H]-DHEA were 1, 2, 5, 10, and 20 μM . Each concentration was evaluated in duplicate.

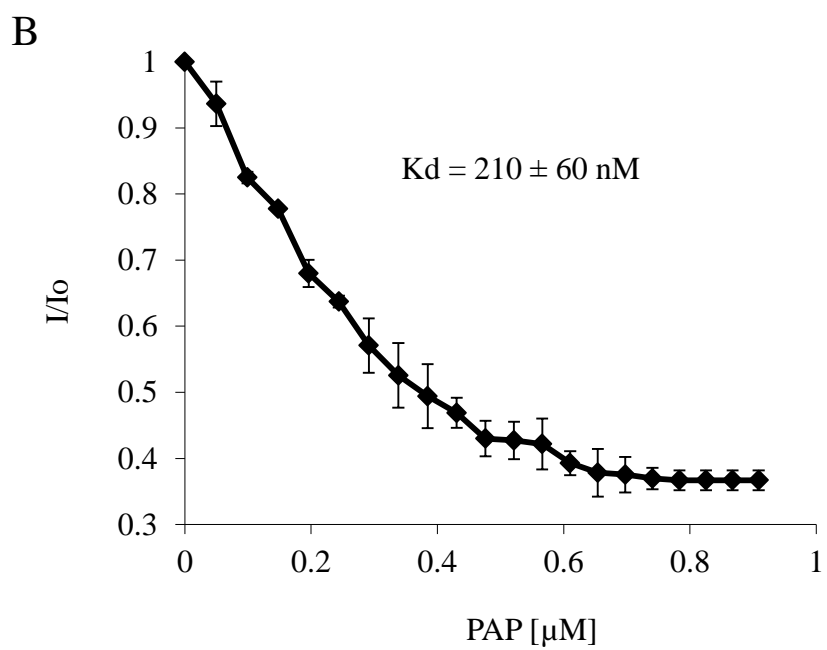
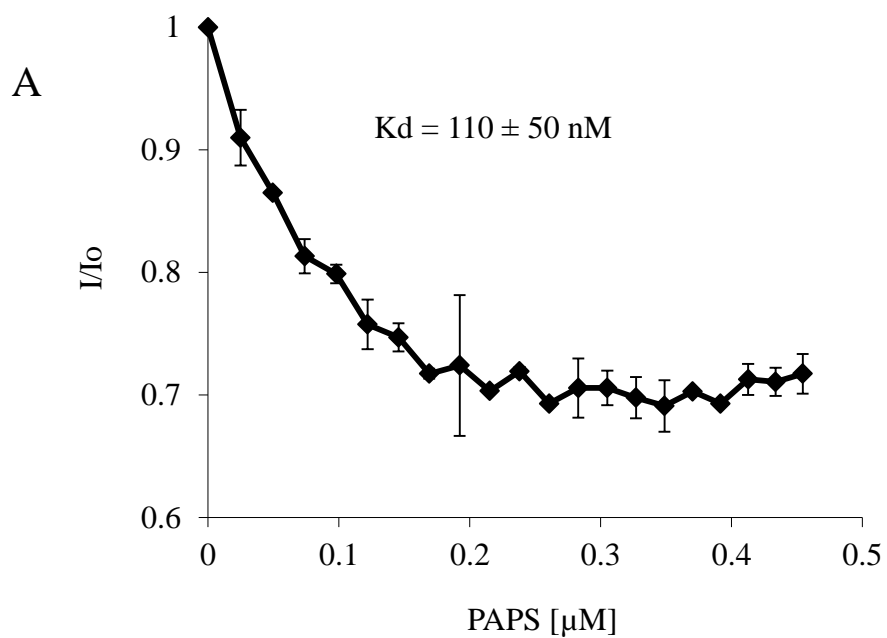


Figure 40. K_d determination of PAPS and PAP binding to L233G/L234G SULT2A1 using intrinsic fluorescence. PAPS and PAP were titrated to 50 nM L233G/L234G SULT2A1 in PBS as described in section I-J. The change in fluorescence was normalized to the initial fluorescence and plotted vs the concentration of A) PAPS or B) PAP. The K_ds were determined by non-linear regression in KaleidaGraph with a single binding site model. Each concentration was evaluated in triplicate and presented as the mean ± SEM.

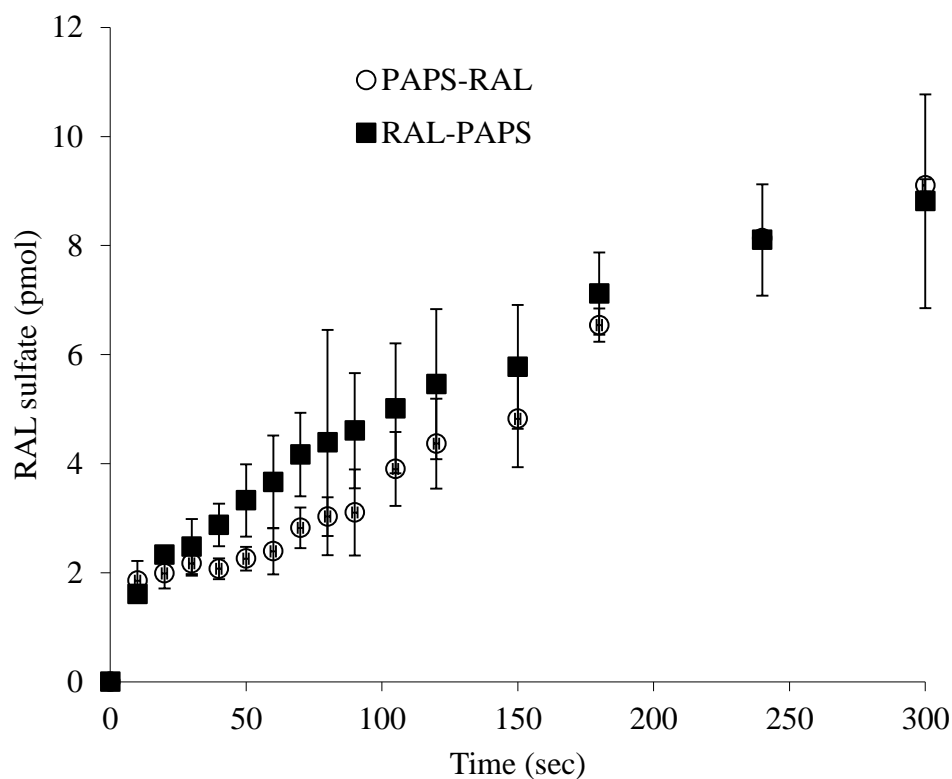


Figure 41. Pre-steady state kinetics of RAL sulfation with the L233G/L234G SULT2A1 mutant. The pre-steady state kinetics were performed with 2 pmol of the L233G/L234G SULT2A1 using the protocol described in section I-I. Reactions were started with the addition of RAL (black squares) or [³⁵S]-PAPS (white circles). Each reaction was evaluated in triplicate and presented as the mean \pm SEM.

The binding of RAL to the mutant was measured with the change in intrinsic fluorescence. The K_d was determined to be 750 nM, and was not statistically different from the K_d for RAL with the WT enzyme (Fig. 42A). When the mutant was saturated with PAP, no change in the K_d was observed (Fig 42B). The affinity of RAL to the SULT2A1 mutant with and without PAP further demonstrates that sulfation is a random ordered reaction mechanism. The results are all consistent with the computer modeling that predicts that the L233G/L234G mutation increased the volume of the closed active site, and permits for larger substrates to bind to the closed conformation and be sulfated.

J) Specific Aim 1 Conclusions

All of the data presented in aim 1 was consistent with the hypothesis that the binding of PAPS changes the structure with resulting effects on the substrate selectivity of SULT2A1. The results consistently demonstrated that small planar substrates have a random reaction mechanism where either substrate or PAPS may bind the enzyme first. In contrast, large non-planar substrates can only bind SULT2A1 if PAPS is not present, resulting in an apparent ordered reaction mechanism where the substrate must bind first.

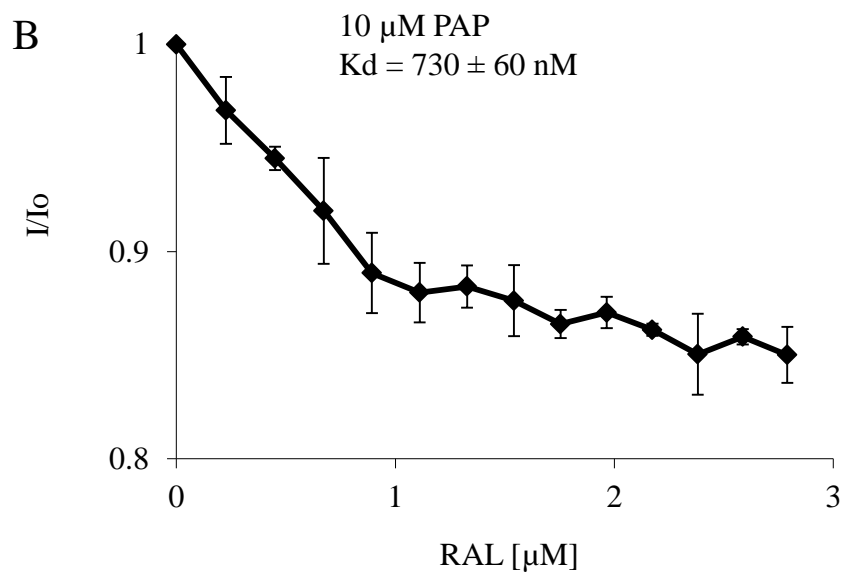
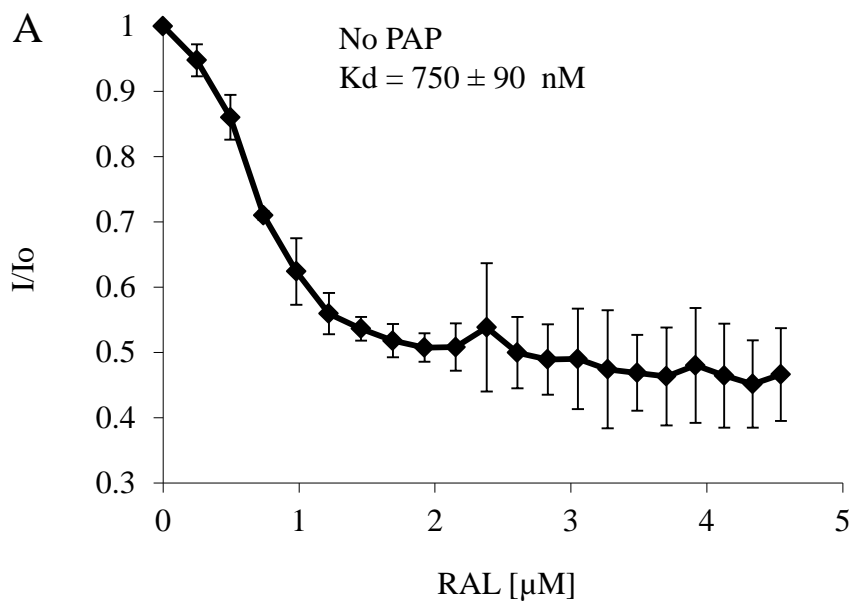


Figure 42. K_d determination of RAL binding to L233G/L234G SULT2A1 using intrinsic fluorescence. RAL was titrated to 100 nM L233G/L234G SULT2A1 in PBS as described in section I-J. The change in fluorescence was normalized to the initial fluorescence and plotted vs the concentration of RAL. Titrations were performed with SULT2A1 pre-incubated with A) no PAP or B) 10 μ M PAP. K_ds were determined by non-linear analysis in KaleidaGraph with the single binding site model. Each titration was evaluated in triplicate and presented as the mean \pm SEM.

II. THE SUBUNIT INTERACTIONS OF THE SULT2A1 HOMODIMER ASSOCIATED PAPS BINDING

We hypothesis that the binding of PAPS induces a structural change across the SULT2A1 homodimer that changes the catalytic activity of SULT2A1?

SULT2A1 is a reported homodimer, and the dimerization domain has been identified as a conserved KTVE interface. Loop 3 was identified as the major region involved in the structural rearrangement induced by PAPS binding and is adjacent to the KTVE dimerization domain and may interact across the homodimer. Dynamic modeling was utilized to determine whether dimerization had any predictable effect on the stability of loop 3. In addition, the attachment of a MBP tag to SULT2A1 caused a loss of the dimeric form of the enzyme based on size exclusion chromatography. Therefore comparison of the kinetic characteristics, DHEA sulfation in Cos-7 cells, and substrate binding of MBP-SULT2A1 and SULT2A1 was performed to identify significant difference in the function of the two constructs.

A) MBP-SULT2A1: Monomerization and Sulfation Activity

MBP-SULT2A1 was generated using the pMAL expression system and was an intermediate product in the generation of pure SULT2A1. The 43 kDa MBP is useful in affinity purification; however, the MBP could interfere with the normal structure and kinetics of SULT2A1. Therefore, it was necessary to study the structure and kinetics of MBP-SULT2A1. Both SULT2A1 and MBP-SULT2A1 were loaded onto a Sephadex G-100 column. The column had been standardized with molecular mass standards; dextran blue, bovine serum albumin, equine fumarase, and human cytochrome C. Elution of

SULT2A1 and MBP-SULTA1 was monitored by UV absorbance at 260 nm as well as DHEA sulfation activity. SULT2A1 elution was consistent with a homodimer, as reported in the literature (Falany, Vazquez et al. 1989). MBP-SULT2A1 was a monomer based upon size exclusion chromatography, indicating that inclusion of the MBP moiety interfere with the dimerization of SULT2A1 (Fig. 43).

DHEA sulfation activity of MBP-SULT2A1 was compared to SULT2A1 to examine the kinetic properties of the monomer as compared to the dimer. Increasing DHEA concentrations showed that both MBP-SULT2A1 and SULT2A1 had a similar K_m of 1.5 μM , but MBP-SULT2A1 did not show substrate inhibition (Fig. 44). In addition to the similar K_m s, the V_{max} of MBP-SULT2A1 was not statistically different from the predicted V_{max} of SULT2A1, if there was no substrate inhibition. The affinity of PAPS and DHEA to MBP-SULT2A1 was studied by intrinsic fluorescence using the same conditions as used with SULT2A1. The calculated K_d of PAPS binding to MBP-SULT2A1 was 260 nM, and was not statistically different from the K_d for binding with WT SULT2A1 (Fig. 45A). DHEA titration showed only a single binding site for DHEA in MBP-SULT2A1. The K_d for DHEA binding to MBP-SULT2A1 was 260 nM and was not statistically different from the high affinity K_d binding site for DHEA observed in WT SULT2A1 (Fig. 45B). Both PAPS and DHEA had the same stoichiometry of binding as SULT2A1 with 1 PAPS molecule and 2 DHEA molecules for each MBP-SULT2A1 molecule (Fig. 46). The lack of a second DHEA binding site in the K_d titrations and a binding ratio of 2 DHEA molecules for each MBP-SULT2A1 molecule, indicates that the lower affinity site is present in MPB-SULT2A1, but does not change the fluorescence of the molecule. This can occur if binding causes no significant structural

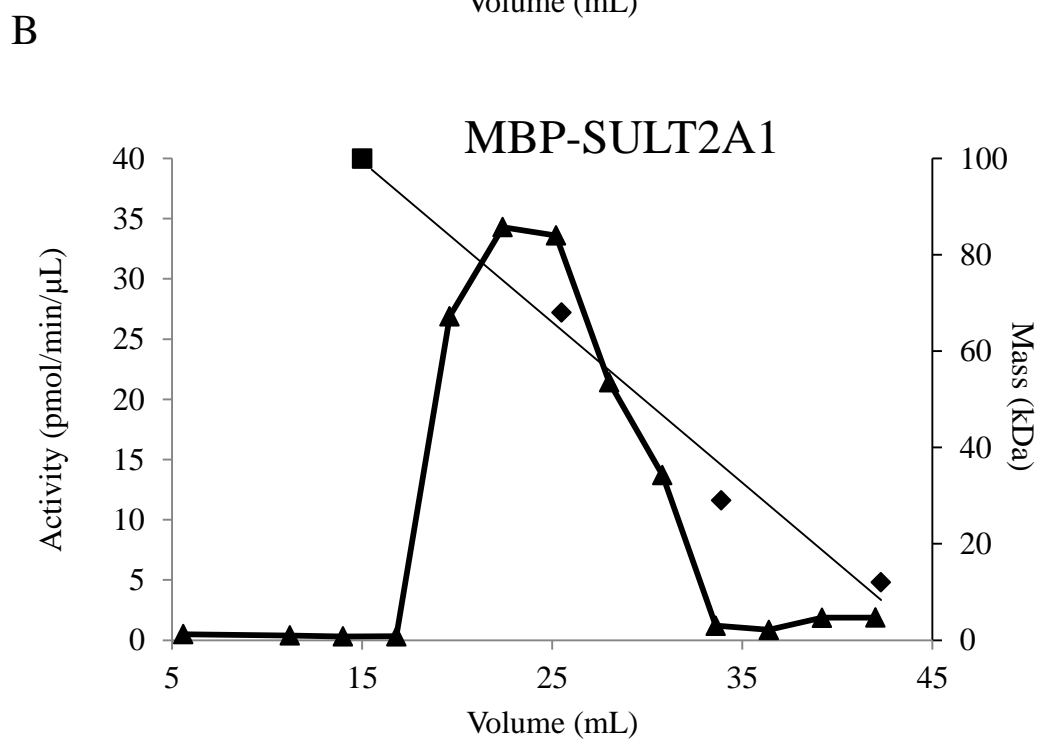
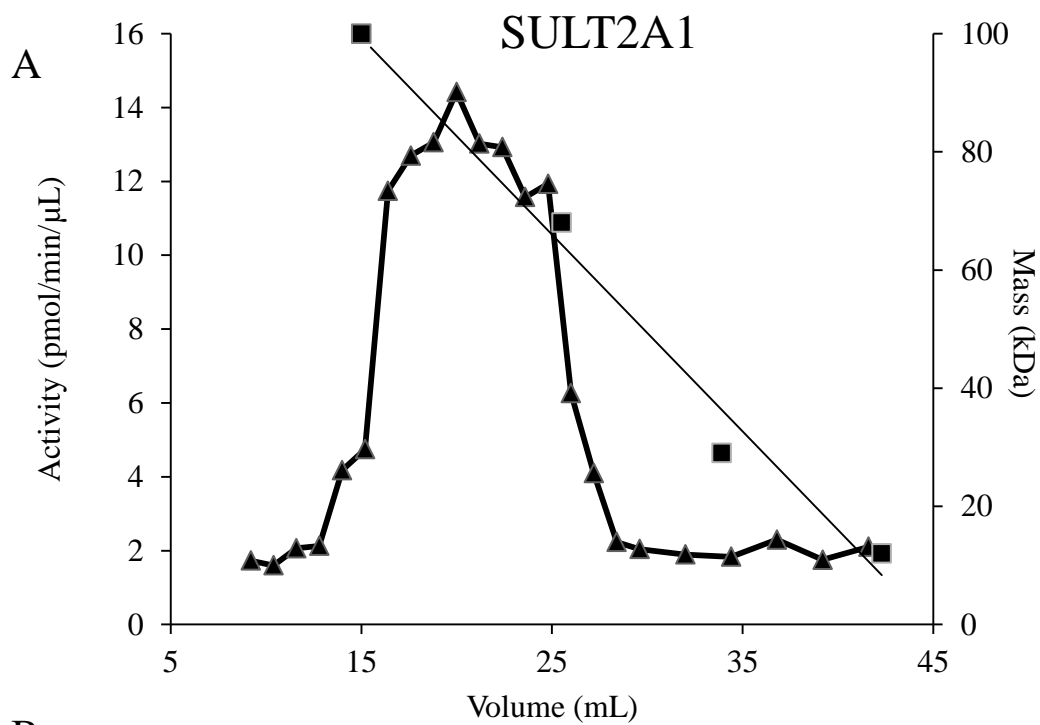


Figure 43. Size exclusion chromatography of SULT2A1 and MBP-SULT2A1. SULT2A1 and MBP-SULT2A1 were loaded on a 45 mL G-100 Sephadex column that was equilibrated with 10 mM sodium phosphate (pH 7.0) at a flow rate of 1.2 mL h⁻¹ as described in section II-C. The column was calibrated with blue dextran (2000 kDa), bovine serum albumin (66.7 kDa), equine fumarase (48.5 kDa), and human cytochrome C (12.1 kDa). Elution of enzyme was monitored by DHEA sulfation activity and UV absorbance at 260 nm.

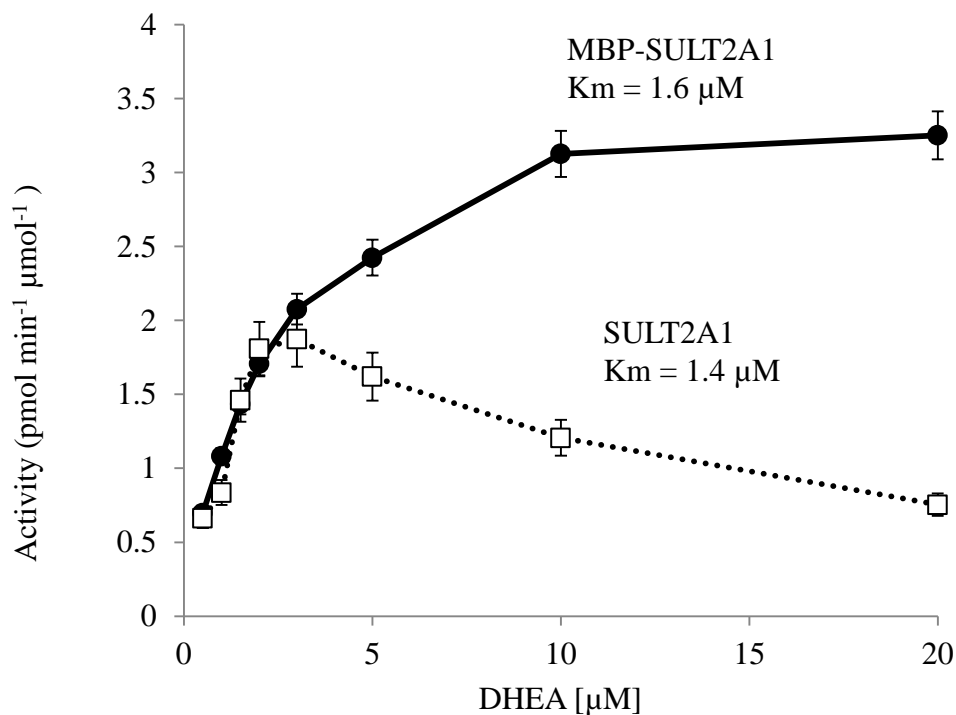


Figure 44. DHEA sulfation by SULT2A1 and MBP-SULT2A1 and the loss of substrate inhibition for the monomer isoform. The DHEA sulfation activity for SULT2A1 and MBP-SULT2A1 was assayed with increasing DHEA concentrations using the [³H]-DHEA and chloroform extraction assay described in section I-B. The K_m and V_{max} were determined based on non-linear regression analysis in the Enzyme Kinetics program. Each concentration was evaluated in triplicate and presented as the mean \pm SEM.

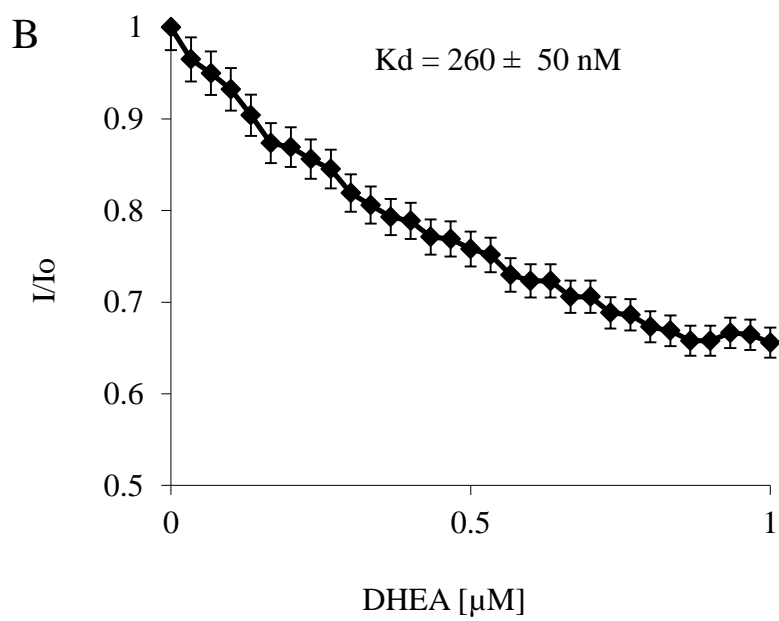
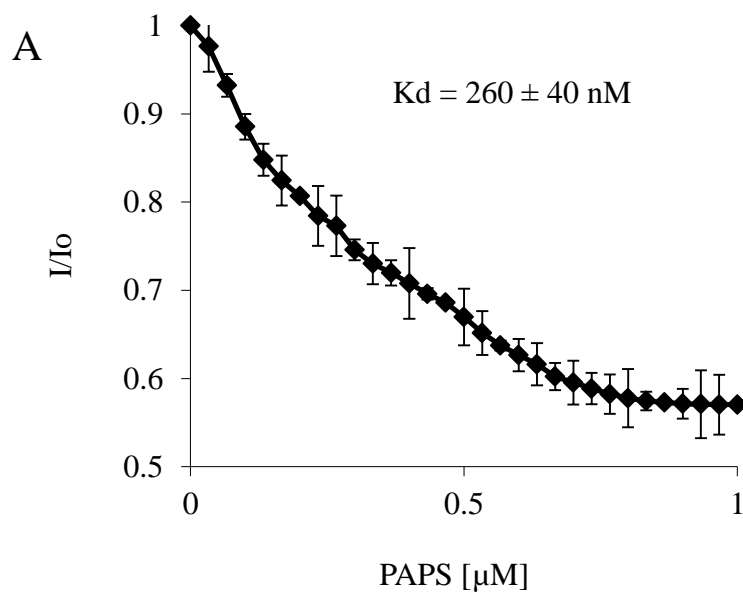


Figure 45. K_d determination of PAPS and DHEA binding to MBP-SULT2A1 using intrinsic fluorescence. A) PAPS and B) DHEA were titrated to 50 or 100 nM MBP-SULT2A1, respectively as described in section I-J. The change in fluorescence was normalized to initial fluorescence and plotted vs the concentration of ligand. K_ds were determined using non-linear regression analysis in KaleidaGraph with the single binding site model. Each titration was evaluated in triplicate and presented as the mean \pm SEM.

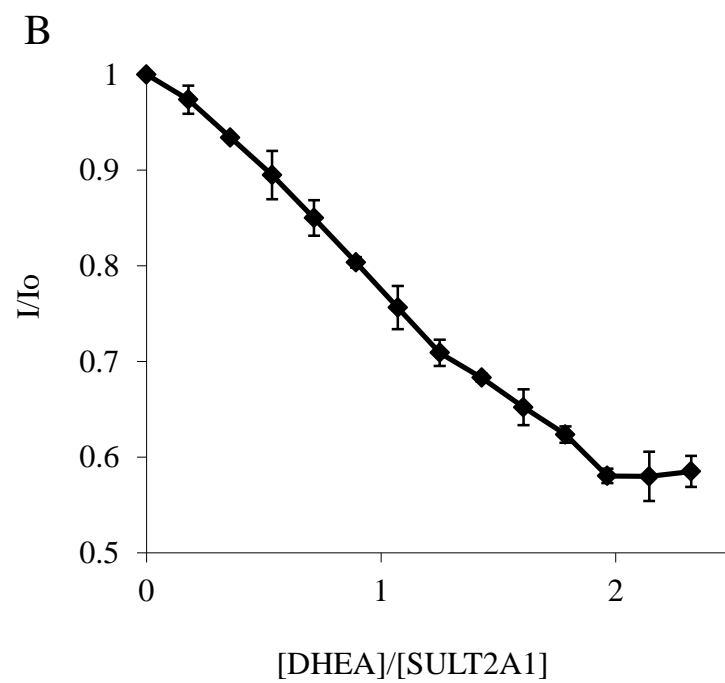
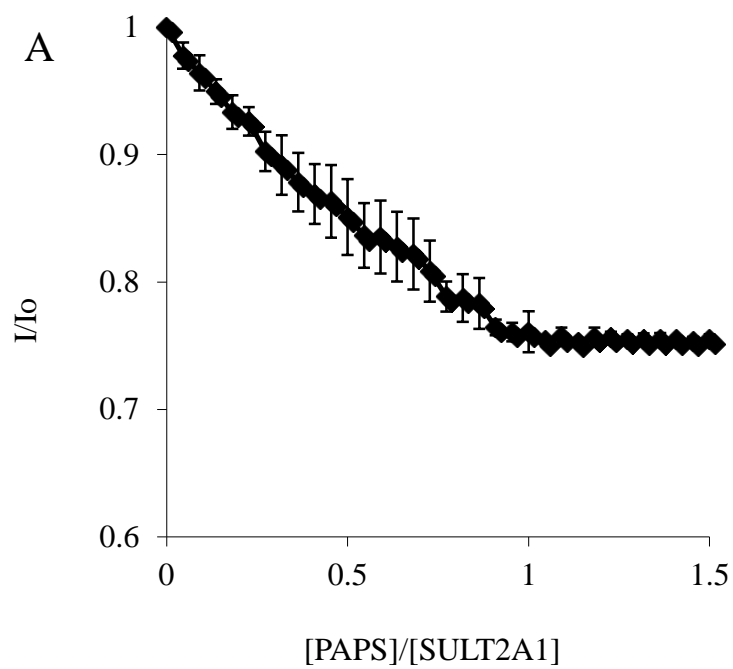


Figure 46. Stoichiometry of binding of PAPS and DHEA to MBP-SULT2A1. PAPS and DHEA were titrated to 5 μ M MBP-SULT2A1 in PBS as described in section I-J. The change in fluorescence was normalized to the initial fluorescence and plotted vs. the ratio of [ligand]/[MBP-SULT2A1]. Each titration was evaluated in triplicate and presented as the mean \pm SEM.

change or if the binding of the second site causes a small change in fluorescence that is insignificant to the background noise. Because the K_d determination titrations are performed at 20-fold lower concentration of enzyme than the stoichiometry titrations, the fluorescence signal is much weaker in the K_d titrations compared to the stoichiometry titrations. Additionally, the MBP tag on MBP-SULT2A1 increased the fluorescence background of the fusion protein compared to the SULT2A1 protein because of the presence of the aromatic residues in the MBP protein. Also possible is the affinity of the second binding site in MBP-SULT2A1 is much lower and is not forming until the DHEA concentration gets high.

B) DHEA Stoichiometry in Substrate Inhibition

Binding of a second DHEA molecule to SULT2A1 appears to be a significant factor in substrate inhibition. To model binding of the second molecule of DHEA, the open model of SULT2A1 was made with a DHEA molecule in the active site based on the modeling described previously. A second DHEA molecule was docked to the open model with the first DHEA fixed in the active site. The second DHEA molecule was able to bind to the open active site with a BFE of -9.7 kJ and was largely stabilized by pi stacking with Y238 (Fig. 47). The second molecule was in a position that would block the binding of the active DHEA site, the release of DHEAS product, or inhibit the binding of PAPS by limiting the loop 3 dynamics and the R247 interaction. The closed model was too small to permit placement of a second DHEA molecule in the active site, suggesting that substrate inhibition is related to the concentration of PAPS. The modeling also sug-

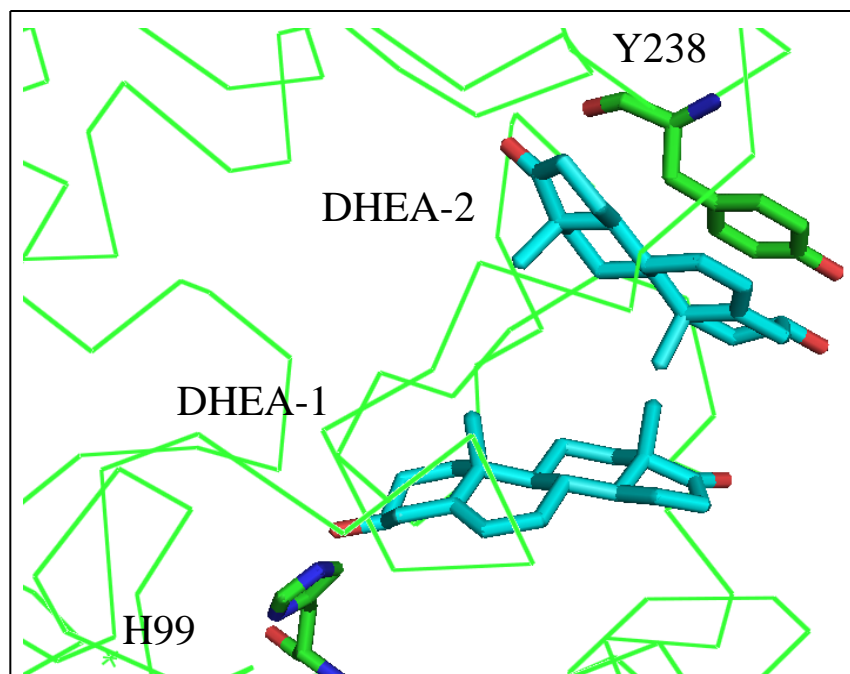


Figure 47. Docking of a second DHEA molecule to the open active site of the SULT2A1. The open model of SULT2A1 was modified with the addition of DHEA. The DHEA molecule was positioned in the active site based on the lowest energy orientation predicted in the previous docking of DHEA in Fig 20A. A second DHEA molecule was docked to the active site as described in section I-E. The second DHEA molecule bound with a predicted BFE of -9.7 kJ.

gests that the binding of DHEA to the catalytic site does not inhibit the binding of the allosteric site.

The modeling predicts that substrate inhibition is related to the concentration of PAPS, and that substrate inhibition will be reduced with higher concentrations of PAPS. Increasing concentration of PAPS was assayed with the DHEA chloroform extraction assay described in the Methods. At 2 μ M DHEA, a concentration below substrate inhibition concentrations, normal Michaelis–Menten characteristics were observed with a K_m of 300 nM (Fig. 48A). When the concentration of DHEA was increased to 20 μ M, where substrate inhibition is observed, PAPS demonstrated substrate activation (Fig. 48B). This substrate activation observed with PAPS suggests that a high concentration of PAPS, the level of substrate inhibition is decreased. In contrast to SULT2A1, MBP-SULT2A1 had no substrate activation with PAPS at 2 or 20 μ M DHEA (Fig. 49). The lack of substrate activation by PAPS at high concentrations of DHEA demonstrates that substrate activation of PAPS is directly related to substrate inhibition by DHEA in SULT2A1.

C) MBP-SULT2A1 Sulfation of RAL

To identify homodimer interactions of SULT2A1 besides substrate inhibition that are important for turnover of the enzyme, the pre-steady state sulfation of RAL by MBP-SULT2A1 was measured. When MBP-SULT2A1 was saturated with RAL, there was a burst of RAL-sulfate formed, representative of a single turnover and then a slow steady state formation of RAL sulfate. The steady state after the burst was only 20% of the rate observed for the steady state rate observed in SULT2A1. When MBP-SULT2A1 was saturated with PAPS first, no activity was observed (Fig. 50) and no activity was ob-

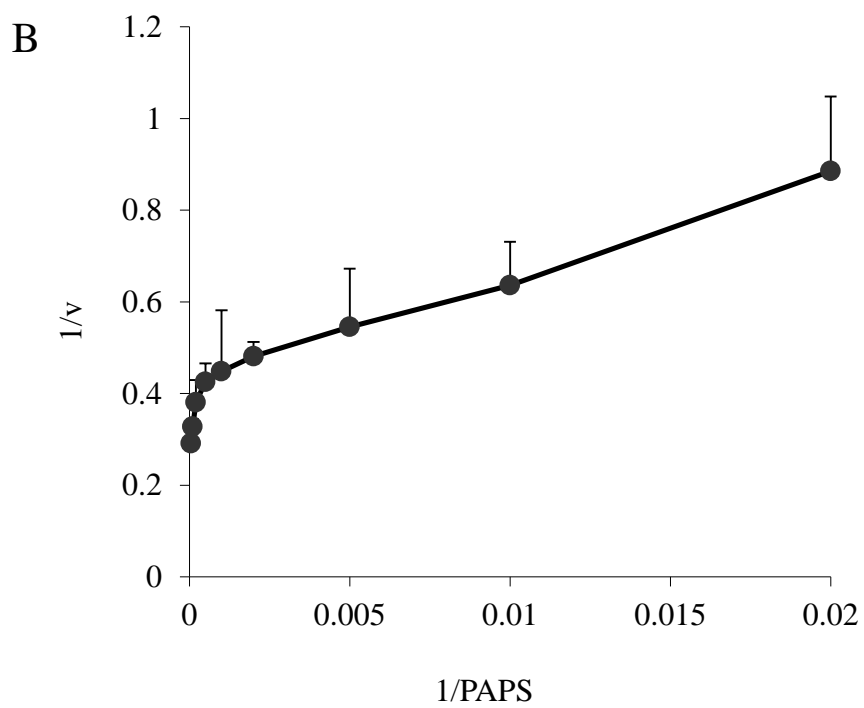
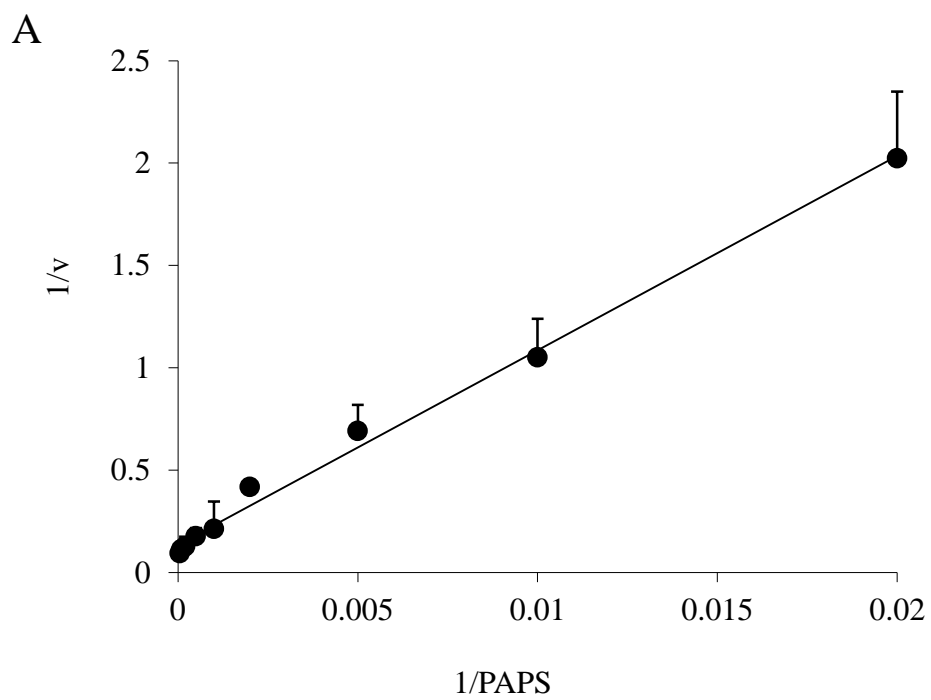


Figure 48. Double reciprocal plot of SULT2A1 activity at 2 μ M and 20 μ M DHEA with increasing PAPS. The DHEA sulfation activity with increasing PAPS concentration was assayed using [3 H]-DHEA and chloroform extraction method described in section I-B. The concentration of [3 H]-DHEA was A) 2 μ M or B) 20 μ M. Each concentration was evaluated 5 times and presented as the mean \pm 95% confidence interval.

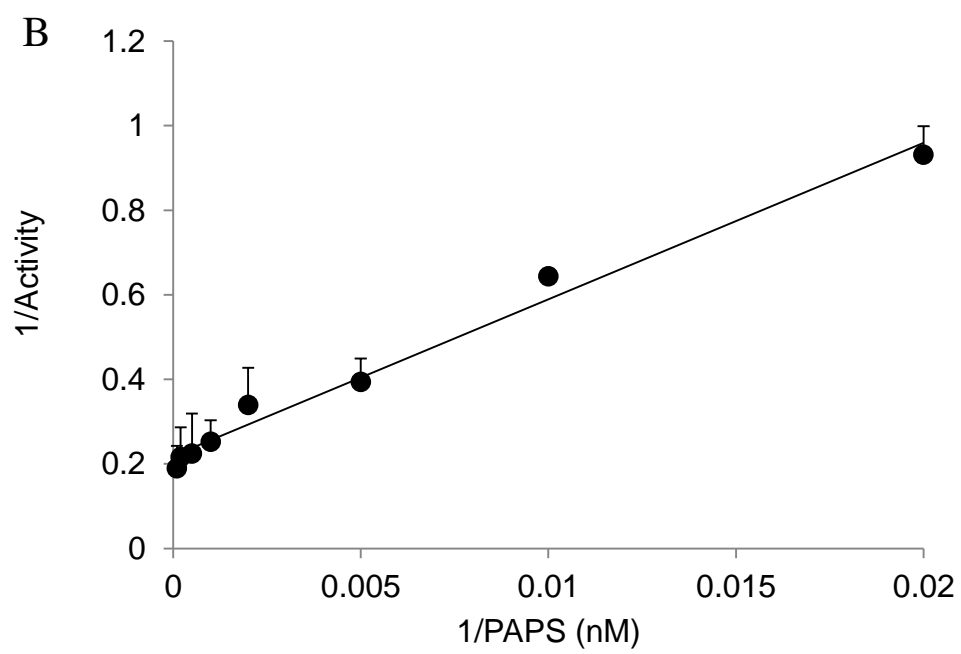
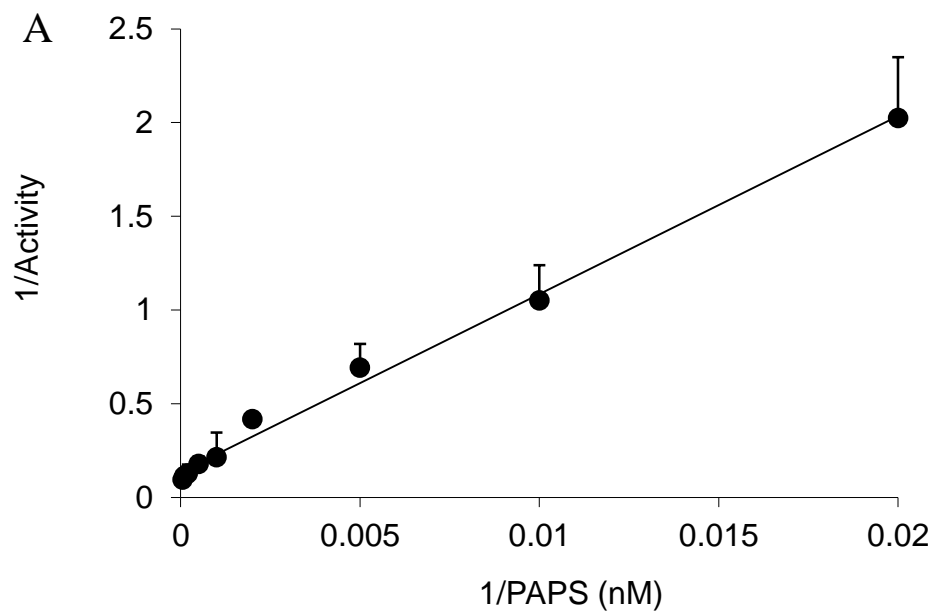


Figure 49. Double reciprocal plot of MBP-SULT2A1 activity at 2 μ M and 20 μ M DHEA with increasing PAPS. DHEA sulfation activity with increasing PAPS concentrations was assayed using the [3 H]-DHEA and chloroform extraction method described in section I-B. The concentration of [3 H]-DHEA was A) 2 μ M and B) 20 μ M. Each concentration was evaluated 5 times and presented as the mean \pm 95% confidence interval.

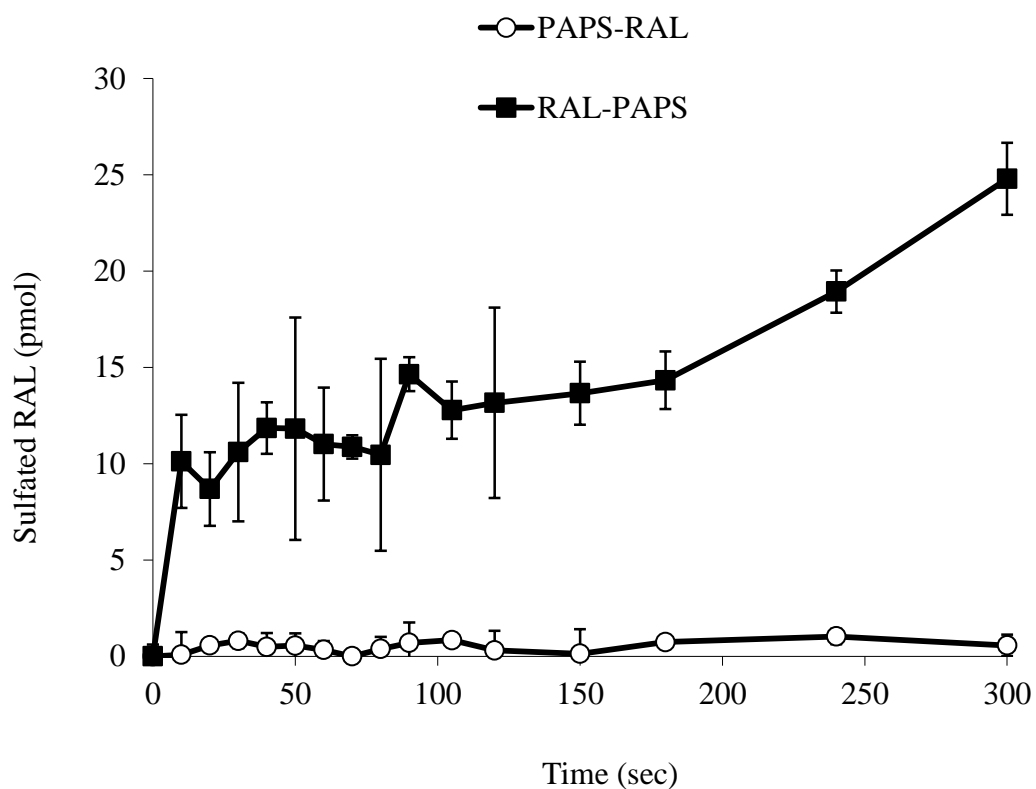


Figure 50. Pre-steady state kinetics for MBP-SULT2A1 with RAL. Pre-steady kinetics were performed with 10 pmole of MBP-SULT2A1, 10 μ M of PAPS, and 20 μ M of RAL using the method described in section I-I. Reactions were initiated with the addition of PAPS (white circles) or RAL (black squares). Each reaction was evaluated in triplicate and presented as the mean \pm SEM.

served even when the reaction was incubated for 10 min. The mechanism for the lack of RAL sulfation when MBP-SULT2A1 was saturated with PAPS first is not clear, but likely is related to the inability of the monomer to release PAP(S) as efficiently as the homodimer.

D) Dynamic Modeling of SULT2A1

Using GROMACS, a dynamic simulation of SULT2A1 was modeled for 5 nsec. Dynamic modeling simulates the natural fluctuations of a protein in solution. The simulation was performed on the monomer crystal structure and the reported SULT dimer (Petrotchenko, Pedersen et al. 2001). The fluctuation of the SULT2A1 model was measured by the Root Mean Squared Fluctuations (RMSF) of the alpha-carbons on the enzyme backbone (Fig. 51). The monomer and KTVE-dimer demonstrated that most of the enzyme had similar fluctuations. A few key regions predicted a significant change in flexibility between the two models. The region from 33-65 was significantly less flexible in the dimer when compared to the monomer. This region is the PAPS binding domain and may indicate a potential involvement of the binding of PAPS in the homodimer. In both simulations, loop 3 had greater flexibility than the rest of the enzyme, but the flexibility of loop 3 in the monomer simulation was twice as dynamic as the dimer, particularly from amino acids 240 to 252. Centered in this region is Q243, which was predicted to interact with Q155 in the homodimer (Fig. 9) and may be the reason for the increased stability in the dimer simulation.

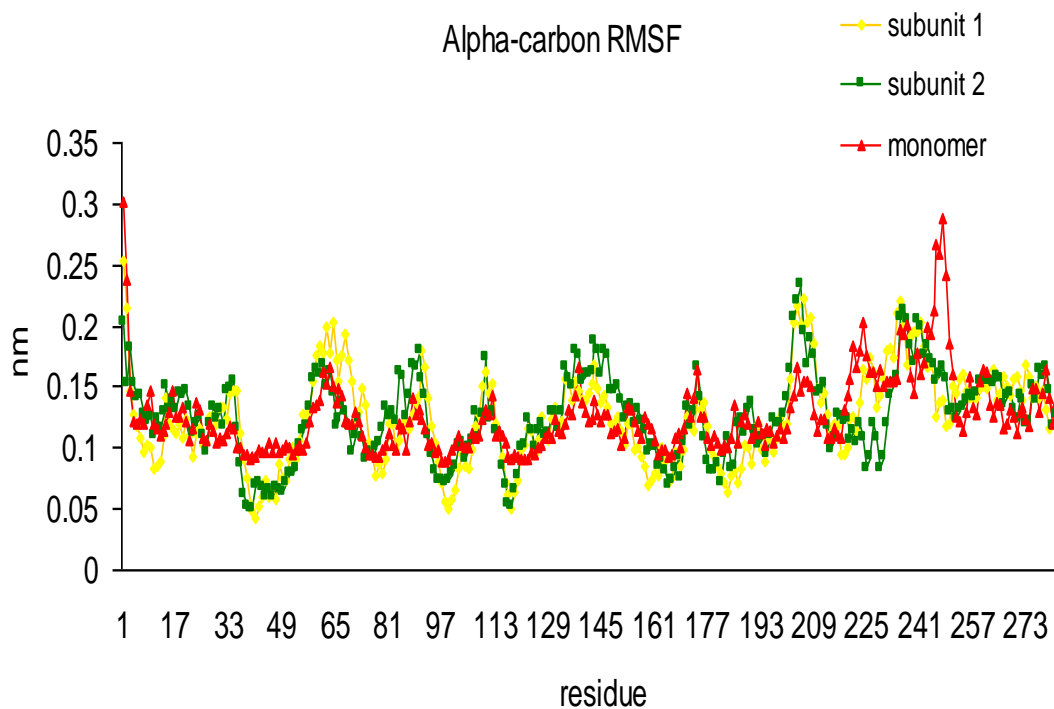


Figure 51. Dynamic modeling of the monomer and homodimer of SULT2A1. Dynamic modeling was performed using GROMACS. The SULT2A1 subunit model was constructed from the SULT2A1 crystal structure generated with bound DHEA (1J99) using the method described in section II-B. The SULT2A1 homodimer was generated by duplicating the subunit and aligning the subunits at the KTVE dimerization domain as described in section II-B. The simulation then initiated and run 5 nsec of simulated time as described in section II-B. The RMSF of the alpha carbon was measured for each residue and is shown above. The monomer is in red and the two subunits of the dimer are in green and yellow.

E) Homodimer Mutations of SULT2A1

The mutation of the valine in the KTVE dimerization domain to a glutamate has been shown to convert SULT1A1 and SULT1E1 to monomers (Petrotchenko, Pedersen et al. 2001). Based upon these reports, the mutation of V260E should convert SULT2A1 to a monomer. In addition to the KTVE mutation, Q155 and Q245 were predicted to have an interaction across the homodimer. To test the homodimer interactions, V260E, Q155A, and Q245A SULT2A1 mutants were generated using the QuickChange II site-directed mutagenesis kit by Stratagene. Mutations were confirmed by the UAB sequencing core. Mutants were then expressed and purified using the same method described for pMAL-SULT2A1.

The sizes of the mutant enzymes were examined by size exclusion chromatography with a G-100 Sephadex column. The Q155A and Q245A mutants were both identified as homodimers. In contrast, the V260E mutant was identified as a monomer (Fig. 52). These results are consistent with those found with the SULT1A1 and SULT1E1 mutations (Petrotchenko, Pedersen et al. 2001). With the V260E mutation confirmed to be a monomer, the activity for DHEA sulfation activity was compared to SULT2A1. The DHEA concentration sulfation plot showed a decreased affinity and an accurate K_m could not be calculated (Fig. 53A). While the K_m was estimated to be 80-100 μM , DHEA has a maximum solubility in aqueous solution of 30 μM , limiting the ability to further analyze activity. The PAPS concentration plot had a calculated K_m of 20 μM with a V_{max} of 52 pmol/min/mg, compared to the WT SULT2A1 K_m of 0.2 μM and V_{max} of 17,200 pmol/min/mg. While no substrate inhibition was observed with the monomer, the poor activity of the mutant makes any conclusions regarding substrate in-

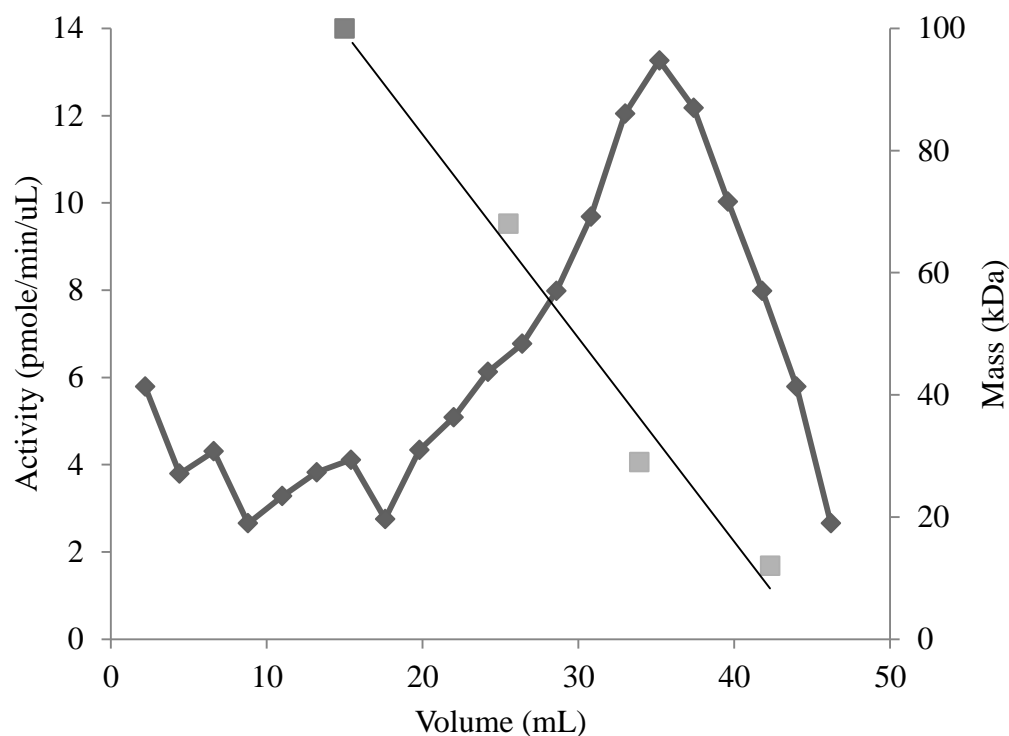


Figure 52. Monomerization of SULT2A1 by the V260E mutation in the KTVE dimerization domain. Size exclusion chromatography was performed with a G-100 Sephadex column (45 mL) equilibrated in 10 mM sodium phosphate (pH 7.4) as described in section II-C. The column was calibrated with blue dextran (2000 kDa), bovine serum albumin (66.7 kDa), equine fumarase (48.5 kDa), and human cytochrome C (12.1 kDa). Elution of enzyme was monitored by DHEA sulfation activity and UV absorbance at 260 nm

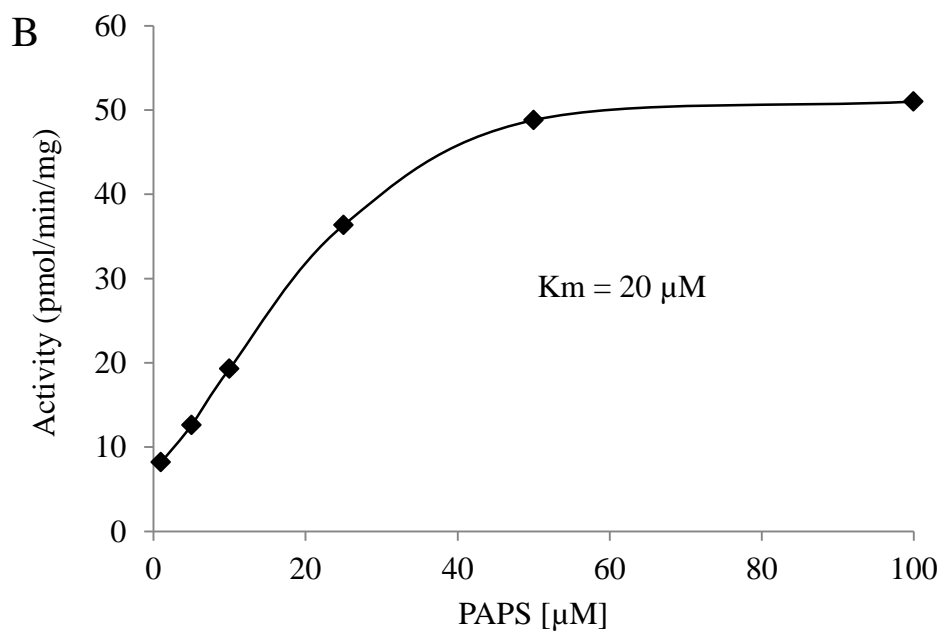
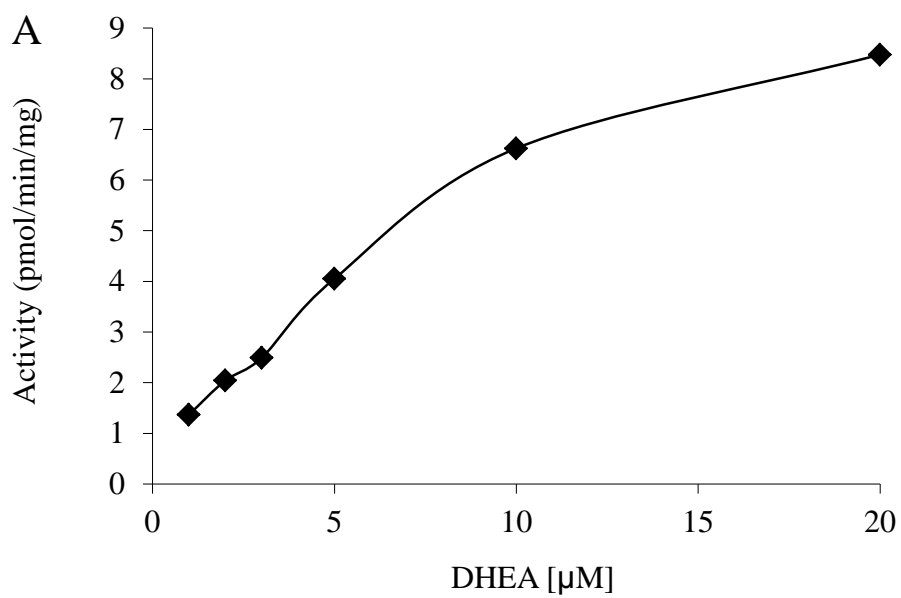


Figure 53. DHEA sulfation with increasing concentration of DHEA and PAPS concentration curves with V260E SULT2A1. DHEA sulfation activity of the V260E SULT2A1 was performed with [³H]-DHEA and chloroform extraction described in the methods section I-B. A) DHEA sulfation was assayed with 20 μM of PAPS and 1, 2, 3, 5 10 or 20 μM [³H]-DHEA. B) PAPS sulfation was assayed with 20 μM [³H]-DHEA and 1, 5, 10, 25, 50, or 100 μM PAPS. Km and Vmax were determined for PAPS based on the Lineweaver-Burk plot. No Km or Vmax could be calculated for DHEA due to the inability to reach saturating DHEA concentration. Each concentration was evaluated in duplicate.

hibition inconclusive. The results demonstrate that the V260E mutation significantly reduces the affinity of SULT2A1 for both PAPS and DHEA.

DHEA sulfation activity for Q155A and Q245A SULT2A1 was not significantly different from WT SULT2A1. A DHEA concentration plot showed that both mutants behaved in a manner statistically similar to WT (Fig. 54), suggesting one of two possibilities. The first is that the Q155 and Q245 interaction is not real but is an artifact of the simulation. The second possibility is that there are redundant interactions in the sequence that can compensate for the Q155 and Q245 interactions. The nearby residues of C154, T157, K246, and D243 may also have interactions that could cross the homodimer.

F) Cos-7 Cell DHEA Sulfation

To study the effect of dimerization and substrate inhibition in a more physiological environment, Cos-7 cells were transfected with SULT2A1 and MBP-SULT2A1 using the pcDNA 3.1(-) vector. Expression of SULT2A1 and MBP-SULT2A1 was confirmed by Western blot analysis using a SULT2A1 polyclonal antibody (Fig. 55). The cells were then treated with [³H]-DHEA and the production of [³H]-DHEAS was monitored by chloroform extraction of the media (Fig. 56). DHEA sulfation activity for SULT2A1 transfected cells showed a Km of 7 μM with substrate inhibition at 15 μM. MBP-SULT2A1 had a Km of 10 μM, with no substrate inhibition observed. The cell assay demonstrated that the WT SULT2A1/Cos-7 cells and the MBP-SULT2A1/Cos-7 had similar affinities for DHEA. However; the WT SULT2A1/Cos-7 showed substrate inhibition over 12.5 μM and no substrate inhibition was not observed with MBP-SULT2A1/Cos-7.

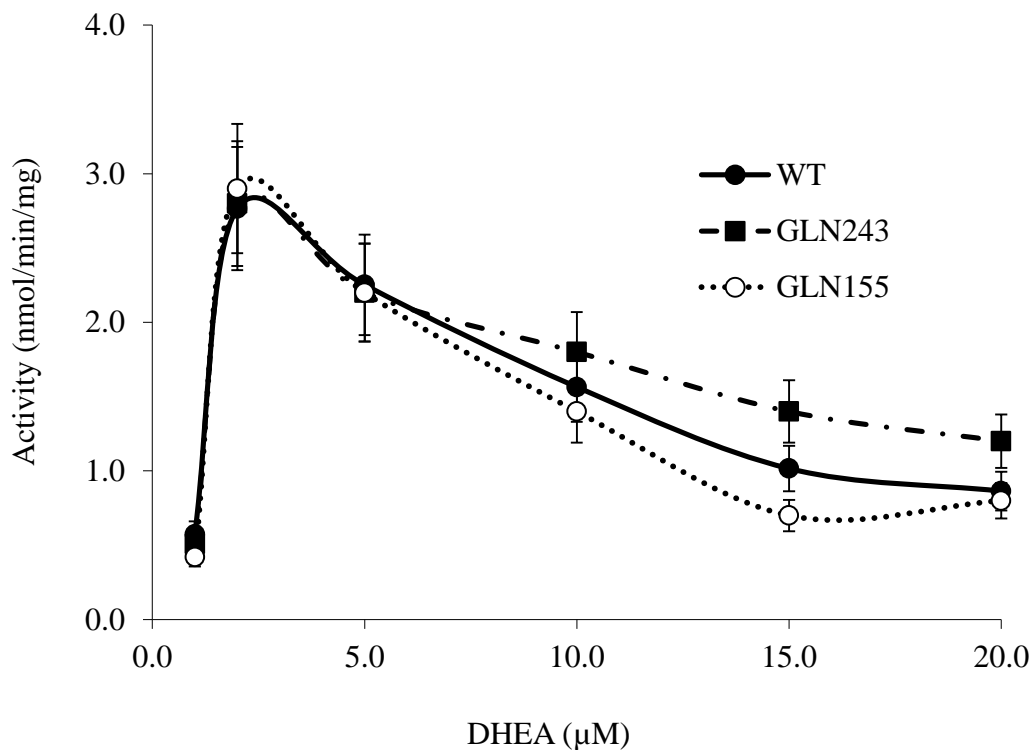


Figure 54. DHEA sulfation of Q155A and Q243A SULT2A1 mutants. Increasing DHEA concentration sulfation activity of WT (black circles), Q155A (white circles), and Q243A (black squares) SULT2A1 was assayed using the chloroform extraction assay described in section I-B. DHEA sulfation was evaluated with 20 μM PAPS and 1, 2, 5, 10, 15, or 20 μM [³H]-DHEA. Each reaction was evaluated in triplicate and presented as the mean ± SEM.

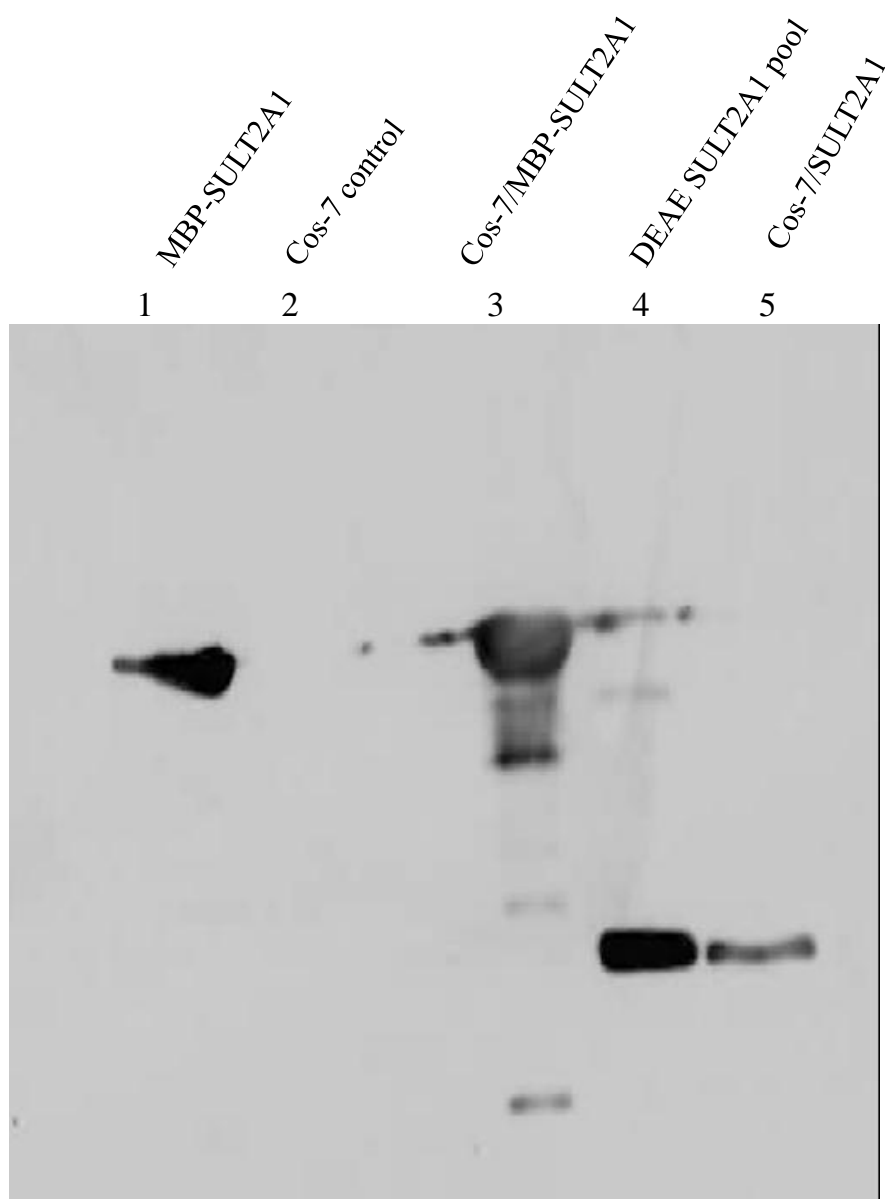


Figure 55. SDS-PAGE and immunoblot analysis of Cos-7 stably transfected cells. Expression levels of MBP-SULT2A1 and SULT2A1 in stably transfected COS-7 cells were determined by immunoreactivity with a rabbit anti-human liver SULT2A1 IgG as described in section II-H. Lanes 2, 3, and 5 were loaded with 100 μ g of COS-7 cell extract, lane 1 was loaded with 0.5 μ g of pure MBP-SULT2A1, and lane 4 was loaded with 20 μ g partially purified SULT2A1 pool.

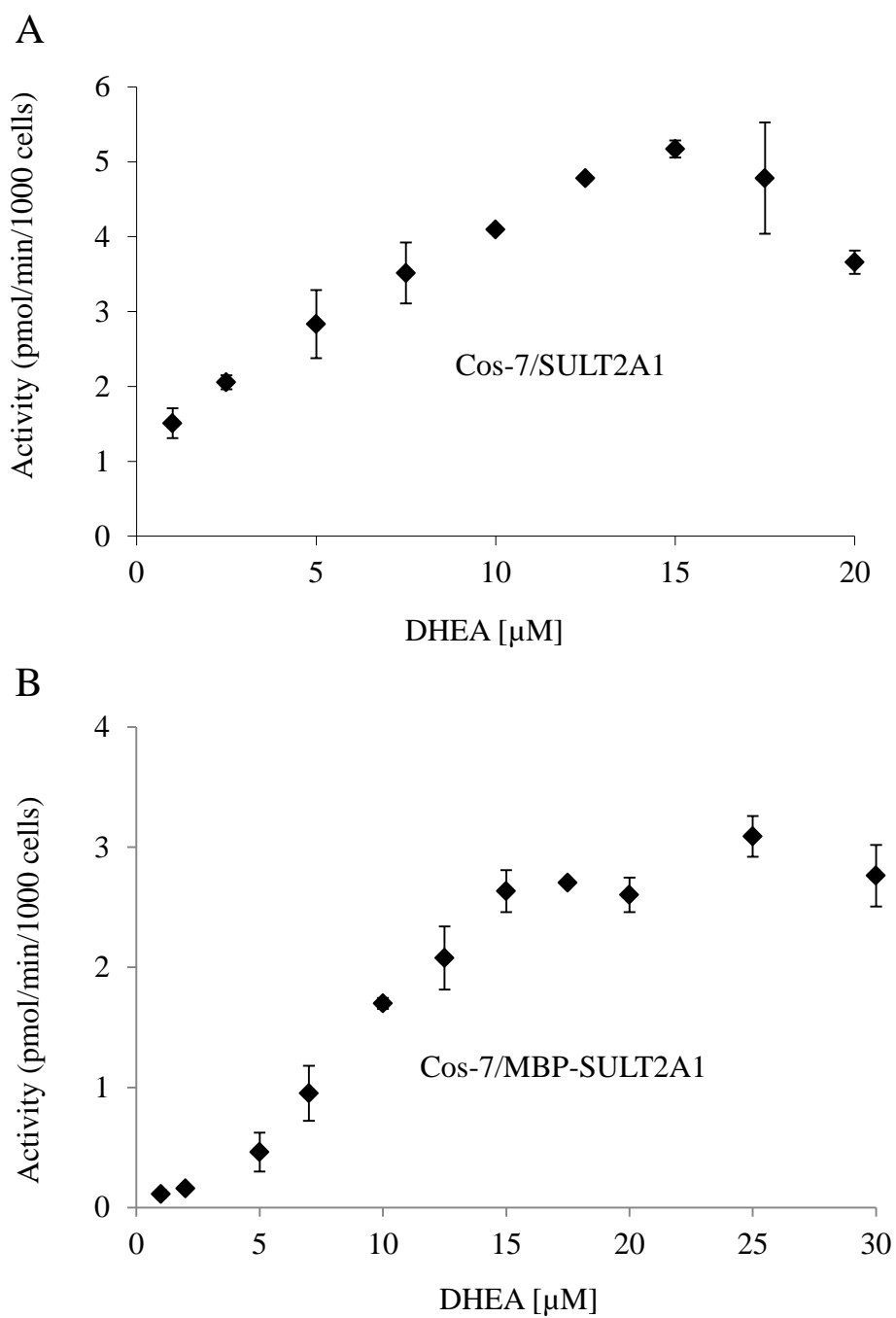


Figure 56. Generation of sulfated DHEA by SUTL2A1 or MBP-SULT2A1 stably transfected Cos-7 cells. DHEA sulfation activity for intact A) SULT2A1 and B) MBP-SULT2A1 stably transfected Cos-7 cells was assayed using [³H]-DHEA and chloroform extraction as described in section II-I. Each reaction was evaluated in triplicate and presented as the mean \pm SEM. The apparent Kms were determined by the Lineweaver Burk plot.

G) Specific Aim 2 Conclusions

In Aim 2, a second allosteric binding site for DHEA was shown to be involved in the mechanism of substrate inhibition. Access to the allosteric binding site was inhibited by the binding of PAPS and the structure and function of the allosteric binding site was also lost in the monomeric form of the enzyme. Furthermore, the results indicated that the effect of the allosteric site was also observed in intact cells as well as purified enzyme. These results are consistent with the hypothesis that the binding of PAPS changes the homodimer interface, and inhibits substrate inhibition.

III. THE STRUCTURAL REARRANGEMENTS OF SULT1A1 AND SULT1E1 ASSOCIATED WITH PAPS BINDING

We propose that the structural rearrangements induced by PAPS binding observed in SULT2A1 are a basic characteristic of the SULT family?

The 3rd specific aim in this thesis was to determine whether the structural changes induced by PAPS binding were unique to SULT2A1 or a characteristic of the SULT family. Homology modeling of SULT1A1 and SULT1E1 predicted that some of the structural changes observed in SULT2A1 would occur in SULT1A1 but probably not in SULT1E1. To test whether the binding of PAPS induced the predicted changes in the structures of SULT1A1 and SULT1E1, the sulfation of FUL and E2 was examined in both SULT1A1 and SULT1E1. The homology modeling and docking studies predicted that binding would be ordered for SULT1A1 and random for SULT1E1. In addition, E2 was predicted to show a random reaction mechanism with SULT1A1 and SULT1E1.

A) Homology Modeling of SULT1A1 and SULT1E1 to the Open SULT2A1 Model

Homology modeling was performed with SULT1A1 and SULT1E1 to the open crystal structure of SULT2A1 generated with bound DHEA (1J99). The sequence of the SULTs were aligned and threaded onto the open SULT2A1 template using MODELLER. The side chains were added and the model was then minimized with AMBER. The open SULT models were then submitted to the NIH SAVES server to check for errors and found to contain no significant errors in structure. The core of the SULT structures was not changed in either SULT1A1 or SULT1E1 and there was less than a 1.5 RMSD over the whole enzyme. The homology model of SULT1A1 predicted several changes with the binding of PAPS (Fig. 57). In loop 1 of SULT1A1, from K85 to P90, the homology model predicted change of 5 Å in the backbone. The loop 1 region was observed to be highly dynamic in the three existing crystal structures of SULT1A1, supporting the predictions of the homology models. The second region of interest in the model was in loop 2 (Y140 to P150), with a predicted a shift of 3 Å in the backbone. The final region predicted to change is loop 3 of SULT1A1 (M237 to W261) that forms the outer surface of the substrate and PAPS binding domain and is analogous to the loop 3 region of SULT2A1. The loop 3 region had a 3 Å change over the substrate side, and a 5 Å shift on the PAPS active site. Thus the homology model indicates that the open active site of SULT1A1 is 50% larger than the closed crystal structure and closes with PAPS binding.

SULT1E1 was modeled using the same method utilized for SULT1A1 with the open SULT2A1 model (Fig. 58). The homology model predicted less structural changes than the SULT1A1 simulation. The loop 1 region of SULT1E1 (R85 to L90) showed a similar shift to that observed in SULT1A1, though no dynamics have been observed in

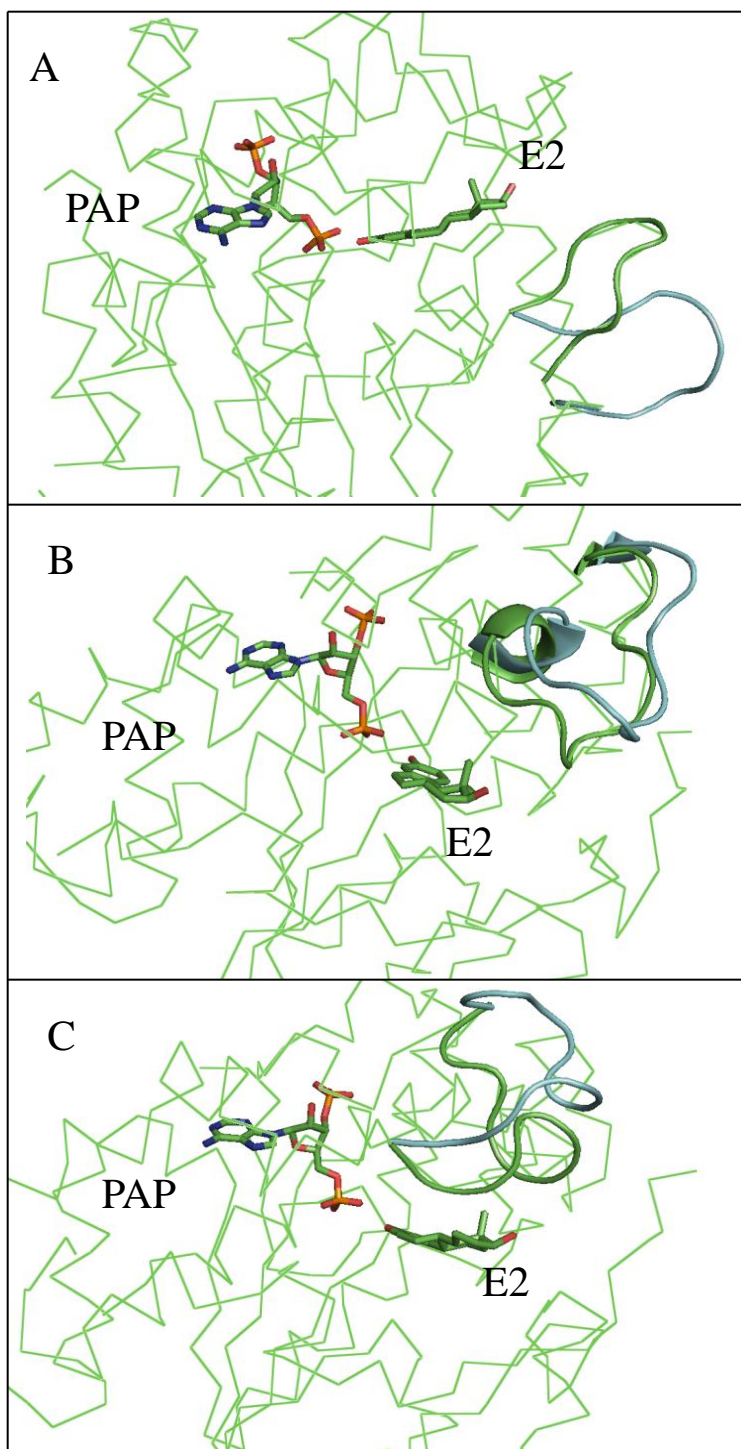


Figure 57. Homology modeling of SULT1A1 to the open SULT2A1 template. Homology modeling was performed with SULT1A1 using the SULT2A1 crystal structure generated with bound DHEA (1J99) as a template, as described in section III-B. The SULT1A1 crystal structure made with PAP and E2 (2DO6) is shown in green with the ligands shown in stick. The SULT1A1 homology model is shown in cyan. The core of the SULT1A1 backbone is in ribbon with the loop region shown in cartoon. Panel A) shows Loop 1 (K85-P90) B), panel B) shows loop 2 (Y140-P150) and panel C) shows loop 3 (M237-W261).

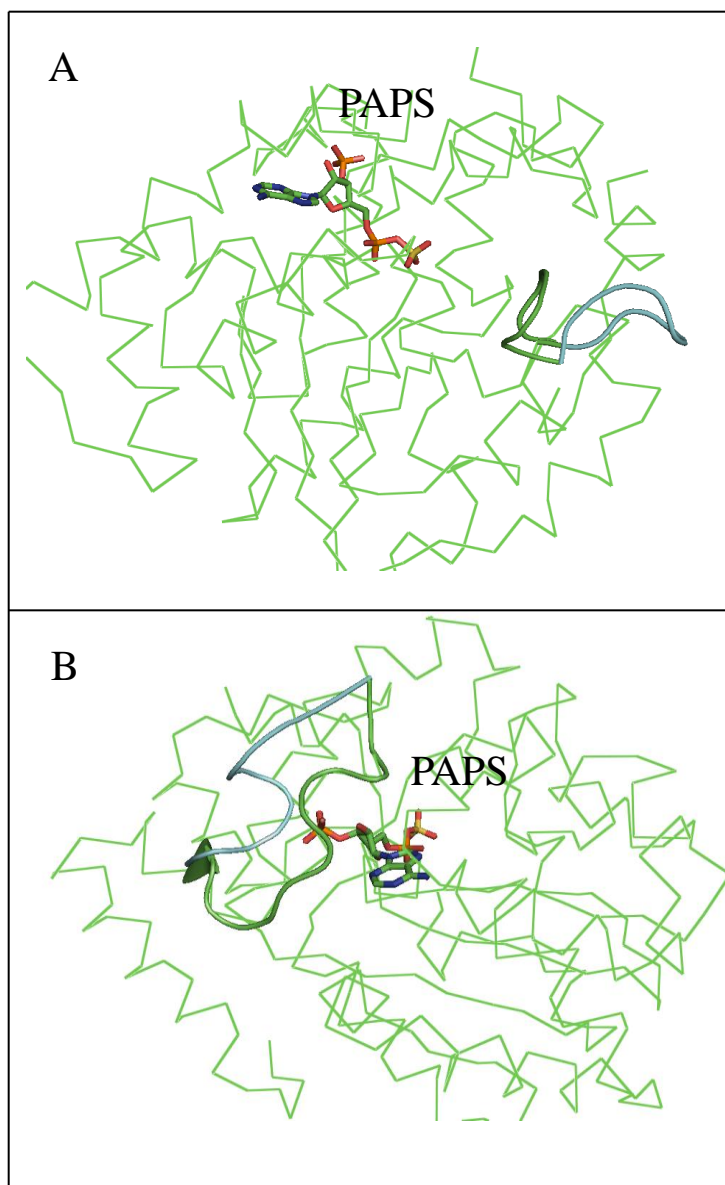


Figure 58. Homology modeling of SULT1E1 to the open SULT2A1 template. Homology modeling was performed with SULT1E1 using the SULT2A1 crystal structure generated with bound DHEA (1J99) as a template, as described in section III-B. The SULT1E1 crystal structure made with bound PAPS (1HY3) is shown in green with the PAPS shown in stick, and the SULT1E1 homology model is shown in cyan. The core of the SULT1E1 backbone is in ribbon. A) Loop 1 of SULT1E1 (R85-L90) and B) Loop3 of SULT1E1 (K250- W262) are shown in cartoon.

the crystal structures of SULT1E1 (Pedersen, Petrotchenko et al. 2002) (Shevtsov, Petrotchenko et al. 2003). The homology model also predicted a structural shift in loop 3. In SULT1E1, the structural rearrangement was observed only on the PAPS binding site of loop3 (K250 to W262). No significant change was observed on the substrate active site in the loop 3 region. The homology modeling of SULT1E1 predicted only a 10% increase in the volume of the active site in the open model.

B) Molecular Docking to SULT1A1 and SULT1E1

1. *SULT1A1 Docking of FUL and E2*

Docking of FUL and E2 to SULT1A1 was performed using the same docking method utilized for SULT2A1 molecular docking. The available SULT1A1 crystal structure formed with bound E2 and PAP (2D06) represented the closed model (Gamage, Tsvetanov et al. 2005). The PDB structure was minimized and the PAP was converted to PAPS. The open model was the homology model described previously. FUL and E2 docking was performed as described in Methods. FUL docking to the open homology model predicted a competent orientation 2.5 Å from the active site H108 with a BFE of -11.8 kJ (Fig. 59A). When FUL was docked to the closed model, no binding was predicted for FUL to the active site. The lowest energy orientation places FUL with the side chain in the active site and has a BFE of -3.4 kJ (Fig. 59B). Based on the docking, FUL sulfation by SULT1A1 is predicted to be an ordered reaction mechanism with FUL as the lead substrate.

E2 is a known substrate of SULT1A1 (Falany, Krasnykh et al. 1995; Gamage, Tsvetanov et al. 2005), and was docked to both the open and closed SULT1A1 models.

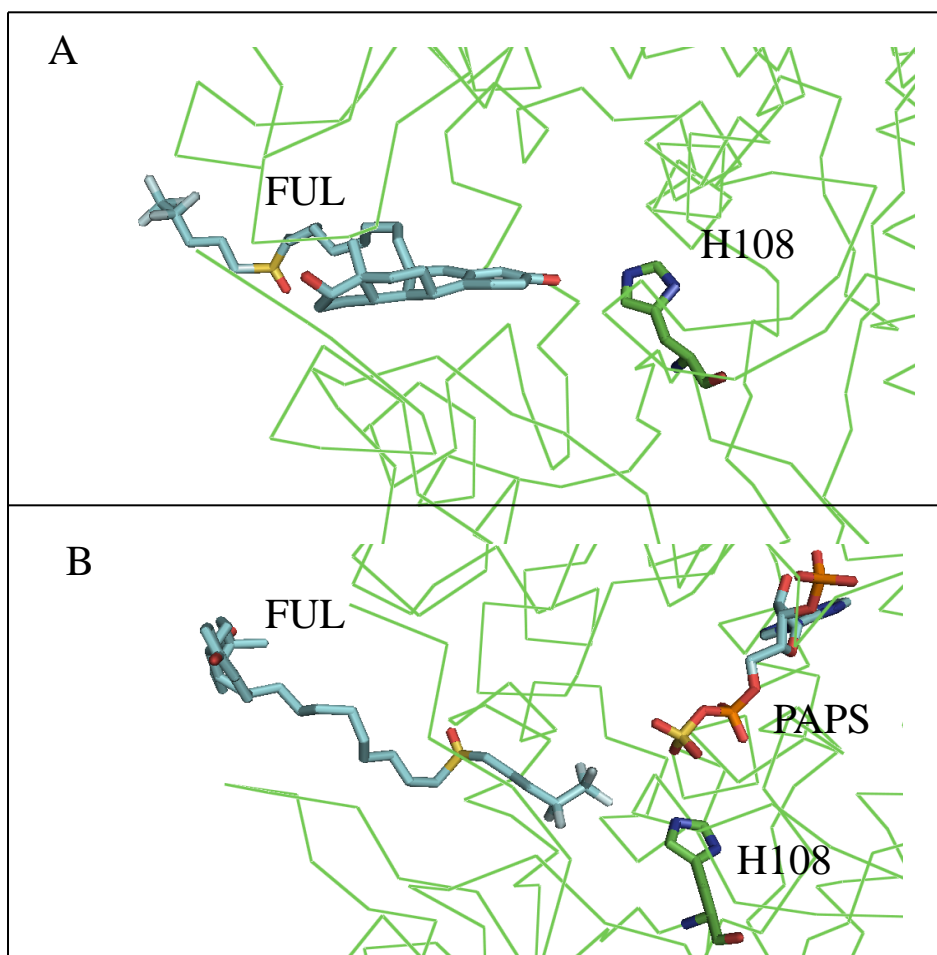


Figure 59. Docking of FUL to the open and closed models of SULT1A1. Docking of FUL was performed using the programs in MOE as described in the section III-C. The closed model was built using the SULT1A1 crystal structure made with bound PAP and E2 (2DO6) and the open model was built from the homology model of SULT1A1 with the SULT2A1 open structure as a template. A) The lowest energy orientation of FUL in the open model. FUL docked with a predicted BFE of binding of -11.8 kJ. A hydrogen bond was predicted between the H99 and 3-OH group of FUL. B) The lowest energy orientation of FUL docked in the closed model. The BFE for the docking was -3.4 kJ. No hydrogen bond was observed in the docking. SULT1A1 is in green and FUL and PAPS are in cyan. H108, PAPS, and FUL are in stick and the backbone of SULT1A1 is in ribbon.

The docking of E2 to the open SULT1A1 structure predicted a catalytically competent orientation with a BFE of -7.9 kJ (Fig. 60A). E2 was also able to bind to the closed active site with a BFE of -8.5 kJ also in a catalytically competent orientation (Fig. 60B). E2 docking with the closed model showed less than 0.5 Å RMSD compared to the PAP*SULT1A1*E2 crystal structure. In both models, E2 was less than 3 Å from the active site H108. The docking results predict that SULT1A1 sulfation of E2 is a random ordered Bi Bi reaction mechanism.

2. *SULT1E1 Docking of E2 and FUL*

Docking simulations with SULT1E1 were performed using the homology model for the open model and the SULT1E1 crystal structure generated with bound PAPS (1HY3) for the closed model. Docking of E2 to SULT1E1 was performed with the closed and open model and predicted a competent orientation for E2 in both models (Fig. 61). The BFE was -16.4 kJ for the closed and -15.3 kJ for the open structure, predicting a random ordered Bi Bi reaction mechanism. This result is consistent with the reported reaction mechanism for SULT1E1 by Zhang et al. (Zhang, Varlamova et al. 1998). FUL was then docked to the open and closed model of SULT1E1 and was predicted to bind in a catalytic orientation with the H106 to both SULT1E1 models (Fig. 62). FUL bound to the SULT1E1 open model with a BFE of -11.7 kJ and to the closed model with a BFE of -11.2 kJ. The FUL docking to SULT1E1 predicts a random ordered Bi Bi reaction mechanism.

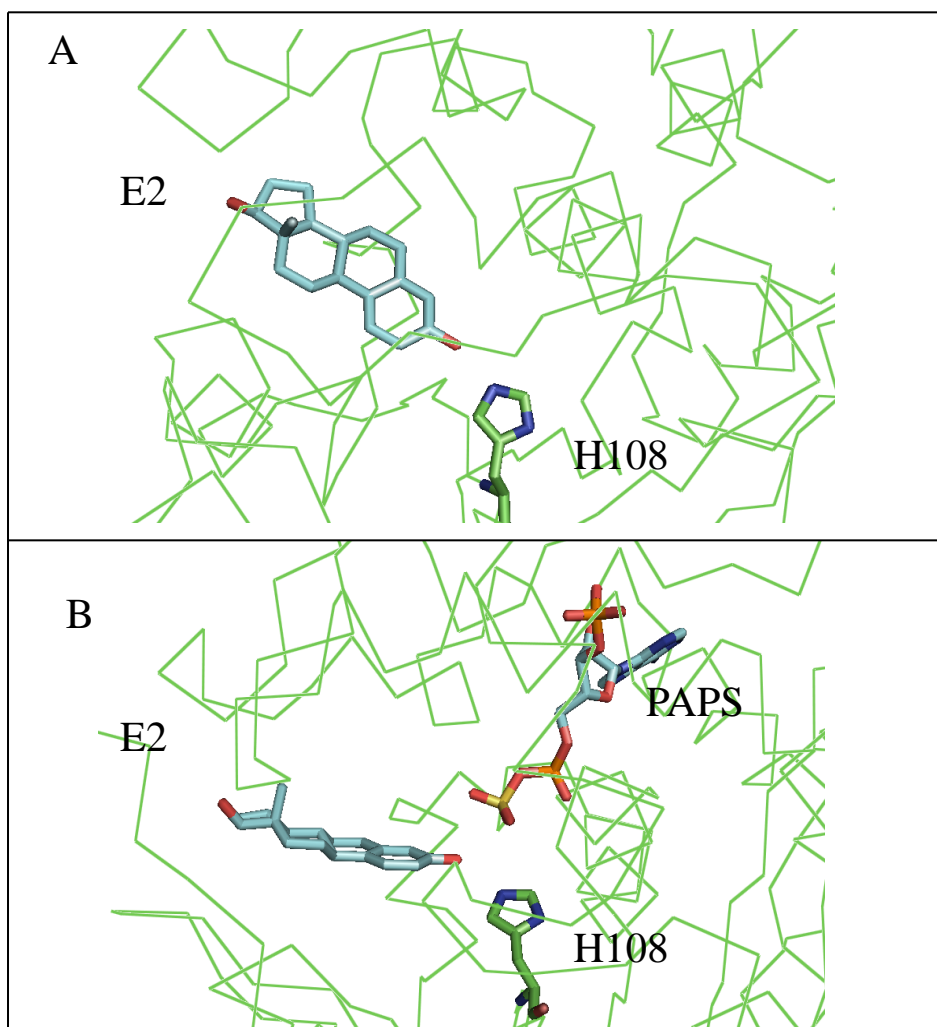


Figure 60. Docking of E2 to the open and closed models of SULT1A1. E2 docking was performed using the programs in MOE as described in the method section III-C. A) The lowest energy orientation of E2 in the open model. E2 docked with a predicted BFE of binding of -7.9 kJ. B) The lowest energy orientation of E2 docked in the closed model. The BFE for the docking was -8.5 kJ. In both models a hydrogen bond was predicted with the H99 and 3-OH of E2. SULT1A1 is in green and E2 and PAPS are in cyan. H108, PAPS, and E2 are in stick and the backbone of SULT1A1 is in ribbon.

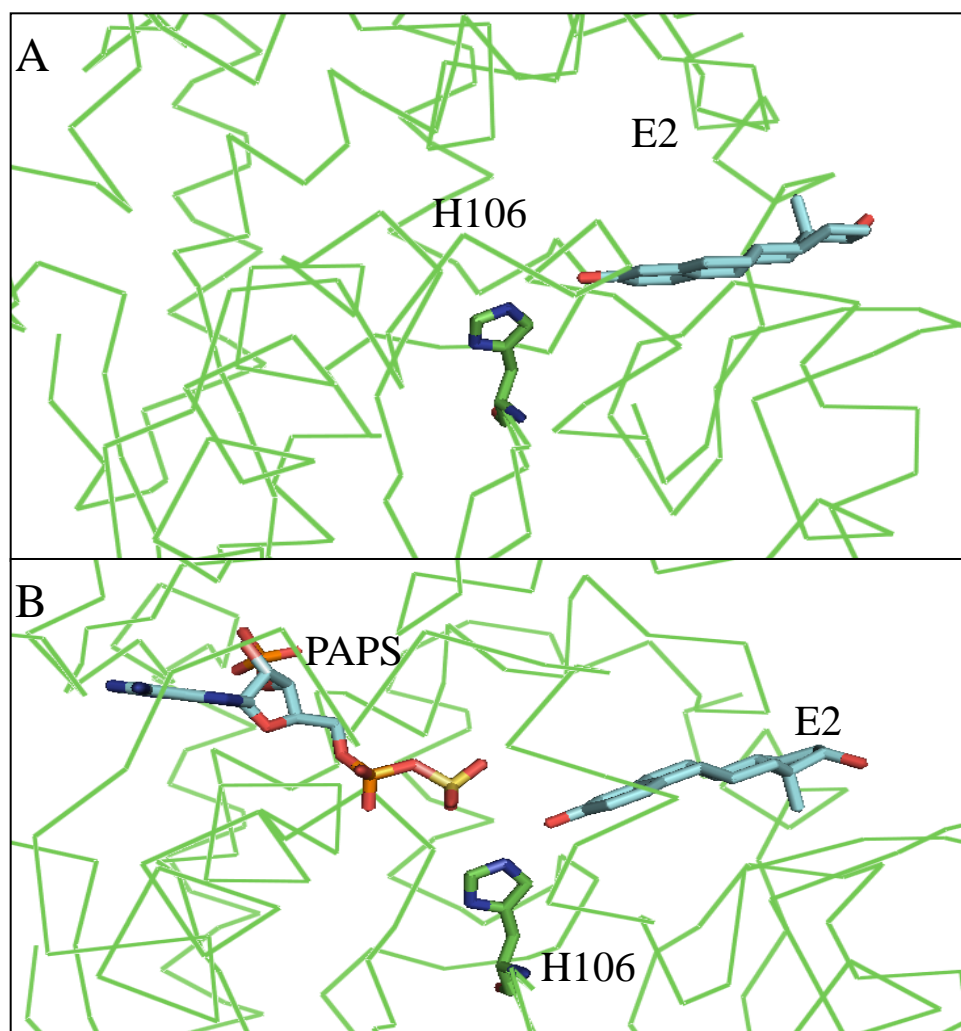


Figure 61. Docking of E2 to the open and closed models of SULT1E1. Docking of E2 was performed using the programs in MOE using the protocol described in the methods section III-C. The closed model was built with the SULT1E1 crystal structure made with bound PAPS (1HY3) and the open model was built from the homology model of SULT1E1 with the SULT2A1 open structure as a template. A) The lowest energy orientation of E2 in the open model. E2 docked with a predicted BFE of binding of -15.3 kJ. B) The lowest energy orientation of E2 docked in the closed model. The BFE for the docking was -16.4 kJ. In both models a hydrogen bond was predicted with the H99 and 3-OH of E2. SULT1E1 is in green and E2 and PAPS are in cyan. H106, PAPS, and E2 are in stick and the backbone of SULT1E1 is in ribbon.

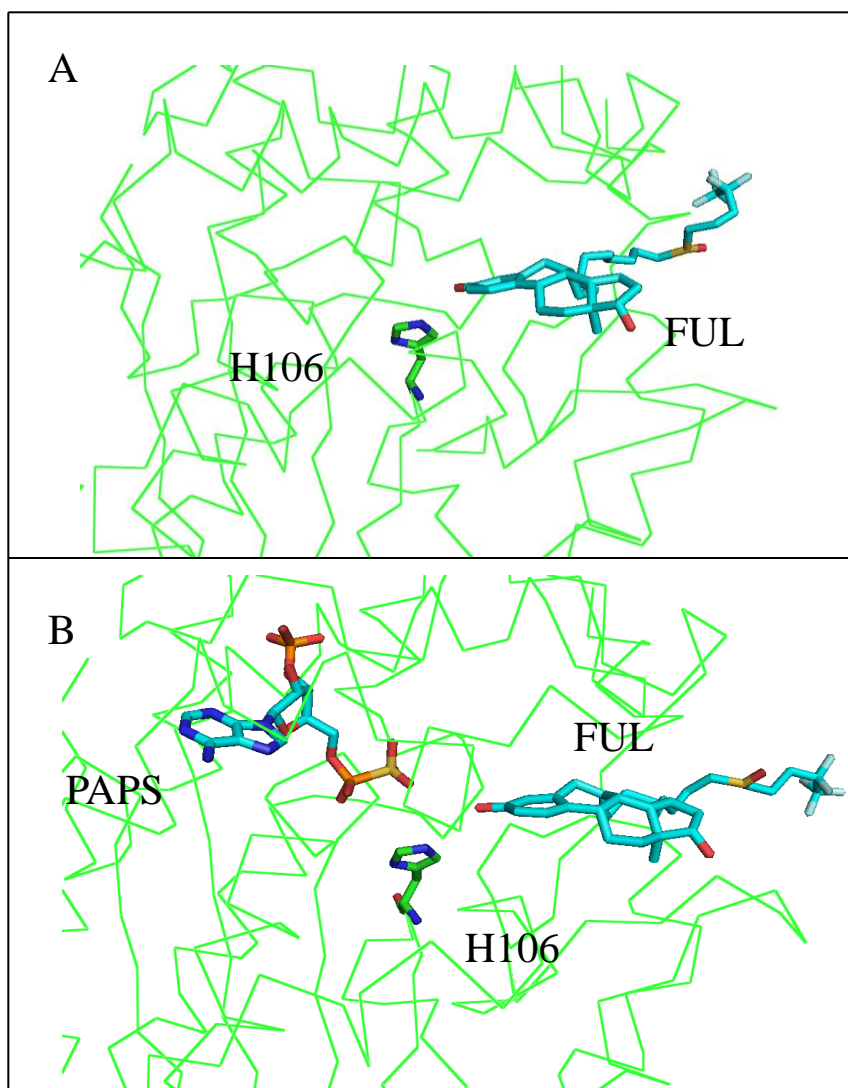


Figure 62. Docking of FUL to the open and closed models of SULT1E1. Docking of FUL was performed using the programs in MOE as described in the methods section III-C. A) The lowest energy orientation of FUL in the open model. FUL docked with a predicted BFE of binding of -11.7 kJ. B) The lowest energy orientation of FUL docked in the closed model. The BFE for the docking was -11.2 kJ. In both models a hydrogen bond was predicted with the H99 and 3-OH of FUL. SULT1E1 is in green and FUL and PAPS are in cyan. H106, PAPS, and FUL are in stick and the backbone of SULT1E1 is in ribbon.

C) FUL Sulfation by SULT1A1 and SULT1E1

FUL sulfation was performed with [³⁵S]-PAPS and TLC separation as described in the Methods. The K_m and V_{max} values of FUL sulfation by SULT1A1 were calculated based on the double reciprocal plot of the two substrate kinetic plots (Fig. 63A). The K_m for FUL sulfation was 4.2 μM and the K_m for PAPS was 1.2 μM . The V_{max} was 7.8 $\text{pmol min}^{-1} \mu\text{g}^{-1}$. Product inhibition was performed with 0.5 and 1.0 μM of PAP. The inhibition by PAP was un-competitive for FUL with a K_i of 0.65 μM (Fig. 63B). The un-competitive inhibition is consistent with an ordered reaction mechanism with FUL as the leading substrate. The affinity of SULT1A1 for FUL was measured with the change in intrinsic fluorescence as described in methods. The K_d for FUL binding to SULT1A1 was 2.3 μM (Fig 64A). However, when PAP was bound to the active site, no binding of FUL was observed (Fig 64B).

SULT1E1 sulfation activity for FUL was performed as described in the Methods (Fig. 65A). The K_m for FUL sulfation with SULT1E1 was 0.23 μM and the K_m for PAPS in the sulfation reaction was 0.1 μM . The V_{max} for the sulfation of the FUL by SULT1E1 was 62.5 $\text{pmol min}^{-1} \mu\text{g}^{-1}$. Product inhibition with PAP was performed with 1.0 and 0.5 μM PAP and was a mixed inhibitor for FUL with a K_i of 0.6 μM (Fig. 65B). The mixed competitive inhibition demonstrates that FUL sulfation by SULT1E1 is a random ordered Bi Bi reaction mechanism. The K_d for FUL binding to SULT1E1 was determined using the change in intrinsic fluorescence with an excitation of 285 nm and emission of 355 nm with a SULT1E1 concentration of 50 nM. The FUL titration was repeated in the presence of a saturating concentration of 10 μM PAP. The K_d for FUL binding

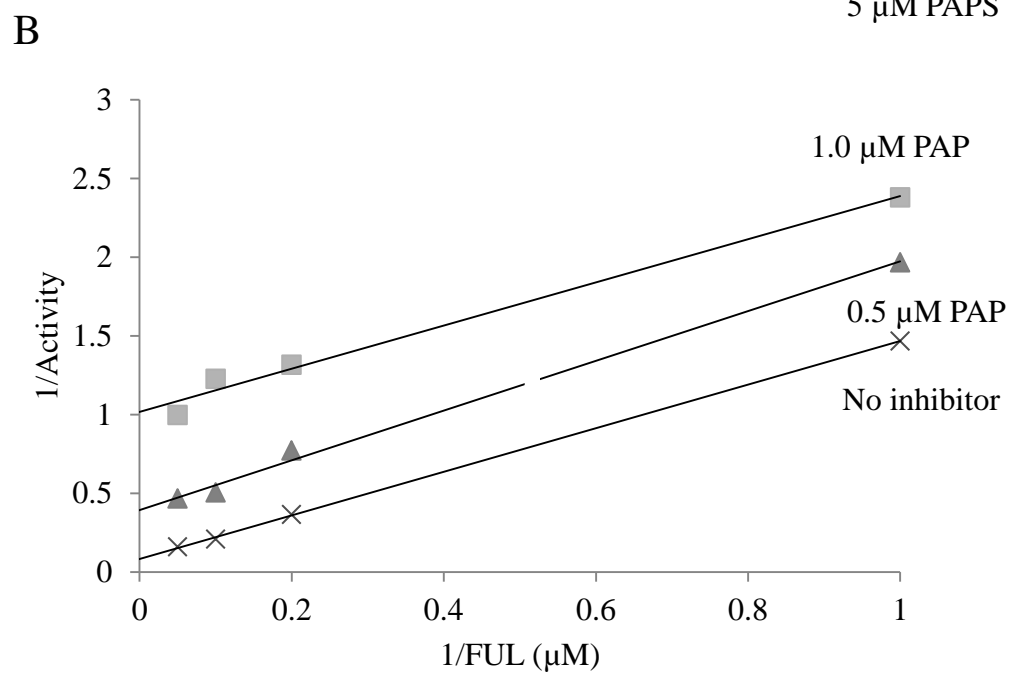
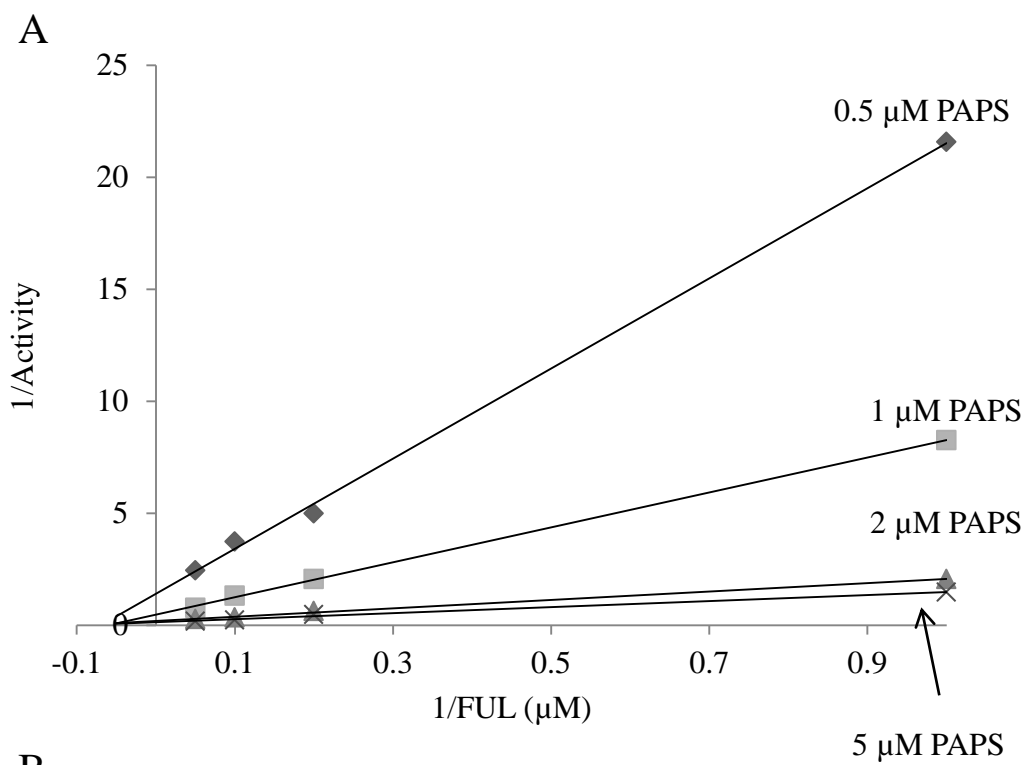


Figure 63. FUL sulfation by SULT1A1. FUL sulfation by SULT1A1 was assayed using [³⁵S]-PAPS with TLC separation as described in the methods section III-F and I-H. A) The kinetic constants were determined by the re-plots of the intercepts and slopes vs the concentration of PAPS. B) Product inhibition of FUL sulfation with 1.0 and 0.5 μM PAP using the TLC method described in the methods section III-F. Each reaction was performed in duplicate.

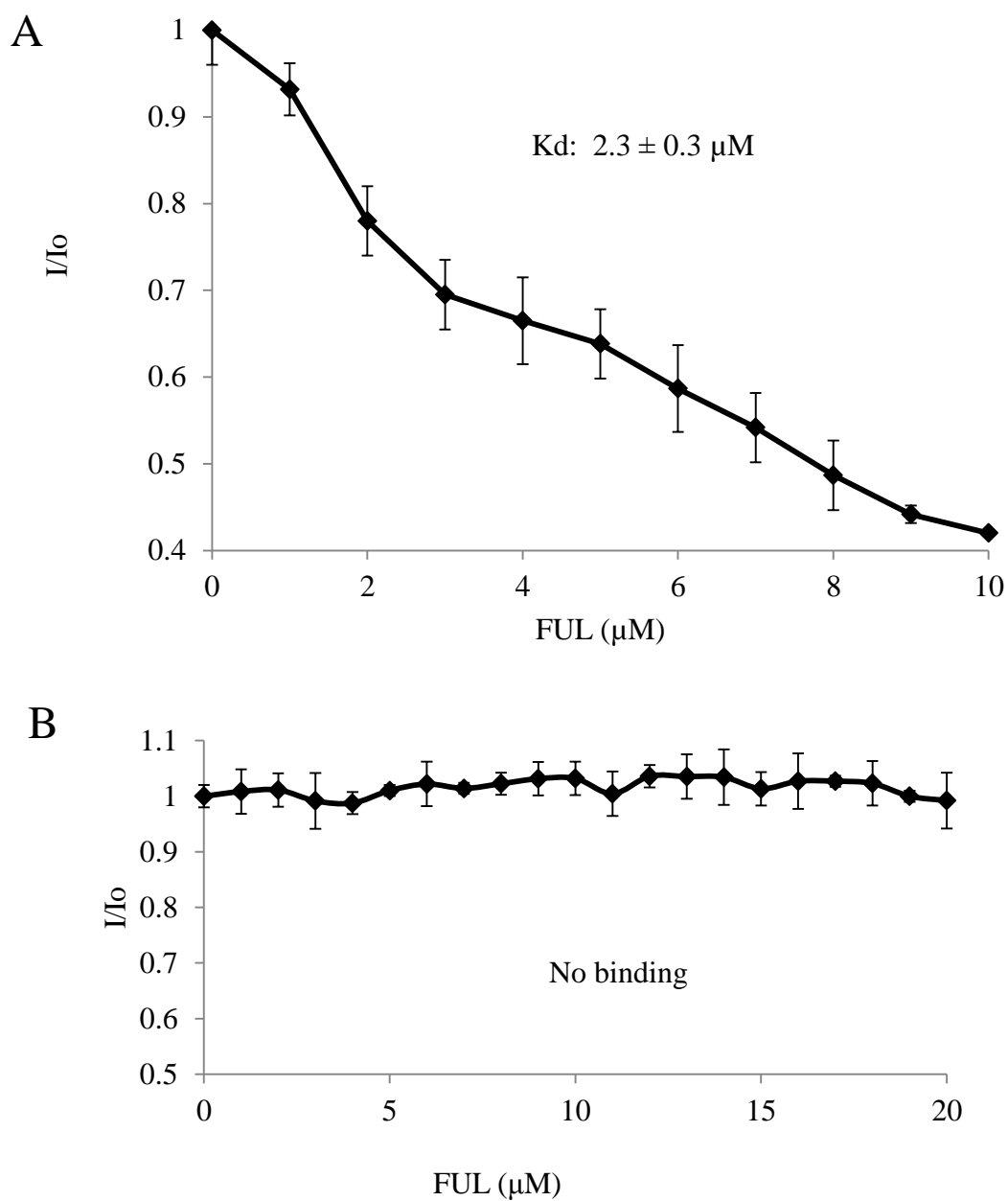


Figure 64. K_d determination of FUL binding to SULT1A1 using intrinsic fluorescence. FUL was titrated to 100 nM SULT1A1 as described in the sections III-G and I-J. The SULT1A1 was pre-incubated with A) no PAP or B) 10 μM PAP. The change in intrinsic fluorescence was plotted vs. the concentration of FUL. Each concentration was evaluated in triplicate and presented as the mean \pm SEM.

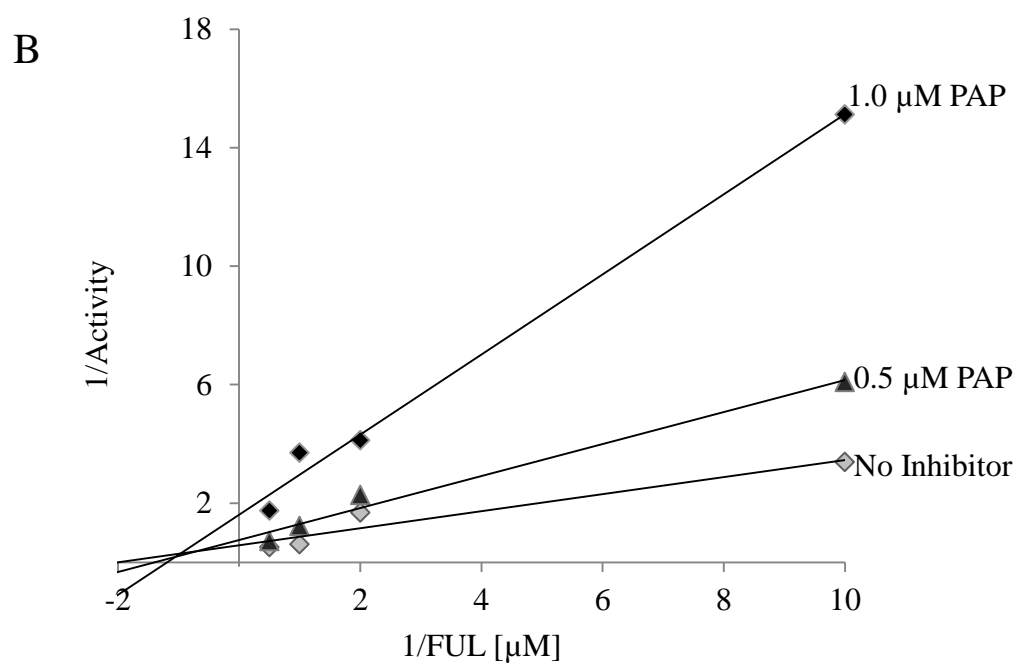
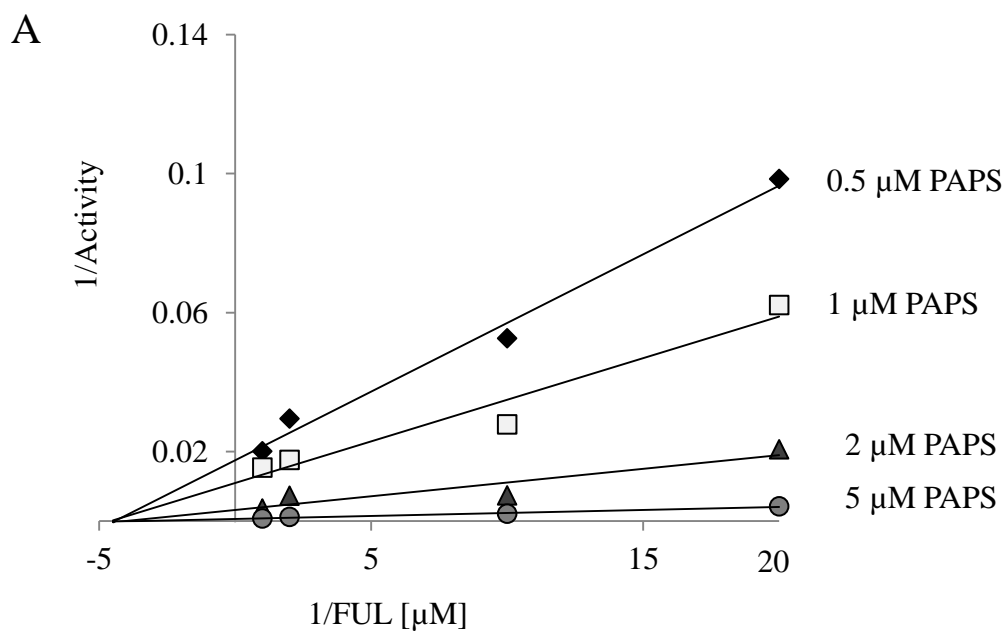


Figure 65. SULT1E1 sulfation of FUL. FUL sulfation by SULT1E1 was assayed using the [³⁵S]-PAPS and TLC method described in the methods sections III-G and I-J. A) The kinetic constants were determined by the re-plots of the intercepts and slopes vs the concentration of PAPS. B) Product inhibition of FUL sulfation with PAP was evaluated using the TLC method described III-F. Each reaction was performed in duplicate.

to SULT1E1 was 0.2 μM with and without PAP (Fig. 66). The affinity of FUL for SULT1E1 is consistent with the random ordered Bi Bi mechanism.

The pre-steady state kinetics of FUL sulfation was assayed with 2 pmole of SULT1A1 or 10 pmole of SULT1E1. The concentration of substrate in each reaction was 20 μM FUL and 10 μM PAPS. When SULT1A1 was saturated with FUL and the reaction was started with PAPS, there was a burst of FUL sulfation that represented a single turnover. After the burst, a steady state formation of FUL sulfate was observed. If SULT1A1 was saturated with PAPS, PAPS had to dissociate from the enzyme before the reaction could progress. SULT1A1 burst kinetics was consistent with an ordered reaction mechanism with FUL as the lead substrate (Fig. 67A). SULT1E1 had a single turnover in the first 10 sec with either PAPS or FUL bound to the enzyme, consistent with a random ordered Bi Bi reaction mechanism (Fig. 67B).

D) SULT1A1 Sulfation of E2

SULT1A1 sulfation of E2 was performed with [^3H]-E2 using a chloroform extraction assay similar to the assay for DHEA sulfation activity with SULT2A1. A two substrate double reciprocal plot was performed to determine the K_m and V_{max} values (Fig. 68). The K_m for E2 was 2.4 μM and the K_m for PAPS of 0.4 μM . The V_{max} for E2 sulfation of SULT1A1 was 16.2 $\text{pmol min}^{-1} \mu\text{g}^{-1}$. Product inhibition assays with PAP and E2-sulfate (Fig. 69) showed that both products were mixed inhibitors, consistent with a random ordered Bi Bi reaction mechanism with the K_{is} for the inhibitors shown in Table 2. The K_{is} of the products show that E2-sulfate has a poor affinity for the PAPS*SULT1A1 complex, likely because the two sulfates are required to be within 5 Å

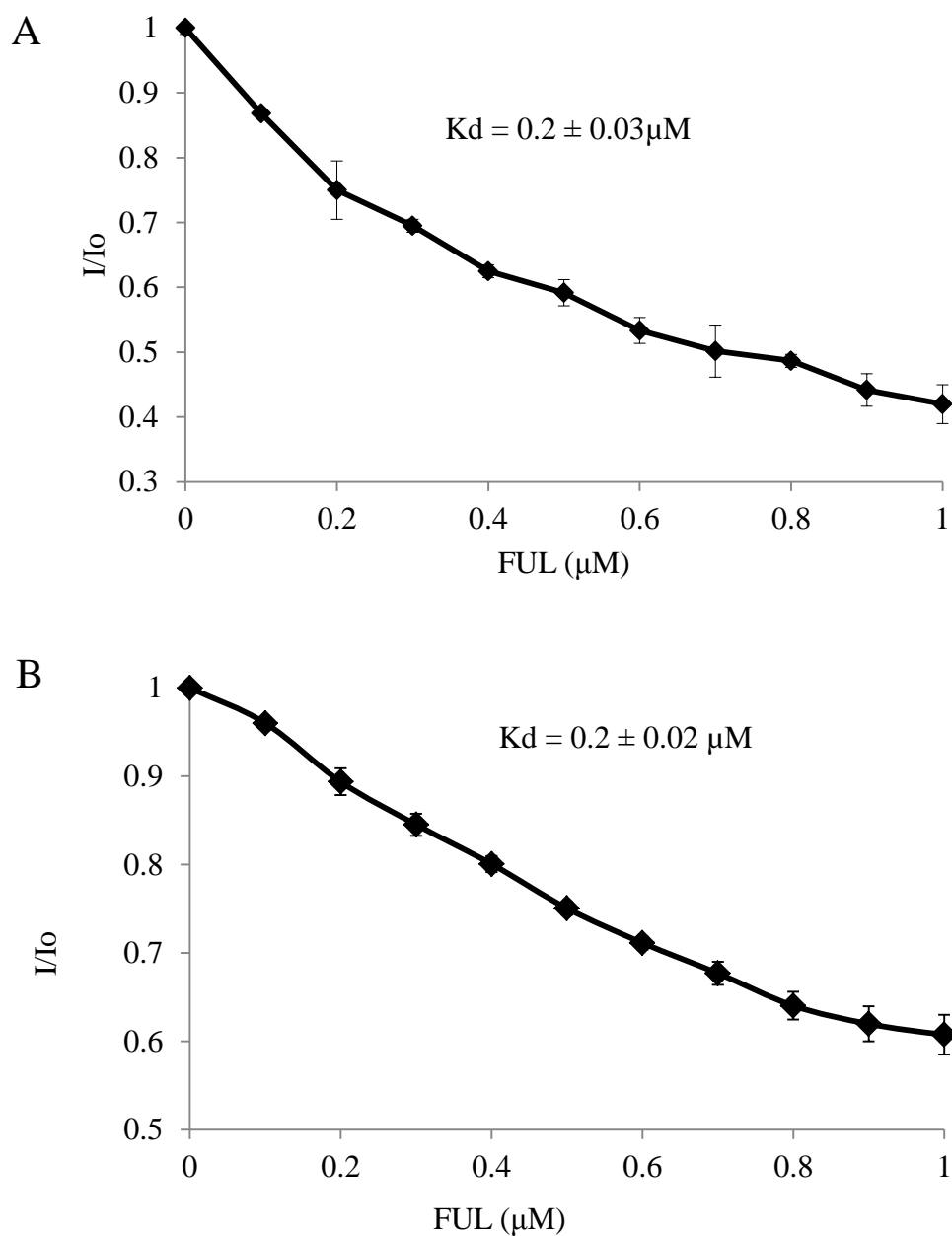
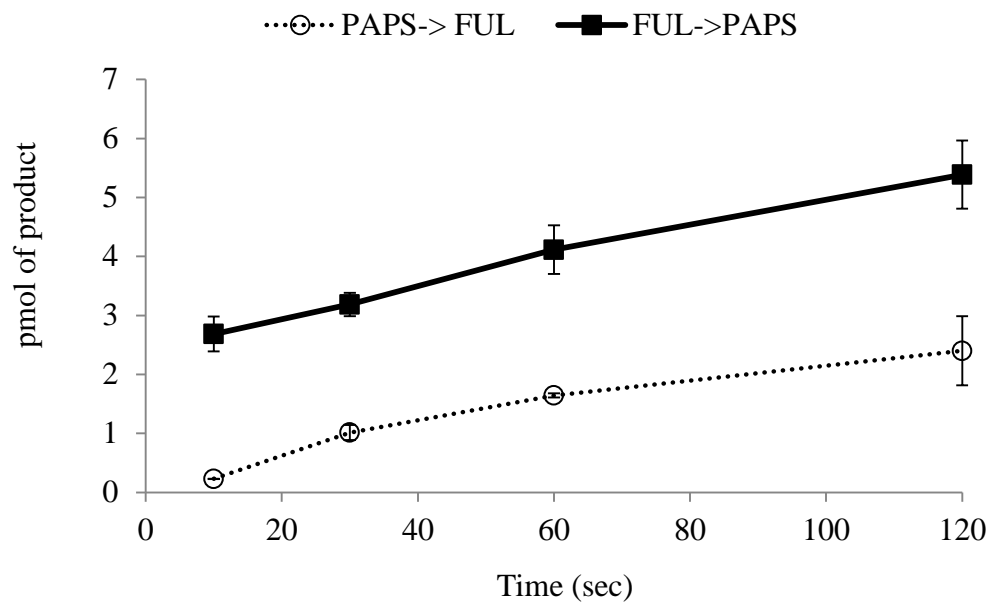


Figure 66. K_d determination of FUL binding to SULT1E1 using intrinsic fluorescence. FUL was titrated to 50 nM SULT1E1 from a stock solution of 10 μM FUL as described in the methods sections III-G and I-J. The SULT1E1 was pre-incubated with A) no PAP or B) 10 μM PAP. The change in intrinsic fluorescence was normalized to the initial fluorescence and plotted vs. the concentration of FUL. Each concentration was evaluated in triplicate and presented as the average \pm SEM.

A



B

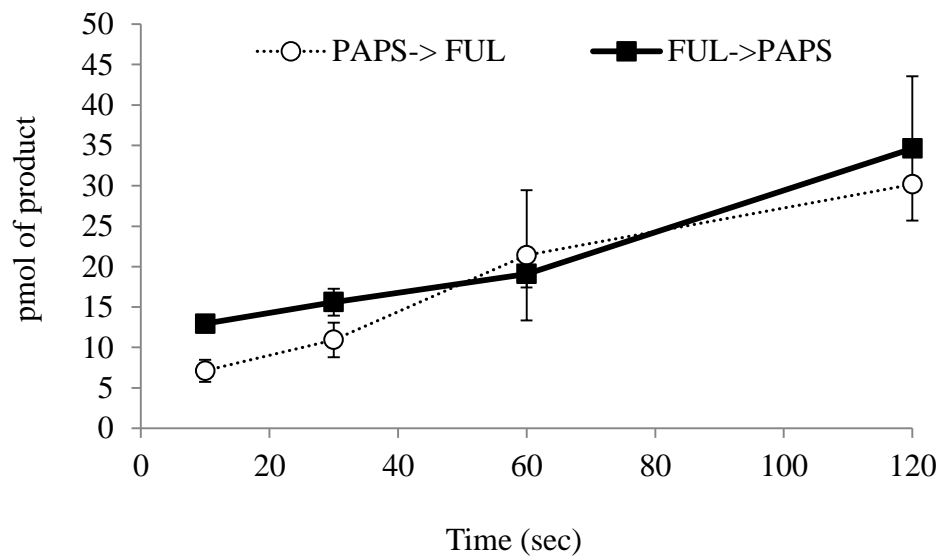


Figure 67. Pre-steady state kinetics of SULT1A1 or SULT1E1 for FUL sulfation. Pre-steady state FUL sulfation was evaluated with 10 μM [^{35}S]-PAPS and 20 μM of FUL. Reactions were assayed either A) 2 pmol of SULT1A1 or B) 10 pmol of SULT1E1 using the methods described in sections III-F and I-I. Each reaction was evaluated in triplicate, presented as the mean \pm SEM.

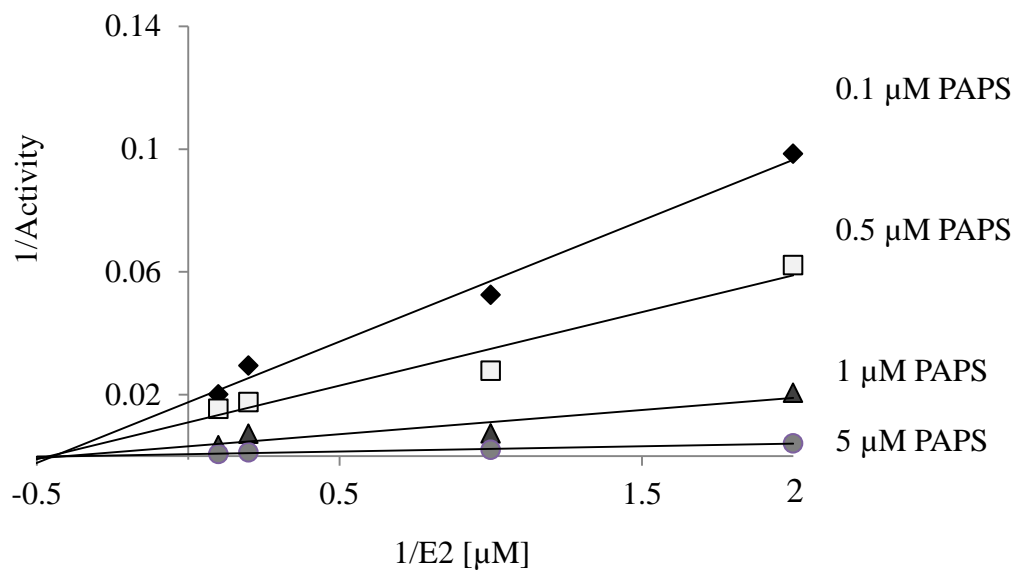


Figure 68. SULT1A1 double reciprocal plot for E2 sulfation. E2 sulfation by SULT1A1 was examined using [³H]-E2 and chloroform extraction as described previously in sections III-E and I-B. The K_m and V_{max} were determined using the re-plots of the slopes and intercepts. Each reaction was performed in duplicate.

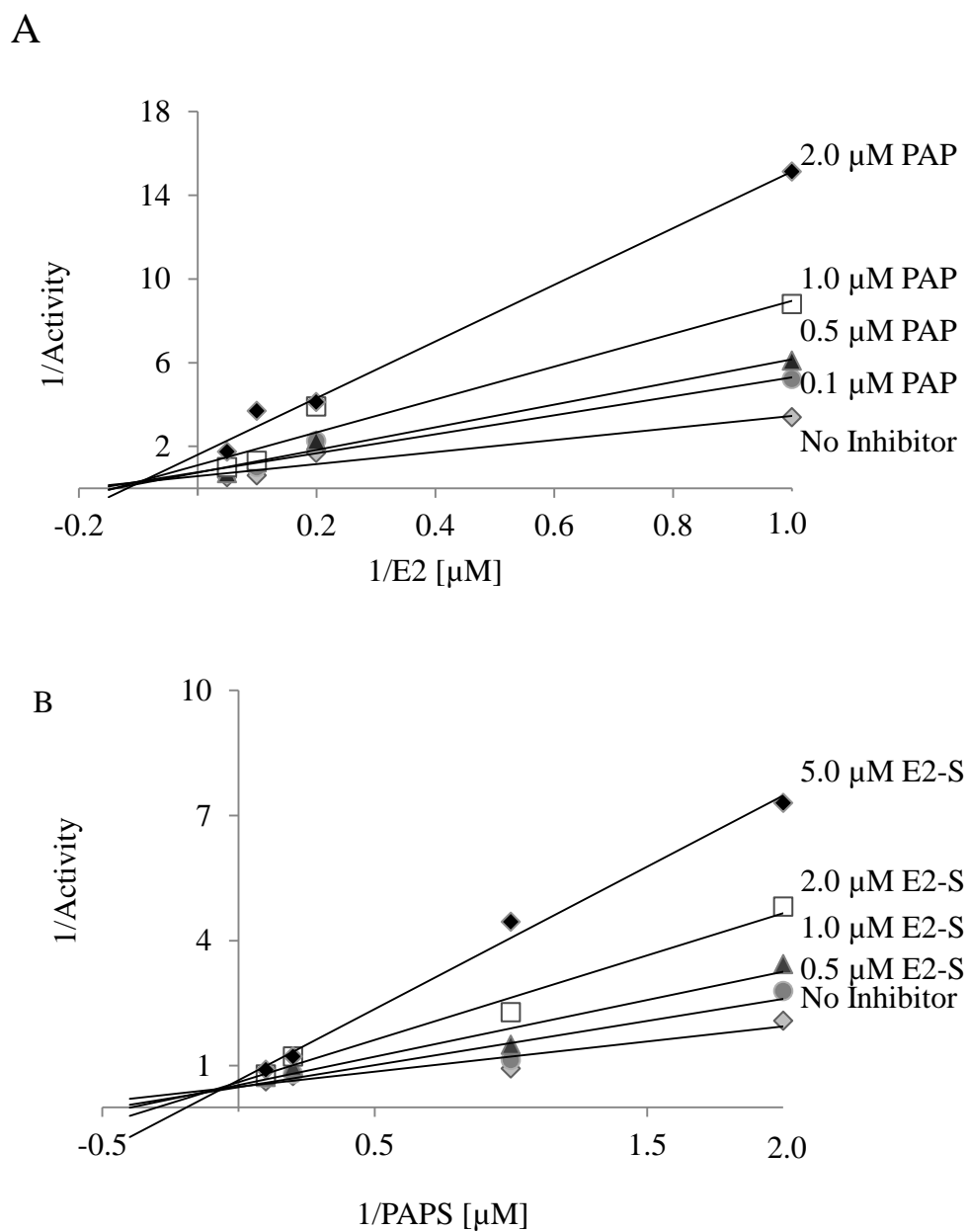


Figure 69. Product inhibition of E2 sulfation with PAP and E2-S in SULT1A1. Inhibition SULT1A1 E2 sulfation by the products A) PAP and B) E2-S was assayed using the chloroform extraction assay described in sections III-E and I-B. The K_{is} are presented in Table 2. Each reaction was performed in duplicate.

of each other. In addition, the PAP molecule has a poor affinity for the E2-SULT1A1 complex, which would indicate a preference of PAPS for the free enzyme.

E2 binding to SULT1A1 demonstrated a random ordered Bi Bi reaction mechanism for the sulfation of E2 by SULT1A1 with a preference in PAPS binding first followed by E2 binding (Fig. 70). The titration of E2 to the open SULT1A1 protein had a K_d of 2.6 μM . When SULT1A1 was saturated with PAP at a concentration of 10 μM , the affinity of E2 significantly improved with a K_d of 1.2 μM . The change in affinity combined with the K_i of PAP for the E2-SULT1A1 complex demonstrates that while the reaction mechanism for SULT1A1 sulfation of E2 is a random Bi Bi reaction, although there is a preference for the PAPS to bind first and E2 second.

| | K_i | K_i' |
|------|---------------------------|----------------------------|
| PAP | $6.4 \pm 1.4 \mu\text{M}$ | $12.4 \pm 1.8 \mu\text{M}$ |
| E2-S | $6.8 \pm 1.1 \mu\text{M}$ | $82.7 \pm 6.2 \mu\text{M}$ |

Table 2. K_i s for PAP and E2-S product inhibition of E2 Sulfation by SULT1A1. The K_i 's were determined using the Lineweaver-Burk plots of the product inhibition curves (Fig 69). The K_i is the affinity of the product inhibitor to SULT1A1 and the K_i' is the affinity to E2*SULT1A1 complex for PAP and the PAPS*SULT1A1 complex for E2-S. Each reaction was performed in triplicate and presented with the mean \pm SEM.

E) Specific Aim 3 Conclusions

The results of aim 3 indicate that the binding of PAPS significantly alters the substrate specificity of SULT1A1. The binding of substrates to SULT1A1 was ordered with FUL and random with E2, as predicted in the modeling. The mechanism for the structural rearrangement of SULT1A1 is similar to SULT2A1, however there are distinct differ-

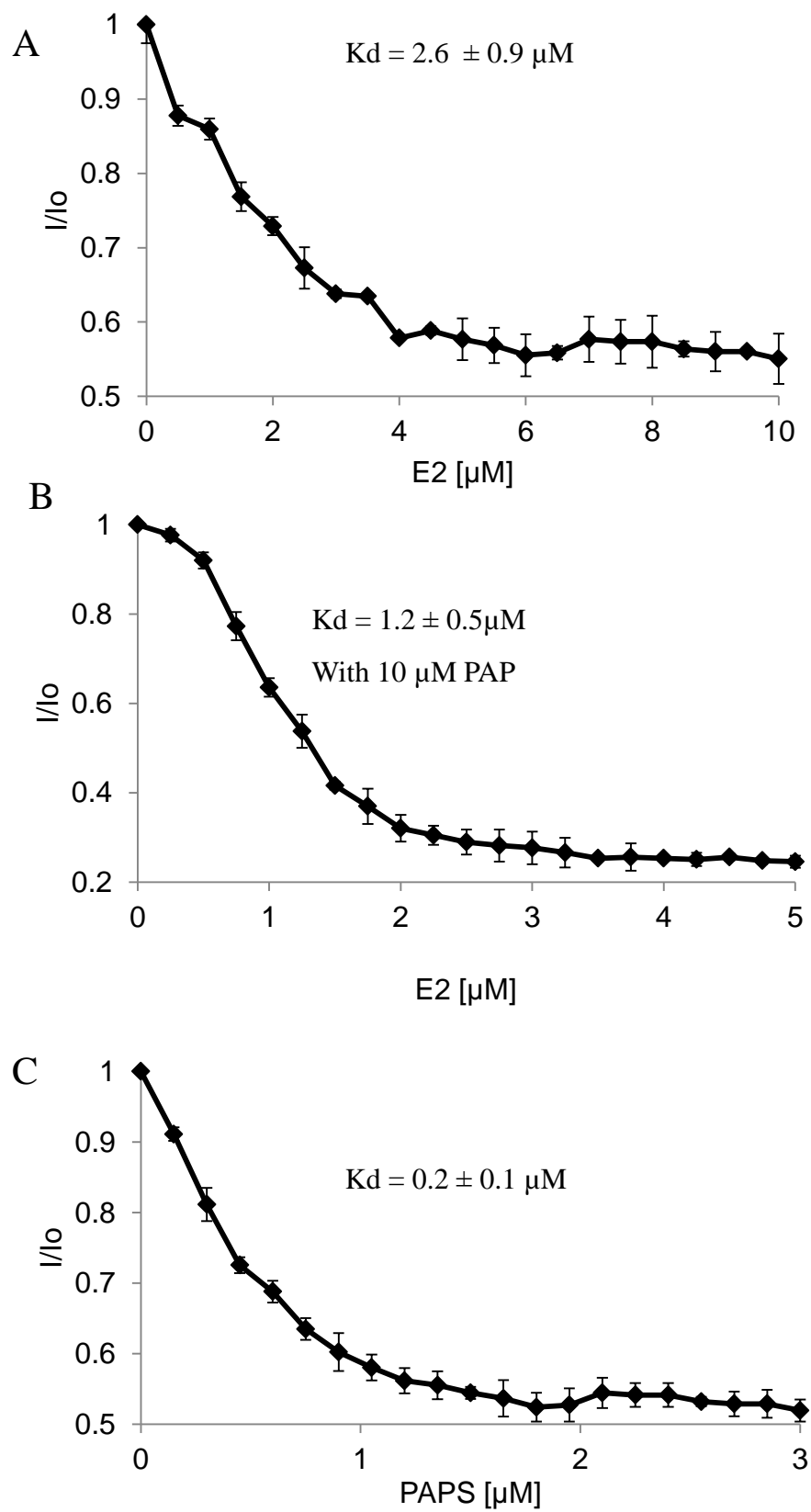


Figure 70. Determination of E2 and PAPS binding to SULT1A1 using intrinsic fluorescence. E2 was titrated to 100 nM SULT1A1 in PBS as described in the methods sections III-G and I-J. The relative change in fluorescence plotted vs the concentration of E2 or PAP. K_d was determined based on the non-linear regression analysis in KaleidaGraph using the single binding site model. For E2, SULT1A1 was pre-incubated with A) no PAP or B) 10 μ M PAP. C) The titration of PAPS to SULT1A1 is presented. Each titration was evaluated in triplicate, presented as the mean \pm SEM.

ences between SULT isoforms. The SULT1 family possesses a short loop (aa 85-90) that is absent in the SULT2 family. This 5 aa loop is flexible and forms a portion of the substrate binding site. The results with SULT1E1 indicate a lesser degree of flexibility in the substrate binding pocket with the binding of PAPS. The more rigid binding pocket may be associated with the high specificity for estrogen sulfation by SULT1E1 as compared to a broader role in drug/xenobiotic sulfation for SULT1A1.

DISCUSSION

This thesis represents a fundamental shift in our understanding of the SULTs and is the first report of active site plasticity in a Phase II drug metabolizing enzyme. The major conclusion of this study is that the binding of PAPS can significantly alter the substrate specificity of the SULTs. These results mean that the concentration of PAPS and the order of the addition substrate and PAPS to the SULT will have a major impact on reactivity and substrate selectivity of some SULTs. Failure to account for the effects of PAPS binding can result in significantly different kinetics and reaction rates of sulfation of a drug with a given SULT isoform. Understanding these interactions will provide valuable insights for understanding the *in vitro* properties of the SULTs and predicting the *in vivo* sulfation of drugs and xenobiotics.

This project was initiated to identify possible mechanisms for the numerous reported discrepancies between the apparently favorable *in vitro* sulfation of some drugs and xenobiotics and the absence of *in vivo* sulfated metabolites (Snyder, Sparano et al. 2000; Falany, Pilloff et al. 2006; Wempe, Wachter et al. 2008). In this dissertation we have demonstrated by multiple methods that for SULT2A1, PAPS binding changes the substrate specificity of SULT2A1 to selectively sulfate small planar compounds like hydroxysteroids. Additionally, the binding of PAPS changed the structure of the SULT homodimer and reduced substrate inhibition by the apparent disruption of an inhibitory allosteric binding site. A similar change in SULT1A1's substrate specificity was observed

with the binding of PAPS, demonstrating that the relationship of PAPS binding and substrate specificity is not unique to SULT2A1. The discrepancy between *in vitro* and *in vivo* substrate reactivity may be caused in part by a failure of *in vitro* experiments to accurately model the *in vivo* PAPS concentration and binding. Most published sulfation assays initiate the reaction with the addition of PAPS (Duffel and Jakoby 1981; Whittemore, Pearce et al. 1985; Whittemore, Pearce et al. 1986; Falany, Krasnykh et al. 1995; Her, Wood et al. 1998; Zhang, Varlamova et al. 1998; Dajani, Sharp et al. 1999; Falany, Pilloff et al. 2006; Dumas, He et al. 2008; Tyapochkin, Cook et al. 2009). By doing so, the assays are likely to have favorable kinetics for a larger range of substrate than if the reaction was initiated with the addition of substrate. *In vivo*, the SULTs are localized in the cytosol in the presence of PAPS, and the acceptor compound enters the cell, and binds the SULT*PAPS complex to form the reactive ternary complex. A better assay to model the *in vivo* sulfation reaction would be to saturate the SULT isoforms with PAPS first and initiate the reaction with the addition of substrate.

This dissertation examined the structural and kinetic changes in the SULTs that occur with the binding of PAPS and demonstrated that the binding of PAPS changes the substrate specificity of the SULTs. When this dissertation began, the structural rearrangements of the SULTs elicited by PAPS binding were hypothesized but the effects on the kinetic properties of the different SULT isoforms had not been described. Allali-Hassani et al. had reported a change in the substrate binding properties of several SULT enzymes associated with PAPS, but did not determine the mechanism for the change in substrate specificity or the impact of the change in substrate binding on the kinetics and substrate selectivity of the SULTs (Allali-Hassani, Pan et al. 2007). Other than the report

presented by Allali-Hassan et al., no other reports have proposed a kinetic change in the SULTs associated with the binding of PAPS (Allali-Hassani, Pan et al. 2007).

PAPS interactions with SULT2A1 were predicted by *in silico* modeling and confirmed with *in vitro* kinetics. In addition, the binding of the substrates for sulfation were examined using intrinsic fluorescence. The substrates examined were 24(S)-OH-Chol, RAL, DHEA, emodin, digitoxin, and 3-CTP for SULT2A1. 24(S)-OH-Chol kinetics predicted that the open SULT2A1 active site was necessary for the formation of 24(S)-OH-Chol disulfate. The affinity of RAL for SULT2A1 was significantly reduced by the binding of PAPS. The change in RAL affinity by PAPS binding forced the reaction mechanism of RAL sulfation to be an ordered reaction with RAL binding to SULT2A1 before PAPS. The binding of PAPS to SULT2A1 showed no change in DHEA sulfation and was a random ordered reaction mechanism. However, substrate inhibition for DHEA sulfation was reduced at high PAPS concentrations, and substrate inhibition was eliminated in the MBP-SULT2A1 monomer.

In SULT1A1, the binding of PAPS decreased the affinity of FUL for binding SULT1A1 causing the reaction to become ordered with FUL as the lead substrate. SULT1A1 affinity for E2 was improved with the binding of PAPS; resulting in an apparent ordered reaction with PAPS as the lead substrate. The conclusion of all these results is that the binding of PAPS has a significant impact on the substrate selectivity and reactivity of SULT1A1 and SULT2A1. These results indicate that *in vitro* SULT substrates may not be substrates *in vivo* and that the concentration of PAPS in the cells can significantly influence the substrate specificity.

I. THE STRUCTURAL REARRANGEMENTS ASSOCIATED WITH PAPS BINDING IN THE SULT2A1 SUBUNIT

A) 24(S)-OH-Chol Sulfation

This dissertation began with the investigation of the sulfation of 24(S)-OH-Chol, the major metabolite of cholesterol in the brain. Sulfation has been reported to play a significant role in the elimination of 24(S)-OH-Chol from the body (Björkhem, Lütjohann et al. 1997; Meng, Griffiths et al. 1997). The major metabolite of 24(S)-OH-Chol detected in human urine and bile is 24(S)-Chol-3-sulfate-24-glucuronide (Meng, Griffiths et al. 1997; Björkhem and Meaney 2004). In addition to the elimination of oxysterols, sulfation also changes the biological activity of oxysterols, such as 24(S)-OH-Chol from a LXR agonist to a LXR antagonist (Ren, Li et al. 2007; Cook, Duniac-Dmuchowski et al. 2009). The sulfation of 24(S)-OH-Chol by SULT2A1 was investigated and showed that at low concentrations of 24(S)-OH-Chol, the formation of disulfate was favored over that of monosulfate. The mechanism for the formation of disulfate at low concentrations was the high affinity of the 24(S)-Chol-24-sulfate for SULT2A1. The affinity of 24(S)-Chol-24-sulfate was much greater than of 24(s)-OH-Chol. As 24(S)-Chol-24-sulfate was formed, the 24(S)-Chol-24-sulfate would bind SULT2A1 preferentially over 24(S)-OH-Chol binding SULT2A1 and form the disulfate.

The docking of 24(S)-OH-Chol and 24(S)-Chol-3-sulfate were consistent with observations from the kinetics for SULT2A1. However, when 24(S)-Chol-24-sulfate was docked to SULT2A1, no competent binding was predicted. The docking result for 24(S)-Chol-24-sulfate was inconsistent with the observed 24(S)-Chol-24-sulfate kinetics.

24(S)-Chol-24-sulfate had a higher V_{max}/K_m for than 24(S)-sulfate-Chol for SULT2A1. If the docking with the closed model was accurate, 24(S)-Chol-24-sulfate would not be a substrate, and the 3-sulfate would be a poor substrate. This would result in the formation of monosulfate at all concentrations and small level of disulfate appearing at only at high 24(S)-OH-Chol concentrations.

To correlate the docking with the kinetics, a new model of SULT2A1 was required. SULT2A1 is the only SULT isoform with a crystal structure resolved at a high resolution without PAP or PAPS bound (Pedersen, Petrotchenko et al. 2000). The PAP bound SULT2A1 crystal structure was significantly different from the other SULT2A1 structures in the loop 3 region that forms the outer surface of the substrate and PAPS binding site. In all the crystal structures without PAP, loop 3 region was extended into the solvent, and the active site was open to the environment (Rehse, Zhou et al. 2002; Chang, Shi et al. 2004; Lu, Hsieh et al. 2008). The SULT2A1 crystal structure made with bound PAP (1EFH) showed loop 3 was shifted into the active site by 10 Å, reducing the volume of the active site by over 50% (Pedersen, Petrotchenko et al. 2000). Comparison of the SULT2A1 crystal structures to other SULT crystal structures showed that 1EFH was structurally more similar to the other SULTs in loop 3 than to the open SULT2A1 structures (Pedersen, Petrotchenko et al. 2002; Gamage, Duggleby et al. 2003; Shevtsov, Petrotchenko et al. 2003; Gamage, Tsvetanov et al. 2005; Allali-Hassani, Pan et al. 2007). These results indicate that the PAP crystal structure of SUTL2A1 was not an artifact, and that the binding of PAPS changes the structure SULT2A1. The docking of 24(S)-Chol-24-sulfate was originally performed with 1EFH; therefore, a second model of SULT2A1 was made using the SULT2A1 crystal structure with only bound DHEA

(1J99) (Rehse, Zhou et al. 2002). The 24(S)-Chol-24-sulfate docked in an orientation and with a BFE that agreed with the *in vitro* kinetics. The modeling suggested that SULT2A1 can either be PAPS free and “open” or PAPS bound and “closed”. At the time this project was initiated, little had been published on the structural rearrangement of any of the SULTs with the binding of PAPS or substrate. The mechanism for the molecular rearrangement is likely interaction of the 5'-phosphate of PAPS with R247; however, published literature indicates that mutation of R247 caused a significant loss in DHEA sulfation activity (Radomska, Drake et al. 1996). The titration of APS to SULT2A1 in this dissertation also demonstrates that without the 5'-phosphate and Arg247 interaction, SULT2A1 is inactive.

The 24(S)-OH-Chol data predicts that the disulfate formation observed *in vitro* is an artifact of the *in vitro* methods. In the liver, where 24(S)-OH-Chol metabolism is observed, the concentration of PAPS is between 23-80 μM (Cappiello, Franchi et al. 1989; Klaassen and Boles 1997). The K_d of PAPS for SULT2A1 is only 200 nM, which means that in the liver almost all of SULT2A1 should be closed. With no open SULT2A1, there will be almost no disulfate formation. The major metabolite of 24(S)-OH-Chol reported from the liver is the 24(S)-Chol-3-sulfate-24-glucuronide, with some 24(S)-OH-Chol-3-sulfate and 24(S)-Chol-24-glucuronide (Meng, Griffiths et al. 1997; Björkhem, Lütjohann et al. 1998). No detectable level of disulfate or 24(S)-Chol-24-sulfate has been observed *in vivo*. The *in vivo* results support that SULT2A1 is unable to form disulfate in the high PAPS environment of the liver. Further investigation is required to determine if there is any cooperatively between glucuronidation of 24(S)-OH-Chol and sulfation of 24(S)-OH-Chol. The double conjugate comprised more than 50% of the 24(S)-OH-Chol ad-

ministered (Meng, Griffiths et al. 1997). The major UGT responsible for glucuronidation of 24(S)-OH-Chol has been identified as UGT1A3, with an affinity of 52 μ M (Verreault, Senekeo-Effenberger et al. 2006). The result in this work and the published metabolism of 24(S)-OH-Chol suggest two pathways in the formation of the double conjugate. If 24(S)-OH-Chol-3-sulfate has an affinity for UGT1A3 that is greater than the affinity of 24(S)-OH-Chol, then the 24(S)-OH-Chol-3-sulfate will rapidly be converted to the double conjugate. Alternatively, if the 24(S)-Chol-24-glucuronide has a higher affinity for SULT2A1 than 24(S)-OH-Chol, the result would be the rapid sulfation of the 24(S)-glucuronide-Chol to the double conjugate. The two proposed pathways are not mutually exclusive and both can be correct. The high level of double conjugate relative to single conjugate 24(S)-OH-Chol demonstrates that at least one of the two pathways described above is correct.

B) Structural Rearrangement of SULT2A1 by PAPS Binding

The open and closed models of SULT2A1 suggested that the substrate selectivity of SULT2A1 may be regulated by the concentration of PAPS. To test this hypothesis, the SULT2A1 substrates DHEA and RAL were evaluated using intrinsic fluorescence, steady state kinetics, and pre-steady state kinetics to determine the kinetic constants and reaction mechanisms of DHEA and RAL sulfation by SULT2A1. DHEA is the most characterized substrate for SULT2A1 and is the most physiologically relevant SULT2A1 substrate. Modeling of DHEA to the SULT2A1 active site predicted that DHEA could bind to either the open or closed conformation of SULT2A1 with similar affinities. Kinetic assays of DHEA sulfation in steady state and pre-steady state kinetics were con-

sistent with a random Bi Bi reaction mechanism. The intrinsic fluorescence of DHEA binding revealed that two molecules of DHEA could bind to each molecule of SULT2A1 with a high affinity and low affinity binding site. When SULT2A1 was saturated with PAP, the low affinity binding was inhibited. DHEA could still bind at the high affinity site with no change in K_d . The two binding sites of DHEA in SULT2A1 are a likely mechanism for substrate inhibition and were further examined using the MBP-SUTL2A1 monomer, which lacks DHEA substrate inhibition.

RAL is a selective estrogen modulator, and has been reported by Falany et al. to be sulfated *in vitro* by SULT2A1 on the thionylphenol hydroxyl (Falany, Pilloff et al. 2006). Docking of RAL to the open model of SULT2A1 predicted a catalytically competent orientation with the thionylphenol hydroxyl in position for sulfation. In the closed model, the docking energy was significantly higher and RAL was in a non-catalytic orientation with the side chain in the active site. Pre-steady state kinetics demonstrated that the reaction mechanism was an ordered reaction with RAL as the leading substrate. Intrinsic fluorescence of RAL binding to SULT2A1 showed that RAL bound the PAP free SULT2A1. When SULT2A1 was saturated with PAP, RAL still bound to the complex but at a much lower K_d . When the kinetic constants were calculated using steady state kinetics for RAL, the affinity of PAPS was 20% the affinity of PAPS observed in DHEA sulfation. The significant change in PAPS K_m indicates that the binding of RAL causes a structural change in the PAPS active site that inhibits the binding of PAPS. The most likely cause for the increase in the PAPS K_m is that the binding of RAL inhibits the interaction of the R247 with the 3'phosphate of PAPS by preventing the full closure of loop 3.

In conclusion, the DHEA and RAL experiments with SULT2A1 demonstrates that SULT2A1 has at least two different reaction mechanisms for sulfation, an ordered reaction with the acceptor binding first or a random ordered Bi Bi reaction. The reaction mechanism for SULT2A1 is dependent on the size of the substrate and the affinity of the substrate to the “closed” structure. For small, planar substrates, such as DHEA and emodin, the reaction mechanism is a random ordered Bi Bi reaction. For these substrates, the binding of PAPS does not significantly change the affinity of the substrate. For large acceptor substrates, including RAL and digitoxin, or non-planar substrates such as 3-CTP, SULT2A1 has an ordered reaction mechanism with the sulfate acceptor as the leading substrate.

C) Pharmacophore Modeling of SULT2A1 Substrates

The pharmacophore method presented in this dissertation represents a significant improvement in the SULT field in substrate screening. The streamlined algorithms of a pharmacophore study allow for 10,000 compounds to be screened to an active site in the same time that a docking program can do a single compound. By screening a chemical library, new potential substrates, or hits, can be identified much faster than traditional screening methods. The main limitation of pharmacophore is the structural input of the enzyme. The open model of SULT2A1 generated 3 times more hits than the closed model. While the closed model predicted emodin as a substrate, the closed model missed digitoxin and 3-CTP. Additionally, both RAL and DHEA were added to the chemical library manually, and the closed model only identified the DHEA. In contrast, the open model identified RAL, DHEA, digitoxin, 3-CTP, and emodin as substrates. While the

open model increased number of hits, there are two major limitations with the open model when compared to the closed model. The first is the increased rate of false positives. Pharmacophore screening is an excellent first step in identifying substrates; however the false positive rate of a pharmacophore screening has been reported to range from 20-80% and the size of the active site has been shown to increase the false positive rate (Tanrikulu, Rau et al. 2009). Without testing all of the hits, the false positive rate is unknown for either model. If the open and closed models follow the literature trends, then the open model likely has a higher false positive rate than the closed model. The second limitation of the open model is physiological. If a substrate is only a substrate when PAPS concentration is low, and the PAPS concentration is high in the liver and adrenals, where SULT2A1 is expressed, then sulfation of the substrate by SULT2A1 is unlikely to be physiologically relevant.

D) SULT2A1 Reaction Mechanism

While the reaction mechanism for the SULTs has been studied for nearly 30 years, a uniform reaction mechanism for all the SULTs remains poorly defined. SULT1A1 sulfation of PNP by Duffel et al. described a random Bi Bi reaction mechanism (Duffel and Jakoby 1981). SULT1E1 was also reported to be random Bi Bi reaction mechanism by Zhang et al. (Zhang, Varlamova et al. 1998). Whittemore et al. reported that SULT1A3 and SULT1A1 sulfation had ordered reaction mechanism, with PAPS as the leading compound (Whittemore, Pearce et al. 1985; Whittemore, Pearce et al. 1986). Recently, Tyapochkin et al. reported that SULT1A1 sulfation is an ordered reaction mechanism (Tyapochkin, Cook et al. 2008; Tyapochkin, Cook et al. 2009). However,

Tyapochkin et al. had examined the reverse reaction of PNPS and PAP converted to PNP and PAPS. Additionally, SULT2A1 sulfation of bile acid in rhesus monkey has been reported to be an ordered reaction mechanism with bile acid as the leading substrate (Barnes, Waldrop et al. 1986). The work presented here demonstrates that the structural rearrangement induced by PAPS binding causes the reaction mechanism for at least some of the SULTs to be substrate dependent.

If the binding of PAPS does not significantly change the affinity of a substrate, then the reaction would be a random ordered reaction mechanism. This was observed for DHEA and SULT2A1. However, if PAPS causes a structural rearrangement that significantly reduces the affinity of the acceptor substrate with the active site, the result would appear to be an ordered reaction mechanism where the sulfate acceptor must bind first. If the binding of PAPS completely inhibits the binding of acceptor, the reaction mechanism will be an obligatory ordered reaction mechanism with acceptor binding first. This ordered reaction mechanism with acceptor as the leading substrate was observed with RAL, 3-CTP, and digitoxin for SULT2A1 and FUL for SULT1A1. Finally, if the binding of PAPS caused the active site to increase the affinity of a substrate, this could result in a pseudo-ordered reaction mechanism where the reaction will have a preference for PAPS binding first. This was observed with E2 and SULT1A1, where the affinity for E2 was significantly increased if PAPS bound first and PAPS binding was inhibited by E2 binding. While either substrate could bind to SULT1A1, the changes in affinities demonstrate a tendency for PAPS to bind first. In an extreme case the binding of PAPS may be required for the substrate to bind the enzyme and result in an obligatory ordered reaction mechanism at physiological conditions. This may be the case in the reaction of PNP and

SULT1A1. PNP is a small molecule and SULT1A1 has a large active site. The active site of SULT1A1 was resolved with two molecules of PNP bound to the active site in the crystal structure, with PAP present (Gamage, Duggleby et al. 2003). Based on the data presented, this is the smaller closed structure of SULT1A1, and the open SULT1A1 active site is likely larger. With the large active site, PNP may be able to bind in many non-catalytic orientations in the open SULT1A1 active site. This would result in a high K_m for PNP sulfation by SULT1A1. If the binding of PAPS causes the structural rearrangements that are observed in SULT2A1, then in SULT1A1 the active site will become significantly smaller. A smaller active site would limit the number of non-catalytic binding orientations of PNP and greatly decrease the K_m of PNP. The result would be that PNP is a pseudo-ordered reaction mechanism, or even an obligatory ordered reaction mechanism if the change in affinity is large enough.

II. THE SUBUNIT INTERACTIONS OF THE SULT2A1 HOMODIMER ASSOCIATED WITH PAPS BINDING

Nearly all of the SULTs have been reported to be homodimers, with the exception of mouse SULT1E1 (Petrotchenko, Pedersen et al. 2001). The dimer interface was first proposed by Pedersen et al. and was based on sequence homology of the SULTs (Petrotchenko, Pedersen et al. 2001). The KTVE sequence was observed in all SULTs except mouse SULT1E1, where the KTVE sequence is replaced with a KPTE sequence (Petrotchenko, Pedersen et al. 2001). When human SULT1E1 and SULT1A1 were mutated from a KTVE to a KTEE sequences, both enzymes became monomers. In a gain of

function experiment, the mouse SULT1E1 was mutated to a KTVE sequence. The mouse KTVE SULT1E1 mutant formed a dimer (Petrotchenko, Pedersen et al. 2001).

Despite strong evidence demonstrating that the dimerization interface is the small highly conserved KTVE sequence, no heterodimers has been observed *in vivo*. The only published report of a SULT heterodimer was between SULT1A1 and SULT1A3 by Kiehlbauch et al. and only in an *in vitro* environment were both enzymes were overexpressed (Kiehlbauch, Lam et al. 1995). The KTVE dimerization domain has three points of contact, a salt bridge on both sides between the K and E residues and a hydrophobic interaction in the center with both the T and the V residues. With only three points of contact that are identical in all SULTs, it seems unlikely that the SULTs would not readily form heterodimers. However, to date no heterodimers have been observed *in vivo*. The data in this dissertation support the hypothesis that the KTVE sequence in SULT2A1 is critical for dimer formation. Despite a major loss in activity, the SULT2A1 K260E mutant was a monomer. While the KTVE domain is required for dimerization, it is also clear that the dimerization domain must include more points of contact for the selectivity in dimerization than is observed in the SULTs *in vivo*.

The physiological relevance of the SULT homodimer has remained elusive. The mouse SULT1E1 is the only native monomer SULT and lacks substrate inhibition (Petrotchenko, Pedersen et al. 2001; Stjernschantz, Reinen et al. 2010). This would suggest that the formation of the dimer is important in substrate inhibition. The MBP-SULT2A1 monomer also lacked substrate inhibition, supporting this observation. However, the SULT1A1 and SULT1E1 KTEE mutant monomers have no reported change in substrate inhibition. According to the report by Pedersen et al. the monomer

and dimer of SULT1A1 and SULT1E1 behaved in a kinetically identical manner (Petrotchenko, Pedersen et al. 2001). One hypothesis proposed by Lu et al. is that the dimerization is important for stability of the SULT in cells, and the monomer is more susceptible to enzymatic degradation (Lu, Chiang et al. 2009). A third hypothesis proposed by Sun et al. is that in SULT1E1, the dimerization is important for the internal equilibrium. Sun et al. reported only half of the homodimer went through a full catalytic cycle. The binding of PAPS to one active site caused a structural change that inhibited the binding of PAPS to the other active site. The formation of the half site was critical to stabilizing the internal equilibrium and the formation of E2 sulfate at low nM concentrations in SULT1E1 (Sun and Leyh 2010).

A) MBP-SULT2A1 Structural and Kinetic Properties

The pMAL vector was used to generate SULT2A1 with an MBP tag on the amino terminal. The MBP allowed for rapid affinity purification with an amylose column. Then the MBP tag was cleaved with Factor Xa to generate a pure WT SULT2A1. When MBP-SULT2A1 was passed through a size exclusion column, the size of MBP-SULT2A1 was consistent with a monomer. The MBP was interfering with the dimerization of SULT2A1. When the MBP tag was cut, SULT2A1 would form back into a homodimer. DHEA sulfation assays of MBP-SUTL2A1 showed that while the V_{max}/K_m was unchanged; however, the MBP-SULT2A1 showed no substrate inhibition. The lack of change in the V_{max}/K_m of the MBP-SULT2A1 compared to SULT2A1 indicates that the binding and catalysis of PAPS and DHEA is unchanged in the MBP-SULT2A1. The results indicate that the MBP is blocking substrate inhibition by the loss of dimerization

in SULT2A1. The mechanism for substrate inhibition is currently not understood. While the most likely reason for the loss of substrate inhibition in MBP-SULT2A1 is because of the disruption in dimerization, interaction of the MBP tag and the active site may also contribute to the loss of substrate inhibition.

When MBP-SULT2A1 was saturated with RAL, MBP-SULT2A1 sulfated RAL at a rate 5 times slower than SULT2A1 after the initial turnover. When MBP-SULT2A1 was saturated with PAPS, no activity was observed with RAL for up to 10 min. SULT2A1 saturated with PAPS could sulfate RAL 30-60 sec after the addition of RAL. This result indicates that the PAPS*SULT2A1 complex could dissociate and form free SULT2A1 that could then bind RAL. The lack of any RAL sulfation to the PAPS saturated MBP-SULT2A1 indicates that when the PAPS*MBP-SULT2A1 complex forms, the enzyme cannot readily dissociate to free enzyme. Without free MBP-SULT2A1, RAL cannot bind and be sulfated. When the affinity of PAPS for MBP-SULT2A1 was compared to SULT2A1, there was no significant change in the affinity of PAPS. This means that the lack of dissociation of the MBP-SULT2A1*PAPS complex is not because of an increase in PAPS affinity.

A possible mechanism for the release of PAPS is the hydrolysis of the sulfonate. PAPS can be hydrolyzed to PAP without sulfating an acceptor molecule and releasing the free sulfate by the SULTs (Pedersen, Petrotchenko et al. 2002; Sun and Leyh 2010). The hydrolysis of PAPS may be necessary for the release of the PAP and opening of the active site. In SULT2A1 and MBP-SULT2A1, when PAPS binds, the active site closes and prevents RAL from binding. SULT2A1 can hydrolyze the PAPS to PAP, even without acceptor substrate and release PAP and free sulfate. If this were the case, then the active

site of SULT2A1 would open and allow RAL to bind and be sulfated. If MBP-SULT2A1 cannot hydrolyze PAPS without an acceptor substrate, because the MBP-SULT2A1 cannot complete the catalytic cycle without an acceptor and hydrolyze PAPS, the SULT2A1 active site will not open for RAL. This is not observed with DHEA because the DHEA molecule can bind to the PAPS*MBP-SULT2A1 complex and complete the catalytic cycle.

B) Mechanism of Substrate Inhibition in SULT2A1

Substrate inhibition is a common characteristic of the SULTs. The mechanism for substrate inhibition has been proposed to involve the binding of substrate at an allosteric binding site, formation of a dead-end product complex, and gating of the active site. The binding of an allosteric binding site is supported by a report that two E2 molecules could bind to each subunit of SULT1E1 (Zhang, Varlamova et al. 1998) and in the SULT1A1 crystal structure with PNP and PAP, with two PNP molecules were resolved in the active site (Gamage, Duggleby et al. 2003). Dead-end product formation has been reported in SUTL1A1 by Tyapochkin et al. (Tyapochkin, Cook et al. 2009), SULT2A1 by Glucan et al. (Gulcan and Duffel 2011) and SUTL1E1 by Sun et al. (Sun and Leyh 2010). In the dead-end product formation model, the substrate binds to the PAP*SULT complex at high concentrations. Lu et al. report that the M137 and Y238 in SULT2A1 can act as a gate to the active site and inhibit activity at high concentrations of substrate (Lu, Hsieh et al. 2008).

In this study, the intrinsic fluorescence of SULT2A1 demonstrated that 2 molecules of DHEA bound to SULT2A1, but only one DHEA molecule could bind if the

SULT2A1 was saturated with PAP. This was confirmed kinetically with a Lineweaver–Burk plot of PAPS at a high concentration of DHEA. The kinetics showed that the level of substrate inhibition was inversely proportional to the concentration of PAPS. A second DHEA molecule was modeled in the open active site of SULT2A1 and was predicted to bind the Y238 in loop 3. Lu et al. reported that mutating the Y238 caused the loss of substrate inhibition in SULT2A1 (Lu, Hsieh et al. 2008), demonstrating the importance of Y238 in substrate inhibition. The results in this dissertation demonstrate that the mechanism for substrate inhibition is the binding of a second DHEA molecule in the active site at Y238. This binding inhibits activity by blocking the active site and preventing access to the catalytic site. The binding can also block release of the DHEAS product. The allosteric binding site is lost when PAPS binds to SULT2A1. Based on the results with MBP-SULT2A1, the second binding site is present in the monomer, but has a much lower affinity and is unable to inhibit the catalytic cycle. Interactions across the homodimer increase the affinity of the second binding sites to relevant concentrations and are necessary for the binding site to inhibit the catalytic cycle. The mechanism for this homodimer interaction is likely the loop 3 region. The loop 3 region is adjacent to the KTVE dimer site and contains the Y238 that is predicted to be important for the second binding site. Initial examination of the region suggested that Q243 may be a key residue in the homodimer interactions. However, mutation of Q243 did not change the dimerization, K_m , V_{max} , or substrate inhibition of SULT2A1. Other residues near Q243 may have been able to compensate for the Q243A mutation. To date, the understanding of the molecular interactions of the homodimer in the SULTs remains elusive.

C) PAPS Concentration, Reaction Mechanism, and Substrate Inhibition *in vivo*

The reaction mechanism for different substrates in the same enzyme can have a significant influence on the physiological sulfation of drugs. For SULT2A1 the K_m for the sulfation of RAL is not significantly different from the K_m for DHEA. Based on these results alone, RAL would be predicted to be significantly sulfated in the liver by SULT2A1. However, the concentration of PAPS in the human liver has been estimated to be approximately 80 μM (Klaassen and Boles 1997) (Kim, Madhu et al. 1995). At this concentration, nearly all SULT2A1 molecules will be saturated with PAPS. Based on the data presented here, RAL would not be significantly sulfated by SULT2A1 and have a higher bioavailability than predicted by the *in vitro* kinetics. These results may explain why no RAL-sulfate has been observed *in vivo* (Jeong, Liu et al. 2005).

The problem with the estimated PAPS concentration used above is that the concentration was based on the sulfation of E2 by SULT1E1 using liver extract as a PAPS source. The first issue is using SULT1E1 or other any SULT activity as a means for determining the concentration of PAPS is highly sensitive to the presence of PAP. The PAP in the tissue extracts will inhibit the activity and will result in an underestimate of the concentration of PAPS. The second issue with the method is that PAPS is not a stable compound and decomposes to PAP relatively quickly. A rapid method that could quickly measure the concentration of PAPS before a significant amount of PAPS degrades is necessary for a better measurement of PAPS concentration *in vivo*. The third problem with this method of PAPS is the sensitivity of the reaction to other substrates. Any contaminating SULT1E1 substrates in the liver extract would change the determined PAPS concentration. Finally, the liver extract did not differentiate between cell types and sub-

cellular localization. PAPS is predominantly synthesized in the nucleus and must be divided between the cytosolic SULTs and the Golgi SULTs. There are two reported PAPS transporters to the Golgi; however, the mechanism for transport from the nucleus to the cytosol has not been reported. Additionally, different cell types in the liver almost certainly possess different levels of PAPS.

While the liver is the site a most of drug metabolism, there is increasing research showing that non-hepatic metabolism plays a very important physiological role. The concentration of PAPS in non-hepatic tissues of different species has not been well reported (Kim, Madhu et al. 1995; Klaassen and Boles 1997). In addition to tissue differences, there are likely to be developmental changes in PAPS levels, as well as changes due pathological conditions, like cancer, that could change PAPS levels in the cytosol. PAPS synthesis is also dependent on the availability of inorganic sulfate and ATP (Kim, Madhu et al. 1995). Any conditions that would lower inorganic sulfate concentration or ATP production will likely lower PAPS levels as well, such as inflammation (Ha and Snyder 1999).

III. THE STRUCTURAL REARRANGEMENTS OF SULT1A1 AND SULT1E1 ASSOCIATED WITH PAPS BINDING

SULT2A1 is the one of two SULTs with crystal structures made without PAP or PAPS bound, the other SULT crystallized without PAPS is SULT4A1. In the SULT4A1 crystal structure, no residues in the loop 3 domain were resolved. Additionally, there is no data supporting the binding of PAPS to SULT4A1. To predict the structural rearrangement of PAPS binding, homology modeling of SUTL1A1 and SULT1E1 was per-

formed with the SUTL2A1 crystal structure with DHEA (1J99) (Rehse, Zhou et al. 2002) as a template. A major limitation in the homology modeling was the SULT2A1 crystal structure. If either SULT1A1 or SULT1E1 have a significantly larger active site in the open confirmation than SUTL2A1, then the full size of the open active site may not be modeled in the homology modeling. A crystal structure of SULT1A1 and SULT1E1 without PAP(S) bound would be the ideal method to determine the structure of the open enzymes.

A) SULT1A1 Structure

SULT1A1 is one of the most important SULTs in drug metabolism. SULT1A1 is the most highly expressed SULT in the liver and has the largest number of substrates reported in the literature (Falany, Krasnykh et al. 1995; Nowell and Falany 2006). The homology modeling of SULT1A1 with the open SULT2A1 structure revealed a more open active site than observed in any of the SULT1A1 crystal structures (Gamage, Duggleby et al. 2003; Gamage, Tsvetanov et al. 2005; Lu, Li et al. 2010). The loop 3 region showed a significant opening of both the PAPS and substrate binding site of approximately 3 Å in the back-bone. However, an even larger change was observed in the K85-P90 region, or loop 1. SULT2A1 has no homology to loop 1, making any prediction of the loop 1 region difficult in the homology modeling. However, analysis of the three crystal structures of SULT1A1 shows that the loop 1 region is highly dynamic, with 5 Å shift in the back bone from SULT1A1 with PAP and E2 (2DO6) (Gamage, Tsvetanov et al. 2005) to SULT1A1 with PAP and PNP (1L6S) (Gamage, Duggleby et al. 2003). The

homology model of SULT1A1 predicted an even larger opening in the loop 1 region than in the largest volume crystal structure (2DO6) by an additional 3 Å in the backbone.

The homology modeling predicted that the binding of PAPS will cause a major change in the structure of SULT1A1. Because of the limitations of homology modeling, the structural rearrangements predicted in the model are likely smaller than the actual rearrangements in SULT1A1 from PAPS binding. This is because SULT1A1 has the largest closed active site of all the SULTs (Gamage, Duggleby et al. 2003). Because SULT1A1 has the largest closed active site of the SULTs, and the largest range of substrates, including some small peptides, a reasonable hypothesis would be that the open active site of SULT1A1 is larger than what is predicted in the homology modeling with SULT2A1. The optimal method to determine the open structure of SULT1A1 would be to crystallize SULT1A1 without PAP(S).

B) SULT1E1 Structure

SULT1E1 homology modeling to the open structure of SULT2A1 predicted relatively few changes in the active site. The most significant change was in loop 3 but was limited to only the PAPS binding domain. The region of loop 3 that forms the upper surface of the PAPS binding domain was extended away from the core of the enzyme compared to crystal structures of SULT1E1. Unlike SULT1A1, the region of loop 3 that formed the upper surface of the substrate binding site did not move in the homology modeling. The lack of any major structural change is likely a result of the highly specialized role of SULT1E1. SULT1E1 sulfates E2 with a K_m in the low nM range. The very high affinity is a unique feature of SULT1E1. While SULT1E1 can sulfate substrates

other than E2, the dominant physiological role of SULT1E1 is sulfation of E2. The lack of dynamics in the active site of SULT1E1 may be related to the narrow substrate selectivity of SULT1E1.

C) SULT1A1 and SULT1E1 Activity and PAPS Dependent Substrate Specificity

The docking of FUL and E2 to SULT1A1 was predictive of the kinetics for sulfation. FUL sulfation by SULT1A1 was an ordered reaction mechanism with FUL as the lead substrate. In contrast to FUL, E2 sulfation by SULT1A1 was a random Bi Bi reaction mechanism. Further analysis of E2 sulfation revealed that there was a pseudo order to the binding where the reaction preferred the binding of PAPS first and then E2. K_d determination for E2 to the open and closed structures showed that the affinity of E2 was increased 2-3 fold when SULT1A1 was saturated with PAP. Additionally, product inhibition kinetics showed that the affinity of PAPS decreased 5-10 fold if E2 bound to the enzyme first. These results suggest a non-obligatory ordered reaction. In this reaction model, E2 or PAPS can bind to the free SULT1A1; however, E2 will have a poor affinity and PAPS will have a high affinity. If PAPS binds to the enzyme first, the affinity for E2 will dramatically improve and the E2 will be sulfated. If E2 bound the enzyme first, the affinity for PAPS will be significantly decreased, though PAPS could still bind and sulfate E2. FUL sulfation by SULT1E1 was a random Bi Bi ordered reaction mechanism because the affinity of FUL to SULT1E1 was unchanged by the binding of PAPS.

One major conclusion from the FUL sulfation data is that in an environment with SULT1A1, FUL sulfation will be low. However, if SULT1E1 is present, FUL sulfation will be high. In normal breast tissue, the most prevalent SULT is SULT1E1, while most

breast cancer cell lines have been reported to down-regulate SULT1E1 and up-regulated SULT1A1 (Falany, Macrina et al. 2002). This difference in SULT expression between normal breast and breast cancer will result in a difference in FUL activity. In normal breast tissue, SULT1E1 will rapidly sulfate and inactivate FUL. The down-regulation of SULT1E1, and the up-regulation of SULT1A1, means that breast cancer will not be able to sulfate FUL to the extent that normal tissue can sulfate FUL. Breast cancer will be more susceptible to FUL than normal cells. The difference in FUL sulfation of normal and cancer tissue would result in selectivity for cancer tissue for FUL conjugation.

IV. CONCLUSIONS

The structural changes in the SULTs resulting from the binding of PAPS and the kinetic implications have only recently been studied. The data presented in this thesis demonstrate that the binding of PAPS causes a significant change in the structure of the acceptor binding site of SULT2A1. The changes in the structure modifies the substrate specificity of SULT2A1 resulting in different apparent reaction mechanisms for different acceptor substrates. Substrates that can bind to the open and closed structures will have random Bi Bi reaction mechanisms, while substrates that bind only the open structure will have ordered reactions with the sulfate acceptor as the lead compound. The result is that SULT2A1 has a different substrate specificity at a high concentration of PAPS than at low concentration of PAPS. In addition to regulating the substrate specificity, the binding of PAPS was also shown to decrease substrate inhibition of DHEA in SULT2A1. The substrate inhibition of DHEA in SULT2A1 was dependent on the for-

mation of the homodimer. The formation of the homodimer would generate a second allosteric binding site for DHEA that could inhibit activity. If PAPS bound to SULT2A1, the second binding site was disrupted and substrate inhibition reduced.

The binding of PAPS was also shown to change the sulfate acceptors affinity for SULT1A1, but not for SULT1E1. In SULT1A1, the results show a change the affinity associated with the binding of PAPS was observed for both FUL and E2. For FUL, the data shows that the binding of PAPS prevented the binding of FUL and resulted in an apparent ordered reaction mechanism with FUL as the lead substrate. E2 sulfation was a random order reaction mechanism; however, the binding of PAPS improved the affinity of E2 and resulted in an apparent ordered reaction mechanism with PAPS binding first. While the data in this dissertation clearly shows that SULT1A1 and SULT2A1 have significant structural rearrangements when PAPS binds, there is currently no evidence for such a structural change in SULT1E1. The lack of any significant change observed with SULT1E1 is likely a result of SULT1E1's high affinity for estrogens.

The concentration of PAPS changes the substrate specificity of SULT2A1 and SULT1A1 and this can result in different apparent reaction mechanism. The change in substrate specificity induced by the binding of PAPS would explain the discrepancy in the reaction mechanism of the SULTs. The reaction mechanism for the SULTs has been reported to be an ordered mechanism, both with PAPS and substrate binding first and a random mechanism depending on the isoform and substrate (Barnes, Waldrop et al. 1986; Zhang, Varlamova et al. 1998; Tyapochkin, Cook et al. 2008). In the proposed model, the differences in reaction mechanism can be explained as the change in substrate selectivity caused by the binding of PAPS in SULT isoforms.

In addition to the reaction mechanism, PAPS binding can also reduce substrate inhibition. In SULT2A1, DHEA substrate inhibition was caused by the binding of DHEA at an allosteric site that inhibited the catalytic activity of SULT2A1. When PAPS bound the enzyme and closed the active site, DHEA could only bind once in the catalytically active orientation. As the concentration of PAPS was increased; the level of substrate inhibition was decreased. The reported concentrations of PAPS in the liver are high enough to saturate SULT2A1, so that less than 1% of the enzyme is in the open state (Cappiello, Franchi et al. 1989; Klaassen and Boles 1997; Xu, Wood et al. 2001). If the PAPS concentration decreased substantially, substrate inhibition would increase. Without substrate inhibition, SULT2A1 activity would only decrease with the level of PAPS. However, with substrate inhibition, SULT2A1 activity would decrease faster, significantly reducing the utilization of PAPS by SULT2A1. If a similar mechanism were observed in SULT1A1, the other major SULT in the liver, cytosolic SULT activity would drop dramatically under conditions of depleted PAPS level. This decrease would be greater than the decrease in PAPS could explain. The result is a potential scavenging pathway, to reduce the level of PAPS consumption and maintain PAPS and ATP for other functions. A depletion of PAPS at the magnitude required to see such a change has been reported in rat liver with the administration of acetaminophen (Hjelle, Hazelton et al. 1985)

The dynamic model of SULT2A1 presented in this dissertation represents a major change in the SULT field. Instead of static models, the model made by combining the crystal structures of SULT2A1 is an attempt to study the dynamics of SULT2A1's structure. The crystal structures used in the SULT2A1 modeling were the extreme conformations of SULT2A1 and were used to maximize the structural change. The dynamic

modeling with GROMACS demonstrates that the loop 3 region is highly flexible and suggests that there are more conformations than the two conformations in this work. The different conformations are regulated by more factors than just the concentration of PAPS. The two-substrate kinetics of DHEA and RAL for SULT2A1 and FUL and E2 for SULT1A1 show that the binding of PAPS changes with different acceptor substrates. The changes to the structure of the SULTs that are induced by the binding of sulfate acceptor are unknown, but large acceptor substrates inhibit the binding of PAPS based on the data in this dissertation.

The PAPS dependent substrate specificity in SULT2A1 and SULT1A1 will have significant influence on the *in vivo* kinetics of these enzymes. In tissues that are high in PAPS, such as the liver, the enzymes will have a selectivity that will favor the closed model. Both SULT2A1 and SULT1A1 are highly expressed in the liver. Based on the data presented in this dissertation, large substrates like RAL and FUL will pass the liver un-sulfated by SULT1A1 or SULT2A1. The selectivity of SULT1A1 and SULT2A1 will be similar to the liver in any tissues with sufficiently high concentration of PAPS. An example of this relationship of substrate selectivity and PAPS is in the sulfation of RAL in MCF-7 cells. RAL has been shown to be a substrate for SULT1A1, and SULT1A1 is the major SULT expressed in MCF-7 cells. The SULT1A1 in MCF-7 cells is active and intact MCF-7 cells have been shown to sulfate other SULT1A1 substrates. However, no RAL-sulfate has been observed in MCF-7 cells. The work presented in this dissertation suggests that the concentration of PAPS in the cytosol of MCF-7 cells is high enough to saturate most of the SULT1A1.

V. IMPORTANCE OF *IN VIVO* PAPS CONCENTRATION AND SULT SUBSTRATE SPECIFICITY

This dissertation demonstrates the importance of PAPS concentrations in regulating not only SULT activity but substrate specificity as well. This highlights the importance of measuring the concentration of PAPS *in vivo* to design more accurate *in vitro* assays of SULT activity. Currently, PAPS concentrations *in vivo* are measured using tissue homogenates, usually liver, as a PAPS source. The homogenate is added to SULT1E1 and E2 and the conversion of E2 to E2-sulfate is used to determine the concentration of PAPS (Klaassen and Boles 1997). However, using any enzymatic method to determine *in vivo* concentration can easily result in an inaccurate PAPS determination. Factors including contaminating estrogens and PAPs in the liver, can result in significantly different values. Despite the flaws in this method, there are several reports on the concentration of PAPS in tissues. Klaassen et al. reported a range of concentrations for PAPS in humans from 79 μM in the liver to 3.4 μM in the placenta (Klaassen and Boles 1997). More recently, Xu, Z. H. et al reported a concentration of 43 μM in human liver (Xu, Wood et al. 2001). Cappiello et al. reported that the human liver PAPS concentration was 22.6 μM using an assay with SULT1A1 and measuring β -naphthol sulfate formation (Cappiello, Franchi et al. 1989). There are also significant species differences in PAPS concentration, with 70, 33, 29, and 17 μM for rat, rabbit, mouse, and dog liver, respectively (Cappiello, Franchi et al. 1989; Klaassen and Boles 1997).

Xu et al also reported that the PAPS synthesis activity in the liver can range from less than 2 nmol/hr/mg of protein to 27 nmol/hr/mg of protein with the average at 10 nmol/hr/mg of protein (Xu, Wood et al. 2001). While the concentration of PAPS in the

livers trended with the PAPSS activity, the correlation was not statistically significant. Comparison of the sulfation activity reported in the liver to the rates of PAPSS activity indicates that at maximum sulfation, the SULTs in the liver can deplete PAPS in less than 5 min (Klaassen and Boles 1997; Xu, Wood et al. 2001). There have been several SNPs identified for both PAPSS-1 and PAPSS-2 that can influence PAPSS activity. In PAPSS-1, two coding SNPs have been identified, and they result in a R333C and E531Q mutation. The two SNPs have been reported to change the ATP-sulfurylase activity of PAPSS-1 (Xu, Thomae et al. 2003). While neither mutant caused a change in the liver PAPS concentration, that is likely because PAPSS-2 is the major liver PAPSS isoform. The change in PAPS concentration of the PAPSS-1 SNPs in most non-hepatic tissues has not reported, however both SNPs reduced PAPS concentration in the brain (Xu, Thomae et al. 2003). A major mutation identified in PAPSS-2 results in the loss of function for the protein. The mutation is the conversion of Ser438 to a stop codon, resulting in a truncation of PAPSS-2 and was observed in a large inbred family in Pakistan. In humans, this mutation results causes severe bone and joint problems and dwarfism (Xu, Freimuth et al. 2002). The PAPS levels in human liver are also greatly reduced in the PAPSS-2 mutant (Faiyaz ul Haque, King et al. 1998)

The concentration of PAPS in rats, but not mice, has been shown to be significantly depleted (>50%) after the administration of acetaminophen and it takes over 12 hours for PAPS levels to regenerate to their basal level (Hjelle, Hazelton et al. 1985; Kim, Rozman et al. 1995). If a similar pattern is observed for a SULT substrate in humans, then the sulfation profile of liver SULTs can change dramatically in a short period as the substrate specificity changes. In addition, as the substrate specificity broadens, the sulfation will

slow down for the random order substrates and the consumption of PAPS will be reduced.

In addition to PAPS synthesis, another important factor influencing cytosolic PAPS concentration is PAPS transport. Most PAPS synthesis is localized to the nucleus where PAPSS are usually expressed (Besset, Vincourt et al. 2000). PAPS must be transported to the Golgi SULTs for essential cell function like cell-cell adhesion (Bistrup, Bhakta et al. 1999; Tangemann, Bistrup et al. 1999), cell proliferation (Rapraeger 1995), cell differentiation (Fan, Uchimura et al. 1999; Cornelison, Filla et al. 2001; Rapraeger 2001), blood clotting (Michnick, Pittman et al. 1994; Barbucci, Lamponi et al. 1998; Anderson, Fredenburgh et al. 2001), and chemokine activation (Selvan, Ihrcke et al. 1996; Lipscombe, Nakhoul et al. 1998). The transport of PAPS to the Golgi is by the PAPS transporters (PAPST-1 and PAPST-2). The two isoforms have different tissue expressions and are critical for Golgi SULT activity (Kamiyama, Suda et al. 2003; Bhattacharya, Townley et al. 2009; Kamiyama, Ichimiya et al. 2011). No reports are currently available on PAPS concentrations by cell type or the subcellular concentration of PAPS. Inhibition of PAPST activity in intestine cells has shown to result in a significant deficiency in the Golgi SULTs activity (Kamiyama, Ichimiya et al. 2011). However, the change PAPS concentration or cytosolic SULT activity was not examined in these studies. The most likely result of inhibiting PAPST activity on PAPS concentration would be a decrease in PAPS activity in the Golgi and an increase of PAPS in the cytosol.

A new accurate method for determining the concentration of PAPS *in vivo* is needed in order to improve *in vitro* sulfation assays and understanding of *in vivo* sulfation activity. The current method is inconsistent and difficult to reproduce. An ideal method would

be to use mass spectrometry; however the isolation of PAPS from ATP will be required for a mass spectrometry method to work. ATP and PAPS, have very similar mass, charge, and physical properties making separation difficult. Currently, efforts are under way to use recombinant human CD39/ENTPD1 to remove contaminating ATP. In theory, the CD39/ENTPD1 will selectively hydrolyze the ATP and not PAPS. If successful, PAPS concentration could be measured using normal LC/MS following digestion of ATP.

VI. COMPARISON OF *IN VIVO* UGT AND SULT ACTIVITY

Sulfation is an important Phase II drug metabolism pathway, however; glucurindation by the UGTs accounts for most Phase II metabolism and is 2-3 time greater than sulfation. As discussed in the introduction, the UGTs catalyze the transfer of the glucuronic acid of UDPGA to a wide range of acceptor substrate (Liston, Markowitz et al. 2001). Both the SULTs and UGTs add a bulky negatively charged conjugate to their substrates that enhance excretion and there is a large amount of overlap between in substrate specificity between the UGTs and SULTs (Liston, Markowitz et al. 2001) (Falany 1997). Despite the similarities between the two pathways, there are several major differences. One major difference is that the drug metabolizing SULTs are mostly localized in the cytosol, and the UGTs are membrane-dependent proteins localized on the luminal side of the ER (Falany, Green et al. 1986; Liston, Markowitz et al. 2001). The substrate binding domain of the UGTs is associated with the phospholipid membrane, and changes to membrane have been shown to greatly alter the activity of the UGT (Falany, Green et al. 1986). In general, the UGTs also have a lower affinity for substrates and a higher capacity com-

pared to the SULTs (Liston, Markowitz et al. 2001). Only a handful of glucuronides have been reported to be biologically active and glucuronidation is usually non-reversible (Tephly, Green et al. 1998). In contrast, the number of biologically active sulfated metabolites is quite large and includes many drugs, xenobiotics, neural hormones, and steroids (Whittemore, Pearce et al. 1985; Goldstein, Swoboda et al. 1999; Glatt 2000; Cook, Duniac-Dmuchowski et al. 2009). The sulfation of many compounds is reversible by the sulfatase family and has been shown to be a major factor *in vivo* (Pion, Conrad et al. 1966; Parker 1999). The importance of sulfatase activity is clearly demonstrated by the use of sulfatase inhibitors in the treatment of estrogen positive breast cancer. In many estrogen breast cancers, steroid sulfatase is up-regulated, resulting in increased levels of active estrogens. Sulfatase inhibitors decrease steroid sulfatase activity and concentration of active estrogens.

Both sulfated and glucuronidated steroid hormones have been reported in human plasma and urine (Hernández, Watson et al. 1992; Gall, Zawada et al. 1999). Sulfated steroids have been shown to bind plasma proteins and can be regenerated by steroid sulfatase (Pion, Conrad et al. 1966; Parker 1999). Some steroid hormones have also been shown to be biologically active (Goldstein, Swoboda et al. 1999; Cook, Duniac-Dmuchowski et al. 2009). In contrast, glucuronidated steroids are rapidly excreted and are not biologically active. The result is that glucuronidation of steroids is an inactivation pathway that results in elimination of the steroid while sulfation regulates the activity but does not necessarily enhance elimination of the steroid (Gall, Zawada et al. 1999).

The data presented in this project shows that steroids are a random ordered binding substrate for the SULTs. For SULT2A1 the binding of PAPS improved the activity for

DHEA by limiting the level of substrate inhibition. In *SULT1A1*, the binding of PAPS improved the affinity of E2 by two fold, and will likely have a similar influence on other steroidal compounds. These results indicate that in an environment with high level of PAPS, sulfation will be the dominate pathway for steroid conjugation. As the concentration of PAPS is lowered, the specificity and activity of the *SULTs* for the steroids will decrease, significantly reducing steroid sulfation and promoting other metabolic pathways such as the glucuronidation. In low PAPS environments, glucuronidation will become the dominate pathway and result in a higher rate of hormone elimination from the body.

VII. ACTIVE SITE PLACTICIY IN PHASE I AND PHASE II DRUG METABOLIZING ENSYMES

There is a growing consensus in the literature indicating a high level of active site plasticity in the drug metabolizing *CYPs* (Ekroos and Sjögren 2006; Hritz, de Ruiter et al. 2008). The *CYPs* are the major Phase I drug metabolism family and are responsible for ~75% of total drug metabolism. Within the *CYP* gene superfamily, the first three families (*CYP1*, *CYP2*, and *CYP3*) are considered the major drug metabolizing *CYPs* (Martignoni, Groothuis et al. 2006). The drug metabolizing *CYPs* are highly expressed in the intestine, liver, lung, and skin, the major sites of drug and xenobiotic metabolism (Smith 1994; Parkinson 1996; Martignoni, Groothuis et al. 2006). Most of the drug metabolizing *CYPs* also have broad substrate ranges that include many different classes of substrates (Ekroos and Sjögren 2006; Hritz, de Ruiter et al. 2008). The other *CYP* families, such as *CYP19* and *CYP46* have specific physiological functions, such as the syn-

thesis of important steroid hormones. The tissue expression of these CYPs is more dependent on their physiological function (Simpson, Zhao et al. 1997; Vega and Weiner 2007). For example, CYP46 catalyze the 24(S)-hydroxylation of cholesterol, the major cholesterol metabolite in the brain (Vega and Weiner 2007). The 24(S)-OH-Chol then regulates cholesterol levels in the brain through activation of the LXR receptor, which stimulates the efflux of cholesterol from the brain to the liver (Björkhem, Lütjohann et al. 1997).

Starting with CYP2B4 in 2006 (Blobaum, Harris et al. 2005), the crystal structures of several drug metabolizing CYPs have shown a high level of structural variability in their active sites and could have a significant level of active site plasticity (Hritz, de Ruiter et al. 2008). *In vitro* experiments have shown that the binding of substrates, cytochrome P450 reductase, temperature, pH, and the oxidative state of the heme group can affect the shape of the active sites and the substrate specificity of CYP2B4, CYP3A4, and CYP2D6 (Blobaum, Harris et al. 2005; Ekroos and Sjögren 2006; Hritz, de Ruiter et al. 2008). CYP3A4 has the highest variability in the active site, with as much as an 80% change in the volume. This is interesting as CYP3A4 also has the widest reported range of substrates in the CYPs (Ekroos and Sjögren 2006). The active site plasticity of the CYPs adds another level of complexity to the CYP mediated metabolism of drugs and xenobiotics.

The active site plasticity of the drug metabolizing CYPs reported in the literature mirrors the data reported in this thesis in the active site of SULT1A1 and SULT2A1. In both families, the plasticity of the active site is an important structural feature for the broad range of substrates. The evolutionary function for active site plasticity is almost

certainly due to the demand for these enzymes to metabolize novel compounds with only a minor change in the structure of the drug metabolizing enzyme.

Identifying the causes of variability in drug response has been a major field of research in the pharmaceutical industry (Tokuriki and Tawfik 2009). Interpatient variability to drug response is one of the biggest causes of adverse drug reactions. A drug dose that is sub-therapeutic for one patient may be toxic for another patient. Additionally, rare side effects that can often be deadly are often not statistically significant in clinical trials, however can be significant when administered to millions worldwide. There have been many attempts to explain interpatient variability to drugs by the induction, inhibition, and polymorphisms of the CYPs but very few of these studies have included the active site plasticity (Smith 1994; Liston, Markowitz et al. 2001; Niemi, Backman et al. 2003; Wilkinson 2005). Currently, a novel method that combines docking and dynamic modeling called dynamic docking is being attempted to improve the *in silico* predictions of the drug metabolizing CYPs (Hritz, de Ruiter et al. 2008). Dynamic docking may be combined in the future with other models of induction, inhibition, and polymorphisms to predict the variability in drug metabolism *in vivo*.

CYP19 (aromatase) is an important enzyme in estrogen synthesis and catalyzes the conversion of testosterone to E2 (Simpson, Zhao et al. 1997). Aromatase has recently been crystalized, and compared to other CYPs, the aromatase crystal structure is similar to CYP2B4 (Ghosh, Griswold et al. 2009), but has an active site 40% smaller than the CYP2B4 “closed” active site (Ghosh, Griswold et al. 2009). Additionally, the crystal structure of aromatase with bound androstenedione was not significantly different from the aromatase crystal structure with no bound substrate (Ghosh, Griswold et al. 2010).

The structures of aromatase suggested a highly specific and efficient enzyme (Ghosh, Griswold et al. 2009; Ghosh, Griswold et al. 2010). This is also observed in substrate binding studies with aromatase. Testosterone has a reported K_d of 49 nM for aromatase, while the K_d s for drug metabolism CYPs are generally at least a 100 fold higher, in the μ M range (Simpson, Zhao et al. 1997). This suggests that the active site of aromatase has significantly less active site plasticity than the drug metabolizing CYPs and is more specialized for the physiological function of the converting testosterone to E2. Similarly, this thesis reports no detectable change in the substrate specificity of SULT1E1 with the binding of PAPS. Like aromatase, SULT1E1 is not important in drug metabolism but has a specific physiological function. The binding affinity of E2 to SULT1E1 is 1000 fold greater than the normal affinities reported for the other SULTs (Zhang, Varlamova et al. 1998). The reports on aromatase and the data presented on SULT1E1 demonstrate suggest that members of the drug metabolism families with specialized roles will have only a small degree if any active site plasticity and their active sites will be highly efficient for their specialized function.

The growing number of reports in the drug metabolizing CYP and the data reported in this thesis with the SULTs indicates that active site plasticity may be a common feature of drug metabolizing enzymes. Enzymes which have a wide range of reported substrates and have been shown to be significant in drug and xenobiotics will likely have a large level of plasticity in their active site. While plasticity has not been reported in the UGTs, the lack of quality crystal structures that show the substrate binding domain makes it difficult to determine any plasticity in the active site of the UGTs (Shao, He et al. 2005; Miley, Zielinska et al. 2007). The plasticity of the active sites in the drug me-

tabolizing enzymes should be included in any model of drug metabolism and may explain reported discrepancy between *in vitro* and *in vivo* experiments as well as interpatient variability

VIII. FUTURE DIRECTIONS

Future studies will need to examine the *in vivo* concentration of PAPS, and the associated changes in sulfation with differences in PAPS concentrations in a more physiological environment. This thesis demonstrates that there are major changes in the activity and selectivity of the SULTs at different concentrations of PAPS. Currently, the enzymatic method for determining PAPS concentration is error-prone and inconsistent. Using mass spectrometry, a new method for determine PAPS concentration is currently being investigated. If successful, a mass spectrometry method should be more consistent and allow the investigation of PAPS concentration concentrations not only at tissue levels, but also cell type and sub-cellular concentrations. Once perfected, a mass spectrometry method will be used to examine the PAPS concentration in the cytosol of several tissues and cell types. Cell sulfation studies may then be performed using several cell types with a range of PAPS concentrations to determine if the change in selectivity with PAPS concentration is detectable in cells.

The mass spectrometry based method will also permit the investigation of PAPS concentrations in a several physiological and pathological conditions. Conditions that limit the availability of sulfate and ATP should lower PAPS levels; however, this has not been explored in depth by the literature (Hjelle, Hazelton et al. 1985). Also, variability of PAPS concentration between individuals has not been well researched. Mutations in

PAPSS may have a significant impact on basal PAPS concentration, and PAPSS activity is significantly less than the potential SULT activity in the liver resulting in the possibility of PAPS depletion. All of these factors can contribute to interpatient variability in drug metabolism. Despite this, there is a surprising lack of research in the variability of PAPS levels between individuals. Cytosolic SULT expression is not limited to the liver, yet there are only a handful of studies that have examined PAPS levels in non-hepatic tissues. While the liver is a major site of drug sulfation, non-hepatic sulfation of drugs will influence biological activity. To better understand non-hepatic sulfation, the PAPS concentration must be examined in a wide variety of tissues.

Examination of the RAL steady state kinetics also showed that the K_m for PAPS was increased 5-fold. The large increase suggests that RAL binding inhibits PAPS binding. The most likely mechanism is by preventing the full closing of loop 3 in the active site. However, this hypothesis has not been examined. In addition to how RAL changes the structure of SULT2A1, the structural changes induced by DHEA and the mechanism by which the binding of DHEA at the allosteric site inhibits activity have not been examined. The research in this dissertation focused on the changes induced by PAPS and how it affects substrate binding and did not examine the reverse to any detail. The release of products from the ternary complex is also unexplored. Currently, there is no data indicating the order of release. It is clear that if the binding of PAPS induces a structural change, then the release of PAP must also induce a structural change. The impact of release on the reaction kinetics has not been examined.

Monomerization of SULT2A1 using the MBP tag resulted in the loss of substrate inhibition. However, when a KTEE SUT2A1 mutant was generated the activity was too

poor to identify any change in substrate inhibition. It should be noted that the KTEE mutant is the normal mutation made to disrupt dimerization in the SULTs (Petrotchenko, Pedersen et al. 2001). The likely reason for the loss of activity is the KTEE mutant in SULT2A1 places a strong negative charge in the PAPS binding domain that inhibits PAPS binding. Interesting, there are no reports of using the KPEV sequence of mouse SULT1E1. The mouse SULT1E1 activity is similar to human SULT1A1, but lacks substrate inhibition. This data suggest that a KPEV mutant in SULT2A1 will disrupt dimerization without inhibiting PAPS binding. If true, a KPVE SULT2A1 mutant will be a better model of the monomer structure.

An interesting paradox in the SULTs is the lack of heterodimers observed *in vivo*. The KTVE dimerization domain is conserved in all of the SULTs and is a small domain with only 3 points of contact. In every SULTs, the points will be chemically identical, presenting no clear mechanism for selectivity. However, only a single report as identified a heterodimer, and the heterodimer was observed *in vitro* under conditions to promote the formation of the heterodimer (Kiehlbauch, Lam et al. 1995). The mechanism for the high level of dimerization specificity is unknown and cannot be explained by the KTVE dimerization domain. Future research should use a combination of chemical labeling, hydrogen/deuterium exchange, and mutagenesis to explore the mechanism for the specificity in dimerization.

Future studies should also examine the structural rearrangement in the binding of PAPS in other SULTs. This dissertation examined the structural characteristic of SULT2A1 in great detail, but only scratched the surface of SULT1A1 and SULT1E1. Furthermore, the other SULT isoforms have not been examined at all. An interesting

SULT is SULT1A3. SULT1A3 has a distinct biological role *in vivo* of sulfating catecholamines such as dopamine and epinephrine. This would suggest that the active site plasticity of SULT1A3 will be limited, as observed in SULT1E1. However, SULT1A3 shares a 93% identity with SULT1A1, which has a significant level of active site plasticity. If SULT1A3 has a more limited level of plasticity as suggested by its specialized physiological role, then that would suggest that a large level of the plasticity observed in SULT1A1 could be a result of only a few aa, and that a SULT1A1 mutant could be designed to have little active site plasticity.

Finally, new crystal structures are necessary for improving the *in silico* modeling. Currently, only SULT2A1 has been crystalized in the absence of PAPS with the active site resolved. There are no crystal structures of any of the SULTs without ligand bound. Future crystallography of the SULTs should look to crystalize the SULTs, specifically SULT1A1, in the absence of PAPS.

BIBLIOGRAPHY

- Aehle, W., H. Sobek, et al. (1993). "Rational protein engineering and industrial application: structure prediction by homology and rational design of protein-variants with improved 'washing performance'--the alkaline protease from *Bacillus alcalophilus*." J Biotechnol **28**(1): 31-40.
- Aksoy, I. A., D. M. Otterness, et al. (1993). "Cholesterol sulfation in human liver. Catalysis by dehydroepiandrosterone sulfotransferase." Drug Metab Dispos **21**(2): 268-276.
- Aksoy, I. A., T. C. Wood, et al. (1994). "Human liver estrogen sulfotransferase: identification by cDNA cloning and expression." Biochem Biophys Res Commun **200**(3): 1621-1629.
- Allali-Hassani, A., P. W. Pan, et al. (2007). "Structural and chemical profiling of the human cytosolic sulfotransferases." PLoS Biol **5**(5): e97.
- Alnouti, Y. and C. D. Klaassen (2006). "Tissue distribution and ontogeny of sulfotransferase enzymes in mice." Toxicol Sci **93**(2): 242-255.
- Alnouti, Y., J. S. Petrick, et al. (2006). "Tissue distribution and ontogeny of organic cation transporters in mice." Drug Metab Dispos **34**(3): 477-482.
- Anderson, J. A., J. C. Fredenburgh, et al. (2001). "Hypersulfated low molecular weight heparin with reduced affinity for antithrombin acts as an anticoagulant by inhibiting intrinsic tenase and prothrombinase." J Biol Chem **276**(13): 9755-9761.
- Anderson, R. J., R. M. Weinshilboum, et al. (1981). "Human platelet phenol sulphotransferase: assay procedure, substrate and tissue correlations." Clin Chim Acta **110**(2-3): 157-167.
- Arlt, V. M., H. Glatt, et al. (2002). "Metabolic activation of the environmental contaminant 3-nitrobenzanthrone by human acetyltransferases and sulfotransferase." Carcinogenesis **23**(11): 1937-1945.

- Arlt, V. M., H. Glatt, et al. (2003). "Activation of 3-nitrobenzanthrone and its metabolites by human acetyltransferases, sulfotransferases and cytochrome P450 expressed in Chinese hamster V79 cells." Int J Cancer **105**(5): 583-592.
- Barbucci, R., S. Lamponi, et al. (1998). "Influence of Sulfation on Platelet Aggregation and Activation with Differentially Sulfated Hyaluronic Acids." J Thromb Thrombolysis **6**(2): 109-115.
- Barnes, S., R. Waldrop, et al. (1986). "Evidence for an ordered reaction mechanism for bile salt: 3'phosphoadenosine-5'-phosphosulfate: sulfotransferase from rhesus monkey liver that catalyzes the sulfation of the hepatotoxin glycolithocholate." J Lipid Res **27**(11): 1111-1123.
- Baumann, E. (1876). "Concerning the occurrence of brencatechin in the urine." Pfl ü gers Arch.Physiol. **12**(69).
- Bell, J. E. and E. T. Bell (1988). Proteins and Enzymes. Englewood Cliffs, New Jersey, Prentice-Hall.
- Belz, G. G., K. Breithaupt-Grögler, et al. (2001). "Treatment of congestive heart failure--current status of use of digitoxin." Eur J Clin Invest **31 Suppl 2**: 10-17.
- Beset, S., J. B. Vincourt, et al. (2000). "Nuclear localization of PAPS synthetase 1: a sulfate activation pathway in the nucleus of eukaryotic cells." Faseb J **14**(2): 345-354.
- Bhattacharya, R., R. A. Townley, et al. (2009). "The PAPS transporter PST-1 is required for heparan sulfation and is essential for viability and neural development in *C. elegans*." J Cell Sci **122**(Pt 24): 4492-4504.
- Bistrup, A., S. Bhakta, et al. (1999). "Sulfotransferases of two specificities function in the reconstitution of high endothelial cell ligands for L-selectin." J Cell Biol **145**(4): 899-910.
- Björkhem, I., D. Lütjohann, et al. (1997). "Importance of a novel oxidative mechanism for elimination of brain cholesterol. Turnover of cholesterol and 24(S)-hydroxycholesterol in rat brain as measured with ¹⁸O₂ techniques in vivo and in vitro." J Biol Chem **272**(48): 30178-30184.
- Björkhem, I., D. Lütjohann, et al. (1998). "Cholesterol homeostasis in human brain: turnover of 24S-hydroxycholesterol and evidence for a cerebral origin of most of this oxysterol in the circulation." J Lipid Res **39**(8): 1594-1600.
- Björkhem, I. and S. Meaney (2004). "Brain cholesterol: long secret life behind a barrier." Arterioscler Thromb Vasc Biol **24**(5): 806-815.

- Blanchard, R. L., R. R. Freimuth, et al. (2004). "A proposed nomenclature system for the cytosolic sulfotransferase (SULT) superfamily." Pharmacogenetics **14**(3): 199-211.
- Blobaum, A. L., D. L. Harris, et al. (2005). "P450 active site architecture and reversibility: inactivation of cytochromes P450 2B4 and 2B4 T302A by tert-butyl acetylenes." Biochemistry **44**(10): 3831-3844.
- Boccuzzi, G. and E. Brignardello (1996). "Adrenal androgen action in breast cancer." Ann N Y Acad Sci **784**: 349-361.
- Bower, M. M., F. E. Cohen, et al. (1997). "Prediction of Protein Side-chain Rotamers from a Backbone Dependent Rotamer Library: A New Homology Modeling Tool." J. Mol. Biol. **267**: 1268-1282.
- Boylard, E. and L. F. Chasseaud (1969). "The role of glutathione and glutathione S-transferases in mercapturic acid biosynthesis." Adv Enzymol Relat Areas Mol Biol **32**: 173-219.
- Cappiello, M., M. Franchi, et al. (1989). "Distribution of 2-naphthol sulphotransferase and its endogenous substrate adenosine 3'-phosphate 5'-phosphosulphate in human tissues." Eur J Clin Pharmacol **37**(3): 317-320.
- Chang, H. J., R. Shi, et al. (2004). "Identifying androsterone (ADT) as a cognate substrate for human dehydroepiandrosterone sulfotransferase (DHEA-ST) important for steroid homeostasis: structure of the enzyme-ADT complex." J Biol Chem **279**(4): 2689-2696.
- Chao, P. M., Y. H. Kuo, et al. (2010). "The metabolic benefits of Polygonum hypoleucum Ohwi in HepG2 cells and Wistar rats under lipogenic stress." J Agric Food Chem **58**(8): 5174-5180.
- Comer, K. A. and C. N. Falany (1992). "Immunological characterization of dehydroepiandrosterone sulfotransferase from human liver and adrenal." Mol Pharmacol **41**(4): 645-651.
- Comer, K. A., J. L. Falany, et al. (1993). "Cloning and expression of human liver dehydroepiandrosterone sulphotransferase." Biochem J **289** (Pt 1): 233-240.
- Condra, J. A., H. Neibergs, et al. (2007). "Evidence for two schizophrenia susceptibility genes on chromosome 22q13." Psychiatr Genet **17**(5): 292-298.
- Cook, I. T., Z. Duniac-Dmuchowski, et al. (2009). "24-Hydroxycholesterol Sulfation by Human Cytosolic Sulfotransferases: Formation of Monosulfates and Disulfates,

Molecular Modeling, Sulfatase Sensitivity and Inhibition of LXR Activation." Drug Metab Dispos.

- Cook, I. T., T. S. Leyh, et al. (2010). "Lack of Substrate Inhibition in a Monomeric Form of Human Cytosolic SULT2A1." Hormone Molecular Biology and Clinical Investigation **3**(1): 367-374.
- Cook, I. T., T. S. Leyh, et al. (2010). "Structural Rearrangement of SULT2A1: effects on dehydroepiandrosterone and raloxifene sulfation." Horm Mol Biol Clin Invest **1**(1).
- Cornelison, D. D., M. S. Filla, et al. (2001). "Syndecan-3 and syndecan-4 specifically mark skeletal muscle satellite cells and are implicated in satellite cell maintenance and muscle regeneration." Dev Biol **239**(1): 79-94.
- Coughtrie, M. W., R. A. Gilissen, et al. (1999). "Phenol sulphotransferase SULT1A1 polymorphism: molecular diagnosis and allele frequencies in Caucasian and African populations." Biochem J **337** (Pt 1): 45-49.
- Dajani, R., A. M. Hood, et al. (1998). "A single amino acid, glu146, governs the substrate specificity of a human dopamine sulfotransferase, SULT1A3." Mol Pharmacol **54**(6): 942-948.
- Dajani, R., S. Sharp, et al. (1999). "Kinetic properties of human dopamine sulfotransferase (SULT1A3) expressed in prokaryotic and eukaryotic systems: comparison with the recombinant enzyme purified from Escherichia coli." Protein Expr Purif **16**(1): 11-18.
- De Witt, E. H. and L. Lack (1980). "Effects of sulfation patterns on intestinal transport of bile salt sulfate esters." Am J Physiol **238**(1): G34-39.
- Demeio, R. H., M. Wizerkaniuk, et al. (1953). "Role Adenosine Triphosphate in the Enzymatic Synthesis of Phenyl Sulfated Carbohydrates." J. Biol. Chem **203**: 257-263.
- Duffel, M. W. and W. B. Jakoby (1981). "On the mechanism of aryl sulfotransferase." J Biol Chem **256**(21): 11123-11127.
- Dumas, N. A., D. He, et al. (2008). "Sulfotransferase 2B1b in human breast: differences in subcellular localization in African American and Caucasian women." J Steroid Biochem Mol Biol **111**(3-5): 171-177.
- Eisenberg, D., R. Luthy, et al. (1997). "VERIFY3D: assessment of protein models with three-dimensional profiles." Methods Enzymol **277**: 396-404.

- Ekroos, M. and T. Sjögren (2006). "Structural basis for ligand promiscuity in cytochrome P450 3A4." Proc Natl Acad Sci U S A **103**(37): 13682-13687.
- Elmlinger, M. W., W. Kühnel, et al. (2002). "Reference ranges for serum concentrations of luteinizing hormone (LH), follicle-stimulating hormone (FSH), estradiol (E2), prolactin, progesterone, sex hormone-binding globulin (SHBG), dehydroepiandrosterone sulfate (DHEAS), cortisol and ferritin in neonates, children and young adults." Clin Chem Lab Med **40**(11): 1151-1160.
- Eswar, N., B. Webb, et al. (2006). "Comparative protein structure modeling using Modeller." Curr Protoc Bioinformatics **Chapter 5**: Unit 5.6.
- Faiyaz ul Haque, M., L. M. King, et al. (1998). "Mutations in orthologous genes in human spondyloepimetaphyseal dysplasia and the brachymorphic mouse." Nat Genet **20**(2): 157-162.
- Falany, C. N. (1991). "Molecular enzymology of human liver cytosolic sulfotransferases." Trends Pharmacol Sci **12**(7): 255-259.
- Falany, C. N. (1997). "Enzymology of human cytosolic sulfotransferases." Faseb J **11**(4): 206-216.
- Falany, C. N., M. D. Green, et al. (1986). "Substrate specificity and characterization of rat liver p-nitrophenol, 3 alpha-hydroxysteroid and 17 beta-hydroxysteroid UDP-glucuronosyltransferases." Biochem J **238**(1): 65-73.
- Falany, C. N., D. He, et al. (2006). "Human cytosolic sulfotransferase 2B1: isoform expression, tissue specificity and subcellular localization." J Steroid Biochem Mol Biol **102**(1-5): 214-221.
- Falany, C. N., V. Krasnykh, et al. (1995). "Bacterial expression and characterization of a cDNA for human liver estrogen sulfotransferase." J Steroid Biochem Mol Biol **52**(6): 529-539.
- Falany, C. N., M. E. Vazquez, et al. (1989). "Purification and characterization of human liver dehydroepiandrosterone sulphotransferase." Biochem J **260**(3): 641-646.
- Falany, C. N., M. E. Vazquez, et al. (1989). "Purification and characterization of human liver dehydroepiandrosterone sulphotransferase." Biochem J **260**(3): 641-646.
- Falany, C. N., J. Wheeler, et al. (1994). "Steroid sulfation by expressed human cytosolic sulfotransferases." J Steroid Biochem Mol Biol **48**(4): 369-375.

- Falany, J. L. and C. N. Falany (1996). "Regulation of estrogen sulfotransferase in human endometrial adenocarcinoma cells by progesterone." Endocrinology **137**(4): 1395-1401.
- Falany, J. L. and C. N. Falany (2007). "Interactions of the human cytosolic sulfotransferases and steroid sulfatase in the metabolism of tibolone and raloxifene." J Steroid Biochem Mol Biol **107**(3-5): 202-210.
- Falany, J. L., N. Macrina, et al. (2002). "Regulation of MCF-7 breast cancer cell growth by beta-estradiol sulfation." Breast Cancer Res Treat **74**(2): 167-176.
- Falany, J. L., D. E. Pilloff, et al. (2006). "Sulfation of raloxifene and 4-hydroxytamoxifen by human cytosolic sulfotransferases." Drug Metab Dispos **34**(3): 361-368.
- Fan, Q. W., K. Uchimura, et al. (1999). "Spatially and temporally regulated expression of N-acetylglucosamine-6-O-sulfotransferase during mouse embryogenesis." Glycobiology **9**(9): 947-955.
- Feher, M. and J. M. Schmidt (2000). "Multiple flexible alignment with SEAL: a study of molecules acting on the colchicine binding site." **40**: 495-502.
- Frame, L. T., S. Ozawa, et al. (2000). "A simple colorimetric assay for phenotyping the major human thermostable phenol sulfotransferase (SULT1A1) using platelet cytosols." Drug Metab Dispos **28**(9): 1063-1068.
- Franzon, V. L., M. A. Gibson, et al. (1999). "Molecular cloning of a novel human PAPS synthetase which is differentially expressed in metastatic and non-metastatic colon carcinoma cells." Int J Biochem Cell Biol **31**(5): 613-626.
- Freimuth, R. R., M. Wiepert, et al. (2004). "Human cytosolic sulfotransferase database mining: identification of seven novel genes and pseudogenes." Pharmacogenomics J **4**(1): 54-65.
- Gall, W. E., G. Zawada, et al. (1999). "Differential glucuronidation of bile acids, androgens and estrogens by human UGT1A3 and 2B7." J Steroid Biochem Mol Biol **70**(1-3): 101-108.
- Gamage, N. U., R. G. Duggleby, et al. (2003). "Structure of a human carcinogen-converting enzyme, SULT1A1. Structural and kinetic implications of substrate inhibition." J Biol Chem **278**(9): 7655-7662.
- Gamage, N. U., S. Tsvetanov, et al. (2005). "The structure of human SULT1A1 crystallized with estradiol. An insight into active site plasticity and substrate inhibition with multi-ring substrates." J Biol Chem **280**(50): 41482-41486.

- Ghosh, D., J. Griswold, et al. (2009). "Structural basis for androgen specificity and oestrogen synthesis in human aromatase." Nature **457**(7226): 219-223.
- Ghosh, D., J. Griswold, et al. (2010). "X-ray structure of human aromatase reveals an androgen-specific active site." J Steroid Biochem Mol Biol **118**(4-5): 197-202.
- Glatt, H. (1997). "Sulfation and sulfotransferases 4: bioactivation of mutagens via sulfation." FASEB J **11**(5): 314-321.
- Glatt, H. (2000). "Sulfotransferases in the bioactivation of xenobiotics." Chem Biol Interact **129**(1-2): 141-170.
- Glatt, H. (2000). "Sulfotransferases in the bioactivation of xenobiotics." Chem Biol Interact **129**(1-2): 141-170.
- Glatt, H., H. Boeing, et al. (2001). "Human cytosolic sulphotransferases: genetics, characteristics, toxicological aspects." Mutat Res **482**(1-2): 27-40.
- Goldstein, D. S., K. J. Swoboda, et al. (1999). "Sources and physiological significance of plasma dopamine sulfate." J Clin Endocrinol Metab **84**(7): 2523-2531.
- Gong, D. W., S. Ozawa, et al. (1991). "Purification of hepatic N-hydroxyarylamine sulfotransferases and their regulation by growth hormone and thyroid hormone in rats." J Biochem **110**(2): 226-231.
- Grunwell, J. R. and C. R. Bertozzi (2002). "Carbohydrate sulfotransferases of the GalNAc/Gal/GlcNAc6ST family." Biochemistry **41**(44): 13117-13126.
- Gulcan, H. O. and M. W. Duffel (2011). "Substrate inhibition in human hydroxysteroid sulfotransferase SULT2A1: studies on the formation of catalytically non-productive enzyme complexes." Arch Biochem Biophys **507**(2): 232-240.
- Ha, H. C. and S. H. Snyder (1999). "Poly(ADP-ribose) polymerase is a mediator of necrotic cell death by ATP depletion." Proc Natl Acad Sci U S A **96**(24): 13978-13982.
- Hadley, M. E. (1992). *Endocrinology*. New Jersey, Prentice Hall.
- Hashimoto, H., K. Toide, et al. (1993). "Gene structure of CYP3A4, an adult-specific form of cytochrome P450 in human livers, and its transcriptional control." Eur J Biochem **218**(2): 585-595.

- He, D. and C. N. Falany (2006). "Characterization of proline-serine-rich carboxyl terminus in human sulfotransferase 2B1b: immunogenicity, subcellular localization, kinetic properties, and phosphorylation." Drug Metab Dispos **34**(10): 1749-1755.
- He, D., A. R. Frost, et al. (2005). "Identification and immunohistochemical localization of Sulfotransferase 2B1b (SULT2B1b) in human lung." Biochim Biophys Acta **1724**(1-2): 119-126.
- Hebbring, S. J., A. A. Adjei, et al. (2007). "Human SULT1A1 gene: copy number differences and functional implications." Hum Mol Genet **16**(5): 463-470.
- Her, C., G. P. Kaur, et al. (1997). "Human sulfotransferase SULT1C1: cDNA cloning, tissue-specific expression, and chromosomal localization." Genomics **41**(3): 467-470.
- Her, C., C. Szumlanski, et al. (1996). "Human jejunal estrogen sulfotransferase and dehydroepiandrosterone sulfotransferase: immunochemical characterization of individual variation." Drug Metab Dispos **24**(12): 1328-1335.
- Her, C., T. C. Wood, et al. (1998). "Human hydroxysteroid sulfotransferase SULT2B1: two enzymes encoded by a single chromosome 19 gene." Genomics **53**(3): 284-295.
- Hernandez-Guzman, F. G., T. Higashiyama, et al. (2001). "Purification, characterization and crystallization of human placental estrone/dehydroepiandrosterone sulfatase, a membrane-bound enzyme of the endoplasmic reticulum." J Steroid Biochem Mol Biol **78**(5): 441-450.
- Hernández, J. S., R. W. Watson, et al. (1992). "Sulfation of estrone and 17 beta-estradiol in human liver. Catalysis by thermostable phenol sulfotransferase and by dehydroepiandrosterone sulfotransferase." Drug Metab Dispos **20**(3): 413-422.
- Heroux, J. A., C. N. Falany, et al. (1989). "Immunological characterization of human phenol sulfotransferase." Mol Pharmacol **36**(1): 29-33.
- Heroux, J. A. and J. A. Roth (1988). "Physical characterization of a monoamine-sulfating form of phenol sulfotransferase from human platelets." Mol Pharmacol **34**(2): 194-199.
- Hildebrandt, M. A., O. E. Salavaggione, et al. (2004). "Human SULT1A3 pharmacogenetics: gene duplication and functional genomic studies." Biochem Biophys Res Commun **321**(4): 870-878.

- Hjelle, J. J., G. A. Hazelton, et al. (1985). "Acetaminophen decreases adenosine 3'-phosphate 5'-phosphosulfate and uridine diphosphoglucuronic acid in rat liver." Drug Metab Dispos **13**(1): 35-41.
- Hoffman, A. F. (1988). Bile Acids. The Liver: Biology and Pathobiology. W. B. Jakoby, I. A. Arias, H. Popper, D. Schachter and D. A. Shafritz. New York, Raven Press: 795-796.
- Hritz, J., A. de Ruiter, et al. (2008). "Impact of plasticity and flexibility on docking results for cytochrome P450 2D6: a combined approach of molecular dynamics and ligand docking." J Med Chem **51**(23): 7469-7477.
- Hui, Y., S. Yasuda, et al. (2008). "On the sulfation and methylation of catecholestrogens in human mammary epithelial cells and breast cancer cells." Biol Pharm Bull **31**(4): 769-773.
- Jeong, E. J., Y. Liu, et al. (2005). "Species- and disposition model-dependent metabolism of raloxifene in gut and liver: role of UGT1A10." Drug Metab Dispos **33**(6): 785-794.
- Kakuta, Y., L. G. Pedersen, et al. (1997). "Crystal structure of estrogen sulphotransferase." Nat Struct Biol **4**(11): 904-908.
- Kamiyama, S., T. Ichimiya, et al. (2011). "Expression and the role of 3'-phosphoadenosine 5'-phosphosulfate transporters in human colorectal carcinoma." Glycobiology **21**(2): 235-246.
- Kamiyama, S., T. Suda, et al. (2003). "Molecular cloning and identification of 3'-phosphoadenosine 5'-phosphosulfate transporter." J Biol Chem **278**(28): 25958-25963.
- Kastenholz, M. A., M. Pastor, et al. (2000). "GRID/CPCA: a new computational tool to design selective ligands." J Med Chem **43**(16): 3033-3044.
- Kiehlbauch, C. C., Y. F. Lam, et al. (1995). "Homodimeric and heterodimeric aryl sulfotransferases catalyze the sulfuric acid esterification of N-hydroxy-2-acetylaminofluorene." J Biol Chem **270**(32): 18941-18947.
- Kim, H. J., C. Madhu, et al. (1995). "In vivo modification of 3'-phosphoadenosine 5'-phosphosulfate and sulfate by infusion of sodium sulfate, cysteine, and methionine." Drug Metab Dispos **23**(8): 840-845.
- Kim, H. J., P. Rozman, et al. (1995). "Acetaminophen does not decrease hepatic 3'-phosphoadenosine 5'-phosphosulfate in mice." J Pharmacol Exp Ther **275**(3): 1506-1511.

- Klaassen, C. D. and J. W. Boles (1997). "Sulfation and sulfotransferases 5: the importance of 3'-phosphoadenosine 5'-phosphosulfate (PAPS) in the regulation of sulfation." FASEB J **11**(6): 404-418.
- Kurima, K., M. L. Warman, et al. (1998). "A member of a family of sulfate-activating enzymes causes murine brachymorphism." Proc Natl Acad Sci U S A **95**(15): 8681-8685.
- Labrie, F. (1991). "Intracrinology." Mol Cell Endocrinol **78**(3): C113-118.
- Labrie, F., A. Bélanger, et al. (1998). "DHEA and the intracrine formation of androgens and estrogens in peripheral target tissues: its role during aging." Steroids **63**(5-6): 322-328.
- Labute, P. (2005). "On the perception of molecules from 3D atomic coordinates." J Chem Inf Model **45**(2): 215-221.
- Laskowski, MacArthur, et al. (2001). PROCHECK: validation of protein structure coordinates. *International Tables of Crystallography, Volume F. Crystallography of Biological Macromolecules*, Rossmann M G & Arnold E, Dordrecht, Kluwer Academic Publishers,: 722-725.
- Lee, K. A., H. Fuda, et al. (2003). "Crystal structure of human cholesterol sulfotransferase (SULT2B1b) in the presence of pregnenolone and 3'-phosphoadenosine 5'-phosphate. Rationale for specificity differences between prototypical SULT2A1 and the SULT2BG1 isoforms." J Biol Chem **278**(45): 44593-44599.
- Lehmann, J. M., S. A. Kliewer, et al. (1997). "Activation of the nuclear receptor LXR by oxysterols defines a new hormone response pathway." J Biol Chem **272**(6): 3137-3140.
- Lipscombe, R. J., A. M. Nakhoul, et al. (1998). "Interleukin-5 binds to heparin/heparan sulfate. A model for an interaction with extracellular matrix." J Leukoc Biol **63**(3): 342-350.
- Liston, H. L., J. S. Markowitz, et al. (2001). "Drug glucuronidation in clinical psychopharmacology." J Clin Psychopharmacol **21**(5): 500-515.
- Lu, J., H. Li, et al. (2010). "Crystal structures of SULT1A2 and SULT1A1 *3: insights into the substrate inhibition and the role of Tyr149 in SULT1A2." Biochem Biophys Res Commun **396**(2): 429-434.
- Lu, L. Y., H. P. Chiang, et al. (2009). "Dimerization is responsible for the structural stability of human sulfotransferase 1A1." Drug Metab Dispos **37**(5): 1083-1088.

- Lu, L. Y., Y. C. Hsieh, et al. (2008). "Identification and characterization of two amino acids critical for the substrate inhibition of human dehydroepiandrosterone sulfotransferase (SULT2A1)." Mol Pharmacol **73**(3): 660-668.
- Luthy, R., J. U. Bowie, et al. (1992). "Assessment of protein models with three-dimensional profiles." Nature **356**(6364): 83-85.
- Mackenzie, P. I., J. O. Miners, et al. (2000). "Polymorphisms in UDP glucuronosyltransferase genes: functional consequences and clinical relevance." Clin Chem Lab Med **38**(9): 889-892.
- Maisels, M. J. and A. F. McDonagh (2008). "Phototherapy for neonatal jaundice." N Engl J Med **358**(9): 920-928.
- Mandon, E. C., M. E. Milla, et al. (1994). "Purification of the Golgi adenosine 3'-phosphate 5'-phosphosulfate transporter, a homodimer within the membrane." Proc Natl Acad Sci U S A **91**(22): 10707-10711.
- Martignoni, M., G. M. Groothuis, et al. (2006). "Species differences between mouse, rat, dog, monkey and human CYP-mediated drug metabolism, inhibition and induction." Expert Opin Drug Metab Toxicol **2**(6): 875-894.
- Meinl, W., C. Donath, et al. (2008). "SULT1C3, an orphan sequence of the human genome, encodes an enzyme activating various promutagens." Food Chem Toxicol **46**(4): 1249-1256.
- Meinl, W. and H. Glatt (2001). "Structure and localization of the human SULT1B1 gene: neighborhood to SULT1E1 and a SULT1D pseudogene." Biochem Biophys Res Commun **288**(4): 855-862.
- Meinl, W., U. Pabel, et al. (2006). "Human sulphotransferases are involved in the activation of aristolochic acids and are expressed in renal target tissue." Int J Cancer **118**(5): 1090-1097.
- Meisheri, K. D., L. A. Cipkus, et al. (1988). "Mechanism of action of minoxidil sulfate-induced vasodilation: a role for increased K⁺ permeability." J Pharmacol Exp Ther **245**(3): 751-760.
- Meloche, C. A. and C. N. Falany (2001). "Expression and characterization of the human 3 beta-hydroxysteroid sulfotransferases (SULT2B1a and SULT2B1b)." J Steroid Biochem Mol Biol **77**(4-5): 261-269.
- Meloche, C. A., V. Sharma, et al. (2002). "Sulfation of budesonide by human cytosolic sulfotransferase, dehydroepiandrosterone-sulfotransferase (DHEA-ST)." Drug Metab Dispos **30**(5): 582-585.

- Meng, L. J., W. J. Griffiths, et al. (1997). "High levels of (24S)-24-hydroxycholesterol 3-sulfate, 24-glucuronide in the serum and urine of children with severe cholestatic liver disease." J Lipid Res **38**(5): 926-934.
- Michnick, D. A., D. D. Pittman, et al. (1994). "Identification of individual tyrosine sulfation sites within factor VIII required for optimal activity and efficient thrombin cleavage." J Biol Chem **269**(31): 20095-20102.
- Migeon, C. J., A. R. Keller, et al. (1957). "Dehydroepiandrosterone and androsterone levels in human plasma: effect of age and sex; day-to-day and diurnal variations." J Clin Endocrinol Metab **17**(9): 1051-1062.
- Miley, M. J., A. K. Zielinska, et al. (2007). "Crystal structure of the cofactor-binding domain of the human phase II drug-metabolism enzyme UDP-glucuronosyltransferase 2B7." J Mol Biol **369**(2): 498-511.
- Miller, W. L. and J. B. Tyrrell (1995). The Adrenal Cortex, in: L.A. Frohman (Ed) Endocrinology and Metabolism. New York, McGraw-Hill: 555-711.
- Murias, M., M. Miksits, et al. (2008). "Metabolism of resveratrol in breast cancer cell lines: impact of sulfotransferase 1A1 expression on cell growth inhibition." Cancer Lett **261**(2): 172-182.
- Nagar, S., S. Walther, et al. (2006). "Sulfotransferase (SULT) 1A1 polymorphic variants *1, *2, and *3 are associated with altered enzymatic activity, cellular phenotype, and protein degradation." Mol Pharmacol **69**(6): 2084-2092.
- Niemi, M., J. T. Backman, et al. (2003). "Pharmacokinetic interactions with rifampicin : clinical relevance." Clin Pharmacokinet **42**(9): 819-850.
- Nowell, S. and C. N. Falany (2006). "Pharmacogenetics of human cytosolic sulfotransferases." Oncogene **25**(11): 1673-1678.
- Nowell, S., B. Green, et al. (2005). "Examination of human tissue cytosols for expression of sulfotransferase isoform 1A2 (SULT1A2) using a SULT1A2-specific antibody." Mol Pharmacol **67**(2): 394-399.
- Okuda, H., A. Hiratsuka, et al. (1986). "A hydroxymethyl sulphate ester as an active metabolite of the carcinogen, 5-hydroxymethylchrysene." Biochem Pharmacol **35**(3): 535-538.
- Ottersness, D. M. and R. Weinshilboum (1994). "Human dehydroepiandrosterone sulfotransferase: molecular cloning of cDNA and genomic DNA." Chem Biol Interact **92**(1-3): 145-159.

- Otterness, D. M., E. D. Wieben, et al. (1992). "Human liver dehydroepiandrosterone sulfotransferase: molecular cloning and expression of cDNA." Mol Pharmacol **41**(5): 865-872.
- Park, B. C., Y. C. Lee, et al. (1999). "Testosterone sulfotransferase: evidence in the guinea pig that this reaction is carried out by 3 alpha-hydroxysteroid sulfotransferase." Steroids **64**(8): 510-517.
- Parker, C. R. (1999). "Dehydroepiandrosterone and dehydroepiandrosterone sulfate production in the human adrenal during development and aging." Steroids **64**(9): 640-647.
- Parkinson, A. (1996). Biotransformation of Xenobiotics, in: Casarett and Douls Toxicology: The Basic Science of Poisons. New York, McGraw-Hill: 113-186.
- Pedersen, L. C., E. Petrotchenko, et al. (2002). "Crystal structure of the human estrogen sulfotransferase-PAPS complex: evidence for catalytic role of Ser137 in the sulfuryl transfer reaction." J Biol Chem **277**(20): 17928-17932.
- Pedersen, L. C., E. V. Petrotchenko, et al. (2000). "Crystal structure of SULT2A3, human hydroxysteroid sulfotransferase." FEBS Lett **475**(1): 61-64.
- Peet, D. J., S. D. Turley, et al. (1998). "Cholesterol and bile acid metabolism are impaired in mice lacking the nuclear oxysterol receptor LXR alpha." Cell **93**(5): 693-704.
- Petrotchenko, E. V., L. C. Pedersen, et al. (2001). "The dimerization motif of cytosolic sulfotransferases." FEBS Lett **490**(1-2): 39-43.
- Pion, R. J., S. H. Conrad, et al. (1966). "Pregnenolone sulfate-an efficient precursor for the placental production of progesterone." J Clin Endocrinol Metab **26**(2): 225-226.
- Radomska, A., R. R. Drake, et al. (1996). "Photoaffinity labeling of human recombinant sulfotransferases with 2-azidoadenosine 3',5'-[5'-³²P]bisphosphate." J Biol Chem **271**(6): 3195-3199.
- Raftogianis, R. B., T. C. Wood, et al. (1997). "Phenol sulfotransferase pharmacogenetics in humans: association of common SULT1A1 alleles with TS PST phenotype." Biochem Biophys Res Commun **239**(1): 298-304.
- Raftogianis, R. B., T. C. Wood, et al. (1999). "Human phenol sulfotransferases SULT1A2 and SULT1A1: genetic polymorphisms, allozyme properties, and human liver genotype-phenotype correlations." Biochem Pharmacol **58**(4): 605-616.

- Rapraeger, A. C. (1995). "In the clutches of proteoglycans: how does heparan sulfate regulate FGF binding?" Chem Biol **2**(10): 645-649.
- Rapraeger, A. C. (2001). "Molecular interactions of syndecans during development." Semin Cell Dev Biol **12**(2): 107-116.
- Rehse, P. H., M. Zhou, et al. (2002). "Crystal structure of human dehydroepiandrosterone sulphotransferase in complex with substrate." Biochem J **364**(Pt 1): 165-171.
- Rein, G., V. Glover, et al. (1982). "Multiple forms of phenolsulphotransferase in human tissues: selective inhibition by dichloronitrophenol." Biochem Pharmacol **31**(10): 1893-1897.
- Reiter, C. and R. M. Weinshilboum (1982). "Acetaminophen and phenol: substrates for both a thermostable and a thermolabile form of human platelet phenol sulfotransferase." J Pharmacol Exp Ther **221**(1): 43-51.
- Ren, S., X. Li, et al. (2007). "Sulfated oxysterol, 25HC3S, is a potent regulator of lipid metabolism in human hepatocytes." Biochem Biophys Res Commun **360**(4): 802-808.
- Robbins, P. W. and F. Lipmann (1957). "Isolation and identification of active sulfate." J Biol Chem **229**(2): 837-851.
- Robbins, P. W. and F. Lipmann (1958). "Enzymatic synthesis of adenosine-5'-phosphosulfate." J Biol Chem **233**(3): 686-690.
- Robbins, P. W. and F. Lipmann (1958). "Separation of the two enzymatic phases in active sulfate synthesis." J Biol Chem **233**(3): 681-685.
- Runge-Morris, M. and T. Kocarek (2011). PAPS Knockout in *Hep G2* Cells. Detroit, Mi, Wayne State University.
- Sakakibara, Y., K. Yanagisawa, et al. (1998). "Molecular cloning, expression, and characterization of novel human SULT1C sulfotransferases that catalyze the sulfonation of N-hydroxy-2-acetylaminofluorene." J Biol Chem **273**(51): 33929-33935.
- Sambrook, J. and D. Russel (2001). Molecular Cloning: A Laboratory Manual. Cold Spring Harbor, NY, Cold Spring Harbor Laboratory Press.
- Scherer, C. A., C. L. Magness, et al. (2007). "Distinct gene expression profiles in peripheral blood mononuclear cells from patients infected with vaccinia virus, yellow fever 17D virus, or upper respiratory infections." Vaccine **25**(35): 6458-6473.

- Schmoltdt, A., I. Blömer, et al. (1992). "Hydroxysteroid sulfotransferase and a specific UDP-glucuronosyltransferase are involved in the metabolism of digitoxin in man." *Naunyn Schmiedebergs Arch Pharmacol* **346**(2): 226-233.
- Sekura, R. D., M. W. Duffel, et al. (1981). "Aryl sulfotransferases." *Methods Enzymol* **77**: 197-206.
- Selvan, R. S., N. S. Ihrcke, et al. (1996). "Heparan sulfate in immune responses." *Ann N Y Acad Sci* **797**: 127-139.
- Shao, H., X. He, et al. (2005). "Crystal structures of a multifunctional triterpene/flavonoid glycosyltransferase from *Medicago truncatula*." *Plant Cell* **17**(11): 3141-3154.
- Shevtsov, S., E. V. Petrotchenko, et al. (2003). "Crystallographic analysis of a hydroxylated polychlorinated biphenyl (OH-PCB) bound to the catalytic estrogen binding site of human estrogen sulfotransferase." *Environ Health Perspect* **111**(7): 884-888.
- Shworak, N. W., J. Liu, et al. (1997). "Molecular cloning and expression of mouse and human cDNAs encoding heparan sulfate D-glucosaminyl 3-O-sulfotransferase." *J Biol Chem* **272**(44): 28008-28019.
- Simpson, E. R., Y. Zhao, et al. (1997). "Aromatase expression in health and disease." *Recent Prog Horm Res* **52**: 185-213; discussion 213-184.
- Smith, D. A. (1994). "Design of drugs through a consideration of drug metabolism and pharmacokinetics." *Eur J Drug Metab Pharmacokinet* **19**(3): 193-199.
- Snyder, K. R., N. Sparano, et al. (2000). "Raloxifene hydrochloride." *Am J Health Syst Pharm* **57**(18): 1669-1675; quiz 1676-1668.
- Stjernschantz, E., J. Reinen, et al. (2010). "Comparison of murine and human estrogen sulfotransferase inhibition in vitro and in silico--implications for differences in activity, subunit dimerization and substrate inhibition." *Mol Cell Endocrinol* **317**(1-2): 127-140.
- Sun, M. and T. S. Leyh (2010). "The human estrogen sulfotransferase: a half-site reactive enzyme." *Biochemistry* **49**(23): 4779-4785.
- Takahashi, A., N. Tanida, et al. (1990). "Difference in enzymatic sulfation of bile acids between the mouse and rat." *Tokushima J Exp Med* **37**(1-2): 1-8.

- Tangemann, K., A. Bistrup, et al. (1999). "Sulfation of a high endothelial venule-expressed ligand for L-selectin. Effects on tethering and rolling of lymphocytes." J Exp Med **190**(7): 935-942.
- Tanrikulu, Y., O. Rau, et al. (2009). "Structure-based pharmacophore screening for natural-product-derived PPARgamma agonists." Chembiochem **10**(1): 75-78.
- Tephly, T. R., M. D. Green, et al. (1998). "Metabolism of endobiotics and xenobiotics by UDP-glucuronosyltransferase." Adv Pharmacol **42**: 343-346.
- Teramoto, T., Y. Sakakibara, et al. (2008). "Crystal structure of mSULT1D1, a mouse catecholamine sulfotransferase." FEBS Lett **582**(28): 3909-3914.
- Tokuriki, N. and D. S. Tawfik (2009). "Protein dynamism and evolvability." Science **324**(5924): 203-207.
- Tseng, L. and H. C. Liu (1981). "Stimulation of arylsulfotransferase activity by progestins in human endometrium in vitro." J Clin Endocrinol Metab **53**(2): 418-421.
- Tsoi, C., C. N. Falany, et al. (2001). "Identification of a new subfamily of sulphotransferases: cloning and characterization of canine SULT1D1." Biochem J **356**(Pt 3): 891-897.
- Tyapochkin, E., P. F. Cook, et al. (2008). "Isotope exchange at equilibrium indicates a steady state ordered kinetic mechanism for human sulfotransferase." Biochemistry **47**(45): 11894-11899.
- Tyapochkin, E., P. F. Cook, et al. (2009). "para-Nitrophenyl sulfate activation of human sulfotransferase 1A1 is consistent with intercepting the E[middle dot]PAP complex and reformation of E[middle dot]PAPS." J Biol Chem **284**(43): 29357-29364.
- Van Der Spoel, D., E. Lindahl, et al. (2005). "GROMACS: fast, flexible, and free." J Comput Chem **26**(16): 1701-1718.
- Vega, G. L. and M. F. Weiner (2007). "Plasma 24S hydroxycholesterol response to statins in Alzheimer's disease patients: effects of gender, CYP46, and ApoE polymorphisms." J Mol Neurosci **33**(1): 51-55.
- Venkatachalam, K. V. (2003). "Human 3'-phosphoadenosine 5'-phosphosulfate (PAPS) synthase: biochemistry, molecular biology and genetic deficiency." IUBMB Life **55**(1): 1-11.

- Verreault, M., K. Senekeo-Effenberger, et al. (2006). "The liver X-receptor alpha controls hepatic expression of the human bile acid-glucuronidating UGT1A3 enzyme in human cells and transgenic mice." Hepatology **44**(2): 368-378.
- Visser, T. J. (1994). "Role of sulfation in thyroid hormone metabolism." Chem Biol Interact **92**(1-3): 293-303.
- Wang, J., J. L. Falany, et al. (1998). "Expression and characterization of a novel thyroid hormone-sulfating form of cytosolic sulfotransferase from human liver." Mol Pharmacol **53**(2): 274-282.
- Weinshilboum, R. M. and D. M. Otterness (1994). Sulfotransferase Enzymes, in: F.C. Kauffman (Ed). *Conjugation-Deconjugation Reactions in Drug Metabolism and Toxicity*. New York, Springer-Verlag: 45-78.
- Weinshilboum, R. M., D. M. Otterness, et al. (1997). "Sulfation and sulfotransferases 1: Sulfotransferase molecular biology: cDNAs and genes." FASEB J **11**(1): 3-14.
- Wempe, M. F., V. J. Wacher, et al. (2008). "Pharmacokinetics of raloxifene in male Wistar-Hannover rats: influence of complexation with hydroxybutenyl-beta-cyclodextrin." Int J Pharm **346**(1-2): 25-37.
- Whittemore, R. M., L. B. Pearce, et al. (1985). "Purification and kinetic characterization of a dopamine-sulfating form of phenol sulfotransferase from human brain." Biochemistry **24**(10): 2477-2482.
- Whittemore, R. M., L. B. Pearce, et al. (1986). "Purification and kinetic characterization of a phenol-sulfating form of phenol sulfotransferase from human brain." Arch Biochem Biophys **249**(2): 464-471.
- Wildman, S. A. and G. M. Crippen (2001). "Evaluation of ligand overlap by atomic parameters." J Chem Inf Comput Sci **41**: 446-450.
- Wildman, S. A. and G. M. Crippen (2002). "Three-dimensional molecular descriptors and a novel QSAR method." J Mol Graph Model **21**(3): 161-170.
- Wildman, S. A. and G. M. Crippen (2003). "Validation of DAPPER for 3D QSAR: conformational search and chirality metric." J Chem Inf Comput Sci **43**: 629-636.
- Wilkinson, G. R. (2005). "Drug metabolism and variability among patients in drug response." N Engl J Med **352**(21): 2211-2221.
- Wilson, L. A., G. E. Reynolds, et al. (2004). "cDNA cloning, functional expression, and characterization of chicken sulfotransferases belonging to the SULT1B and SULT1C families." Arch Biochem Biophys **428**(1): 64-72.

- Wood, T. C., C. Her, et al. (1996). "Human dehydroepiandrosterone sulfotransferase pharmacogenetics: quantitative Western analysis and gene sequence polymorphisms." J Steroid Biochem Mol Biol **59**(5-6): 467-478.
- Wu, S. G. and K. D. Straub (1976). "Purification and characterization of N-hydroxy-2-acetylaminofluorene sulfotransferase from rat liver." J Biol Chem **251**(21): 6529-6536.
- Xu, Z., T. C. Wood, et al. (2001). "Human 3'-phosphoadenosine 5'-phosphosulfate synthetase: radiochemical enzymatic assay, biochemical properties, and hepatic variation." Drug Metab Dispos **29**(2): 172-178.
- Xu, Z. H., R. R. Freimuth, et al. (2002). "Human 3'-phosphoadenosine 5'-phosphosulfate synthetase 2 (PAPSS2) pharmacogenetics: gene resequencing, genetic polymorphisms and functional characterization of variant alleles." Pharmacogenetics **12**(1): 11-21.
- Xu, Z. H., B. A. Thoma, et al. (2003). "Pharmacogenetics of human 3'-phosphoadenosine 5'-phosphosulfate synthetase 1 (PAPSS1): gene resequencing, sequence variation, and functional genomics." Biochem Pharmacol **65**(11): 1787-1796.
- Yamazoe, Y., K. Nagata, et al. (1994). "Structural similarity and diversity of sulfotransferases." Chem Biol Interact **92**(1-3): 107-117.
- Yu, A. M., J. R. Idle, et al. (2004). "Polymorphic cytochrome P450 2D6: humanized mouse model and endogenous substrates." Drug Metab Rev **36**(2): 243-277.
- Zhang, H., O. Varlamova, et al. (1998). "Sulfuryl transfer: the catalytic mechanism of human estrogen sulfotransferase." J Biol Chem **273**(18): 10888-10892.